

The background of the cover is a 3D visualization of a crystal lattice. The atoms are represented by small grey spheres connected by thin grey lines. Superimposed on this lattice are numerous arrows of various colors (red, orange, yellow, green, cyan, blue, purple, black) pointing in different directions, representing magnetic moments or spin orientations. The arrows are arranged in a pattern that suggests a phase transition or a specific magnetic configuration.

Elastic Coupling at Quantum Phase Transitions and in Chiral Magnets

Lars Franke

2025



This document is licensed under a Creative Commons Attribution 4.0 International License (CC BY 4.0): <https://creativecommons.org/licenses/by/4.0/deed.en>

Elastic Coupling at Quantum Phase Transitions and in Chiral Magnets

Zur Erlangung des akademischen Grades eines

Doktors der Naturwissenschaften (Dr. rer. nat.)

von der KIT-Fakultät für Physik des

Karlsruher Instituts für Technologie (KIT)

angnommene Dissertation von

Lars Franke

Tag der mündlichen Prüfung: *01.08.2025*

Referent: *Prof. Dr. Markus Garst* (TFP)

Koreferent: *Prof. Dr. Jörg Schmalian* (TKM)

2025

Contents

List of symbols	7
Introduction	10
1. Theory of elasticity	13
1.1. Lattice oscillations in the harmonic approximation	13
1.2. Continuum mechanics	16
1. Criticality in Elastic Media	25
2. Introduction to the theory of critical phenomena	26
2.1. Statistical field theory and Landau theory	27
2.2. The renormalization group idea	29
2.3. Imaginary time formalism for quantum criticality	36
2.4. Example: Lorentz-invariant ϕ^4 -theory	38
2.5. Cubic anisotropy and cubic fixed point	43
3. Classical criticality on compressible lattices: A review	47
3.1. Thermodynamics of phase transitions on compressible lattices	48
3.2. Larkin-Pikin mechanism	51
3.3. Renormalization group approach on an anisotropic cubic lattice . . .	56
3.4. Discussion	65
4. Tricritical elasticity	67
5. Quantum criticality on a compressible lattice	70
5.1. Breakdown of the Larkin-Pikin mechanism at quantum criticality . .	72
5.2. RG analysis of quantum criticality in an isotropic elastic medium . .	73
5.3. Microscopic and macroscopic instability of the crystal lattice	88
6. Ferroelectric quantum criticality in an elastic medium	93
6.1. Quantum criticality in the presence of dipolar interaction	94
6.2. RG flow equations of an isotropic elastic ferroelectric	99
6.3. Classical isotropic elastic ferroelectric criticality	107
6.4. Isotropic elastic ferroelectric quantum phase transition	112

II. Chiral Magnetoelasticity	115
7. Chiral magnets in the micromagnetic framework	116
7.1. The continuum limit of magnetism	116
7.2. The minimal micromagnetic model for bulk chiral magnets	118
8. Theory of magnetoelastic coupling in chiral magnets	124
8.1. Microscopic origins of magnetoelastic coupling	124
8.2. Classification of magnetoelastic couplings	126
8.3. Selected examples	129
9. Magnetoelastic effects on chiral surface twists	135
9.1. Surface twist in the field polarized and helical state	135
9.2. Skyrmion surface twist	142
Conclusion and outlook	149
Acknowledgements	151
A. Calculation of self-energy diagram with transversal and longitudinal projectors	152
Bibliography	156

List of symbols

A	Magnetic exchange stiffness
a	Lattice constant
α	Critical exponent (specific heat)
β	Critical exponent (r -dependence of order parameter)
b	RG scaling parameter
γ	Critical exponent (r -dependence of susceptibility)
Γ	Vertex correction of the self-interaction
c	Critical mode velocity
c_l	Longitudinal acoustic phonon velocity
c_t	Transversal acoustic phonon velocity
C_{ijkl}, C_{mn}	Stiffness tensor
d	Number of spatial dimensions
d_{eff}	Effective dimensions $d + z$
D	Dzyaloshinsky-Moriya interaction
D_{ij}	Dynamical matrix
\mathcal{D}	Path integral measure
δ	Critical exponent (h -dependence of order parameter)
δ_{ij}	Kronecker symbol
$\partial_{\#}$	Partial derivative
ϵ	Dimensional expansion parameter
ϵ_{ijk}	Levi-Civita tensor
ε	Strain tensor
$\tilde{\varepsilon}$	Traceless strain tensor $\varepsilon - \mathbb{1} \text{tr} \varepsilon / d$
\mathcal{E}	Thermodynamic strain variable $\langle \text{tr}\{\varepsilon\} \rangle$
E_{ij}	Spatially homogeneous strain
E	Energy
\mathcal{E}	Energy density
\mathcal{F}	Free energy

F	Green's function of displacement field \mathbf{u}
G	Green's function of critical modes ϕ
\mathbf{h}, h	Magnetic/external field
H	Hamiltonian
η	Anomalous dimension
Θ	Heavyside function
I_n, I_{mn}	Integrals appearing RG corrections TOOD
K	Bulk modulus
\mathcal{K}	Uniaxial anisotropy
κ	Dimensionless uniaxial anisotropy
ℓ	Logarithmic RG scale $\ell = \log b$
λ	Coupling constant of the elastic interaction
$\lambda_{ijkl}, \lambda_{mn}$	Magnetostrictive/electrostrictive coupling tensor
Λ	Ultraviolet cutoff
\mathbf{M}	Magnetization vector
M_s	Saturation magnetization
\mathbf{m}	Unit vector in magnetization direction
μ	Shear modulus
μ_{ijkl}, μ_{mn}	Magnetoelastic DMI coupling tensor
ν	Critical exponent (correlation length)
ν_{ijkl}, ν_{mn}	Magnetoelastic exchange coupling tensor
O	Observable
$O(N)$	Orthogonal group in N dimensions
$\mathcal{O}(\#)$	Terms on the order of $\#$
Π	Self-energy of displacement field \mathbf{u}
\mathbf{q}	Wave vector
$\hat{\mathbf{q}}$	Unit vector in wave vector direction
\mathbf{r}	Spatial coordinate in chapters where the tuning parameter does <i>not</i> appear
r	Tuning parameter
ρ	Mass density
\mathcal{S}	Action
σ_{ij}	Stress tensor
Σ	Self-energy of critical modes ϕ
t	Time coordinate
τ	Imaginary time coordinate
T	Temperature
\mathbf{u}, u_i	Displacement field

u	Coupling constant of $O(N)$ -symmetric self-interaction
v	Coupling constant of cubic anisotropy in the self-interaction or ϕ^6 -interaction in the discussion of the tricritical point
w	Coupling constant of infinite range interaction $(\int \phi^2)^2$
w_{ij}	Lifshitz invariant
ω	Frequency
ω_{ij}	Rotation of displacement field
\mathbf{x}	Spatial coordinate in chapters where r is used for the tuning parameter
χ	Skyrmion helicity
z	Dynamical exponent
\mathcal{Z}	Partition function
Z_ϕ	Z-factor (wave function renormalization) of the critical field ϕ
Z_u	Z-factor (wave function renormalization) of the displacement field \mathbf{u}
$\#^V$	Voigt notation matrix of a fourth order tensor $\#$
$\#^M$	Mandel notation matrix of a fourth order tensor $\#$

Introduction

The ways in which physical processes are changed by elasticity are of fundamental interest in many areas of condensed matter science. In some cases, elastic coupling is just a small perturbation, in others, the inclusion of elastic coupling drastically changes the outcomes. The most interesting cases are of course the latter, where elastic coupling does not just lead to purely quantitative change, which may be absorbed into macroscopic model parameters, but instead leads to a qualitative change through the breaking of a symmetry or the introduction of a new length- or energy scale. In this work, we explore two topics in which elastic coupling to microscopic degrees of freedom changes the physics at large scales: Phase transitions and magnetism.

When a system is tuned close a continuous phase transitions, critical fluctuations drive the system toward universal behavior, which is only determined by symmetry and dimension. In reality, phase transitions do not happen in perfect lattices, where each degrees of freedom, is rigidly pinned to a specific position in space, as introductory statistical physics courses may have you believe. Instead, these degrees of freedom are usually carried by a medium, which can move, bend, and stretch. We should not be surprised that the fluctuations in the degrees of freedom undergoing the transition, and the fluctuations of the underlying lattice are intimately connected. Thus, continuous phase transitions, where fluctuations strongly affect macroscopic properties, the influence of elastic coupling can be felt. We seek to understand under which conditions this coupling is non-perturbative, and thus changes the universal behavior, i.e. does the inclusion of lattice coupling change the universality class of a phase transition?

For classical phase transitions this question was answered in the 60s and 70s (Bergman & Halperin, 1976; Fisher, 1968; Larkin & Pikin, 1969; Moura et al., 1976; Nattermann, 1977; Sak, 1974), but how this applies to quantum phase transitions has only recently become a focus of interest (Chandra et al., 2020; Han, Lee, & Moon, 2021; Samanta, Shimshoni, & Podolsky, 2022; Sarkar et al., 2023). We will attempt to address this question in this work for the case of high symmetry, where the leading coupling is quadratic in the order parameter. This case is relevant in quantum paraelectrics, which are close to a ferroelectric quantum critical point (Coak et al., 2020; Rowley et al., 2014) and antiferromagnetic quantum phase transitions (Rüegg et al., 2008). In the less symmetric case, a bilinear coupling is present, the order parameter strongly hybridizes with elastic excitations and critical

elasticity is an effective description of the transition (Cowley, 1976; Zacharias, Paul, & Garst, 2015), such is the case in piezoelectric ferroelectrics (Levanyuk & Sobyanin, 1970; Villain, 1970), Mott metal-insulator transitions (Gati et al., 2016; Zacharias, Bartosch, & Garst, 2012) and nematic quantum phase transitions (Paul & Garst, 2017; Reiss et al., 2019).

Another fascinating case where the physics at large scales shows a strong elastic influence is seen in chiral magnets. The breaking of inversion symmetry in these materials allows for an antisymmetric exchange interaction called Dzyaloshinsky-Moriya interaction (DMI) (Dzyaloshinsky, 1958; Moriya, 1960), which favors a twist in the magnetization. As a consequence, chiral magnets host a diverse set of modulated spin textures, such as magnetic helices, cycloids, and skyrmions (Bogdanov & Yablonskii, 1989; Muhlbauer et al., 2009). Through magnetoelastic coupling, chiral magnets also host modulated strain textures. The low symmetry of the crystal structure of chiral magnets with tetrahedral point group allows for chiral magnetoelastic coupling contributions which can cause strain textures of a similarly chiral nature.

At the boundaries of bulk chiral magnets, uncompensated DMI leads to phenomena known as chiral surface twists. Most phases in chiral magnets show a surface twist such as the fully polarized state (Rybakov, Borisov, & Bogdanov, 2013) and the skyrmion lattice (Zhang et al., 2018). However, experimental observations show that the length scale on which the skyrmion surface twist extends into the bulk is an order of magnitude larger than theory predicts (Schneider et al., 2018; Tan et al., 2024; Zhang et al., 2018). We explore magnetoelastic coupling as a possible explanation. However, it turns out that in this particular case, the effect of the elastic coupling is perturbative, meaning that it only leads to slight modifications of the surface twist on the order of the magnetoelastic energy scale. Nonetheless the complicated interplay of magnetic and elastic degrees of freedom, both coming with non-trivial boundary conditions, has some interesting surface effects.

The body of this thesis is structured as follows: First, the basics of elasticity theory are covered in chapter 1, introducing concepts that will be used throughout the whole thesis. It also introduces some non-standard notation, therefore it is recommended that even readers with prior knowledge of elasticity at least skim the section on continuum mechanics.

The first part of the thesis is dedicated to critical phenomena and how they interact with elasticity, with a focus on highly symmetric models with a generic quadratic coupling to strain. An introduction chapter on critical phenomena is given in chapter 2, introducing the renormalization group (RG) method and how it is used to derive the universal properties of classical and quantum phase transitions. Readers already familiar with the matter may safely skip this chapter, without loss of insight. If in later chapters specific formulas are used, they will be referenced explicitly. In chapter 3 we build up an understanding of the theory of classical phase transitions with lattice coupling. This chapter is essentially a literature review, that is concerned

with some seminal contributions to this topic, like the Fisher-renormalization of the critical exponents (Fisher, 1968), which occurs in the presence of lattice coupling at constant volume, the Larkin-Pikin mechanism (Larkin & Pikin, 1969), which allows us to describe the compressible system in terms of an effective Landau theory as a function of the free energy of the rigid system, and an RG analysis of a phase transition on an anisotropic cubic lattice, performed by Bergman & Halperin (1976), which connects the Fisher-renormalized exponents to fixed points in the RG flow at finite elastic coupling. We then apply this theory to the tricritical point in chapter 4. We go through the works on the classical transition on compressible lattices in detail not just because they are interesting in their own right, which they are, but also because they are laying the groundwork for the theory of the corresponding quantum phase transition coupled to a compressible lattice, which is the topic of chapter 5. Specifically, it is important to understand how some of the approaches to the classical theory fail, because the breaking of Lorentz invariance by the elastic coupling introduces a non-analyticity that breaks some of the assumptions that lead to Fisher-renormalization. In the RG analysis, the quantum theory turns out to be quite different from the classical counterpart, exhibiting additional instabilities. Finally, in chapter 6 we discuss the ferroelectric quantum phase transition with lattice coupling, where the order parameter represents an optical phonon, which couples to the acoustic phonons in ways that go beyond a purely compressive interaction, by also allowing for coupling to shear modes. Additionally, in a ferroelectric long-range dipolar interaction becomes important, which already has interesting effects in the rigid model.

The second part of the thesis explores the effects of elastic coupling on the non-collinear spin texture in chiral magnets. In chapter 7 a brief introduction to micromagnetism is given and the relevant magnetic phases are discussed in a purely magnetic theory. This is another introductory chapter that may be skipped if the reader feels they do not need it. The nature of the lattice coupling in bulk chiral magnets with tetrahedral symmetry is then discussed in chapter 8. We find that a wide variety of different couplings may be considered and we explore some examples in which the effects of the different couplings such as magnetostriction and coupling to DMI-like terms become apparent, with a focus on the chiral symmetry breaking of these couplings. Finally, in chapter 9 we discuss chiral surface twists both in the collinear and the skyrmion phase. We show how they are affected by magnetoelastic coupling using a mix of analytical and numerical methods. In the end, we will see that magnetoelastic coupling can not explain experimental observations of the skyrmion surface twist, leaving the question open for further investigation.

1. Theory of elasticity

In this chapter, concepts from elasticity theory are introduced that will be used throughout this text. We start from an atomistic view of displacements and lattice vibrations, then move on to develop an understanding of continuum mechanics. Many of these concepts can also be found in classic textbooks such as (Landau & Lifshitz, 1959). However, some non-standard notation used in later chapters is also introduced here.

1.1. Lattice oscillations in the harmonic approximation

In an idealized picture, a crystal consists of a perfectly regular lattice of atoms. Classically, we describe the positions of atoms in the solid with a vector \mathbf{r}_n , with some label n . Regularity here means it can be created by repetition of an arrangement of atoms, called the *unit cell*. If the arrangement with the smallest number of atoms that generates the lattice, called the *primitive unit cell*, still contains more than one atom, it is convenient to label the positions as $\mathbf{r}_{n,\alpha}$, where the Greek letter indices label the atoms within one unit cell, while the index n labels the unit cells within the crystal. The vector decomposes as follows

$$\mathbf{r}_{n,\alpha} = \mathbf{R}_n + \mathbf{T}_\alpha + \mathbf{u}_{n,\alpha} . \quad (1.1)$$

\mathbf{R} refers to the *Bravais lattice* vectors, which in turn can be decomposed into basis vectors

$$\mathbf{R}_n \equiv \mathbf{R}_{n_a, n_b, n_c} = n_a \mathbf{a} + n_b \mathbf{b} + n_c \mathbf{c} \quad (1.2)$$

where \mathbf{T} refers to the equilibrium positions of the atoms within the unit cell and \mathbf{u} is the deviation from the equilibrium position due to its momentary *displacement*.

The atoms have arranged themselves in a particular crystal structure because of some effective potential in which they have found an equilibrium. The displacements are merely small perturbations around the equilibrium arrangement. We can model the system with the Hamiltonian

$$H = \sum_{n,\alpha} \frac{\mathbf{p}_{n,\alpha}^2}{2m_\alpha} + U(\{\mathbf{r}\}) , \quad (1.3)$$

where U represents the effective potential and depends on the position of all atoms. In general, the form of the potential is unknown and may be quite complicated. However, assuming displacements are small compared to the lattice spacing, we expand U in \mathbf{u}

$$U(\{\mathbf{r}\}) = U|_{\mathbf{u}=0} + \frac{1}{2} \sum_{m,n,\alpha,\beta,i,j} \left(\frac{\partial^2 U}{\partial r_{m,\alpha,i} \partial r_{n,\beta,j}} \right)_{\mathbf{u}=0} u_{m,\alpha,i} u_{n,\beta,j} + \mathcal{O}(u^3). \quad (1.4)$$

The 0th order is simply a constant and can be ignored in the following discussion. The 1st order would contradict the assumption that we expand around an equilibrium position and has to vanish. The first non-trivial order is therefore the quadratic one. We use the coefficients of the above expansion to define the *Dynamical Matrix*

$$D_{mn,\alpha\beta,ij} = \frac{1}{\sqrt{m_\alpha m_\beta}} \left(\frac{\partial^2 U}{\partial r_{m,\alpha,i} \partial r_{n,\beta,j}} \right)_{\mathbf{u}=0}. \quad (1.5)$$

If we stop the expansion at this point, we end up with a quadratic Hamiltonian. We can then learn everything there is to know about this Hamiltonian by diagonalizing the dynamical matrix and looking at the eigenmodes, effectively solving the classical equations of motion

$$\ddot{v}_{m,\alpha,i} = - \sum_{n,\beta,j} D_{mn,\alpha\beta,ij} v_{n,\beta,j} \quad (1.6)$$

where we introduced rescaled displacements to remove the masses from the equation

$$v_{n,\alpha,i} = \sqrt{m_\alpha} u_{n,\alpha,i}. \quad (1.7)$$

Assuming an infinite crystal or applying periodic boundary conditions, we can reduce the size of the matrix that we have to diagonalize considerably by using translational invariance with respect to Bravais lattice vectors

$$D_{mn,\alpha\beta,ij} = D_{\alpha\beta,ij}(\mathbf{R}_m - \mathbf{R}_n), \quad (1.8)$$

which enables us to define the Fourier transform of the dynamical matrix

$$D_{\alpha\beta,ij}(\mathbf{q}) = \sum_n D_{\alpha\beta,ij}(\mathbf{R}_n) e^{-i\mathbf{q}\cdot\mathbf{R}_n}. \quad (1.9)$$

The result is a $(d \cdot \mu) \times (d \cdot \mu)$ matrix (with μ atoms per unit cell) for every \mathbf{q} vector in the first Brillouin zone. It has at most $d \cdot \mu$ distinct eigenmodes or *branches*.

To simplify notation, we combine the coordinate and atomic species to a single branch index $\lambda = (\alpha, i)$. May $\omega_\lambda^2(\mathbf{q})$ be the eigenvalues of $D(\mathbf{q})$ and $\phi_\lambda(\mathbf{q})$ the corresponding eigenvectors. Then we can write

$$H = \frac{1}{2} \sum_{\mathbf{q} \in 1^{\text{st}}\text{BZ}} \sum_{\lambda} \left(\pi_\lambda(\mathbf{q}) \pi_\lambda(-\mathbf{q}) + \omega_\lambda^2(\mathbf{q}) \phi_\lambda(\mathbf{q}) \phi_\lambda(-\mathbf{q}) \right) \quad (1.10)$$

using an appropriate definition of the canonical momentum π in terms of \mathbf{p}

$$\boldsymbol{\pi}_\alpha(\mathbf{q}) = \sum_n \frac{\mathbf{p}_{n,\alpha}}{\sqrt{m_\alpha}} e^{-i\mathbf{q}\cdot\mathbf{R}_n} . \quad (1.11)$$

Such a theory could now be quantized by declaring ϕ and π to be field operators and assuming canonical commutation relations. However, we will not go into the details here and instead focus on the classical description.

To understand the character of the eigenmodes of the dynamical matrix, let us think about a plane displacement wave of a particular mode λ traveling through the crystal. Consider the equation of motion eq. (1.6), with the ansatz

$$v_{n,\alpha,i} = w_{\alpha,i}^{(\lambda)} e^{i\mathbf{q}\cdot\mathbf{R}_n} , \quad (1.12)$$

where $w_{\mu,i}^{(\lambda)}$ is a polarization vector belonging to a certain branch λ . If all atoms in the unit cell are displaced in phase, such that w no longer depends on α , the mode is called an acoustic mode. From the equation of motion, we then get

$$\omega_\lambda^2(\mathbf{q}) w_i^{(\lambda)} e^{i\mathbf{q}\cdot\mathbf{R}_n} = \sum_{m,\beta} D_{mn,\alpha\beta,ij} w_j^{(\lambda)} e^{i\mathbf{q}\cdot\mathbf{R}_m} . \quad (1.13)$$

The above equation can be solved for ω_λ using the fact that w is an eigenvector of the $d \times d$ -matrix $D_{mn,\alpha\beta}$

$$\omega_\lambda^2(\mathbf{q}) = \sum_{m,\beta} D_{mn,\alpha\beta,ij} e^{i\mathbf{q}\cdot(\mathbf{R}_m - \mathbf{R}_n)} . \quad (1.14)$$

Our strategy is now to expand both sides in \mathbf{q} . In 0th order we have

$$\omega_\lambda^2(0) = \sum_{m,\beta,j} D_{mn,\alpha\beta,ij} = 0 \quad (1.15)$$

where in the last step it was used that a constant displacement (independent of m and β) can not cause a force in between the atoms, since it represents simply a shift of the position of the crystal as a whole. eq. (1.15) shows that *the acoustic mode can not have a gap*. This is a fundamental consequence of the fact that the energy is invariant under global translations, the symmetry for which the phonon is the *Goldstone mode*.

The 1st order of the expansion of eq. (1.14) vanishes for symmetry reasons. In 2nd order we have

$$\left(\nabla_{\mathbf{q}} \omega_\lambda(0) \cdot \mathbf{q} \right)^2 = -\frac{1}{2} \sum_{n,\beta,j} D_{mn,\alpha\beta,ij} \left((\mathbf{R}_n - \mathbf{R}_m) \cdot \mathbf{q} \right)^2 \quad (1.16)$$

where we usually write $(\nabla_{\mathbf{q}} \omega(0) \cdot \mathbf{q})^2 = c_\lambda^2(\hat{\mathbf{q}}) q^2$ with the speed of sound c_λ . eq. (1.16) shows that *the acoustic branches go linear with q at small q* . The speed of sound is

then given by

$$c_\lambda^2(\hat{\mathbf{q}}) = - \sum_{\mathbf{R}\beta} D_{\alpha\beta,ii}(\mathbf{R})(\mathbf{R} \cdot \hat{\mathbf{q}})^2 \quad (1.17)$$

For the optical branches, a similar expansion is possible, but they acquire a gap in the 0th order. The linear order on the other hand still vanishes with the same symmetry argument. As a result, we can write the following dispersion relations for a long wavelength theory

$$\omega_\gamma(\mathbf{q}) = \begin{cases} c_\gamma(\hat{\mathbf{q}})q & \text{for acoustic branches} \\ \sqrt{\omega_{0,\gamma}^2 + s_\gamma^2(\hat{\mathbf{q}})q^2} & \text{for optical branches.} \end{cases} \quad (1.18)$$

1.2. Continuum mechanics

In the context of a sufficiently long wavelength theory, it is justified to “zoom out” and consider the continuum version of elasticity. Here, the system is treated as a continuous medium rather than focusing on individual atomic displacements. We analyze the shifts and distortions of small volume elements that contain many unit cells, neglecting the relative displacements of atoms within a unit cell (optical modes) and focusing on the low-energy theory for acoustic modes.

Displacement and strain

The displacement field $\mathbf{u}(\mathbf{r})$ represents the displacement vector of a volume element, which at equilibrium would be at a point \mathbf{r} , but has been moved to a different point \mathbf{r}'

$$\mathbf{r} \rightarrow \mathbf{r}' = \mathbf{r} + E\mathbf{r} + \mathbf{u}(\mathbf{r}), \quad (1.19)$$

where we split off the part of the displacement field that is linear in \mathbf{r} into a matrix E for reasons that will become clear soon. The displacement itself has a degree of freedom that corresponds to global shifts since shifting the crystal as a whole should not change the fundamental physics happening inside the crystal. Usually, we choose a frame of reference where the volume average of \mathbf{u} vanishes

$$\langle \mathbf{u}(\mathbf{r}) \rangle_V = 0, \quad (1.20)$$

which for a material of homogeneous mass density corresponds to the center of mass frame. Therefore the quantities of interest are the derivatives of the displacement field. The gradients of the displacement field $\partial_i u_j$ can be decomposed into three physically meaningful components:

$$\partial_i u_j = \frac{1}{d} \nabla \cdot \mathbf{u} \delta_{ij} + \frac{1}{2} \left(\partial_i u_j + \partial_j u_i - \frac{2}{d} \nabla \cdot \mathbf{u} \delta_{ij} \right) + \frac{1}{2} (\partial_i u_j - \partial_j u_i) \quad (1.21)$$

The first term represents dilation, the second term shear, and the third term rotation. The *strain tensor*, which captures the first two terms, includes the symmetric part of the displacement gradient

$$\varepsilon_{ij} = E_{ij} + \frac{1}{2}(\partial_i u_j + \partial_j u_i) . \quad (1.22)$$

The trace of the strain tensor describes the dilation and the traceless strain tensor

$$\tilde{\varepsilon} = \varepsilon - \frac{1}{d} \text{tr}\{\varepsilon\} \mathbb{1} \quad (1.23)$$

describes shear. Here, we made another decomposition of the strain into a spatially constant tensor E , corresponding to a linear term in the displacement, and a purely local strain. This allows us to apply the additional constraint

$$\langle \partial_i u_j + \partial_j u_i \rangle_{\mathcal{V}} = 0 . \quad (1.24)$$

On the other hand, rotation is represented by the antisymmetric tensor

$$\omega_{ij} = \frac{1}{2}(\partial_i u_j - \partial_j u_i) . \quad (1.25)$$

Here, we do not make the distinction between global and local rotations, since the spatially constant part $\Omega = \langle \omega \rangle_{\mathcal{V}}$ represents a global rotation and this is required to be a symmetry, thus we can make it vanish by choice of a frame of reference. In other words, in a consistent lattice theory, the energy can not depend on Ω . Therefore we can enforce the constraint

$$\langle \partial_i u_j - \partial_j u_i \rangle_{\mathcal{V}} = 0 . \quad (1.26)$$

In combination with eq. (1.24) we have established that we can set $\langle \partial_i u_j \rangle_{\mathcal{V}} = 0$.

Energy and stress

Linear elasticity is the continuum limit of a theory based on the harmonic approximation of the interatomic potential, evoking the image of point-like masses connected by springs. The equations governing such a model are therefore given by a generalized *Hooke's law*, that connects the *stress tensor* σ , the equivalent of force, to the strain tensor ε , the continuum description of displacement, through a set of generalized spring constants, given by the *stiffness tensor* C_{ijkl}

$$\sigma_{ij} = C_{ijkl} \varepsilon_{kl} , \quad (1.27)$$

where the sum over repeated indices is implied. This linear equation can be derived by minimizing a quadratic energy functional

$$E = \int d^d r \mathcal{E} = \int d^d r \left(\frac{1}{2} \varepsilon_{ij} C_{ijkl} \varepsilon_{kl} - \sigma_{ij} \varepsilon_{ij} \right), \quad (1.28)$$

where \mathcal{E} is the energy density. For more compact notation and to avoid the introduction of an overwhelming amount of indices, we can use the $:$ -product that contracts two indices of the involved tensors

$$\mathcal{E} = \frac{1}{2} \varepsilon : C : \varepsilon - \sigma : \varepsilon, \quad (1.29)$$

where $(C : \varepsilon)_{ij} = C_{ijkl} \varepsilon_{kl}$ and $\sigma : \varepsilon = \sigma_{ij} \varepsilon_{ij}$.

In the special case of an isotropic solid, the energy can be expressed using only rotationally invariant quantities. Since the strain tensor transforms like a tensor under rotations, at the quadratic level there are only two such objects, which are $\text{tr}\{\varepsilon\}^2$ and $\text{tr}\{\varepsilon\varepsilon\}$. The energy is then typically parametrized as

$$\mathcal{E} = \frac{1}{2} \left(K - \frac{2}{d} \mu \right) \text{tr}\{\varepsilon\}^2 + \mu \text{tr}\{\varepsilon\varepsilon\}, \quad (1.30)$$

where K is called *bulk modulus* and μ is called *shear modulus*. The corresponding stiffness tensor is of the form

$$C_{ijkl} = \left(K - \frac{2}{d} \mu \right) \delta_{ij} \delta_{kl} + \mu (\delta_{ik} \delta_{jl} + \delta_{jk} \delta_{il}). \quad (1.31)$$

The bulk modulus can be defined in terms of the stiffness tensor

$$K = \frac{1}{d^2} C_{iijj}. \quad (1.32)$$

If we define the bulk modulus as the stiffness of the system to volume changes in response to hydrostatic pressure, then this definition is useful even in the presence of anisotropy.

Voigt and Mandel notation

Taking a close look at the energy functional eq. (1.28) we notice that the stiffness tensor C_{ijkl} necessarily has to satisfy the symmetries

$$C_{ijkl} = C_{jikl} = C_{klij}. \quad (1.33)$$

The first equality is a consequence of the strain tensor being a symmetric matrix. As a result of this symmetry ε has only six independent components in three

dimensions. The idea of Voigt notation is to rewrite symmetric second-rank tensors as six-component vectors

$$\varepsilon^V = (\varepsilon_{11}, \varepsilon_{22}, \varepsilon_{33}, 2\varepsilon_{23}, 2\varepsilon_{13}, 2\varepsilon_{12}) \quad (1.34)$$

effectively traversing the matrix in the pattern

$$\begin{pmatrix} \varepsilon_{11} & \varepsilon_{12} & \varepsilon_{13} \\ \varepsilon_{12} & \varepsilon_{22} & \varepsilon_{23} \\ \varepsilon_{13} & \varepsilon_{23} & \varepsilon_{33} \end{pmatrix} .$$

Consequently, fourth-rank tensors can then be written as 6×6 -matrices

$$C^V = \begin{pmatrix} C_{1111} & C_{1122} & C_{1133} & C_{1123} & C_{1113} & C_{1112} \\ C_{2211} & C_{2222} & C_{2233} & C_{2223} & C_{2213} & C_{2212} \\ C_{3311} & C_{3322} & C_{3333} & C_{3323} & C_{3313} & C_{3312} \\ C_{2311} & C_{2322} & C_{2333} & C_{2323} & C_{2313} & C_{2312} \\ C_{1311} & C_{1322} & C_{1333} & C_{1323} & C_{1313} & C_{1312} \\ C_{1211} & C_{1222} & C_{1233} & C_{1223} & C_{1213} & C_{1212} \end{pmatrix} . \quad (1.35)$$

We will simply write $C_{ij} \equiv C_{ij}^V$. There is no ambiguity because of the different number of indices.

The second equality in eq. (1.33) tells us that C^V must also be a symmetric matrix, further reducing the number of independent components to a maximum of 21. For specific crystal structures, the corresponding symmetries allow more detailed statements about the form of such tensors. For example, in a cubic crystal, there are only three independent parameters C_{11} , C_{12} , and C_{44} . The cubic anisotropy can then be quantified using the *Zener ratio*

$$A = \frac{2C_{44}}{C_{11} - C_{12}} \quad (1.36)$$

where $A = 1$ corresponds to the case of an isotropic crystal of the form eq. (1.30), in which case we can identify $K = (C_{11} + 2C_{12})/3$ and $\mu = C_{44}$.

Voigt notation is constructed to preserve quadratic forms like the one in the energy

$$\varepsilon : C : \varepsilon = (\varepsilon^V)^T C^V \varepsilon^V . \quad (1.37)$$

This is ensured by the factors of 2 in front of the shear strain components in eq. (1.34). However, one needs to be careful when dealing with more than one fourth-rank tensor, because products between these are in general not preserved under Voigt notation:

$$C_1^V C_2^V \neq (C_1 : C_2)^V . \quad (1.38)$$

To fix this issue, we introduce *Mandel notation* (Mandel, 1965), effectively shifting a factor of $\sqrt{2}$ from shear vector components to the corresponding matrix components, defining

$$\varepsilon^M = (\varepsilon_{11}, \varepsilon_{22}, \varepsilon_{33}, \sqrt{2}\varepsilon_{23}, \sqrt{2}\varepsilon_{13}, \sqrt{2}\varepsilon_{12}) \quad (1.39)$$

and

$$C^M = \begin{pmatrix} C_{1111} & C_{1122} & C_{1133} & \sqrt{2}C_{1123} & \sqrt{2}C_{1113} & \sqrt{2}C_{1112} \\ C_{2211} & C_{2222} & C_{2233} & \sqrt{2}C_{2223} & \sqrt{2}C_{2213} & \sqrt{2}C_{2212} \\ C_{3311} & C_{3322} & C_{3333} & \sqrt{2}C_{3323} & \sqrt{2}C_{3313} & \sqrt{2}C_{3312} \\ \sqrt{2}C_{2311} & \sqrt{2}C_{2322} & \sqrt{2}C_{2333} & 2C_{2323} & 2C_{2313} & 2C_{2312} \\ \sqrt{2}C_{1311} & \sqrt{2}C_{1322} & \sqrt{2}C_{1333} & 2C_{1323} & 2C_{1313} & 2C_{1312} \\ \sqrt{2}C_{1211} & \sqrt{2}C_{1222} & \sqrt{2}C_{1233} & 2C_{1223} & 2C_{1213} & 2C_{1212} \end{pmatrix}. \quad (1.40)$$

Mandel notation also leaves quadratic forms invariant

$$(\varepsilon^M)^T C^M \varepsilon^M = (\varepsilon^V)^T C^V \varepsilon^V = \varepsilon : C : \varepsilon \quad (1.41)$$

but now we can use it for matrix products as well

$$C_1^M C_2^M = (C_1 : C_2)^M. \quad (1.42)$$

In conclusion, Mandel notation is more general and convenient. However, the literature standard is Voigt notation. To avoid confusion with literature values in this text the component without explicit superscript C_{ij} will still refer to Voigt notation. For example, in an isotropic crystal, the stiffness tensor component $C_{44} = \mu$ refers to the shear modulus, not twice the shear modulus.

Dynamics, microscopic and macroscopic modes

When describing the dynamics of the displacement field we minimize the actions instead of the energy, including time derivatives of \mathbf{u} . Ignoring externally applied stress the action is

$$\mathcal{S} = \int dt d^d x \mathcal{L} = \int dt d^d x \frac{1}{2} \left(\rho (\partial_t u_i)^2 - \varepsilon_{ij} C_{ijkl} \varepsilon_{kl} \right), \quad (1.43)$$

where ρ is the mass density. We use the Fourier transformation of the displacement field

$$\mathbf{u}(\mathbf{r}, t) = \int_{\mathbf{q}, \omega} e^{i(\mathbf{q}\cdot\mathbf{r} - \omega t)} \mathbf{u}(\mathbf{q}, \omega) \quad \mathbf{u}(\mathbf{q}, \omega) = \int dt d\mathbf{r} e^{-i(\mathbf{q}\cdot\mathbf{r} - \omega t)} \mathbf{u}(\mathbf{r}, t) \quad (1.44)$$

where we have defined the shorthand notation

$$\int_{\mathbf{q},\omega} = \int_{-\infty}^{\infty} \frac{d\omega}{2\pi} \int \frac{d^d q}{(2\pi)^d} . \quad (1.45)$$

For simplicity, we ignore the global, homogeneous strain E for the moment, since it does not enter the equation of motion for \mathbf{u} anyway. The transformed action is then

$$\mathcal{S} = \int_{\mathbf{q},\omega} \frac{1}{2} u_i(\mathbf{q}, \omega) \left(\rho \omega^2 \delta_{ij} - D_{ij}(\mathbf{q}) \right) u_j(-\mathbf{q}, -\omega) \quad (1.46)$$

where we have defined the *dynamical matrix* D in the continuum theory as

$$D_{ij}(\mathbf{q}) = C_{iklj} q_k q_l . \quad (1.47)$$

The equation of motion for \mathbf{u} is then simply the eigenvalue equation for D and is diagonalized by the acoustic phonon modes,

$$\rho \omega^2 u_i = D_{ij}(\mathbf{q}) u_j , \quad (1.48)$$

with a linear dispersion given by the respective phonon velocities $\omega = c_\lambda(\hat{q})q$. c_λ is the phonon velocity for the respective branch λ and in general, depends on the direction of the momentum in a way that is determined by the stiffness tensor C . In the isotropic case, the dependence on the direction of \mathbf{q} disappears and we obtain the velocity of the single longitudinal phonon and the $d - 1$ fold degenerate transversal phonon

$$\begin{aligned} c_l &= \sqrt{\frac{K + (2 - \frac{2}{d})\mu}{\rho}} \\ c_t &= \sqrt{\frac{\mu}{\rho}} . \end{aligned} \quad (1.49)$$

It is important to note that in a finite crystal, the phonon picture does not tell the whole story. At a scale of the system size L , one has to include the effects of geometry and boundary conditions. For a finite isotropic elastic body, one has to find solutions of the Navier-Lamé equation

$$\rho \partial_t^2 \mathbf{u} = \left(K + \left(1 - \frac{2}{d} \right) \mu \right) \nabla(\nabla \cdot \mathbf{u}) + \mu \nabla^2 \mathbf{u} . \quad (1.50)$$

with the appropriate boundary conditions. The low-energy solution will then be macroscopic dynamic modes, while the high energy modes will behave as described above in the phonon picture.

Assuming an infinitely large crystal, the phonon picture is valid at any finite q . However, the macroscopic regime is still present at $q = 0$ in the form of the macroscopic strain E , which was defined in eq. (1.22). Note that there are no time derivatives of E in the action in eq. (1.43). We can image an infinite crystal being

strained by a force that acts on it at every point in space, however, there is no path from the strained to the unstrained infinite crystal in terms of dynamics within a finite amount of time. Nonetheless, if we view the infinite system as a limit of a finite system that remains close to equilibrium, small perturbations from equilibrium are in the thermodynamic limit characterized by the eigenvalue equation

$$C : E = \kappa E , \tag{1.51}$$

which in general has 6 eigenmodes. As an example, in a cubic solid in three dimensions there is a singlet with eigenvalue $C_{11} + 2C_{12}$ (corresponding to the bulk modulus), a doublet with $C_{11} - C_{12}$, and a triplet with $2C_{44}$ (the eigenvalues are the ones of C^M , not C^V). In the isotropic case where $A = 1$ the doublet and triplet merge to a 5-fold mode with eigenvalue 2μ .

This introduces an important subtlety with the handling of acoustic phonon in field theory: If one were to write the global and local strain as a single field, the corresponding Green's function would be non-analytic around $q = 0$, causing problems when integrating said function over a domain that contains the Γ -point. The Green's function for the microscopic mode—the acoustic phonon—vanishes at $q = 0$. The macroscopic modes fill this hole with a different elastic constant. In other words, on a microscopic scale, the medium appears to have different elastic properties than on the scale of the crystal.

Coupling of strain to vector fields

Throughout this work, we will consider the coupling of different degrees of freedom to elasticity. Let us assume that these degrees of freedom are represented by some generic vector field ϕ . For example, in the case of magnetoelastic coupling, it would be the magnetization \mathbf{M} or, in the case of a ferroelectric, the polarization \mathbf{P} . Both of these cases will be considered in later chapters, but for now, we remain agnostic about the exact nature of ϕ .

From a phenomenological standpoint, ϕ and ε can couple in any way that is allowed by the symmetry of the system. One may formally expand the energy functional in these fields and their gradients and keep at every order only the terms that are invariant under symmetry transformations. Of course, the contributions get smaller at higher orders in this expansion and for topics covered in this work we will only need to go to quadratic order in ϕ . There can in principle be a linear coupling, most generally written as an energy term of the form

$$\varepsilon_{ijl} \iota_{ijk} \phi_k . \tag{1.52}$$

This coupling may be forbidden, if the vector field obeys an Ising-type symmetry, i.e. invariance under $\phi \rightarrow -\phi$, e.g. time reversal symmetry in the case of magnetism.

On the other hand, if ϕ is a polarization, the above term is known as piezoelectricity and is common in materials with sufficiently low symmetry. One should also note that the only rank three tensor that is invariant under rotations is the antisymmetric tensor ϵ_{ijk} . However, since the strain tensor is symmetric, such a contribution to ι_{ijk} would vanish. The above term is therefore necessarily anisotropic.

Another kind of linear coupling is the coupling to strain gradients, or equivalently

$$\epsilon_{ij}\kappa_{ijkl}\partial_k\phi_l. \quad (1.53)$$

In the case where ϕ refers to polarization, this coupling is known as flexoelectricity. We will not get into the details of the effects of this coupling in this work and only mention it for completeness.

If the linear coupling is forbidden by symmetry, the leading coupling is expected to be the quadratic one

$$\epsilon_{ij}\lambda_{ijkl}\phi_k\phi_l, \quad (1.54)$$

In contrast to linear coupling, quadratic coupling is generic in the sense that it is present even for highly symmetric systems.

The coupling is parametrized by a fourth-rank tensor λ . Similarly, to the stiffness tensor, it has to satisfy $\lambda_{ijkl} = \lambda_{jikl} = \lambda_{ijlk}$, which allows us to use Voigt notation. However, in general $\lambda_{ijkl} \neq \lambda_{klij}$. In other words, λ^V may not be a symmetric matrix.

Specifically, in the case of point group 23, which describes the bulk chiral magnets that we will investigate in chapter 8, it is of the form

$$\lambda^{23,V} = \begin{pmatrix} \lambda_{11} & \lambda_{12} & \lambda_{21} & 0 & 0 & 0 \\ \lambda_{21} & \lambda_{11} & \lambda_{12} & 0 & 0 & 0 \\ \lambda_{12} & \lambda_{21} & \lambda_{11} & 0 & 0 & 0 \\ 0 & 0 & 0 & \lambda_{44} & 0 & 0 \\ 0 & 0 & 0 & 0 & \lambda_{44} & 0 \\ 0 & 0 & 0 & 0 & 0 & \lambda_{44} \end{pmatrix}. \quad (1.55)$$

with four independent components.

In the case of an isotropic solid the number of components is further reduced by the conditions $\lambda_{21} = \lambda_{12}$ and $\lambda_{11} - \lambda_{12} = 2\lambda_{44}$. As a result, λ can be written in the same form as eq. (1.31)

$$\lambda_{ijkl}^{\text{iso}} = \lambda_{11}\delta_{ij}\delta_{kl} + \lambda_{44}(\delta_{ik}\delta_{jl} + \delta_{il}\delta_{jk}) \quad (1.56)$$

and will become important in chapter 6. In all of the above, we assumed that symmetry transformations act on the vector field ϕ the same way they act on the strain tensor ϵ . We can also imagine an in a sense even more symmetric case, where

ϕ can be transformed independently from spatial degrees of freedom. In this case, we can simply write

$$\lambda_{ij\alpha\beta} = \lambda\delta_{ij}\delta_{\alpha\beta} \tag{1.57}$$

where the indices α and β may be summed over a different range than i and j . This describes the generic elastic coupling that we will meet again in chapter 3 and chapter 5.

Part I.

Criticality in Elastic Media

2. Introduction to the theory of critical phenomena

In most situations in our everyday lives, regular thermodynamics is sufficient to explain what is happening around us. The reason is that a fundamental assumption of thermodynamics is satisfied: Fluctuations do not matter in the thermodynamic limit. However, in the vicinity of continuous phase transitions, things are different. Here, fluctuations do change the macroscopic behavior of the system. These fluctuations become correlated over longer and longer length scales, until at the critical point, the correlation length diverges and beyond this point, the system acquires long-range order.

As the system approaches the critical point from the disordered phase, correlated regions are forming and getting larger. At the scale of the correlation length, the system behaves according to renormalized system parameters, for example, an ensemble of correlated Ising spins will behave differently from a single Ising spin. The macroscopic details of the system and its interactions get lost at large length scales. The phenomenon of universality emerges: Approaching a critical point, the system asymptotically shows behavior that is solely determined by symmetry and dimension. These two factors determine the *universality class* of a continuous phase transition. For example, the Ising transition at zero field turns out to be in the same universality class as the critical endpoint of a liquid-vapor transition. This is a remarkable proposition. It allows us to freely choose the model within a given universality class, which we may investigate and make exact statements about universal properties that hold for the entire class.

The purpose of this chapter is to give a brief introduction to a theoretical approach for describing critical phenomena, focusing on concepts needed in later chapters. The physics of classical phase transitions in the Landau theory and renormalization group approach will be introduced in sections 2.1 and 2.2, as it gives important context for the discussion in chapter 3. For the treatment of quantum phase transitions, the tool of imaginary time formalism is introduced in section 2.3. These tools are then applied to a basic ϕ^4 theory in section 2.4 as a baseline for comparison with later results when we extend the theory with elastic coupling and a ϕ^4 theory with cubic anisotropy in section 2.5, which will become relevant when discussing dipolar interaction.

For a more in-depth discussion of the physics of quantum phase transitions with historical and experimental perspectives see (Sachdev, 2011). For details on the mathematical subtleties of the renormalization group method, I recommend (Zinn-Justin, 2021).

2.1. Statistical field theory and Landau theory

In statistical mechanics, the thermal expectation value of an observable is given by the sum over all states weighted with the probability of the particular state being realized. In field theory, where states are described by a function ϕ of space and, depending on context, also of time, the “sum over states” is then given by a path integral

$$\langle O \rangle = \frac{1}{\mathcal{Z}} \int \mathcal{D}\phi O(\phi) e^{-\mathcal{S}[\phi]}, \quad (2.1)$$

where $O(\phi)$ is the value of the observable in the particular state ϕ , \mathcal{S} is the *action* and \mathcal{Z} —the normalization factor—is called the *partition function*. It is given by

$$\mathcal{Z} = \int \mathcal{D}\phi e^{-\mathcal{S}[\phi]}. \quad (2.2)$$

The symbol $\mathcal{D}\phi$ represents the integration over all possible field configurations. It can be understood as the limit of infinitely many integrals over independent variables, representing the field values at discrete points in space. The expectation values of operators that are products of fields can be written as derivatives of $\mathcal{F} = -\log \mathcal{Z}$, where \mathcal{F} is called the *free energy*.

The action is assumed to be analytical in the field ϕ , such that it can be expanded in a power series of the field and its derivatives, typically close to some minimum, which corresponds to thermodynamic equilibrium. In a conventional naming of the parameters we write

$$\mathcal{S}[\phi] = \int d^d x \left(\text{const.} + h\phi + \frac{r}{2}\phi^2 + \frac{c^2}{2}(\nabla\phi)^2 + \dots \right). \quad (2.3)$$

The constant in 0th order only leads to a constant factor in both the numerator and denominator of eq. (2.1) that cancels and therefore doesn't change observable outcomes. The 1st order describes an external field h , which changes the equilibrium value of ϕ and can be used as an experimental knob to probe the system. An important quantity describing this response of the system to an applied field is the susceptibility. It is given by

$$\chi = \partial_h \langle \phi \rangle = \partial_h^2 \mathcal{F} = \langle \phi^2 \rangle - \langle \phi \rangle^2. \quad (2.4)$$

In the disordered phase at $h = 0$ we have $\langle \phi \rangle = 0$ and the susceptibility is simply

the two point correlation function $\langle \phi(x)\phi(y) \rangle$ of the field values at two points in space(-time) x and y , often referred to as the *Green's function* G . In a theory with translation invariance, it χ is only a function of $x - y$

$$G(x - y) = \chi(x, y)|_{h=0} \quad (2.5)$$

To make this notion more concrete let us look at an analytically solvable example. If the action only has quadratic terms,

$$\begin{aligned} \mathcal{S}_G[\phi] &= \int d^d x \frac{1}{2} (r\phi^2 + c^2(\nabla\phi)^2) \\ &= \int \frac{d^d q}{(2\pi)^d} \frac{1}{2} (c^2 q^2 + r)\phi_q \phi_{-q} , \end{aligned} \quad (2.6)$$

eq. (2.2) is a Gaussian integral and everything can be calculated explicitly

$$\mathcal{Z}_G = \int \mathcal{D}\phi e^{-\int \frac{1}{2}\phi G_0^{-1}\phi + h\phi} \propto e^{\frac{1}{2}h^T G_0 h} . \quad (2.7)$$

The Green's function in Fourier space can be directly read off the action

$$\langle \phi_q \phi_{-q} \rangle_0 = \partial_h^2 \log \mathcal{Z}_G|_{h=0} = G_0(q) = \frac{1}{c^2 q^2 + r} , \quad (2.8)$$

where the subscript 0 refers here to the expectation value with respect to the Gaussian action \mathcal{S}_G . Performing the inverse Fourier transform back to real space in three spatial dimensions gives the result

$$G_0(x) = \frac{1}{4\pi} \frac{e^{-\sqrt{r}x}}{x} . \quad (2.9)$$

This shows that at finite r the system has an intrinsic length scale, the correlation length $\xi = r^{-\frac{1}{2}}$. It is defined by the long-distance behavior of the correlation function $\langle \phi(x)\phi(0) \rangle \propto e^{-\frac{x}{\xi}}$ as $x \rightarrow \infty$. If r vanishes, the correlation length diverges, and there is no intrinsic length scale anymore. The correlation function then becomes a power law at large distances. Specifically x^{-1} in three dimensions, more generally x^{2-d} in d dimensions.

This makes the tuning parameter r another important experimental knob. If a system can be described as a perturbation around the Gaussian theory, r is in a sense the “distance” to the critical point. Only at positive r is the expansion of \mathcal{S} in eq. (2.3) around a stable minimum. If r becomes negative an instability may develop, spontaneously breaking a symmetry. For classical phase transitions we can assume the tuning parameter to be linear in the reduced temperature $r \propto (T - T_c)/T_c$, but it may also depend on other parameters like pressure. The thermodynamic quantity that characterizes the response of the system to changes in r is the (generalized)

specific heat \mathcal{C} , which we define as

$$\mathcal{C} = -\partial_r^2 \mathcal{F} = \partial_r^2 \log \mathcal{Z} = \langle \phi^4 \rangle - \langle \phi^2 \rangle^2, \quad (2.10)$$

which corresponds to the density-density correlation function.

If we were to take the point of view that fluctuations do not matter, as will be the case in high enough dimension or far away from any phase transition, then instead of integrating over all possible states ϕ , the system can be sufficiently described to be in one particular state ϕ_0 , at which it is at equilibrium or, in other words, the state which minimizes the free energy. This state ϕ_0 can then be found via the saddle point approximation of the integral \mathcal{Z}

$$\mathcal{F} \approx \mathcal{S}[\phi_0], \quad (2.11)$$

where we take ϕ_0 to be defined by

$$\frac{\delta \mathcal{F}}{\delta \phi_0} = 0. \quad (2.12)$$

In other words, ϕ_0 is a solution of the Euler-Lagrange equation of the *Ginzburg-Landau theory* defined by the free energy functional

$$\mathcal{F} = \int d^d x \left(-h\phi_0 + \frac{r}{2}\phi_0^2 + \frac{c^2}{2}(\nabla\phi_0)^2 + \dots \right). \quad (2.13)$$

Using eq. (2.12) we can eliminate ϕ_0 and are left with a function $\mathcal{F}(h, r, c, \dots)$ of the parameters, which can then be used to calculate thermodynamic quantities, such as χ and \mathcal{C} .

2.2. The renormalization group idea

To find out how system parameters are renormalized by fluctuations in the vicinity of the critical point, we employ the tool of the renormalization group (RG). The name is somewhat misleading, since mathematically there is no group structure here, only a semigroup, and this structure is not a focus of the method. Also, even though in what has become the standard formulation of this theory renormalization is an important part of a non-trivial RG analysis, it is only one step of the procedure. Despite the unfortunate naming, RG is a powerful tool for the investigation of critical phenomena. After all, most theories are not exactly solvable like the Gaussian model. As soon as interactions are introduced to the problem we usually have to resort to perturbation theory to make progress. If perturbations are small it makes sense to use the Gaussian theory as a point of reference and describe the system relative to its Gaussian counterpart.

Let us consider a generic $O(N)$ symmetric model, where a rotation of the vector ϕ leaves the action invariant, all odd orders must vanish, except in the presence of external fields, which explicitly breaks the symmetry. We therefore consider the action

$$\mathcal{S}[\phi] = \int d^d x \left(\frac{r}{2} \phi^2 - \frac{c^2}{2} \phi^T \nabla^2 \phi + u(\phi^2)^2 + \dots \right) \quad (2.14)$$

where u as well as all higher-order coefficients are small. We have integrated by parts to compactly rewrite the gradient term. Usually, a theory like this is derived by taking the scaling limit of a microscopic theory. The validity of this theory can then only be safely assumed up to some small length scale a , e.g. the lattice constant of a solid, or equivalently a momentum space cutoff $\Lambda \sim a^{-1}$.

If for the moment we ignore the existence of this cutoff, assuming that the above theory is valid at all scales a rescaling transformation $x = bx'$ does not change the phase space. At the critical point, where intrinsic length scales disappear this transformation should not change anything. Anywhere else than the critical point, the transformation will map to a renormalized theory, where the function ϕ and the parameters r, c, u, \dots are changed appropriately.

Let $\phi(x) = b^{-s_\phi} \phi'(bx)$, where s_ϕ is the *scaling dimension* of ϕ . Consequently, all the parameters of the action have scaling dimensions. We can then restore the original form of the action by defining

$$\begin{aligned} \phi(x) &= b^{-s_\phi} \phi'(x') \\ r &= b^{2s_\phi - d} r' \\ c^2 &= b^{2s_\phi - d + 2} c'^2 \\ u &= b^{4s_\phi - 3d} u' \end{aligned} \quad (2.15)$$

after which we obtain again eq. (2.14), but with primed symbols. So the above parameters of the action are, in general, scale-dependent.

We must now make a choice. Since a constant factor in front of the action does not affect any observable outcomes, and b to any power is a constant in this sense, we have the freedom to eliminate one of the above scaling relations. This choice is called the *RG condition* and will effectively set s_ϕ . The other relations will then tell us how the parameters scale relative to the one we keep fixed. A common choice in the classical theory is to fix c^2 , or equivalently

$$G^{-1}|_{r=0} = c^2 q^2 \quad (2.16)$$

which implies $s_\phi = (d-2)/2$. This is consistent with our earlier result for $\langle \phi(x)\phi(0) \rangle_0$, which scales with $2s_\phi = d - 2$ at long distances.

The other parameters in the expansion of \mathcal{S} can now be classified according to their scaling dimension. If the scaling dimension is positive, the parameter is called

relevant. If it is negative, the parameter is *irrelevant*. If it vanishes, the parameter is *marginal*. For example in the above 0th order scaling we find

$$\frac{d \log r}{d \log b} = 2 , \quad (2.17)$$

which means r is relevant in any dimension. In other cases, the scaling dimension may depend on the dimension, such as

$$\frac{d \log u}{d \log b} = 4 - d . \quad (2.18)$$

We see that u is relevant in $d < 4$. In this case, the ϕ^4 term will have a strong influence on the critical behavior. It is irrelevant for $d > 4$, in which case u will eventually become negligible at large enough scales and we end up with a Gaussian theory again. In the marginal case, $d = 4$, we can not make a statement about the effect the ϕ^4 term has on the critical behavior from this superficial argument.

In general, the number of relevant parameters is also the number of experimental knobs which must be adjusted to tune the system to the transition. The number of irrelevant parameters gives the dimension of a hypersurface in parameter space called the *critical surface* on which the physics are equivalent to the critical point. Thus, if an interaction is relevant or irrelevant in the RG sense, has drastic effects on the critical behavior. The dimension at which the interaction becomes irrelevant is called the *upper critical dimension* of the theory, above which the Gaussian theory is exact. For the $O(N)$ model the upper critical dimension is 4 as we have seen. There is also a lower critical dimension at which the phase transition is completely suppressed by fluctuations, which become more dominant at lower dimensions. However, we will not discuss low dimensions in this text.

In general, when including the effects of the interactions, the correlation function may scale differently from the Gaussian theory at the critical point. With perturbative RG the ϕ may also have an anomalous scaling dimension, relative to the Gaussian one

$$2s_\phi = d - 2 + \eta \quad (2.19)$$

where η is the *anomalous dimension*. We can have $\eta \neq 0$ if the q^2 term in the above action is renormalized by some interaction, which we have not included so far. To make the appearance of an anomalous dimension more transparent, we introduce a so-called *Z-factor*, with $G \rightarrow Z_\phi G$, which is then renormalized and also has a scaling dimension

$$Z'_\phi = b^\eta Z_\phi , \quad (2.20)$$

where Z_ϕ is a so far arbitrary number. Its bare value is usually set to unity.

The number η is one of the *critical exponents*, which is a relatively small set of numbers that capture the universal critical behavior of the phase transition. From

the above arguments, we can already calculate all the critical exponents for the Gaussian theory. The anomalous dimension, as described above is defined by

$$\eta = \frac{d \log Z_\phi}{d \log b} \quad (2.21)$$

and has the Gaussian value $\eta_G = 0$. The correlation length exponent, defined by $\xi \propto r^{-\nu}$, can be calculated with the following formula and has the Gaussian value

$$\nu = \left(\frac{d \log r}{d \log b} \right)^{-1} \quad \nu_G = \frac{1}{2}. \quad (2.22)$$

The specifically heat exponent, defined by $\mathcal{C} \propto r^{-\alpha}$ is connected to the correlation length exponent via the *hyperscaling relation*

$$\alpha = 2 - \nu d \quad \alpha_G = 2 - \frac{d}{2}. \quad (2.23)$$

Notably, $\alpha_G = 0$ in $d = 4$ dimensions. Hyperscaling is a consequence of the free energy, \mathcal{F} , being an extensive quantity, while the only relevant length scale is the correlation length ξ . Therefore it must hold $\mathcal{F} \propto \xi^{-d} \propto r^{\nu d}$, but also $\mathcal{F} \propto r^{2-\alpha}$ via eq. (2.10). In a setup where there is another length scale, for example introduced by dangerously irrelevant operators, hyperscaling may not hold. However, we will not study these cases in this text.

The analysis in later chapters will focus on the three exponents α , ν , and η , but for completeness, the remaining canonical exponents are given here. The susceptibility scales like $\chi \propto r^{-\gamma}$ and previously we established $\chi \propto \xi^{2-\eta} \propto r^{-(2-\eta)\nu}$, therefore

$$\frac{\gamma}{\nu} = 2 - \eta \quad \gamma_G = 1 \quad (2.24)$$

In the ordered phase the order parameter depends on the tuning parameter with $\langle \phi \rangle \propto r^\beta$. From the scaling relation for ϕ we know $\phi'(x') = b^{(d-2+\eta)/2} \phi(x)$. If we evaluate this at $b^* = \xi$ we get

$$\frac{\beta}{\nu} = (d - 2 + \eta)/2 \quad \beta_G = \frac{d - 2}{2}. \quad (2.25)$$

In $d = 4$ dimensions, this means $\beta_G = 1$.

Considering the effect of an externally applied field at the critical point $r = 0$, the power law of the form $\langle \phi \rangle \propto h^{\frac{1}{\delta}}$ defines the exponent δ . We can calculate it from the fact that $\langle \phi \rangle$ scales with b^{s_ϕ} , while h can be connected to the correlation length in analogy with the definition of ν . We find

$$\left(\frac{d \log h}{d \log b} \right)^{-1} = d - s_\phi = \frac{d + 2 + \eta}{2} \quad (2.26)$$

and as a result, the general expression for δ and its Gaussian value are

$$\delta = \frac{d - s_\phi}{s_\phi} = \frac{d + 2 - \eta}{d - 2 + \eta} \quad \delta_G = \frac{d + 2}{d - 2} \quad (2.27)$$

Overall, we can conclude that with all the scaling relations calculating two exponents from the RG equations is enough to fix the complete critical behavior. We will usually solve the system to find $Z_\phi(b)$ and $r(b)$ and calculate the exponents η and ν from there.

The momentum shell RG procedure

As the system approaches criticality, the correlation length diverges and the system becomes more and more self-similar. We want to use this fact by mapping the theory onto a scaled version of itself and analyze the properties of this mapping to find out how the system parameters are renormalized within correlated domains. There are many ways to produce such mappings, but a common way is to go to momentum space and integrate out the small wavelength/large momentum modes. The integrals involved are algebraically divergent in $d < 4$ dimensions and logarithmically divergent in $d = 4$ dimensions. The latter case can be remedied by renormalizing and we use an ϵ -expansion to go to $d = 4 - \epsilon$ dimensions using perturbation theory in ϵ , see (K. G. Wilson & Fisher, 1972).

Here, it becomes important that the momentum integral in \mathcal{S} only goes up to some cutoff Λ . In a solid with lattice constant a , it is reasonable to assume $\Lambda \sim \frac{1}{a}$, but it should not matter much, since we are only interested in the cutoff independent physics. We split the fields into modes that are on a momentum space shell between the original and rescaled cutoff $\Lambda/b < \Lambda$, which we want to integrate out, and the longer wavelength modes, which will remain

$$\phi_q = \phi_q^< + \phi_q^> , \quad (2.28)$$

where we have defined the functions

$$\phi_q^< = \phi_q \Theta(\Lambda/b - q) \quad \phi_q^> = \phi_q \Theta(q - \Lambda/b) . \quad (2.29)$$

Θ refers to the Heavyside function. We will treat these as independent fields and integrate out $\phi^>$, mapping the theory to an effective theory for only $\phi^<$, with a reduced phase space

$$\mathcal{Z} = \int \mathcal{D}\phi^< \mathcal{D}\phi^> e^{-\mathcal{S}[\phi^<, \phi^>]} \equiv \int \mathcal{D}\phi^< e^{-\mathcal{S}'[\phi^<]} , \quad (2.30)$$

where, assuming the original action can be written as a Gaussian theory plus

interactions $\mathcal{S} = \mathcal{S}_G + \mathcal{S}_{\text{int}}$, the new action \mathcal{S}' is

$$\mathcal{S}'[\phi^<] = \mathcal{S}_G[\phi^<] - \log \left\langle e^{-\mathcal{S}_{\text{int}}[\phi^<, \phi^>]} \right\rangle_0 - \log \mathcal{Z}_G . \quad (2.31)$$

The average $\langle \dots \rangle_0^>$ here is with respect to the Gaussian theory only for the high energy modes $\phi^>$. In general, it is not possible to calculate the integral in the expectation value exactly. Instead, we calculate perturbatively the contributions to the action \mathcal{S}' generated by the interaction term. Assuming the interaction is small, we can expand the exponential function

$$\left\langle e^{\mathcal{S}_{\text{int}}[\phi^<, \phi^>]} \right\rangle_0^> = \sum_n \frac{1}{n!} \left\langle (\mathcal{S}_{\text{int}}[\phi^<, \phi^>])^n \right\rangle_0^> . \quad (2.32)$$

From this expansion, we can see that in principle corrections at any order in $\phi^<$ can appear, however, we only need to take into account those that are relevant or marginal in the RG sense. What is left is to calculate the average over the $\phi^>$ fields using Wick's theorem

$$\left\langle \phi_{i_1}^> \dots \phi_{i_n}^> \right\rangle_0^> = \sum_P \left\langle \phi_{P(i_1)}^> \phi_{P(i_2)}^> \right\rangle_0^> \dots \left\langle \phi_{P(i_{n-1})}^> \phi_{P(i_n)}^> \right\rangle_0^> , \quad (2.33)$$

where the sum is over all pairings of fields. Wick's theorem can be derived by using the Gaussian integral eq. (2.7) including a “force” term $\mathbf{h} \cdot \boldsymbol{\phi}$ and expressing the n -point functions as derivatives with respect to \mathbf{h}

$$\langle \phi_{i_1} \dots \phi_{i_n} \rangle = \partial_{h_{i_1}} \dots \partial_{h_{i_n}} \log \mathcal{Z} . \quad (2.34)$$

It turns out that many of these pairings evaluate to the same contribution. They can be organized in Feynman diagrams with external lines representing the $\phi^<$ fields. And internal lines representing the bare two-point functions G_0 , connected with vertices representing the interaction. For example with ϕ^4 interaction u from eq. (2.14) can be represented as

$$\begin{array}{c} \diagup \quad \diagdown \\ \times \\ \diagdown \quad \diagup \end{array} \quad (2.35)$$

The linked cluster theorem states that we only have to include fully connected diagrams. Furthermore, after renormalization, only one particle irreducible diagrams have to be considered. We do not go into the details here, since these principles have been written down in textbooks in many different ways (Altland & Simons, 2023; Cardy, 1996; Zinn-Justin, 2021).

Finally, we arrive at the modified action. If we take all the corrections at the order of ϕ^2 we get the *dressed Green's function* G . The difference between the bare and

dressed Green's function is called the *self-energy correction* Σ

$$G^{-1} = G_0^{-1} - \Sigma , \quad (2.36)$$

where Σ is the sum of all one-particle irreducible diagrams that allow for two external lines to be attached

$$\Sigma = \text{---} \text{---} \text{---} = \text{---} \text{---} \text{---} + \text{---} \text{---} \text{---} + \dots \quad (2.37)$$

And interactions such as u get a vertex correction

$$u = u_0 + \Gamma , \quad (2.38)$$

where in terms of diagrams the vertex function Γ is

$$\Gamma = \text{---} \text{---} \text{---} = \text{---} \text{---} \text{---} + \text{---} \text{---} \text{---} + \dots \quad (2.39)$$

Since in this text, we will generally stay in the vicinity of the upper critical dimension, where terms with additional gradients are irrelevant, we will neglect the momentum dependence of Γ . Hence, all the diagrams in the above expansion can be calculated with external momentum set to zero.

To bring the theory back to the original phase space and complete the RG procedure, we need to perform a scale transformation, such that Λ/b is the new cutoff. So we write $q = q'/b$ and $\phi_q = \sqrt{Z_\phi} b^{\frac{d-2}{2}} \phi'_{q'}$. If the theory is *renormalizable*, we end up with the same action as before, just with the primed quantities

$$S'(c'^2, r', u', \dots) = S(c^2, r, u, \dots) . \quad (2.40)$$

This defines the primed parameters, which we may express in terms of an infinitesimal rescaling $b = 1 + d\ell$, e.g.

$$\begin{aligned} r' &= b^2(r - \Sigma|_{k=0}) = r + \frac{dr}{d\ell} d\ell + \mathcal{O}(d\ell^2) , \\ u' &= b^{4-d}(u + \Gamma) = u + \frac{du}{d\ell} d\ell + \mathcal{O}(d\ell^2) . \end{aligned} \quad (2.41)$$

The change in the model parameters under an infinitesimal RG transformation is thus, fully parametrized by their derivatives with respect to ℓ , often called the β -functions. Interpreting these as first-order differential equations generates the RG flow for finite transformations, with $\ell = \log b > 0$. The result of this calculation is thus a set of RG flow equations, e.g.

$$\frac{dr}{d\ell} = 2r + \left. \frac{d\Sigma}{d\ell} \right|_{k=0} , \quad \frac{du}{d\ell} = \epsilon u + \frac{d\Gamma}{d\ell} . \quad (2.42)$$

We can use the fact that we only care about the $\log b$ -derivatives, to make our lives easier when calculating diagrams, because b only enters Σ and Γ only via the cutoff. We may thus ignore all terms which do not depend on Λ , when calculating the loop integrals and still end up with the correct RG equations.

2.3. Imaginary time formalism for quantum criticality

In contrast to classical phase transitions, which are usually driven by thermal fluctuations, quantum phase transitions are abrupt changes in the ground state of a quantum system in the absence of thermal fluctuations. It is important to appreciate how different the picture underlying the model for these quantum phase transitions is from classical statistical mechanics.

Classically, randomness is a consequence of our lack of knowledge of the microscopic details of the system. The system appears in a random microstate every time it is observed and given enough time between observations these states will be entirely uncorrelated. The principle of ergodicity then tells us that every state that is possible under conservation laws will eventually be realized and therefore contributes to the partition function and observables calculated from it. In systems that evolve according to the laws of quantum mechanics, randomness is a more fundamental fact of nature. The quantum state evolves coherently and experiences quantum fluctuations in accordance with the uncertainty principle. The quantum state evolves coherently in time up until a characteristic time scale called the coherence time τ_ϕ . At zero temperature the coherence time may be infinite. At finite temperatures there will additionally be thermal fluctuations, making the initial quantum state unknown.

Therefore, we reframe the partition function instead of a sum over all states as a “sum over histories”. Mathematically this is facilitated by the fact that the density matrix, which can be used to define the partition function

$$\mathcal{Z} = \text{tr}\{e^{-\beta H}\}, \quad (2.43)$$

which depends on the inverse temperature β , is analogous to the time evolution operator known from quantum mechanics

$$U(t, t') = e^{-iH(t-t')}. \quad (2.44)$$

So the partition function of a quantum system is really the trace of the time evolution operator evaluated at an imaginary time

$$\mathcal{Z} = \text{tr}\{U(-i\beta, 0)\}. \quad (2.45)$$

Thermal averages of operators can thus be seen as analytic continuations of time evolved operators evaluated on the imaginary axis. In the path integral formulation, this is expressed with the introduction of a time-like parameter τ , which despite the name “imaginary time” takes on real values

$$\mathcal{Z} = \int \mathcal{D}\phi e^{-\mathcal{S}} = \int \mathcal{D}\phi e^{-\int_0^\beta d\tau L} . \quad (2.46)$$

Since in this text, we only consider the zero temperature limit, where coherence time is unbounded and inverse temperature diverges, the τ integral in the action is on the interval $(0, \infty)$. The field $\phi(x, \tau)$ is now a function of τ and we expand also in its derivatives. Hence, we write

$$\mathcal{S} = \int_0^\infty d\tau \int d^d x \left(r\phi^2 + (\partial_\tau \phi)^2 + c^2(\nabla\phi)^2 + \dots \right) . \quad (2.47)$$

Here, we work under the assumption that the time dimension obeys similar symmetry as the spatial ones, i.e. time-reversal, hence the first non-trivial term is the second derivative. This does not necessarily need to be true. Time reversal and inversion symmetry can in principle be broken. In these cases, the leading order could have only one derivative. An example would be a ferromagnet, where time-reversal symmetry is broken. However, we restrict ourselves to the most generic case, where the above action is valid.

The velocity c now relates space and time dimensions. In the absence of any Lorentz invariance breaking terms, it can be removed by a scaling of the space or time coordinates. In later chapters, however, we will introduce such Lorentz invariance breaking terms by coupling to elasticity.

As a consequence of the symmetries chosen, at the critical point ($r = 0$) the low-energy excitations will have a spectrum described by $\omega \propto q$. Generally, at the critical point, there is some power law $\omega \propto q^z$, where z is called the dynamical exponent. In our case, we have $z = 1$, which applies to e.g. an antiferromagnetic quantum phase transition. In contrast, a ferromagnet would have $z = 2$. The scaling is then determined by the so-called *effective dimension* $d_{\text{eff}} = d + z$. As a consequence, in the case $z = 1$ the upper critical dimension of the ϕ^4 -theory is at $d = 3$ spatial dimensions. Additionally, the scaling relations are modified, such as the hyperscaling relation

$$\alpha_q = 2 - (d + z)\nu . \quad (2.48)$$

2.4. Example: Lorentz-invariant ϕ^4 -theory

In this section, we perform the RG procedure for a Lorentz-invariant $O(N)$ symmetric ϕ^4 theory as a baseline example. The action for a vector field ϕ with N components or “flavors” is given by

$$\mathcal{S} = \int d^d r d\tau \left(\frac{1}{2} \phi^T (-\partial_\tau^2 - c^2 \nabla^2 + r) \phi + u(\phi^2)^2 \right). \quad (2.49)$$

N is called the *flavor number*. For $N = 1$ this model is of Ising-type, $N = 3$ corresponds to a Heisenberg model. The ϕ^4 interaction is interesting because it is marginal in $3 + 1$ dimensions, a common case in reality.

The propagator is an $N \times N$ matrix. Here, the bare propagator is already diagonal

$$G_{ij}^{(0)}(q, \omega) \equiv \langle \phi_{i,q,\omega} \phi_{j,-q,-\omega} \rangle_0 = \frac{\delta_{ij}}{\omega^2 + c^2 q^2 + r} \quad (2.50)$$

We perform the RG procedure outlined in the last section to one-loop order. First, we calculate the self-energy correction, which at one-loop order consists only of one diagram. However, we have to be careful about the different contractions, since the interaction contains two scalar products and we have to keep track of which field index is contracted with external or internal lines. To do this we represent the vertex u with wavy lines

$$\begin{aligned} \text{Diagram} &= \text{Diagram 1} + \text{Diagram 2} \\ \Sigma_{ij}^{(1L)} &= -2u \left(2\delta_{ij} \int_{q,\omega} G_{kk} + 4 \int_{q,\omega} G_{ij} \right) \\ &= -u(4N + 8) \int_{q,\omega} \frac{1}{\omega^2 + c^2 q^2 + r}, \end{aligned} \quad (2.51)$$

again using the shorthand notation from eq. (1.45). We define the integral

$$I_n = \int_{q,\omega} \left(\frac{1}{\omega^2 + c^2 q^2 + r} \right)^n \quad (2.52)$$

The integral I_1 in $d = 3$ spatial dimensions is

$$I_1 = \int_{q,\omega} \frac{1}{\omega^2 + c^2 q^2 + r} = \int_q \frac{1}{2} \frac{1}{\sqrt{c^2 q^2 + r}} = \frac{1}{(2\pi)^2} \int_0^\Lambda dq \frac{q^2}{\sqrt{c^2 q^2 + r}}. \quad (2.53)$$

Since we are only interested in the physics close to criticality ($r = 0$) we can expand

I_1 in small r , which is up to first order

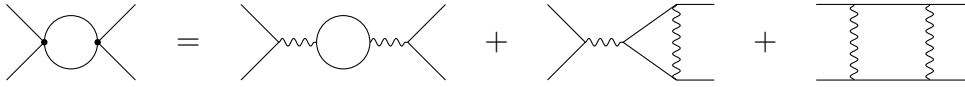
$$I_1 = \frac{1}{8\pi^2 c^3} (c^2 \Lambda^2 - r \log \Lambda) . \quad (2.54)$$

We have here calculated the integral for limits from 0 to an arbitrary cutoff Λ for notational simplicity, but in the end, we only need to integrate over the momentum shell $(\Lambda/b, \Lambda)$.

$$(c^2 \Lambda^2 - r \log \Lambda) \rightarrow (c^2 \Lambda^2 (1 - b^2) - r \log b) \quad (2.55)$$

The log term is therefore not really cutoff dependent, the Λ^2 term, however, is. It is a large term that introduces a fast flow towards a shifted pole of the correction function. In other words, it changes the critical values of r from 0 to some value r_c . Since we are only interested in the asymptotic, universal features of the RG flow, not in cutoff-dependent physics, we simply absorb this shift into $\tilde{r} = r - r_c$ and ignore the Λ^2 term from here on.

The vertex correction Γ has the one-loop contribution



$$(2.56)$$

$$\begin{aligned} \Gamma_{ijkl}^{(1L)} &= \frac{1}{2} u^2 \left(2^3 \delta_{ij} \delta_{kl} \int_{q,\omega} G_{mn} G_{mn} + 2^5 \delta_{ij} \int_{q,\omega} G_{km} G_{ml} + 2^5 \int_{q,\omega} G_{ik} G_{jl} \right) \\ &= \frac{1}{2} u^2 (2^3 N \delta_{ij} \delta_{kl} + 2^5 \delta_{ij} \delta_{kl} + 2^5 \delta_{ik} \delta_{jl}) \int_{q,\omega} \frac{1}{(\omega^2 + c^2 q^2 + r)^2} \end{aligned} \quad (2.57)$$

Here we have already set the external momentum and frequency to zero, since, assuming momentum-dependent contributions are analytical, this would only generate irrelevant terms. The remaining integral can be calculated from the previous integral I_1 by noticing

$$I_2 = \int_{q,\omega} \frac{1}{(\omega^2 + c^2 q^2 + r)^2} = -\frac{\partial I_1}{\partial r} = \frac{1}{8\pi^2 c^3} \log \Lambda . \quad (2.58)$$

Having calculated the corrections to the self-energy and the vertex function, we can execute step 2 of the RG procedure to write the scaling relations for the parameters of the action

$$\begin{aligned} \tilde{r}' &= b^{2z} \left(\tilde{r} - (N+2) \frac{u}{2\pi^2 c^3} \tilde{r} \log b \right) \\ u' &= b^{3z-d} \left(u - (N+8) \frac{u^2}{2\pi^2 c^3} \log b \right) \\ c'^2 &= b^{2z-2} c^2 \end{aligned} \quad (2.59)$$

With $z = 1$ the equation for c becomes trivial. This should not be surprising, since the action was Lorentz-invariant from the start. Corrections calculated from

diagrams that contain only Lorentz-invariant vertices and propagators, cannot break the invariance. Therefore, the q^2 term in the action must scale as the ω^2 term.

The other two parameters, however, are modified and taking the derivative with respect to $\ell = \log b$ results in the RG flow equations for \tilde{r} and $\tilde{u} = u/(2\pi^2 c^3)$

$$\begin{aligned}\frac{d\tilde{r}}{d\ell} &= 2\tilde{r} - (N + 2)\tilde{r}\tilde{u} \\ \frac{d\tilde{u}}{d\ell} &= \epsilon\tilde{u} - (N + 8)\tilde{u}^2,\end{aligned}\tag{2.60}$$

where we set $\epsilon = 3 - d$ and $z = 1$.

In analyzing RG equations the first step is to identify fixed points, where the ℓ derivatives of all parameters vanish. Only the first equation depends on the tuning parameter \tilde{r} and always has a fixed point at $\tilde{r}^* = 0$. The second equation on the other hand has two fixed points: The *Gaussian (G) fixed point* ($\tilde{u}^* = 0$) and the *Wilson-Fisher (WF) fixed point* ($\tilde{u}^* = \epsilon/(N + 8)$).

We can get a qualitative picture of the RG flow by linearizing the above equations around the fixed points and investigating their stability. After inserting $\tilde{u} = \tilde{u}^* + \delta\tilde{u}$ and only keeping linear order in $\delta\tilde{u}$ we obtain for the Gaussian fixed point

$$\frac{d}{d\ell}\delta\tilde{u}|_G = \epsilon\delta\tilde{u},\tag{2.61}$$

with a positive eigenvalue ϵ indicating an unstable fixed point in the \tilde{u} direction. If we do the same for the WF fixed point, on the other hand, we obtain

$$\frac{d}{d\ell}\delta\tilde{u}|_{\text{WF}} = (\epsilon - (N + 8)\tilde{u}^*)\delta\tilde{u} = -\epsilon\delta\tilde{u},\tag{2.62}$$

where the negative eigenvalue $-\epsilon$ indicates a stable fixed point: If the system's initial value \tilde{u}_0 is close to the WF value, it will get closer after an RG transformation. The flow in \tilde{r} and \tilde{u} around these points is shown in fig. 2.1.

There are two distinct domains in the parameter space. One where for large ℓ the tuning parameter \tilde{r} goes to positive infinity, representing the disordered phase, and one where it goes to negative infinity, representing the ordered phase. \tilde{u} on the other hand is attracted to its WF value as long as its initial value is positive. This is effectively a post hoc explanation for the phenomenon of universality. No matter the exact initial values of \tilde{u} , the system will eventually flow towards the same effective parameters.

Each fixed point has associated critical exponents, which will be realized physically if close to the transition the system is driven into the vicinity of the respective fixed point. The critical exponents can be calculated from the corresponding eigenvalues after linearization. The anomalous dimension η can be calculated according to

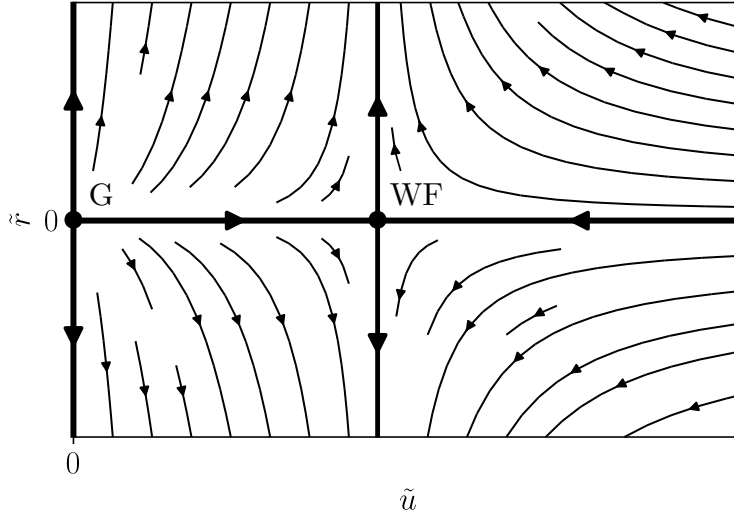


Figure 2.1.: RG flow of the parameters \tilde{u} and \tilde{r} of the ϕ^4 -theory in $d = 3 - \epsilon$ dimensions, with the Gaussian (G) and Wilson-Fisher (WF) fixed points. On the $\tilde{r} = 0$ axis, the flow is towards WF. Off-axis, the flow is towards $\tilde{r} \rightarrow \infty$ or $\tilde{r} \rightarrow -\infty$ depending on the sign of the initial value \tilde{r}_0 , representing the two different phases on either side of the transition.

eq. (2.21) from the RG equation for Z_ϕ , which we did not bother to write down because there is no correction to Z_ϕ at first order in ϵ and therefore $\eta = 0$. This is the case because the only self-energy diagram at one-loop order eq. (2.51) happens to be momentum and frequency-independent. Starting from order ϵ^2 there will be a non-trivial anomalous dimension.

The Gaussian critical exponents have been derived already in section 2.2. Here, we calculate the WF exponents. The correlation length exponent ν , calculated from the linearized RG equations using eq. (2.22), gets a correction. Since we only went to one-loop order, the expressions are only valid in first order of ϵ

$$\frac{d}{d\ell}\delta r = \frac{1}{\nu}\delta r \quad \nu_{\text{WF}} = \frac{1}{2} + \frac{1}{4} \frac{N+2}{N+8} \epsilon + \mathcal{O}(\epsilon^2). \quad (2.63)$$

We conclude then for the critical exponent α using the hyperscaling relation

$$\alpha_{\text{WF}} = 2 - (d+z)\nu_{\text{WF}} = 2 - (4-\epsilon)\nu_{\text{WF}} = \frac{1}{2} \frac{4-N}{N+8} \epsilon + \mathcal{O}(\epsilon^2) \quad (2.64)$$

and the other critical exponents can be calculated in first order in ϵ in a similar fashion. Note that α_{WF} changes sign as a function of N at a critical flavor number $N_c = 4$. In general, the critical flavor number will change with the inclusion of higher loop correction and starting from second order N_c will also depend on ϵ . If we see ϵ as an infinitesimal deviation from the upper critical dimension, the value of

N_c is dominated by the lowest order in ϵ and the one-loop value becomes exact.

RG flow at the upper critical dimension

At the upper critical dimension ($\epsilon = 0$) we can solve the RG flow equations analytically. The equation for \tilde{u} reduces to

$$\frac{d\tilde{u}}{d\ell} = -(N+8)\tilde{u}^2, \quad (2.65)$$

which is solved by

$$\tilde{u}(\ell) = \frac{1}{(N+8)\ell + \tilde{u}_0^{-1}}. \quad (2.66)$$

with the initial value $\tilde{u}_0 = u(\ell = 0)$. Subsequently, after inserting this result into eq. (2.60)

$$\frac{d\tilde{r}}{d\ell} = \left(2 - \frac{N+2}{(N+8)\ell + \tilde{u}_0^{-1}}\right) \tilde{r}, \quad (2.67)$$

it turns out that \tilde{r} has no longer a pure power law dependence on b , but instead acquires a logarithmic correction

$$r(\ell) \propto e^{2\ell} ((N+8)\ell + \tilde{u}_0^{-1})^{-\frac{N+2}{N+8}} \sim b^2 (\log b)^{-\frac{N+2}{N+8}} \quad (2.68)$$

So the scaling is no longer captured by a single critical exponent $\nu = \frac{1}{2}$, but additionally one needs to specify the logarithmic scaling with an exponent $\hat{\nu}$ such that $\xi \propto r^{-\nu} (\log r)^{\hat{\nu}}$. To determine $\hat{\nu}$ we take the log on both sides of eq. (2.68)

$$\log r \propto 2 \log b - \frac{N+2}{N+8} \log \log b \quad (2.69)$$

and neglect the log log term. Substituting this back into eq. (2.68) and evaluating b at the correlation length, we obtain

$$\xi \propto r^{-\frac{1}{2}} (\log r)^{\frac{N+2}{2(N+8)}}. \quad (2.70)$$

Comparing with the above ansatz we find $\hat{\nu} = \frac{N+2}{2(N+8)}$. Similar extensions can be defined for the other critical exponents and there are analogs of scaling relations (Kenna, Johnston, & Janke, 2006), but one has to keep in mind that hyperscaling may not hold at the upper critical dimension (Luijten & Blöte, 1997).

2.5. Cubic anisotropy and cubic fixed point

One might ask how important the $O(N)$ symmetry of the interaction is for the above results, or equivalently, how the RG flow changes, if we include some sort of anisotropy. To explore this question we extend the theory to include cubic anisotropy. This example is discussed in (Cardy, 1996), but we point out some details that will become important later when we discuss the effect of dipolar interactions in chapter 6. The action of this extended model is

$$\mathcal{S} = \int d^d r d\tau \left(\frac{1}{2} \phi^T (-\partial_\tau^2 - c^2 \nabla^2 + r) \phi + u (\phi^2)^2 + v \sum_i \phi_i^4 \right). \quad (2.71)$$

where we have added the cubic anisotropy term v . The bare propagator is of course the same as in the isotropic theory

$$G_{ij}^{(0)}(q, \omega) = \frac{\delta_{ij}}{\omega^2 + c^2 q^2 + r}. \quad (2.72)$$

Here we benefit from the particularity of the cubic anisotropy, that is does not generate anisotropic corrections to the propagator. In fact, a second-rank tensor can not be anisotropic under cubic symmetry.

The two interactions u and v can be written as a single vertex

$$V_{ijkl} = u \delta_{ij} \delta_{kl} + v g_{ijkl}, \quad (2.73)$$

where g_{ijkl} is 1 for $i = j = k = l$ and zero otherwise. The diagrams contributing to self-energy and vertex corrections look the same as in the isotropic theory. However, we must now carefully write down the correct tensor contractions and identify all terms with the isotropic and anisotropic part of the vertex function

$$\Gamma_{ijkl} = \Gamma_u \delta_{ij} \delta_{kl} + \Gamma_v g_{ijkl}. \quad (2.74)$$

As before, let us start with the self-energy correction

$$\begin{aligned} \Sigma_{ij}^{(1L)} &= 2(2V_{ijkl} + 4V_{iklj}) \int_q G_{kl} \\ &= 2 \left(2(u \delta_{ij} N + v g_{ijkl} \delta_{kl}) + 4(u \delta_{ik} \delta_{jk} + v g_{iklj} \delta_{kl}) \right) I_1 \\ &= (4(N + 2)u + 12v) \delta_{ij} I_1 \end{aligned} \quad (2.75)$$

where I_1 is the same as in eq. (2.54) and we used the relations

$$g_{iklj} \delta_{kl} = g_{ijkl} \delta_{kl} = \delta_{ij}, \quad (2.76)$$

where summation over repeated indices is implied. For the calculation of the vertex

correction, we will also need

$$g_{ijkl}g_{klmn} = g_{ijmn} . \quad (2.77)$$

To make the contractions more explicit we label the diagrams with indices

$$(2.78)$$

$$\begin{aligned} \Gamma_{ijkl}^{(1L)} &= \frac{1}{2} \left[2^3 V_{ij'i'k'} V_{j'l'kl} + 2^5 V_{ij'i'k'} V_{j'kl'l} + 2^5 V_{i'l'jk'} V_{j'kl'l} \right] \int_q G_{i'l'} G_{k'l} \\ &= \frac{1}{2} \left[2^3 (Nu^2 \delta_{ij} \delta_{kl} + uv \delta_{ij} \delta_{kl} + uv \delta_{ij} \delta_{kl} + v^2 g_{ijkl}) \right. \\ &\quad + 2^5 (u^2 \delta_{ij} \delta_{kl} + uv g_{ijkl} + uv \delta_{ij} \delta_{kl} + v^2 g_{ijkl}) \\ &\quad \left. + 2^5 (u^2 \delta_{ik} \delta_{jl} + uv g_{ikjl} + uv g_{ikjl} + v^2 g_{ikjl}) \right] I_2 \\ &= 4 \left[((N+8)u^2 + 6uv) \delta_{ij} \delta_{kl} + (12uv + 9v^2) g_{ijkl} \right] I_2 , \end{aligned} \quad (2.79)$$

where I_2 is the same as in eq. (2.58). Finally, we end up with the RG equations for $\tilde{u} = u/(2\pi^2 c^3)$ and $\tilde{v} = v/(2\pi^2 c^3)$ with the analogous steps as in the previous section

$$\begin{aligned} \frac{d\tilde{r}}{dl} &= 2r - (N+2)\tilde{u}\tilde{r} - 3\tilde{v}\tilde{r} \\ \frac{d\tilde{u}}{dl} &= \epsilon\tilde{u} - (N+8)\tilde{u}^2 - 6\tilde{u}\tilde{v} \\ \frac{d\tilde{v}}{dl} &= \epsilon\tilde{v} - 12\tilde{u}\tilde{v} - 9\tilde{v}^2 . \end{aligned} \quad (2.80)$$

The above equations reduce to the equations for an isotropic ϕ^4 -theory for $\tilde{v} = 0$ as one would expect. Since $\tilde{v} = 0$ is also a fixed point of the last equation, the Gaussian and WF fixed points are still present. There are, however, two new fixed points: One at $(\tilde{u}^*, \tilde{v}^*) = (0, \epsilon/9)$, which we call Ising (I) fixed point, since it corresponds to a set of N completely decoupled Ising models, and $(\tilde{u}^*, \tilde{v}^*) = (\frac{\epsilon}{3N}, \frac{\epsilon(N-4)}{9N})$, which we call the Cubic (C) fixed point.

Analyzing the stability of the fixed points is crucial for determining the critical behavior. Since we have now two coupled equations, after linearization around a fixed point we get a matrix, describing the flow close to the fixed points. The eigenvalues determine the stability along the principle directions, given by the eigenvectors.

Before introducing the anisotropy, the WF fixed point was stable. Now we obtain close to WF

$$\frac{d}{dl} \begin{pmatrix} \delta\tilde{u} \\ \delta\tilde{v} \end{pmatrix}_{\text{WF}} = \begin{pmatrix} -\epsilon & -\frac{6\epsilon}{N+8} \\ 0 & -\frac{(4-N)\epsilon}{N+8} \end{pmatrix} \begin{pmatrix} \delta\tilde{u} \\ \delta\tilde{v} \end{pmatrix} , \quad (2.81)$$

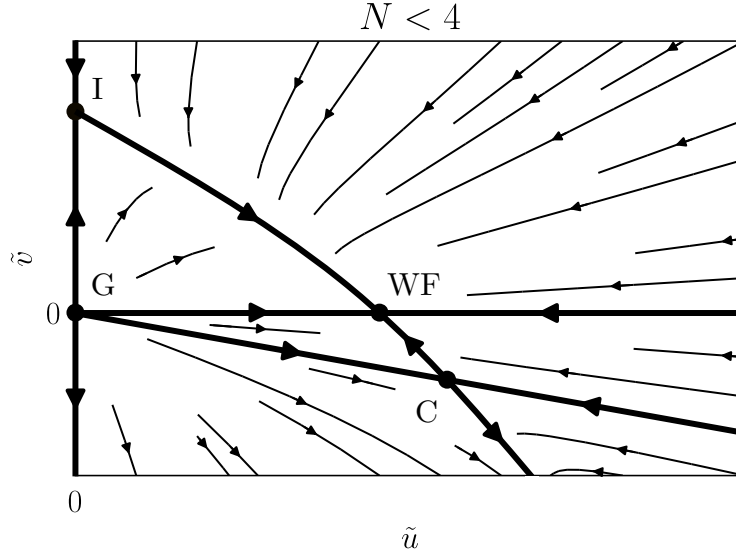


Figure 2.2.: RG flow around the WF and C fixed point below the critical flavor number $N < N_c$. The WF fixed point is stable, while C is repulsive.

where we can simply read the eigenvalues off the diagonal. The stability depends on the flavor number N since the second eigenvalue is positive for $N > 4$. For the C fixed point

$$\frac{d}{d\ell} \begin{pmatrix} \delta\tilde{u} \\ \delta\tilde{v} \end{pmatrix}_C = \begin{pmatrix} -\frac{(N+8)\epsilon}{3N} & -\frac{2\epsilon}{N} \\ -\frac{4(N-4)\epsilon}{3N} & -\frac{(N-4)\epsilon}{N} \end{pmatrix} \begin{pmatrix} \delta\tilde{u} \\ \delta\tilde{v} \end{pmatrix} \quad (2.82)$$

with the two eigenvalues

$$\lambda_C^{(1)} = -\epsilon \quad \lambda_C^{(2)} = \frac{(4-N)\epsilon}{3N} \quad (2.83)$$

This gives us already a qualitative understanding of the RG flow. Below a critical flavor number $N_c = 4$ (see fig. 2.2), the WF fixed point is stable. The C fixed point on the other hand is repulsive and effectively separates the parameter space into two regions. For positive or not too large negative initial values of v the cubic anisotropy term becomes irrelevant. For strong negative anisotropy, on the other hand, the system experiences runaway flow, where cubic anisotropy eventually destabilizes the system at the quartic level. From a Ginzburg-Landau theory perspective, this would necessitate the inclusion of a ϕ^6 term. This generically describes a first-order transition.

Above N_c (see fig. 2.3) the C fixed point is at a positive value of \tilde{v} and becomes stable. The WF fixed point becomes repulsive and for negative initial values of \tilde{v} the situation is again one of runaway flow. If the initial value of v is positive the system will now be attracted to C and as a result, we would observe the critical

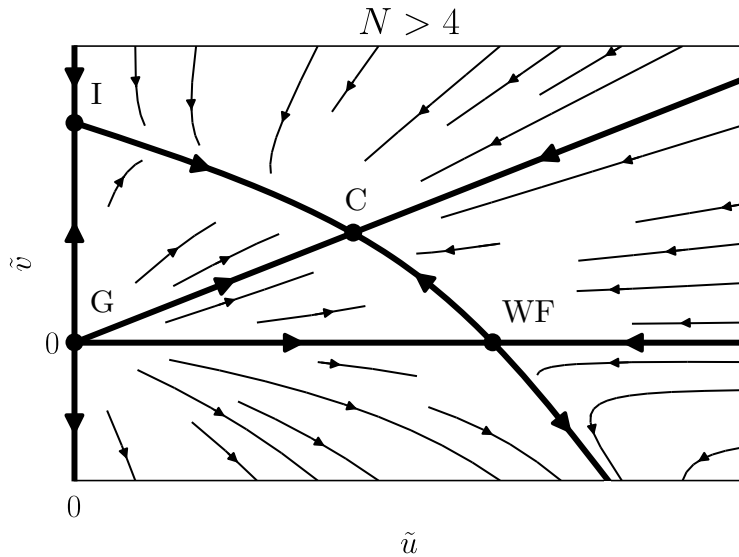


Figure 2.3.: Stable cubic fixed point above critical N

exponents associated with C. For the correlation length exponent, this means

$$\nu_C = \frac{1}{2} + \frac{N-1}{6N}\epsilon + \mathcal{O}(\epsilon^2). \quad (2.84)$$

Consequently for the specific heat exponent

$$\alpha_C = \frac{4-N}{6N}\epsilon + \mathcal{O}(\epsilon^2). \quad (2.85)$$

There is still no Z_ϕ at first order in ϵ , therefore $\eta = 0$.

In conclusion, the effect of cubic anisotropy on critical behavior depends strongly on the flavor number N . Below a critical value, which we find at the one-loop level to be $N_c = 4$, we can safely ignore the effect of cubic anisotropy and the critical exponents are unchanged. However, above N_c the critical behavior is dominated by a new fixed point with different critical exponents.

3. Classical criticality on compressible lattices: A review

This chapter is concerned with the different stages of development of the theory of classical criticality on a compressible lattice, meaning transitions at finite temperature where thermal fluctuations dominate. As has been discussed in section 1.2, there are many ways in which coupling to strain can be realized.

At lowest order—if symmetry allows it—there can be a bilinear coupling, which leads to a strong hybridization between acoustic phonons and critical fluctuations. This elevates strain to a primary order parameter and hence the transition is dominated by critical elasticity (Cowley, 1976; Levanyuk & Sobyenin, 1970). However, as discussed in section 1.2 this is only possible with a combination of inversion symmetry breaking and anisotropy.

Here we focus on the case where the bilinear coupling is forbidden by symmetry. Therefore, the dominating elastic coupling is quadratic in the critical field,

$$\mathcal{L}_{\text{int}} \sim \varepsilon \phi^2, \quad (3.1)$$

and is marginal in 4 dimensions. The fundamental question that we are concerned with in this chapter is how the nature of a continuous transition changes in the presence of the above coupling.

We will address the content of several seminal works as far as we can learn something from it in pursuit of our later goal of understanding the corresponding case for quantum phase transitions. At first, we approach the subject from the most general considerations about the thermodynamics of phase transitions coupling to elastic degrees of freedom, treating them effectively as hidden variables (Fisher, 1968). These early developments are discussed in section 3.1 together with arguments about the non-perturbative nature of the elastic coupling (Domb, 1956; Rice, 1954). Going further to specific microscopic models, we will look at Larkin and Pikin’s approach of integrating out strain (Larkin & Pikin, 1969), mapping the problem on an effective Landau theory that suggests a first-order transition at constant pressure, while confirming Fisher’s theory in the case of constant volume. Here, the subtleties of the macroscopic elastic mode become important and lead to a strong dependence on boundary conditions. Later in section 5.1 we also discuss why this approach fails for the quantum phase transition. Finally, in section 3.3 we discuss

the renormalization group analysis done by Bergman & Halperin (1976), which treats both constant pressure and constant volume in one theory and will be used as a blueprint for the RG analysis of quantum criticality in chapter 5.

3.1. Thermodynamics of phase transitions on compressible lattices

The critical behavior of a system coupled to elasticity, should be contrasted to the critical behavior of the “rigid” system, in the limiting case of vanishing elastic coupling. We assume the rigid system shows a continuous phase transition of a certain universality class, associated with critical exponents system $\alpha_0, \beta_0, \gamma_0, \dots$. For simplicity, we consider the transition at zero field. The free energy as a function of the tuning parameter is then generically of the form

$$\mathcal{F}_0(r) = -Ar^{2-\alpha_0} + Br + \dots, \quad (3.2)$$

such that $\mathcal{C}_0 = -\partial_r^2 \mathcal{F}_0 \propto r^{-\alpha_0}$. There may be many other terms in the free energy, but we write down only the important ones for the following arguments. We have also omitted logarithmic corrections, which only become important when $\alpha_0 = 0$, such is the case for an $O(N)$ model in $d = 4$ dimensions, as seen in section 2.4. In such cases we may write $\mathcal{C} \propto (\log r)^{-\tilde{\alpha}}$ and if $\tilde{\alpha} > 0$ the specific heat diverges logarithmically. Here, we only discuss $\alpha_0 \neq 0$, but the results are straightforwardly generalized (Fisher, 1968; Larkin & Pikin, 1969).

Taking into account elastic coupling the system is described by the full free energy $\mathcal{F}(r, \sigma)$, which is now a function of applied stress σ . This raises the question: How is \mathcal{F} connected to \mathcal{F}_0 and does \mathcal{F} come with modified critical exponents $\alpha, \beta, \gamma, \dots$? In other words, does elastic coupling change the universality class of the transition?

The free energy depends on the usual thermodynamic variables. These variables generally come in pairs of extensive variables (entropy, magnetization, volume) also called generalized coordinates and intensive variables (temperature, magnetic field, pressure) or generalized forces. In the coupled system the new pair of variables is stress and strain, where stress is the generalized force/extensive variable. They can be viewed as a generalization of pressure and volume, which would be sufficient in the absence of shear forces. We usually assign special meaning to the derivative of the generalized coordinate with respect to the generalized force, which indicates a “stiffness” of the system on application of an external force. These must be positive for the system to be thermodynamically stable, i.e. for the free energy to be at a minimum. Examples include the specific heat, the magnetic susceptibility or in the case of stress and strain the compressibility, which we now proceed to calculate.

When applying hydrostatic pressure, equivalent to a uniform stress $\sigma_{ij} = \sigma\delta_{ij}$, the resulting volume change is given by

$$\mathcal{E} \equiv \langle \text{tr}\{\varepsilon\} \rangle = \frac{\partial \mathcal{F}}{\partial \sigma} \sim \frac{\Delta V}{V}. \quad (3.3)$$

Here, we use the symbol \mathcal{E} for the thermodynamic strain variable, while ε is reserved for the microscopic tensor field. At constant pressure/stress, we can define the compressibility which is essentially the strain-strain correlation function

$$\kappa = -\frac{\partial \mathcal{E}}{\partial \sigma} = -\frac{\partial^2 \mathcal{F}}{\partial \sigma^2} = \langle \text{tr}\{\varepsilon\}^2 \rangle - \langle \text{tr}\{\varepsilon\} \rangle^2. \quad (3.4)$$

When operating at constant volume, however, the strain \mathcal{E} of the system has to be set by ensuring appropriate boundary conditions, which causes internal stresses $\sigma(\mathcal{E})$ to develop. The free energy $\mathcal{F} = \mathcal{F}(r, \sigma(\mathcal{E}))$ is now indirectly a function \mathcal{E}

$$\frac{\partial \mathcal{F}}{\partial \mathcal{E}} = \frac{\partial \mathcal{F}}{\partial \sigma} \frac{\partial \sigma}{\partial \mathcal{E}} \equiv -\mathcal{E}K. \quad (3.5)$$

Where we defined the thermal bulk modulus K

$$K = -\frac{\partial \sigma}{\partial \mathcal{E}} = -\frac{\partial^2 \mathcal{F}}{\partial \mathcal{E}^2}. \quad (3.6)$$

It can be identified with the microscopic bulk modulus using Hooke's law (eq. (1.27)). In either case, constant pressure or volume, the condition of thermodynamic stability requires \mathcal{F} to be convex, and therefore κ and K need to be positive. In other words, when the pressure is increased at the boundaries, the system must shrink in volume.

We come to the question of how the singular character of \mathcal{F}_0 is reflected in \mathcal{F} . To make progress we need to make some reasonable assumption about their relation. Domb (1956) and Fisher (1968) assume the free energy \mathcal{F} of the coupled system to be of the form

$$\mathcal{F}(r, \sigma) = \mathcal{F}_0(f(r, \sigma)) + g(r, \sigma) \quad (3.7)$$

where, crucially, f and g are analytic functions that have a series expansion. We will question this assumption later on.

First, we consider the system at constant σ . The critical point is now shifted to a σ -dependent value of the tuning parameter $r = r_c(\sigma)$ defined by $f(r_c, \sigma) = 0$. We expand in $\tilde{r} = r - r_c$

$$f(r, \sigma) = f(r_c + \tilde{r}, \sigma) = \frac{\partial f}{\partial r}(r_c, \sigma)\tilde{r} + \mathcal{O}(\tilde{r}^2). \quad (3.8)$$

We make another assumption that the linear term does not vanish, which is necessarily the case if $\partial f/\partial \sigma \neq 0$, i.e. the singular part of the free energy actually depends on the new variable, and $\partial r_c/\partial \sigma \neq 0$.

We can now check if the exponent α of the coupled system is different from α_0 by calculating the specific heat at constant stress

$$\mathcal{C}_\sigma = - \left(\frac{\partial^2 \mathcal{F}}{\partial r^2} \right)_\sigma = -\mathcal{F}_0''(f) \left(\frac{\partial f}{\partial r} \right)_\sigma^2 - 2\mathcal{F}_0'(f) \left(\frac{\partial^2 f}{\partial r^2} \right)_\sigma - \left(\frac{\partial^2 g}{\partial r^2} \right)_\sigma, \quad (3.9)$$

where the index σ refers to derivatives with fixed stress. By assumption $\partial f/\partial r$ is non-zero and using the known form of \mathcal{F}_0 in eq. (3.2) we can see that the first term is still the only singular one and goes like $\tilde{r}^{-\alpha_0}$ in leading order, hence the critical exponent is unchanged. However, as was pointed out by Domb (1956), if we insert the assumed form of the free energy into the definition of the compressibility, we obtain the analogous expression

$$\kappa = - \left(\frac{\partial^2 \mathcal{F}}{\partial \sigma^2} \right)_r = -\mathcal{F}_0''(f) \left(\frac{\partial f}{\partial \sigma} \right)_r^2 - 2\mathcal{F}_0'(f) \frac{\partial^2 f}{\partial \sigma^2} - \frac{\partial^2 g}{\partial \sigma^2}. \quad (3.10)$$

Again, we assumed $\partial f/\partial \sigma$ not to vanish. A similar line of reasoning as for \mathcal{C}_σ can be used here to show that $\kappa \propto \tilde{r}^{-\alpha_0}$. We can deduce that if $\alpha_0 > 0$ the compressibility will become infinite, or equivalently the thermal bulk modulus $K = \kappa^{-1}$ will vanish. The system is then unstable with respect to volume changes, leading to a phase transition of the lattice. Since here we have made no statement about the symmetry of the medium, the nature of this transition is inaccessible on this level, but in an isotropic medium, this would correspond to an isostructural transition, which is generically first-order.

Note that even if $\alpha_0 < 0$, the first term in eq. (3.10) may just happen to be significant enough to destabilize the system, but it is not guaranteed and will depend on non-universal factors.

Going back to the case of constant strain, we consider the constrained system at a particular strain \mathcal{E}_c . The situation is now somewhat more complicated. Even though, the expansion eq. (3.8) is still valid for the direct dependence of f on \tilde{r} , there is now also an indirect dependence via $\sigma(r, \mathcal{E})$. We can extract the overall relation between f and \tilde{r} using

$$\mathcal{E}_c = \frac{\partial \mathcal{F}}{\partial \sigma} = \mathcal{F}_0'(f) \frac{\partial f}{\partial \sigma} + \frac{\partial g}{\partial \sigma} \quad (3.11)$$

Hence, we write using eq. (3.2)

$$\mathcal{F}_0'(f) \frac{\partial f}{\partial \sigma} = \left(B - (2 - \alpha_0) A f^{1-\alpha_0} \right) \frac{\partial f}{\partial \sigma} = \mathcal{E}_c - \frac{\partial g}{\partial \sigma} \quad (3.12)$$

Expanding both $\partial f/\partial \sigma$ and the right-hand side in \tilde{r} ,

$$\frac{\partial f}{\partial \sigma} = b_0(\sigma) + b_1(\sigma)\tilde{r} + \mathcal{O}(\tilde{r}^2), \quad \frac{\partial g}{\partial \sigma} = c_0(\sigma) + c_1(\sigma)\tilde{r} + \mathcal{O}(\tilde{r}^2) \quad (3.13)$$

and discarding the zeroth order, because $\tilde{r} = 0$ implies $f = 0$, we obtain

$$-(2 - \alpha_0)Af^{1-\alpha_0}b_0(\sigma) = (Bb_1(\sigma) - c_1(\sigma))\tilde{r} \quad (3.14)$$

We conclude that the effective tuning parameter f is related to the bare tuning parameter \tilde{r} in leading order via

$$f \propto \tilde{r}^{\frac{1}{1-\alpha_0}}. \quad (3.15)$$

As a result the coupled system at constant strain then shows *Fisher-renormalized* critical exponents (Fisher, 1968). This is because the leading singular contribution to the free energy is now given by

$$\mathcal{F} \propto f^{2-\alpha_0} \propto r^{\frac{2-\alpha_0}{1-\alpha_0}}. \quad (3.16)$$

Therefore the effective specific heat exponent is

$$\alpha = 2 - \frac{2 - \alpha_0}{1 - \alpha_0} = -\frac{\alpha_0}{1 - \alpha_0} \quad (3.17)$$

The other critical exponents are similarly renormalized,

$$\beta = \frac{\beta_0}{1 - \alpha_0} \quad \gamma = \frac{\gamma_0}{1 - \alpha_0} \quad \dots \quad (3.18)$$

In summary, if at constant stress/pressure the system has a diverging specific heat ($\alpha_0 > 0$), then at constant strain/volume, the specific heat has the Fisher-renormalized exponent α and will remain finite. If $\alpha_0 < 0$ then the leading order critical exponents are unaffected.

This is essentially equivalent to the Harris criterion (Harris, 1974), which states that the nature of the criticality is unaffected by disorder, if $\nu d < 2$, assuming the hyperscaling relation $2 - \alpha = \nu d$ is obeyed. This suggests that fluctuations in strain can be thought of as a kind of disorder.

3.2. Larkin-Pikin mechanism

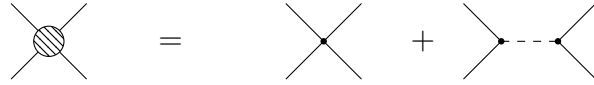
Fisher's theory predicts the critical behavior of the coupled system depending on the thermodynamic ensemble. However, this result is based on the assumption that the free energy depends in a well-behaved way on the free energy of the uncoupled system. Naturally, one would like to test these assumptions on a specific microscopic model.

Sticking to the principle already employed in chapter 2 of always choosing the most generic option, we write down a theory that is $O(N)$ symmetric in ϕ and rotationally

symmetric in space, i.e. isotropic. As explained in section 1.2 the action may then only depend on the trace of tensors constructed from ε . All these constraints result in the action

$$\mathcal{S} = \int d^d x \left(\frac{1}{2} \phi^T (-c^2 \nabla^2 + r) \phi + u(\phi^2)^2 + \frac{1}{2} \left(K - \frac{2}{d} \mu \right) \text{tr}\{\varepsilon\}^2 + \mu \text{tr}\{\varepsilon\varepsilon\} + \lambda \text{tr}\{\varepsilon\}\phi^2 \right), \quad (3.19)$$

equivalent to the model employed by Larkin & Pikin (1969), and we will follow their approach here. Their approach starts by integrating out strain, deriving a modified action with an effective density-density coupling mediated by strain



$$\text{Diagram 1} = \text{Diagram 2} + \text{Diagram 3}, \quad (3.20)$$

and derive an effective Landau theory, which may be identified with the form assumed by Fisher.

Integrating out strain has some subtlety here as was already hinted at in section 1.2. First, let us write the action in terms of the global strain as well as the longitudinal and transversal phonon with the traceless strain tensor $\tilde{\varepsilon} = \varepsilon - \frac{1}{d} \text{tr}\{\varepsilon\} \mathbb{1}$

$$\begin{aligned} \mathcal{S}_\varepsilon &= \int d^d x \left(\frac{1}{2} \left(K - \frac{2}{d} \mu \right) \text{tr}\{\varepsilon\}^2 + \mu \text{tr}\{\varepsilon\varepsilon\} \right) \\ &= \frac{VK}{2} \text{tr}\{E\}^2 + \int d^d x \left(\frac{\rho c_l^2}{2} (\nabla \cdot \mathbf{u})^2 + \rho c_t^2 \text{tr}\{\tilde{\varepsilon}^2\} \right). \end{aligned} \quad (3.21)$$

The longitudinal and transversal sound velocities are given by eq. (1.49) In the following, we ignore the transversal/shear terms, because the coupling is only with the trace of ε .

First, we integrate out the global strain macroscopic strain $\mathcal{E} = \text{tr}\{E\}$. Again, the distinction between ensembles becomes important. At constant volume \mathcal{E} is just a constant and its contribution to the interaction can be accounted for by a shift in the tuning parameter r .

At constant pressure, however, \mathcal{E} is a fluctuating degree of freedom that has to be integrated to obtain the partition function

$$\mathcal{Z} = \int \mathcal{D}\phi \mathcal{D}u d\mathcal{E} e^{-\mathcal{S}} \quad (3.22)$$

We define

$$\psi^2 = \int d^d x \phi^2 \quad (3.23)$$

and complete the square to rewrite

$$\frac{K}{2}\mathcal{E}^2 + \lambda\mathcal{E}\psi^2 = \frac{K}{2}\left(\mathcal{E} + \frac{\lambda}{K}\psi^2\right)^2 - \frac{\lambda^2}{2K}(\psi^2)^2. \quad (3.24)$$

Now we can eliminate ψ^2 in the first term on the right-hand side by a simple shift in the integration variable. The result of the \mathcal{E} integral is a constant factor that can be ignored and only the non-local interaction $(\psi^2)^2$ remains.

A similar procedure may be performed to integrate out \mathbf{u} , regardless of boundary conditions. Completing the square for the longitudinal phonon energy, we obtain

$$\frac{\rho c_l^2}{2}(\nabla\mathbf{u})^2 + \lambda\nabla\mathbf{u}\phi^2 = \frac{\rho c_l^2}{2}\left(\nabla\mathbf{u} + \frac{\lambda}{\rho c_l^2}\phi^2\right)^2 - \frac{\lambda^2}{2\rho c_l^2}(\phi^2)^2. \quad (3.25)$$

One might naively think that the path integral over \mathbf{u} can again be handled by a shift of the integration variable, but this can not account for the spatially constant contribution of ϕ^2 . This is easier seen in momentum space, where the shift

$$\mathbf{u}_q \rightarrow \mathbf{u}_q - \frac{1}{iq}\frac{\lambda}{\rho c_l^2}(\tilde{\phi}^2)_q \quad (3.26)$$

is not possible for $q = 0$, since the second term diverges in this limit. On the other hand the gradient term vanishes for $q = 0$, leaving a ‘‘bosonic hole’’

$$\int \mathcal{D}u \exp\left(-\int_q \frac{\rho c_l^2}{2}\left(i\mathbf{q}\cdot\mathbf{u} + \frac{\lambda}{\rho c_l^2}(\tilde{\phi}^2)_q\right)^2\right) = \mathcal{Z}_u \exp\left(-\frac{\lambda^2}{2\rho c_l^2}(\psi^2)^2\right) \quad (3.27)$$

with a constant \mathcal{Z}_u . In summary, the longitudinal phonon generates both an effective local and non-local self-interaction of the critical modes, while the macroscopic mode generates an effective non-local self-interaction only at constant pressure. As a result, the effective action of the critical modes is

$$\mathcal{S} = \int d^d x \left(\frac{1}{2}\boldsymbol{\phi}^T(-c^2\nabla^2 + r)\boldsymbol{\phi} + \bar{u}(\phi^2)^2\right) + wV^{-1}\left(\int d^d x \phi^2\right)^2, \quad (3.28)$$

where the local interaction has been renormalized by the longitudinal phonon

$$\bar{u} = u - \frac{\lambda^2}{2\rho c_l^2} \quad (3.29)$$

and a new non-local interaction has appeared with a coupling parameter

$$w = \begin{cases} -\frac{\lambda^2}{2\rho c_l^2} < 0 & \mathcal{E} = \text{const.} \\ \left(\frac{\lambda^2}{2K} - \frac{\lambda^2}{2\rho c_l^2}\right) > 0 & \sigma = \text{const.} \end{cases} \quad (3.30)$$

Note that the sign of v depends on the ensemble, since $\rho c_l^2 = K + \frac{4}{3}\mu > K$ and therefore in the constant \mathcal{E} case $v > 0$.

The first term in eq. (3.28) differs from the original ϕ^4 -theory only by a modified bare value of the coupling constant and hence contributes to the free energy a term with the same singular behavior. The question is then: How is the universal behavior changed by the non-local interaction?

Larkin & Pikin (1969) answer this question by performing a Hubbard-Stratonovich transformation, introducing an auxiliary field, which is essentially just reversing the integration of \mathcal{E}

$$\exp\left(wV^{-1}(\psi^2)^2\right) = \int d\mathcal{E} \exp\left(-\frac{\lambda^2\mathcal{E}^2V}{4w} - \lambda\mathcal{E}\psi^2\right). \quad (3.31)$$

The last term represents simply a renormalization of the tuning parameter of the original action. This allows writing the action in terms of the already solved problem of the ϕ^4 theory, representing the uncoupled \mathcal{F}_0 from the previous section

$$\mathcal{Z} = \int d\mathcal{E} \int \mathcal{D}\phi e^{-S_0(r+\lambda\mathcal{E}) - \frac{\lambda^2\mathcal{E}^2V}{4w}} = \int d\mathcal{E} e^{-\mathcal{F}_0(r+2\lambda\mathcal{E}) - \frac{\lambda^2\mathcal{E}^2V}{4w}}. \quad (3.32)$$

At this point, we can apply a saddle point approximation to the \mathcal{E} integral and treat the remaining problem within the framework of Landau theory. We introduce the effective Landau potential

$$\mathcal{V}(\mathcal{E}) = \mathcal{F}_0(r + 2\lambda\mathcal{E}) + \frac{\lambda^2\mathcal{E}^2V}{4w}, \quad (3.33)$$

which is minimized by \mathcal{E}_0 such that $\mathcal{V}'(\mathcal{E}_0) = 0$. In general, $\mathcal{E}_0(\sigma)$ is a function of applied stress and we have the free energy

$$\mathcal{F}(r, \sigma) = \mathcal{F}_0(r + 2\lambda\mathcal{E}_0(\sigma)) + \frac{\lambda^2\mathcal{E}_0(\sigma)^2V}{4w}. \quad (3.34)$$

The effective free energy can be identified with eq. (3.7) with the functions $f(r, \sigma) = r + 2\lambda\mathcal{E}_0(\sigma)$ and $g(r, \sigma) = \lambda^2\mathcal{E}_0(\sigma)^2V/4w$. Clearly, the assumption of analyticity is fulfilled for both of them, provided that \mathcal{E}_0 is analytic, hence, we know to expect Fisher-renormalized exponents at constant volume, if $\alpha_0 > 0$, which is the case for the $O(N)$ model in three dimensions for $N < 4$ in one-loop order. At constant

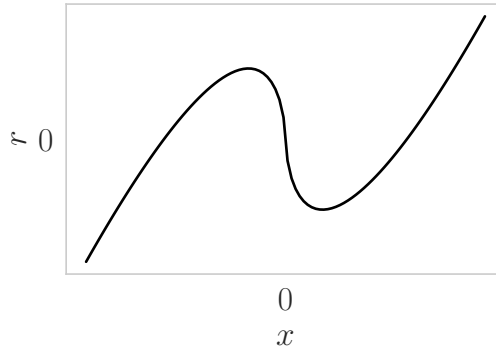


Figure 3.1.: Relation between the auxiliary parameter x and the tuning parameter r at constant pressure. In a region close to the critical point the value of x is not unique. Graph is for $\alpha_0 = \frac{1}{3}$.

pressure, we expect a first-order transition from thermodynamic arguments. To see how this plays out in this specific model, we minimize the Landau potential with respect to the parameter \mathcal{E} .

$$\frac{\partial \mathcal{F}}{\partial \mathcal{E}} = 2\lambda \mathcal{F}'_0(r + 2\lambda \mathcal{E}) + \frac{\lambda^2 \mathcal{E} V}{2w} = 0 \quad (3.35)$$

Pressure would enter via a linear term $-\sigma \mathcal{E}$ at this point, but we ignore it here because the effect is a trivial shift. Solving for \mathcal{E} we find the strain

$$\mathcal{E} = -\frac{4w}{\lambda V} \mathcal{F}'_0(r + 2\lambda \mathcal{E}). \quad (3.36)$$

The significance of this equation is more easily seen by using the shifted variable $x = f(r, \mathcal{E}) = r + 2\lambda \mathcal{E}$. Together with the relation $\mathcal{F}'_0(x) \propto x^{1-\alpha_0}$ from assumption eq. (3.2)

$$r = x - ax^{1-\alpha_0} \quad (3.37)$$

where a is some constant, which we need not bother to write down. The important result is that the right-hand side is a non-monotonic function of x for $\alpha_0 > 0$ as is shown in fig. 3.1. Thus the auxiliary variable x —and thus also \mathcal{E} —is not uniquely defined by the physical parameter r . In a certain range of the tuning parameter r there are two solutions for x (three if signs are taken into account). Therefore we have a first-order transition if $\alpha_0 > 0$, characterized by a jump in volume, signified by the strain variable \mathcal{E} .

The exact point where the transition changes to first-order can be found by the

condition (see Chandra et al. (2020) for details)

$$\frac{\partial r}{\partial x} = 1 - ax^{-\alpha_0} = 0, \quad (3.38)$$

where the second term can then be identified with the specific heat $\mathcal{C}(x)$.

Instead of introducing the Hubbard-Stratonovich field, one could take the theory as framed in eq. (3.28) and perform an RG analysis. This was done in Sak (1974) and Bruno & Sak (1980), obtaining an RG flow that is consistent with the results of Larkin & Pikin (1969). Although the expressions given only match the constant pressure case, a new stable fixed point with Fisher-renormalized exponents can be identified, but seems inaccessible because it is at a value of ν with the opposite sign. We do not go into their calculation in detail and instead focus on the more general analysis in the next section. However, readers trying to follow Sak (1974) should be advised of the typo in eq. (7), which corresponds to the second case in eq. (3.30) of this work after exchanging $-$ with \times .

3.3. Renormalization group approach on an anisotropic cubic lattice

So far both the thermodynamic approach and the microscopic theory for the isotropic solid suggests Fisher-renormalized exponents at constant volume. However, it is worthwhile to see how these modified exponents emerge in the RG picture. To this end we follow here the approach of Bergman & Halperin (1976), who analyzed the effect of lattice coupling for an Ising transition, meaning they only looked at $N = 1$ —an unnecessary restriction that we will not impose here—and find a new fixed point that is associated with Fisher renormalized exponents.

The approach of Bergman and Halperin differs from previous attempts to solve the problem in that they do not integrate out elastic degrees of freedom. Indeed, there is no reason why one should not perform the RG procedure on the original action in terms of the fields ϕ and \mathbf{u} . This approach has the benefit of showing transparently the effect of the transition on the elastic constants, as well as the change in critical behavior. It also avoids the subtleties involved with the integration of the macroscopic mode, since in momentum shell RG the integration domain is always kept far away from the singularity at $q = 0$. As an additional benefit, in Bergman and Halperin’s approach, it becomes feasible to include lattice anisotropy into the model. Hence, we write down the action

$$\mathcal{S} = \int d^d r \left(\frac{1}{2} \phi^T (-c^2 \nabla^2 + r) \phi + u (\phi^2)^2 + \lambda \text{tr} \varepsilon \phi^2 + \frac{1}{2} \varepsilon_{ij} C_{ijkl} \varepsilon_{kl} \right), \quad (3.39)$$

which is slightly more general than eq. (3.19) in that it allows for an anisotropic stiffness tensor. Even though the lattice is anisotropic, the interaction still only depends on the trace because in this theory ϕ and \mathbf{u} are assumed to live in different spaces with distinct symmetries.

Since we want to understand the effect of anisotropy, but don't want to complicate things too much, we will assume a cubic lattice, reducing the number of parameters of the phonon propagator to three, conventionally called C_{11} , C_{12} and C_{44} in Voigt notation (see section 1.2). Readers trying to compare with Bergman & Halperin (1976) should be advised that they are using a different definition of C_{44} , which differs by a factor of 4 from conventional Voigt notation. If the Zener index $A = 2C_{44}/(C_{11} - C_{12})$ is different from unity, the sound velocity will be a function of the direction of momentum $c_l(\hat{q})$. We write the action in Fourier space

$$\mathcal{S} = \int_q \left(\frac{1}{2}(c^2 q^2 + r)(\phi_q \cdot \phi_{-q}) + u \int_{q', q''} (\phi_q \cdot \phi_{q'}) (\phi_{q''} \cdot \phi_{-q-q'-q''}) \right. \\ \left. + \lambda \int_{q'} (i\mathbf{q} \cdot \mathbf{u}_q)(\phi_{q'} \cdot \phi_{-q-q'}) + \frac{1}{2} u_{q,i} D_{ij}(q) u_{-q,j} \right). \quad (3.40)$$

D is the dynamical matrix as defined in eq. (1.47). From a scaling analysis, we can see that, if we fix both the gradient term of the critical field and the dynamical matrix term to fix the scaling dimension of the displacement field, for λ it follows

$$\lambda' = b^{-2s_\phi - s_u - 1 + d} \lambda = b^{\frac{4-d}{2}} \lambda, \quad (3.41)$$

thus the elastic coupling λ is marginal in 4 dimensions, just like u . We therefore perform an ϵ expansion to one-loop order to determine how the coupling λ influences the RG flow.

The diagrams in the perturbation series now have phonon lines, which we represent as dashed, in addition to the critical modes, which still have solid lines. For example for the self-energy correction of the critical field ϕ we get the additional diagram

$$\begin{array}{c} q - q' \\ \circlearrowleft \\ i \xrightarrow{q} \bullet \xrightarrow{q} j \\ \circlearrowright \\ q' \end{array} = \frac{\lambda^2}{2} \int_{q'} \langle \phi_{q',i} \phi_{-q',j} \rangle_0 \langle \text{tr} \varepsilon_{q-q'} \text{tr} \varepsilon_{-q+q'} \rangle_0. \quad (3.42)$$

The correction function of the critical modes is just the Green's function we already encountered in chapter 2

$$\langle \phi_{q,i} \phi_{-q,j} \rangle_0 = G_{ij}^{(0)}(\mathbf{q}) = \frac{\delta_{ij}}{c^2 q^2 + r}. \quad (3.43)$$

The strain-strain correlation function can be calculated from $\langle u_{i,q} u_{j,-q} \rangle_0 = D_{ij}^{-1}(q)$.

The global stain $E = \varepsilon_{q=0}$ can be ignored here, since the q integration will only ever go over momenta close to the cutoff $b\Lambda < q < \Lambda$ with a b that close to unity. The effect of the trace is a projection onto the longitudinal mode

$$\text{-----} = \langle \text{tr } \varepsilon_q \text{ tr } \varepsilon_{-q} \rangle_0 = q_i D_{ij}^{-1}(q) q_j = \frac{1}{\rho c_l^2(\hat{q})}. \quad (3.44)$$

Specifically, for a cubic lattice

$$\rho c_l^2(\hat{q}) = C_{11} - 2(C_{11} - C_{12})(1 - A)Q(\hat{q}), \quad (3.45)$$

where we defined

$$Q(\hat{q}) = \frac{A(\hat{q}_x^2 \hat{q}_y^2 + \hat{q}_x^2 \hat{q}_z^2 + \hat{q}_y^2 \hat{q}_z^2) + (1 - A)(4 - A)\hat{q}_x^2 \hat{q}_y^2 \hat{q}_z^2}{A^2 + 4A(1 - A)(\hat{q}_x^2 \hat{q}_y^2 + \hat{q}_x^2 \hat{q}_z^2 + \hat{q}_y^2 \hat{q}_z^2) + 12(1 - A)^2 \hat{q}_x^2 \hat{q}_y^2 \hat{q}_z^2}. \quad (3.46)$$

Note that $Q > 0$ and it is a necessity for lattice stability that $C_{11} > C_{12}$, hence the sign of the anisotropic contribution to c_l depends strictly on the sign of $1 - A$.

Now we can go about calculating the diagram eq. (3.42). First, we must realize that it is independent of the external momentum \mathbf{q} . We can then expand in q and write

$$\frac{1}{\rho c_l^2 \left(\frac{q-q'}{|q-q'|} \right)} + q_i \partial_{q'_i} \frac{1}{\rho c_l^2(\hat{q}')} + \frac{1}{2} q_i q_j \partial_{q'_i} \partial_{q'_j} \frac{1}{\rho c_l^2(\hat{q}')} + \mathcal{O}(q^3). \quad (3.47)$$

The linear term must vanish just from symmetry. The second term can be reduced using the cubic symmetry which forces the cross terms to vanish $\partial_{q'_i} \partial_{q'_j} \rightarrow \delta_{ij} \nabla_{q'}^2 / d$. Thinking about the angular dependence in terms of spherical harmonics, we can conclude that the gradients will kill the 0th harmonic, which is the only one that would survive the angular integral. As a consequence, the diagram is independent of external momentum and integrand separates into a purely angle-dependent factor and a factor that only depends on the absolute values of momentum

$$\text{---} \circ \text{---} = \frac{2\lambda^2}{\rho \langle c_l^2 \rangle} \int_{\mathbf{q}} G_0(\mathbf{q}) = \frac{2\lambda^2}{\rho \langle c_l^2 \rangle} I_1, \quad (3.48)$$

with I_1 as in eq. (2.54) and where we defined the averaged sound velocity

$$\frac{1}{\langle c_l^2 \rangle} \equiv \int_{\hat{q}} \frac{1}{c_l^2(\hat{q})} \equiv \int \frac{d\Omega}{S_d} \frac{1}{c_l^2(\hat{q})}, \quad (3.49)$$

At first glance, this separation seems like a convenient technicality, but it is what makes the RG treatment of anisotropy feasible in the first place. In fact, all the integrals we encounter in this classical theory will separate in this manner, allowing us to treat anisotropy independently of the other couplings. The critical modes are

then renormalized according to

$$\begin{aligned}
 \text{---} \text{---} \text{---} &= \text{---} \text{---} \text{---} + \text{---} \text{---} \text{---} \\
 \Sigma_{ij}^{(1L)} &= 4(N+2)u_0 I_1 \delta_{ij} - \frac{4\lambda^2}{2\rho \langle c_l^2 \rangle} I_1 \delta_{ij} .
 \end{aligned} \tag{3.50}$$

Since both of the diagrams turned out not to depend on external momentum, only the tuning parameter r is renormalized. Next, we consider the self-energy correction to the phonons. We define the longitudinal displacement field propagator $F(\mathbf{q}) = \hat{q}_i D_{ij}^{-1}(\mathbf{q}) \hat{q}_j$ by projecting the inverse of the dynamical matrix on the wavevector. In the same fashion as for the critical modes we frame the renormalization of the phonon propagator with the phonon self-energy correction Π in terms of a Dyson equation

$$F^{-1}(\mathbf{q}) = F^{(0)-1}(\mathbf{q}) - \Pi(\mathbf{q}) , \tag{3.51}$$

where Π has only the contribution from the one-loop diagram

$$\Pi^{(1L)} = \text{---} \text{---} \text{---} . \tag{3.52}$$

The phonon self-energy correction is in the end a correction to the dynamical matrix

$$D_{ij}(\mathbf{q}) = D_{0,ij}(\mathbf{q}) - 2\lambda_0^2 q_i q_j \int_{q'} G_{kl}^{(0)}(q - q') G_{kl}^{(0)}(q') , \tag{3.53}$$

where the integral is the same as eq. (2.58). The renormalization of the dynamical matrix at the q^2 level translates into a renormalization of the elastic constants C_{ij}

$$D_{ij}(q) = (C_{0,ijkl} - 2N\lambda_0^2 I_2 \delta_{ik} \delta_{jl}) q_k q_l . \tag{3.54}$$

The stiffness of the lattice is therefore lowered by the critical fluctuations. Here we can already discern the possibility of a lattice instability, but the fate of the lattice depends on the flow of the elastic coupling λ .

Moving on to the vertex corrections, there are now two new diagrams with phonon lines contributing to the vertex function of u

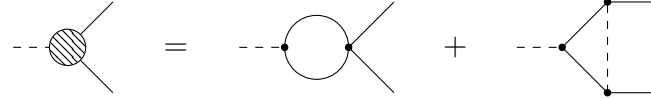
$$\begin{aligned}
 \text{---} \text{---} \text{---} &= \text{---} \text{---} \text{---} + \text{---} \text{---} \text{---} + \text{---} \text{---} \text{---} \\
 u - u_0 &= -4(N+8)u_0^2 I_2 + \frac{24}{\rho \langle c_l^2 \rangle} u_0 \lambda_0^2 I_2 - \frac{4}{\rho^2 \langle c_l^4 \rangle} \lambda_0^4 I_2 ,
 \end{aligned} \tag{3.55}$$

where the definition of I_2 is the same as in eq. (2.58). In the last term (the ‘box’ diagram) we have to average over the fourth power in the sound velocity, which complicates things somewhat because in the presence of anisotropy, it is different

from $\langle c_l^2 \rangle^2$

$$\frac{1}{\rho^2 \langle c_l^4 \rangle} = \int_{\hat{q}} \left(\frac{1}{\rho c_l^2} \right)^2 \neq \left(\int_{\hat{q}} \frac{1}{\rho c_l^2} \right)^2 \quad (3.56)$$

except of course in the special case $A = 1$, in which case the phonon velocity is independent of direction. The elastic coupling λ also gets a vertex correction, which is given by



$$\lambda - \lambda_0 = -4(N+2)\lambda_0 u_0 I_2 + \frac{4}{\rho \langle c_l^2 \rangle} \lambda_0^3 I_2. \quad (3.57)$$

The next step is to rescale fields and parameters with the transformation $\mathbf{q} = \mathbf{q}'/b$

$$\begin{aligned} \phi(\mathbf{q}) &= b^{\frac{d-2}{2}} \phi'(\mathbf{q}'), \\ \mathbf{u}(\mathbf{q}) &= b^{\frac{d-2}{2}} \mathbf{u}'(\mathbf{q}'), \end{aligned} \quad (3.58)$$

It follows then from the RG conditions

$$G^{-1}(q)|_{r=0} = c^2 q^2, \quad F^{-1}(\mathbf{q})|_{r=0} = \rho c_l^2 q^2, \quad (3.59)$$

that the parameters scale like

$$\begin{aligned} c^2 &= c'^2, & c_l^2 &= c_l'^2, & r &= r'/b^2, \\ u &= u'/b^{4-d}, & \lambda &= \lambda'/b^{(4-d)/2}. \end{aligned} \quad (3.60)$$

The RG flow equations are then calculated by differentiating with respect to $\ell = \log b$. For the tuning parameter r we obtain

$$\frac{dr}{d\ell} = 2r - \frac{N+2}{2\pi^2 c^3} u r + \frac{1}{4\pi^2 \rho \langle c_l^2 \rangle c^3} \lambda^2 r \quad (3.61)$$

From the renormalization of the dynamical matrix, we obtain the RG flow equations of the elastic constants

$$\begin{aligned} \frac{dC_{11}}{d\ell} &= -\frac{N}{4\pi^2} \frac{\lambda^2}{c^3} \\ \frac{dC_{12}}{d\ell} &= -\frac{N}{4\pi^2} \frac{\lambda^2}{c^3} \\ \frac{dC_{44}}{d\ell} &= 0. \end{aligned} \quad (3.62)$$

Note that the shear modulus C_{44} is not renormalized, as would be expected, since the interaction is only with the trace of the strain tensor, effectively projecting out the transversal mode. Since C_{11} flows like C_{12} , the difference between them is invariant under RG transformations and consequently, so is the Zener index A

(eq. (1.36)). The only macroscopic elastic modulus that flows is the bulk modulus (eq. (1.32))

$$\frac{dK}{d\ell} = -\frac{N}{4\pi^2} \frac{\lambda^2}{c^3} \quad (3.63)$$

The corresponding microscopic parameter is the longitudinal sound velocity, for which the sound velocity can be derived similarly from eq. (3.45) and eq. (3.62)

$$\frac{dc_l^2}{d\ell} = -\frac{N}{4\pi^2} \frac{\lambda^2}{\rho c^3} . \quad (3.64)$$

Interestingly, the anisotropic contribution to c_l^2 does not flow at all. In fact, it is only C_{11} that changes with an RG transformation, which suggests that the details of the anisotropy do not matter much for the critical behavior, as long as it can be expressed in terms of RG invariants such as A . It also follows from the fact that physically λ has to be real-valued and c has to be positive, the isotropic contribution to c_l^2 will decrease under the RG transformation (or remain constant if $\lambda = 0$), while the anisotropic one remains the same. Therefore, the relative anisotropy

$$R = \frac{C_{11} - C_{12} - 2C_{44}}{C_{11}} = (1 - A) \frac{C_{11} - C_{12}}{C_{11}} \quad (3.65)$$

will increase in magnitude under RG (or again remain constant if $\lambda = 0$)

$$\frac{dR}{d\ell} = \frac{N}{4\pi^2} \frac{\lambda^2}{C_{11} c^3} R . \quad (3.66)$$

All of the above RG flow equations depend on the elastic coupling λ . Thus, to determine the fate of the system we need to find the flow in λ . From the vertex corrections, we obtain the RG flow equations for the couplings, which are then more concisely expressed in the dimensionless variables

$$\tilde{u} = \frac{u}{2\pi^2 c^3} \quad \tilde{\lambda}^2 = \frac{\lambda^2}{4\pi^2 \rho \langle c_l^2 \rangle c^3} . \quad (3.67)$$

For these the equations hold

$$\begin{aligned} \frac{d\tilde{u}}{d\ell} &= \epsilon \tilde{u} - (N + 8) \tilde{u}^2 + 12 \tilde{u} \tilde{\lambda}^2 - 4 \frac{\langle c_l^2 \rangle^2}{\langle c_l^4 \rangle} \tilde{\lambda}^4 \\ \frac{d\tilde{\lambda}^2}{d\ell} &= \epsilon \tilde{\lambda}^2 - 2(N + 2) \tilde{u} \tilde{\lambda}^2 + (N + 4) \tilde{\lambda}^4 \end{aligned} \quad (3.68)$$

In general, a coupled system of nonlinear differential equations like this is hard to solve. However, as Bergman & Halperin (1976) point out the equations can be decoupled in the isotropic limit using the linear transformation

$$\bar{u} = \tilde{u} - \tilde{\lambda}^2 . \quad (3.69)$$

Note that this transformation coincides exactly with the renormalization of the self-interaction found in eq. (3.29). The RG flow equations for the shifted coupling then read

$$\begin{aligned}\frac{d\bar{u}}{d\ell} &= \epsilon\bar{u} - (N+8)\bar{u}^2 + 4\left(1 - \frac{\langle c_l^2 \rangle^2}{\langle c_l^4 \rangle}\right)\tilde{\lambda}^2 \\ \frac{d\tilde{\lambda}^2}{d\ell} &= \epsilon\tilde{\lambda}^2 - 2(N+2)\bar{u}\tilde{\lambda}^2 - N\tilde{\lambda}^4.\end{aligned}\tag{3.70}$$

Note that for isotropic elasticity $\langle c_l^2 \rangle^2 = \langle c_l^4 \rangle$ and therefore the last term in the first equation vanishes.

Solving the equations for zero flow, we find that in $4 - \epsilon$ dimensions for small flavor number $N < 4$ the RG flow is characterized by four fixed points: Additionally to the usual Gaussian and Wilson-Fisher fixed points we find the Fisher-renormalized Gaussian (Fr-G) and Fisher-renormalized Wilson-Fisher (Fr-WF) fixed points at finite elastic coupling. The corresponding fixed point values are given in table 3.1.

Table 3.1.: Fixed points of the classical $O(N)$ model coupled to an isotropic elastic medium in $4 - \epsilon$ dimensions, with values of the dimensionless couplings and the corresponding critical exponents ν and α to first order in ϵ .

Fixed point	\bar{u}	$\tilde{\lambda}^2$	ν	α
G	0	0	$\frac{1}{2}$	$\frac{\epsilon}{2}$
WF	$\frac{\epsilon}{N+8}$	0	1	$\frac{4-N}{2(N+8)}\epsilon$
Fr-G	0	$\frac{\epsilon}{N}$	$\frac{1}{2} + \frac{\epsilon}{4}$	$-\frac{\epsilon}{2}$
Fr-WF	$\frac{\epsilon}{N+8}$	$\frac{4-N}{N(N+8)}\epsilon$	$\frac{1}{2} + \frac{3\epsilon}{2(N+8)}$	$-\frac{4-N}{2(N+8)}\epsilon$

The naming of the fixed points is suggestive and we will show in the following how the Fisher-renormalized fixed points are indeed associated with Fisher-renormalized critical exponents. Since there is no wave function renormalization at this level, the anomalous dimension η vanishes for all fixed points. To calculate the remaining critical exponents we insert the fixed point values into eq. (3.61). For Fr-WF we obtain

$$\begin{aligned}\nu_{\text{Fr-WF}} &= \left(\frac{d \log r}{d \log \ell}\right)^{-1} = \left(2 - (N+8)\bar{u}^* - N(\tilde{\lambda}^*)^2\right)^{-1} \\ &= \frac{1}{2} + \frac{3}{2(N+8)}\epsilon + \mathcal{O}(\epsilon^2),\end{aligned}\tag{3.71}$$

which is indeed the Fisher-renormalized exponent of the corresponding WF exponent, as can be checked with the values from section 2.4

$$\frac{\nu_{\text{WF}}}{1 - \alpha_{\text{WF}}} = \frac{\frac{1}{2} + \frac{1}{4}\frac{N+2}{N+8}\epsilon + \mathcal{O}(\epsilon^2)}{1 - \frac{1}{2}\frac{4-N}{N+8}\epsilon + \mathcal{O}(\epsilon^2)} = \frac{1}{2} + \frac{3}{2(N+8)}\epsilon + \mathcal{O}(\epsilon^2).\tag{3.72}$$

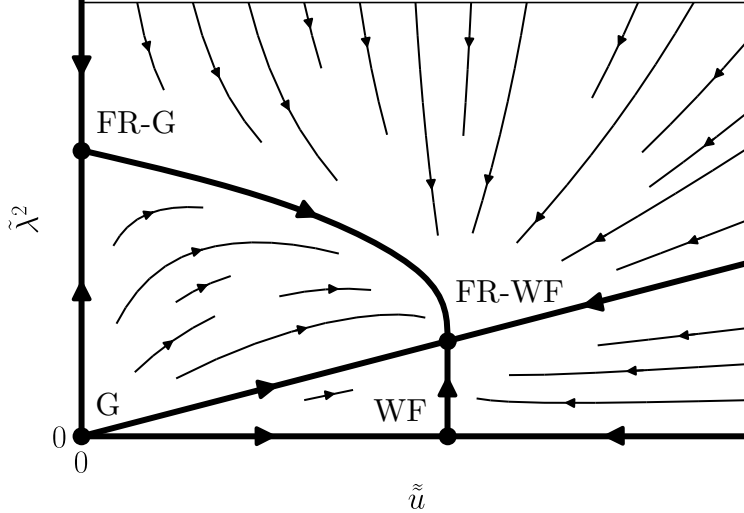


Figure 3.2.: RG flow of the classical ϕ^4 -theory coupled to a compressible lattice in $4 - \epsilon$ dimensions, with $\epsilon > 0$, for $N < 4$ flavors, as calculated by Bergman & Halperin (1976).

The stability of Fr-WF can be analyzed by linearizing the RG equations around the fixed point

$$\frac{d}{d\ell} \begin{pmatrix} \delta\bar{u} \\ \delta\tilde{\lambda}^2 \end{pmatrix}_{\text{Fr-WF}} = \begin{pmatrix} -\epsilon & 0 \\ \frac{2(N-4)(N+2)\epsilon}{3N} & \frac{(N-4)\epsilon}{N+8} \end{pmatrix} \begin{pmatrix} \delta\bar{u} \\ \delta\tilde{\lambda}^2 \end{pmatrix}. \quad (3.73)$$

Since the matrix is already triangular we can just read off the eigenvalues. We find that the Fr-WF fixed point is stable for $N < 4$. The full RG flow for this case is shown in fig. 3.2. This is not entirely surprising since we expect Fisher-renormalized exponents only if $\alpha > 0$. At one-loop order, α_{WF} is positive only for $N < 4$. The $\tilde{\lambda}^2$ value of Fr-WF becomes negative at $N > 4$ corresponding to an imaginary coupling, which is unphysical.

If $N < 4$ and the initial elastic coupling $\tilde{\lambda}_0$ is non-zero, the flow will eventually be towards the Fr-WF fixed point, where $\tilde{\lambda}$ tends towards a finite value. The flow of the elastic constants, which only depends on $\tilde{\lambda}$, can then be approximated with a constant elastic coupling. The solution of eq. (3.62) is then a simple exponential function and with $\ell = \log b$ we find

$$C_{11} \sim b^{-\frac{4-N}{(N+8)}\epsilon}. \quad (3.74)$$

In other words C_{11} tends to zero as a power law. The consequences for the stability of the crystal lattice will become apparent in the subsequent flow of the bulk modulus K and the sound velocity c_l .

For the cubic lattice in three dimensions the bulk modulus in terms of the stiffness

tensor components is

$$K = C_{11} - \frac{2}{3}(C_{11} - C_{12}) . \quad (3.75)$$

In this form it is easy to see that since $C_{11} - C_{12}$ is invariant, while C_{11} approaches zero, the bulk modulus vanishes at a finite RG scale. The vanishing of an elastic modulus causes a macroscopic instability. In case the bulk modulus vanishes the associated instability is isostructural, meaning the lattice symmetry is unchanged. The instability is resolved by a phase transition which is generically first-order and associated with a jump in the lattice constant, except in special fine-tuned cases. However, Bergman & Halperin (1976) point out that such a transition can be avoided by applying appropriate boundary conditions. It turns out that it is not enough to fix the volume to avoid the instability, since the system becomes unstable with respect to surface modes. They propose that fixing the position of every surface atom, so-called “pinned” boundary conditions, will stabilize the crystal even with a negative bulk modulus. Whether it is truly necessary to fix *every* surface atom is a subtle question and that will be addressed in more detail in section 5.3.

There remains the question of microscopic stability, i.e. the stability of phonon modes. In an isotropic system, it holds $c_l = \sqrt{C_{11}/\rho}$ and both vanish asymptotically. However, in an anisotropic system, c_l is modified by a direction-dependent, RG invariant contribution, see eq. (3.45). If $A > 1$ the anisotropy will lower the sound velocity, an effect that is largest in [111] and equivalent directions. It follows that the sound velocity will vanish on lines in phase space. We expect a transition the likes of which have been discussed by Cowley (1976). This is a remarkable fact: Even though the anisotropy index A is invariant, we still found that there is an instability with respect to anisotropy because the isotropic contribution to the sound velocity vanishes asymptotically, thus the relative anisotropy R diverges.

If $A < 1$ it follows that $c_l(\hat{q}) \geq \sqrt{C_{11}/\rho}$ with only the sound velocity along [100] direction and equivalent vanishes asymptotically. Hence, there is no microscopic instability at any finite scale.

On the other hand, if $N > 4$ and consequently $\alpha_{\text{WF}} < 0$, the WF fixed point is stable, as can be seen in the linearized RG equations

$$\frac{d}{d\ell} \begin{pmatrix} \delta\bar{u} \\ \delta\tilde{\lambda}^2 \end{pmatrix}_{\text{WF}} = \begin{pmatrix} -\epsilon & 0 \\ 0 & \frac{4-N}{N+8}\epsilon \end{pmatrix} \begin{pmatrix} \delta\bar{u} \\ \delta\tilde{\lambda}^2 \end{pmatrix} . \quad (3.76)$$

As a result, the elastic coupling will vanish asymptotically and the flow in the elastic constants effectively stops. It may be the case that, if λ_0 is sufficiently large, at the scale at which the λ becomes negligible the elastic constants are already renormalized beyond any of the above-mentioned instabilities. However, this is non-universal, as it depends on the bare values of the parameters.

3.4. Discussion

Throughout this chapter, we have seen three approaches, that illuminate the question of how a classical, finite temperature transition is changed by elastic coupling in varying degrees of detail. Here we discuss the relation between these approaches and the different aspects of the problem that they were able to solve. A much more detailed review of the history of classical transitions coupled to elastic degrees of freedom, containing also more tangential literature can be found in Dünweg (2000). However, since such a comprehensive overview seems to exist only in German, we reiterate some of the points here.

The first approach—in this chapter and historically—is based on thermodynamic relations, which suggests a first-order transition at constant pressure (Rice, 1954). It can be shown that with some reasonable assumptions on the form of the free energy the compressibility diverges with the same exponent as the specific heat (Domb, 1956). For the case of constant volume one has to do a little more work, but it can be shown that the critical exponents will be renormalized (Fisher, 1968). These arguments are fairly general without referring to any specific model. However, Fisher (1968) assumed in his work that in case of constant pressure the transition is the unmodified continuous one except for a shifted critical point, which seems to be at odds with the earlier statements. Another question that this approach leaves open is the nature of the structural transition.

To see how this plays in detail Larkin & Pikin (1969) looked at a concrete, microscopic model, of an Ising-type model coupled to an isotropic medium. They integrate out the elastic degrees of freedom at constant pressure, taking into account the singularity at $q = 0$, which allows them to express the problem in terms of a reparametrized version of the free energy of original Ising criticality. The reparametrization gives a clear picture of how the first-order transition that was predicted at constant pressure arises. At the same time, it validates assumptions proposed in Fisher (1968).

Another famous work that discusses this problem is Baker & Essam (1970), which is unique in that it discusses an exactly solvable model, by only allowing nearest-neighbor interaction for the elastic degrees of freedom in a cubic lattice. However, as a consequence, it has zero shear modulus (Ikea-board instability). Plugging this into eq. (3.30) we see that the non-local interaction vanishes in the case of constant pressure if we set $\mu = 0$, thus the Ising criticality is unmodified. Thus, the Larkin-Pikin mechanism is unique to solids and has no equivalent in fluids, which have $\mu = 0$. At constant volume, the system still shows Fisher-renormalized exponents. A later publication by the same authors (Baker & Essam, 1971) includes a finite shear modulus, at the cost of exact solvability.

The appearance of Fisher-renormalized exponents becomes more transparent in the renormalization group formalism. The Larkin-Pikin action (eq. (3.28)) has been analyzed in this framework in Sak (1974) (also see (Bruno & Sak, 1980)). They find

a Fisher-renormalized fixed point that is accessible at constant volume ($v > 0$) and inaccessible at constant pressure ($v < 0$).

The question of the nature of the elastic transition was addressed by Bergman & Halperin (1976). They simply take the original action, including elastic degrees of freedom, and perform the RG procedure on the displacement field as well, making the effect of the critical fluctuations on the elastic constants transparent. They also include lattice anisotropy in a cubic system and in the extreme case of a vanishing Zener index $A = 0$, reproduce the results of Baker & Essam (1970). Additionally, they provide a more precise notion of the boundary conditions that are necessary to realize the “constant volume” case, by requiring all surface atoms to be pinned to their position, to avoid instabilities caused by surface modes.

A slight generalization of the work by Bergman & Halperin (1976) including cubic anisotropy for the critical modes, is provided by Nattermann (1977). As we have discussed in section 2.5 the WF fixed point is stable with respect to cubic anisotropy, exactly under the conditions at which we expect Fisher-renormalization. Therefore the results are not significantly changed.

4. Tricritical elasticity

Usually, phase transitions can be reached by tuning a single experimental knob, such as temperature T or pressure P , which is connected to the tuning parameter r . The dependence of the other parameters on the knobs is, in general, not important, since at the critical point $r(T_c) = 0$ the other parameters will remain finite and thus will only change slowly if we restrict ourselves to a sufficiently small interval around the critical point.

If, however, we can tune two parameters such that both the tuning parameter $r(P_c, T_c) = 0$ and the quartic interaction $u(P_c, T_c) = 0$ vanish, then the critical behavior around this point is changed considerably. Such a point in the phase diagram is called a *tricritical point*.

In the vicinity of the tricritical point, the critical fluctuations are described by an action that includes the next leading order after the vanishing quartic interaction, namely a ϕ^6 term

$$\mathcal{S}_0 = \int d^d x \left(\frac{r}{2} \phi^2 + \frac{c^2}{2} (\nabla \phi)^2 + u \phi^4 + v \phi^6 \right). \quad (4.1)$$

From a simple scaling analysis, one can see that the ϕ^6 interaction v is marginal in $d = 3$ dimensions. Thus, the classical tricritical point is already at the upper critical dimension, in $d = 3$ spatial dimensions, and we can expect mean field theory to accurately predict the universal critical behavior up to logarithmic corrections (Riedel & Wegner, 1972).

Of course, for small but finite u this is not true. Nonetheless, for simplicity, we look at the problem only in terms of the Landau theory

$$\mathcal{F}_0^{\text{MF}} = r \phi_0^2 + u \phi_0^4 + v \phi_0^6 + \dots, \quad (4.2)$$

We may get rid of v by defining $\tilde{r} = r/v$, $\tilde{u} = u/v$, and $\tilde{\mathcal{F}}_0^{\text{MF}} = \mathcal{F}_0^{\text{MF}}/v$. We define $\psi_0 = \phi_0^2$

$$\tilde{\mathcal{F}}_0^{\text{MF}} = \tilde{r} \psi_0 + \tilde{u} \psi_0^2 + \psi_0^3 \quad (4.3)$$

Note that the symmetry of ψ_0 is different from ϕ_0 , because $\psi_0 > 0$ by definition and odd powers enter the Landau functional.

At $\tilde{r} < 0$ the system is always in the ordered phase and a sign change in u does not make a qualitative difference. If $\tilde{r} > 0$ however, then there will be a first-order

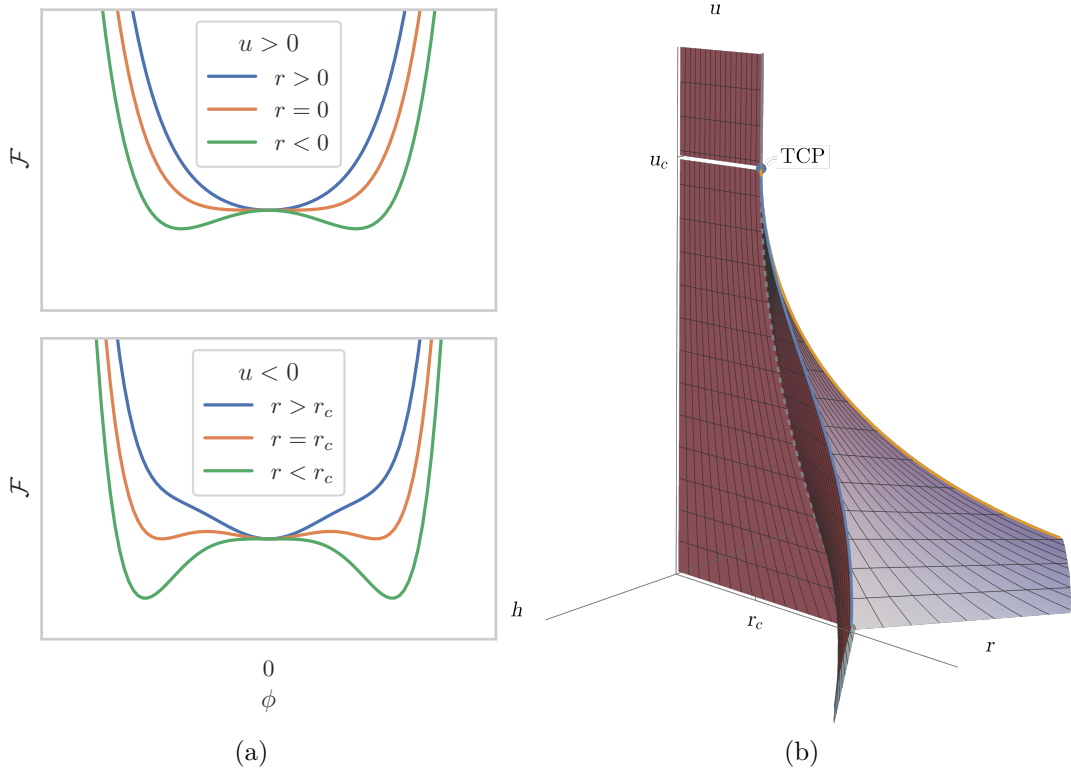


Figure 4.1.: Landau potential for the order parameter ϕ_0 at $h = 0$ in (a). The upper panel shows the case $u > 0$, where as a function of r the minimum splits continuously, while in the lower panel, where $u < 0$, a local minimum at finite ϕ_0 becomes the global minimum at the transition, causing a jump in the order parameter. Panel (b) shows the phase diagram near the tricritical point as a function of u , r and h .

transition as a function of \tilde{u} as a result of the ψ_0^3 potential at a critical value \tilde{u}_c given by $\tilde{u}_c^2/4 = \tilde{r}$. If $\tilde{r} = 0$ then we have a second order transition at $\tilde{u}_c = 0$. This is the tricritical point, since it lies on the border between a first order ($\tilde{u} < 0$) and second order ($\tilde{u} > 0$) transition, With the inclusion of the linear term in the free energy $h\phi_0$, the second-order line splits into two second-order lines, see fig. 4.1, which is where the tricritical point gets its name.

We calculate the exponent α_t at the tricritical point. In the ordered phase ψ_0 is given by

$$\psi_0 = \frac{1}{3} \left(\sqrt{\tilde{u}^2 - 3\tilde{r}} - \tilde{u} \right). \quad (4.4)$$

Inserting this into free energy eq. (4.3) and setting $u = 0$ we obtain

$$\mathcal{F}_0^{\text{MF}}(r < 0, u = 0) = \frac{5(-\tilde{r})^{\frac{3}{2}}}{3\sqrt{3}}. \quad (4.5)$$

The specific heat can be calculated from the second derivative, which has the critical exponent $\alpha_t = \frac{1}{2}$.

More generally, when not dealing with a mean-field theory, but instead, some model that on the second order transition line has the critical exponent $\alpha > 0$, like for example the Ising model in 3 dimensions, we can write the singular part of the free energy as

$$\mathcal{F}_0(r, u) = -Ar^{2-\alpha}\Phi\left(\frac{u}{r^\varphi}\right) \quad (4.6)$$

where φ is a crossover exponent and the scaling function Φ needs to have the limits

$$\Phi(x) = \begin{cases} x^{\frac{\alpha_t-\alpha}{\varphi}} & x \ll 1 \\ \text{const.} & x \gg 1. \end{cases} \quad (4.7)$$

Such that in the vicinity of the tricritical point $\mathcal{F}_0(r, u \ll r^\varphi) \sim r^{2-\alpha_t}$, while when approaching the second order transition line sufficiently far away from the tricritical point $\mathcal{F}_0(r, u \gg r^\varphi) \sim r^{2-\alpha}$. In 3 dimensions it of course still holds that $\alpha_t = \frac{1}{2}$.

The inclusion of a quadratic elastic coupling $\varepsilon\phi^2$ can now be handled with the Larkin-Pikin procedure that was outlined in section 3.2. Integrating out strain is not affected by the inclusion of the ϕ^6 term. We consider the action

$$\mathcal{S} = \mathcal{S}_0 + \int d^d x \left(\lambda\phi^2 \text{tr}\{\varepsilon\} + \frac{1}{2} \left(K - \frac{2}{d}\mu \right) \text{tr}\{\varepsilon\}^2 + \mu \text{tr}\{\varepsilon\varepsilon\} \right) \quad (4.8)$$

and integrate out strain. As we have discussed in chapter 3 the result depends on boundary conditions. For open boundary conditions (constant pressure) we obtain after performing the Hubbard-Stratonovich transformation the effective Landau potential of the strain variable \mathcal{E}

$$\mathcal{V}(\mathcal{E}) = \mathcal{F}_0\left(r - \lambda\mathcal{E}, u - \frac{\lambda^2}{2\rho c_l^2}\right) + \frac{\mathcal{E}^2}{2} \left(\frac{1}{K} - \frac{1}{\rho c_l^2} \right). \quad (4.9)$$

Note that the renormalization of u does not depend on \mathcal{E} , thus u is simply shifted by the elastic coupling. The reasoning from section 3.2 applies without modification. As a consequence, assuming $\alpha > 0$, at constant pressure the second order transition at positive u and zero field becomes first order. Considering also finite field the phase diagram in fig. 4.1b is then modified such that there are two disconnected second-order lines at finite h , hence there is no tricritical point. For pinned boundary conditions (constant volume) we have Fisher renormalized exponents for both α and α_t , meaning

$$\alpha'_t = -\frac{\alpha_t}{1-\alpha_t} = -1. \quad (4.10)$$

The singularity in the specific heat at the tricritical point is thus completely suppressed.

5. Quantum criticality on a compressible lattice

After developing a thorough understanding of how a classical phase transition changes through lattice coupling in chapter 3, we can turn our attention to the quantum phase transition and ask how the story will be different. The questions immediately come to mind whether the Larkin-Pikin mechanism (section 3.2) still applies, which allows us to express the elastically coupled model in terms of the free energy of the rigid model using an effective Landau theory, and whether there is a quantum equivalent of Fisher-renormalization (section 3.1). If the quantum theory can be described by a classical model in higher dimensions, as is the case in the rigid $O(N)$ universality class, we expect the Larkin-Pikin mechanism to hold. However, it will turn out that this is not the case, because, as will be explained in section 5.1, with the inclusion of quantum fluctuations into the theory, the elastic coupling may no longer be reduced to a single, macroscopic strain variable.

Analogous to the classical transition, we concentrate here on the case where the leading coupling is quadratic in the order parameter. In the case of linear coupling, there is again a strong hybridization of strain and order parameter, and the transition is governed by critical elasticity (Zacharias et al., 2015) with the respective consequences for the lattice (Cowley, 1976).

A natural extension of the theory investigated by Larkin & Pikin (1969) and Bergman & Halperin (1976) is to couple the Lorentz invariant model that was already analyzed in section 2.4, with a dynamical exponent $z = 1$, quadratically to compressive strain. An important feature of the elastic coupling is that it explicitly breaks Lorentz invariance. This must necessarily be the case since the elastic medium makes this effectively an ‘aether’ theory.

The breaking of a symmetry, such as Lorentz invariance, is often but not always associated with a change in universality class. This is sufficient motivation to check if critical behavior is significantly changed, provided that the elastic coupling is relevant. The criterion for non-perturbative elastic coupling has a straightforward generalization to quantum criticality. The scaling is governed by the effective dimension $d_{\text{eff}} = d + z$. If the specific heat exponent of the quantum transition

$$\alpha_q = 2 - \nu_q d_{\text{eff}} = 2 - \nu_q (d + z) , \quad (5.1)$$

is positive, then non-perturbative elastic coupling is expected (Anfuso et al., 2008). An equivalent criterion has been discussed by Han et al. (2021). In table 5.1, some universality classes are shown with their specific heat exponents and our expectation for the non-perturbative nature of elastic coupling from the above criterion.

Table 5.1.: Selected universality classes and their specific heat exponent (Di Francesco, Mathieu, & Sénéchal, 1997; Pelissetto & Vicari, 2002; Riedel & Wegner, 1972).

Model	d_{eff}	α_q	Non-perturbative coupling
Ising	2	0	logarithmic
Tricritical Ising	2	$\frac{8}{9}$	yes
Tricritical Ising	3	$\frac{1}{2}$	yes
Three-state Potts	2	$\frac{1}{3}$	yes
Ising	3	~ 0.11	yes
$O(N)$ with $N \geq 2$	3	< 0	no
$O(N)$	4	0	logarithmic

The theory investigated here is directly relevant to a type of antiferromagnetic quantum phase transition, which is well described by the $O(N)$ model, and is realized for example in the material TlCuCl_3 , which, when tuned across the quantum critical point using pressure, has a dynamical exponent $z = 1$ (Rüegg et al., 2008).

The contents of this chapter are structured as follows: In section 5.1 we will first explain in more detail why the classical approach does not work. We conclude that we need to take a deeper look at the effects of fluctuations and perform an RG analysis of the quantum theory section 5.2. In the classical theory, one may argue, the approach of Bergman & Halperin (1976) gives the most transparent picture of the effect of elastic coupling since it shows not only the effect of lattice fluctuations on the transition but also the effect of the critical fluctuations on the lattice and allows reasoning about the nature of the appearing instabilities. We shall favor an analogous approach, not integrating out the phonons, but instead treating them on the same footing as the critical fluctuations. Finally, we also discuss in detail the consequences for the lattice in section 5.3.

The contents of this chapter are an original part of this thesis and the results of section 5.2 have also been published (Sarkar et al., 2023).

5.1. Breakdown of the Larkin-Pikin mechanism at quantum criticality

To extend the Larkin-Pikin model to quantum criticality, we use imaginary time formalism, adding imaginary time derivatives for both critical modes $\boldsymbol{\phi} = (\phi_1, \dots, \phi_N)$ and displacement field. The strain is decomposed into the macroscopic modes E and derivatives of the displacement field. The full action is then

$$\begin{aligned} \mathcal{S} = \int d\tau d^d x \left(\frac{1}{2} \boldsymbol{\phi}^T \left(-\partial_\tau^2 - c^2 \nabla^2 + r \right) \boldsymbol{\phi} + u(\phi^2)^2 + \lambda \phi^2 (\nabla \cdot \mathbf{u}) \right. \\ \left. + \frac{K}{2} \text{tr}\{E\}^2 + \frac{\rho}{2} \left[(\partial_\tau \mathbf{u})^2 + c_l^2 (\nabla \cdot \mathbf{u})^2 + 2c_t^2 \text{tr}\{\tilde{\varepsilon}\tilde{\varepsilon}\} \right] \right). \end{aligned} \quad (5.2)$$

One might ask why this action does not contain time derivatives of the macroscopic strain E . In fact, we assume that E does not depend on time at all. This assumption is well-founded in an infinite system where E is not dynamic, as was discussed in section 1.2. In the case of a finite system, E is just a placeholder for a set of macroscopic modes with wavelengths on the order of the system size, the character of which depends sensitively on geometry and boundary conditions. However, we will restrict ourselves to the thermodynamic limit, thinking of E as static, while leaving finite-size effects a topic of future works.

It is tempting to try and apply the Larkin-Pikin procedure from section 3.2 to this problem, as the classical problem could, at least for the isotropic case, be completely solved by this mechanism. However, after integrating out phonons, we obtain the much more complicated effective action

$$\begin{aligned} \mathcal{S} = \int d\tau d^d x \frac{1}{2} \boldsymbol{\phi}^T \left(-\partial_\tau^2 - c^2 \nabla^2 + r \right) \boldsymbol{\phi} + w V^{-1} \left(\int d\tau d^d x \phi^2 \right)^2 \\ + \int d\tau d^d x \int d\tau' d^d x' \phi(x, \tau)^2 \Gamma(x - x', \tau - \tau') \phi(x', \tau')^2 \end{aligned} \quad (5.3)$$

where w is the same as in eq. (3.30), and there is another non-local interaction with the vertex function in Fourier space given by

$$\Gamma(\mathbf{q}, \omega) = u - \frac{\lambda^2}{2\rho} \frac{q^2}{\omega^2 + c_l^2 q^2}. \quad (5.4)$$

Note that Γ is non-analytic around $(\mathbf{q}, \omega) = (0, 0)$. This can be most easily seen by taking the non-commuting limits $\lim_{q \rightarrow 0} \Gamma = u$ and $\lim_{\omega \rightarrow 0} \Gamma = u - \lambda^2/2\rho c_l^2$. The latter corresponds to the renormalization of the self-interaction that we encountered in the classical theory eq. (3.29).

Larkin-Pikin physics could be recovered by taking the classical limit only for phonons

by taking the mass density to vanish $\rho \rightarrow 0$. The integration is then exactly as described in section 3.2. The consequences of this limit have been explored by Chandra et al. (2020). Alternatively, if there was a manifestly Lorentz invariant coupling to strain in terms of a four-displacement $\phi^2 \partial_\mu u^\mu$, this would lead to a true quantum version of the Larkin-Pikin mechanism. However, there is no time component of the displacement field, and it is not clear what such a field may represent.

If we take into account the quantum nature of elastic fluctuations, the integration of strain leaves us with the non-analytic vertex function above. Assuming that this interaction changes the critical behavior, and we will show later that it does, the theory can no longer be written in terms of the free energy of the rigid system using the Hubbard-Stratonovich transformation to a macroscopic strain-like variable. Instead, the Hubbard-Stratonovich field would have to depend on space and time, effectively reintroducing the strain field. Hence, there is no hidden thermodynamic variable, such as was assumed in Fisher's hidden variable approach, and thus there is no renormalization of the critical exponents (section 3.1).

The question of how the critical behavior is changed by lattice coupling is now open again. Is there a quantum equivalent of Fisher-renormalization? To learn about the critical behavior of the quantum system, we must resort to RG. As in the classical theory, one could perform an RG procedure on the action with phonons already integrated out eq. (5.3) (Sak, 1974), but this is complicated considerably by the non-analytic vertex function. This approach was explored on a similar theory, but without the infinite range interaction w , by Samanta et al. (2022). They expand the vertex function in spherical harmonics, at the cost of generating an infinite number of interaction terms, which are hard to manage. The other option is to perform the RG procedure on the original action, including phonons, which is what is done in the following.

5.2. RG analysis of quantum criticality in an isotropic elastic medium

We take the model already introduced in the previous section for an $O(N)$ quantum phase transition, coupled to an isotropic elastic medium. The only difference is that, since we do not integrate out strain, we can ignore the $q = 0$ strain components, i.e., we drop all terms depending on E and write

$$\mathcal{S} = \int d\tau d^d x \left(\frac{1}{2} \phi^T \left(-\partial_\tau^2 - c^2 \nabla^2 + r \right) \phi + u(\phi^2)^2 + \lambda \phi^2 (\nabla \cdot \mathbf{u}) + \frac{\rho}{2} \left[(\partial_\tau \mathbf{u})^2 + c_l^2 (\nabla \cdot \mathbf{u})^2 + 2c_t^2 \text{tr}\{\hat{\varepsilon}^2\} \right] \right). \quad (5.5)$$

In $3 + 1$ dimensions, both the u and the λ coupling terms are marginal. Following the same procedure that was outlined in section 3.3, we perform a Wilsonian RG by calculating the self-energy and vertex corrections to one-loop, followed by a rescaling of coordinates to derive RG flow around the Gaussian fixed point.

Calculation of the corrections

The fluctuations of the order parameter field at 0th order in the couplings are characterized by the Green function

$$G_{\alpha\beta}^{(0)}(\mathbf{q}, \omega) = \frac{\delta_{\alpha\beta}}{\omega^2 + c^2 q^2 + r}. \quad (5.6)$$

The fluctuations of the displacement field with $\mathbf{q} \neq 0$, on the other hand, are split into a longitudinal and a transversal contribution

$$F_{ij}^{(0)}(\mathbf{q}, \omega) = (\rho\omega^2 + D(\mathbf{q}))_{ij}^{-1} = \frac{1}{\rho} \left[\frac{\hat{q}_i \hat{q}_j}{\omega^2 + c_l^2 q^2} + \frac{\delta_{ij} - \hat{q}_i \hat{q}_j}{\omega^2 + c_t^2 q^2} \right]. \quad (5.7)$$

As the strain enters the elastic coupling only via its trace, analogous to section 3.3, this will project on the longitudinal modes. The bare and dressed Greens functions are connected by

$$\begin{aligned} G^{-1}(\mathbf{q}, \omega) &= G^{(0)-1}(\mathbf{q}, \omega) - \Sigma(\mathbf{q}, \omega), \\ F^{-1}(\mathbf{q}, \omega) &= F^{(0)-1}(\mathbf{q}, \omega) - \Pi(\mathbf{q}, \omega). \end{aligned} \quad (5.8)$$

For notational convenience, we define the integrals

$$\begin{aligned} I_{mn}(\mathbf{q}, \omega) &= \int_{q', \omega'} \left(\frac{1}{d} \text{tr} G^{(0)}(\mathbf{q} - \mathbf{q}', \omega - \omega') \right)^m (\mathbf{q}'^T F^{(0)}(\mathbf{q}', \omega') \mathbf{q}')^n \\ &= \int_{q', \omega} \left(\frac{1}{(\omega - \omega')^2 + c^2 (\mathbf{q} - \mathbf{q}')^2 + r} \right)^m \left(\frac{1}{\rho \omega'^2 + c_l^2 q'^2} \right)^n \end{aligned} \quad (5.9)$$

such that the previously encountered integrals defined in eq. (2.52) are given by $I_n = I_{n0}$. We obtain to one-loop order the self-energy corrections

$$\begin{aligned} \Sigma_{\alpha\beta}(\mathbf{q}, \omega) &= \text{---} \text{---} \text{---} + \text{---} \text{---} \text{---} \\ &= -2(2N + 4)uI_{10}\delta_{\alpha\beta} + 4\lambda^2 I_{11}(\mathbf{q}, \omega)\delta_{\alpha\beta}, \\ \Pi_{ij}(\mathbf{q}, \omega) &= \text{---} \text{---} \text{---} \\ &= 2N\lambda^2 I_{20}q_i q_j, \end{aligned} \quad (5.10)$$

and the vertex corrections

$$\begin{aligned}
u - u_0 &= -(4N + 32)u_0^2 I_{20} + 24\lambda_0^2 u_0 I_{21} - 4\lambda_0^4 I_{22}, \\
\lambda - \lambda_0 &= -(4N + 8)u\lambda I_{20} + 4\lambda^3 I_{21}.
\end{aligned} \tag{5.11}$$

The next step is to calculate the loop integrals. Two of the integrals (I_{10} and I_{20}) are already known from section 2.4. Similar to the realization that I_{20} can be written as an r -derivative of I_{10} , we can make our lives easier by writing I_{21} as an r -derivative of I_{11} and I_{22} as the c_l^2 -derivative of I_{21} . In fact, we only need to calculate one additional integral, which is

$$I_{11}(\mathbf{q}, \omega) = \frac{1}{\rho} \int_{\mathbf{q}', \omega'} \frac{1}{(\omega - \omega')^2 + c^2(\mathbf{q} - \mathbf{q}')^2 + r\omega^2 + c_l^2 q'^2} \frac{q'^2}{}, \tag{5.12}$$

containing one phonon propagator and one critical propagator. The dependence of the integrand on the relative momentum $\mathbf{q} - \mathbf{q}'$ complicates the calculation somewhat. We solve this integral by introducing a Feynman parameter, using the formula

$$\frac{1}{AB} = \int_0^1 dx \frac{1}{xA + (1-x)B}. \tag{5.13}$$

This simplifies the integrals over frequency and momentum considerably. We first execute the frequency integral, which may be simplified by completing the square in the denominator and shifting $\omega' \rightarrow \omega' + (1-x)\omega$

$$\begin{aligned}
&\int_{-\infty}^{\infty} d\omega' \frac{1}{(\omega - \omega')^2 + c^2(\mathbf{q} - \mathbf{q}')^2 + r} \frac{1}{\omega'^2 + c_l^2 q'^2} \\
&= \int_{-\infty}^{\infty} d\omega' \int_0^1 dx \frac{1}{(x[\omega'^2 + c_l^2 q'^2] + (1-x)[(\omega - \omega')^2 + c^2(\mathbf{q} - \mathbf{q}')^2 + r])^2} \\
&= \int_{-\infty}^{\infty} d\omega' \int_0^1 dx \frac{1}{(\omega'^2 + \Delta)^2},
\end{aligned} \tag{5.14}$$

where we have defined the shorthand Δ for the ω' -independent part of the denominator

$$\Delta = x(1-x)\omega^2 + xc_l^2 q'^2 + (1-x)[c^2(\mathbf{q} - \mathbf{q}')^2 + r]. \tag{5.15}$$

Now we can use the integral

$$\int_{-\infty}^{\infty} d\omega' \frac{1}{(\omega'^2 + \Delta)^2} = \frac{\pi}{2} \frac{1}{\Delta^{\frac{3}{2}}}. \tag{5.16}$$

For the q' integral, we first substitute $q' = k/\alpha(x)$, where $\alpha(x) = \sqrt{xc_l^2 + (1-x)c^2}$, and obtain

$$I_{11} = \frac{\pi}{2\rho} \int_0^1 dx \frac{1}{\alpha(x)^{d+2}} \int d^d k \frac{k^2}{[k^2 - 2\beta(x)\mathbf{k} \cdot \mathbf{q} + (1-x)(x\omega^2 + c^2q^2 + r)]^{\frac{3}{2}}} \quad (5.17)$$

with $\beta(x) = (1-x)c^2/\alpha(x)$. After defining another shorthand

$$\Theta = -\beta(x)^2q^2 + (1-x)(x\omega^2 + c^2q^2 + r) \quad (5.18)$$

we again complete the square in the denominator and shift $\mathbf{k} \rightarrow \mathbf{k} + \beta\mathbf{q}$. This creates a $\mathbf{k} \cdot \mathbf{q}$ term in the numerator which is an odd function in \mathbf{k} , thus giving no contribution to the integral

$$\begin{aligned} \int d^d k \frac{k^2}{[(k - \beta(x)q)^2 + \Theta]^{\frac{3}{2}}} &\stackrel{k \rightarrow k + \beta q}{=} \int d^d k \frac{(k + \beta(x)q)^2}{[k^2 + \Theta]^{\frac{3}{2}}} \\ &= \int d^d k \frac{k^2 + \beta(x)^2q^2}{[k^2 + \Theta]^{\frac{3}{2}}}. \end{aligned} \quad (5.19)$$

We now have two integrals with trivial angle dependence. Since we work in $d = 3$ spatial dimensions, the angular integral thus resolves to $S_3 = 4\pi$. For the radial integrals, we can make our lives easier by only considering the cutoff dependence since only these will enter the RG equations. Thus, we get the integrals

$$\int_0^{\alpha\Lambda} dk \frac{k^2}{(k^2 + \Theta)^{\frac{3}{2}}} = \text{Arsinh} \left(\frac{\alpha\Lambda}{\sqrt{\Theta}} \right) - \frac{\alpha\Lambda}{\sqrt{\Theta + \alpha^2\Lambda^2}} \approx \log \left(\frac{2\alpha\Lambda}{\sqrt{\Theta}} \right) - 1 \quad (5.20)$$

and

$$\begin{aligned} \int_0^{\alpha\Lambda} dk \frac{k^4}{(k^2 + \Theta)^{\frac{3}{2}}} &= \frac{3}{2} \left(\alpha\Lambda\sqrt{\Theta + \alpha^2\Lambda^2} - \Theta \text{Arsinh} \left(\frac{\alpha\Lambda}{\sqrt{\Theta}} \right) \right) \\ &\approx \frac{3}{2} \left(\alpha\Lambda^2 - \Theta \log \left(\frac{2\alpha\Lambda}{\sqrt{\Theta}} \right) \right). \end{aligned} \quad (5.21)$$

After this, only the x -integral is left. The complete integral is then given by

$$I_{11} \simeq \frac{K_d}{4\rho} \int_0^1 dx \frac{1}{\alpha^5} \left[\left(\beta^2q^2 - \frac{3\Theta}{2} \right) \log \left(\frac{2\alpha\Lambda}{\sqrt{\Theta}} \right) + \frac{3}{2}\alpha^2\Lambda^2 \right]. \quad (5.22)$$

where the symbol \simeq denotes equality up to cutoff-independent terms. Using the integrals

$$\begin{aligned} \int_0^1 dx \frac{1}{\alpha^3} &= \frac{2}{cc_l(c + c_l)} & \int_0^1 dx \frac{5\beta - 3(1-x)c^2}{2\alpha^5} &= \frac{2c}{3c_l(c + c_l)^3} \\ \int_0^1 dx \frac{(1-x)}{\alpha^5} &= -\frac{2c + c_l}{c^3c_l(c + c_l)^3} & \int_0^1 dx \frac{(1-x)x}{\alpha^5} &= -\frac{2c}{c_l(c + c_l)^3} \end{aligned} \quad (5.23)$$

the above expression can be completely resolved. We finally give the result for I_{11} as well as all the other derived integrals appearing in the self-energy and vertex correction

$$\begin{aligned}
I_{10} &\simeq \frac{1}{8\pi^2 c^3} [c^2 \Lambda^2 - r \log \Lambda], \\
I_{20} &= -\frac{\partial I_{10}}{\partial r} \simeq \frac{1}{8\pi^2 c^3} \log \Lambda, \\
I_{11} &\simeq \frac{1}{8\pi^2 \rho} \frac{1}{c^3 c_l (c + c_l)} \left[c^2 \Lambda^2 - \frac{2c + c_l}{c + c_l} r \log \Lambda \right] \\
&\quad - \frac{1}{4\pi^2 \rho c c_l (c + c_l)^3} \left(\omega^2 - \frac{1}{3} c^2 q^2 \right) \log \Lambda \\
I_{21} &= -\frac{\partial I_{11}}{\partial r} \simeq \frac{1}{8\pi^2 \rho} \frac{2c + c_l}{c^3 c_l (c + c_l)^2} \log \Lambda, \\
I_{22} &= -\frac{1}{\rho} \frac{\partial I_{21}}{\partial c_l^2} \simeq \frac{1}{8\pi^2 \rho^2} \frac{c^2 + 3c c_l + c_l}{c^3 c_l^3 (c + c_l)^2} \log \Lambda.
\end{aligned}$$

Compared to the classical theory, where the projected phonon propagator depended only on the direction of external momentum, not its magnitude, and was trivial in the isotropic case, the evaluation of the integrals in the quantum theory turned out to be quite involved, even in the case of isotropic elasticity. The fact that there is no separation into an angle- and magnitude-dependent contributions make the inclusion of lattice anisotropy unfeasible. The non-trivial dependence on the velocities of both critical and elastic modes is yet another consequence of Lorentz symmetry breaking.

RG flow equations

With the corrections calculated in the previous section we can derive the RG flow equations. The procedure has already been discussed in section 2.4 for the quantum $O(N)$ model with $z = 1$. The inclusion of the displacement field in the RG procedure has been discussed in section 3.3 in the context of a classical model, therefore we keep the discussion here brief.

We integrate out a momentum shell $q \in [\Lambda/b, \Lambda]$ with $b > 1$ and $\ell = \log b \ll 1$. We then rescale momentum and frequencies according to

$$\mathbf{q} = \mathbf{q}'/b, \quad \omega = \omega'/b^z. \quad (5.24)$$

For now, we let the dynamical exponent z be arbitrary. The scaling transformation acts on the fields in the form

$$\begin{aligned}
\phi(\mathbf{q}, \omega) &= \sqrt{Z_\phi} b^{\frac{d+3z}{2}} \phi'(\mathbf{q}', \omega'), \\
\mathbf{u}(\mathbf{q}, \omega) &= \sqrt{Z_u} b^{\frac{d+3z}{2}} \mathbf{u}'(\mathbf{q}', \omega'),
\end{aligned} \quad (5.25)$$

where we introduced two wave function renormalizations, Z_ϕ and Z_u . The parameters of the action are rescaled according to

$$\begin{aligned} c^2 &= c'^2 / (Z_\phi b^{(2z-2)}), & c_l^2 &= c_l'^2 / (Z_u b^{(2z-2)}), \\ u &= u' / (Z_\phi^2 b^{(3z-d)}), & \lambda &= \lambda' / (Z_\phi \sqrt{Z_u} b^{(5z-d-2)/2}), \\ r &= r' / (Z_\phi b^{2z}). \end{aligned} \quad (5.26)$$

Imposing the RG conditions

$$G^{-1}(0, \omega)|_{r=0} = \omega^2, \quad D^{-1}(\mathbf{q}, \omega)|_{r=0} \xrightarrow{\mathbf{q} \rightarrow 0} \rho \omega^2, \quad (5.27)$$

we find the flow of the wave function renormalizations

$$\begin{aligned} \frac{d \log Z_\phi}{d\ell} &= -\frac{1}{\pi^2 \rho} \frac{\lambda^2}{c c_l (c + c_l)^3} \\ \frac{d \log Z_u}{d\ell} &= 0. \end{aligned} \quad (5.28)$$

The full set of RG flow equations up to one-loop order is then complete with

$$\begin{aligned} \frac{dr}{d\ell} &= \left(2z + \frac{1}{2\pi^2 \rho} \frac{3c + c_l}{c^3 (c + c_l)^3} \lambda^2 - \frac{N + 2}{2\pi^2} \frac{u}{c^3} \right) r, \\ \frac{dc^2}{d\ell} &= \left(2z - 2 - \frac{4}{3\pi^2 \rho} \frac{\lambda^2}{c c_l (c + c_l)^3} \right) c^2, \\ \frac{dc_l^2}{d\ell} &= \left(2z - 2 - \frac{N}{4\pi^2 \rho} \frac{\lambda^2}{c_l^2 c^3} \right) c_l^2, \\ \frac{du}{d\ell} &= (3z - d)u - \frac{(N + 8) u^2}{2\pi^2 c^3} \\ &\quad + \frac{1}{\pi^2 \rho} \frac{4c^2 + 9c c_l + 3c_l^2}{c^3 c_l (c + c_l)^3} u \lambda^2 - \frac{1}{4\pi^2 \rho^2} \frac{c^2 + 3c c_l + c_l^2}{c^3 c_l^3 (c + c_l)^3} \lambda^4, \\ \frac{d\lambda}{d\ell} &= \left(\frac{5z - d - 2}{2} + \frac{1}{2\pi^2 \rho} \frac{3c + c_l}{c^3 (c + c_l)^3} \lambda^2 - \frac{N + 2}{2\pi^2} \frac{u}{c^3} \right) \lambda. \end{aligned} \quad (5.29)$$

In contrast to the classical theory, we find a non-trivial RG flow not just for c_l but also for c . The flow of c is caused by the explicit breaking of Lorentz invariance in the elastic coupling term. Alternatively, we can reformulate the above RG flow with a running dynamical exponent z . If we change the RG condition such that we demand $dc^2/d\ell$ to vanish, while z is allowed to change, we can derive an RG flow equation for z . The bare value would of course be unity, but with a correction of order λ^2 . This would be equivalent to changing the RG condition to preserve the $c^2 q^2$ term in the action. We will, however, stick to our original RG condition.

Analogous to section 3.3, the above equations can be simplified by introducing

dimensionless parameters

$$\vartheta = \frac{c_l}{c}, \quad \tilde{u} = \frac{1}{2\pi^2} \frac{u}{c^3}, \quad \tilde{\lambda}^2 = \frac{\lambda^2}{4\pi^2 \rho c_l^2 c^3}, \quad (5.30)$$

where the new parameter ϑ represents the ratio of the velocities of phonons to critical modes. In this representation, the RG flow is governed by only three equations

$$\begin{aligned} \frac{d\vartheta}{d\ell} &= \frac{1}{2} \left(\frac{16}{3} \frac{\vartheta^2}{(1+\vartheta)^3} - N\vartheta \right) \tilde{\lambda}^2, \\ \frac{d\tilde{u}}{d\ell} &= \epsilon\tilde{u} - (N+8)\tilde{u}^2 + \frac{12\vartheta(2+\vartheta)}{(1+\vartheta)^2} \tilde{u}\tilde{\lambda}^2 - \frac{4\vartheta(1+3\vartheta+\vartheta^2)}{(1+\vartheta)^3} \tilde{\lambda}^4, \\ \frac{d\tilde{\lambda}^2}{d\ell} &= \epsilon\tilde{\lambda}^2 - 2(N+2)\tilde{u}\tilde{\lambda}^2 + \left(N+4 - \frac{4}{(1+\vartheta)^2} \right) \tilde{\lambda}^4, \end{aligned} \quad (5.31)$$

where we have set $d = 3 - \epsilon$. Remarkably, the so far arbitrary dynamical exponent z drops out of the equations with the above choice of variables, which means these equations are independent of the above-mentioned change in the RG condition. In a sense, that makes the chosen dimensionless representation the most natural representation of the RG flow.

Note that from the above RG equations, we can reproduce the isotropic limit of the equations derived by Bergman & Halperin (1976) in eq. (3.68) by taking the limit $\rho \rightarrow 0$ of a vanishing mass density, which is equivalent to $c_l \rightarrow \infty$ or $\vartheta \rightarrow \infty$, while keeping the dimensionless couplings constant. Since quantum fluctuations are inherently dynamic, it seems fitting that their effect is connected to the relative velocities, which characterize the dynamics of each mode. Neglecting phonon dynamics restores the classical equations. However, we will see that neglecting dynamics is not permissible.

To calculate the critical exponents, we also need to know the RG flow equations for Z_ϕ and r , which are in terms of the dimensionless variables

$$\begin{aligned} \frac{d \log Z_\phi}{d\ell} &= -\frac{4\vartheta}{(1+\vartheta)^3} \tilde{\lambda}^2 \\ \frac{d \log r}{d\ell} &= 2z - (N+2)\tilde{u} + \frac{2\vartheta^2(3+\vartheta)}{(1+\vartheta)^3} \tilde{\lambda}^2. \end{aligned} \quad (5.32)$$

Note that r is not dimensionless and the appearance of z in its β -function is a result of the choice of RG condition. Had we chosen to keep the gradient term fixed, this would correspond to a reparametrization that effectively scales r with a factor of c^2 . This choice will, however, not affect the results, and we set $z = 1$ in the following.

Fixed points

Compared to the classical case (eq. (3.70)), where at least in the isotropic case the flow of the couplings can be solved independently, in the equations derived above, the situation is complicated by the dependence on ϑ in all terms that stem from the elastic coupling $\tilde{\lambda}$. To get a qualitative picture of the flow, it is instructive to first look at the flow close to the $\tilde{\lambda} = 0$ surface, where the RG equations reduce to the ones of the $O(N)$ model already known from section 2.4 with an unstable Gaussian (G) and a stable Wilson-Fisher (WF) fixed point. We may then ask if the system is stable or unstable with respect to an infinitesimal elastic coupling $\tilde{\lambda}$. This can be checked by calculating its scaling dimension around $\tilde{\lambda}^2 = 0$ from eq. (5.31),

$$\left. \frac{d \log \tilde{\lambda}^2}{d\ell} \right|_{\tilde{\lambda}=0} = \frac{1}{\tilde{\lambda}^2} \left. \frac{d\tilde{\lambda}^2}{d\ell} \right|_{\tilde{\lambda}=0} = \epsilon - 2(N+2)\tilde{u}. \quad (5.33)$$

The elastic coupling is marginally relevant (positive scaling dimension of order ϵ), if the right-hand side is larger than zero. We show that a positive scaling dimension of $\tilde{\lambda}^2$ coincides with the criterion given in eq. (5.1), $\alpha_q > 0$. The correlation length exponent of any fixed point on the $\tilde{\lambda}^2 = 0$ surface is given by

$$1/\nu = \left. \frac{d \log r}{d\ell} \right|_{\tilde{\lambda}=0} = 2 - (N+2)\tilde{u}^*. \quad (5.34)$$

Assuming hyperscaling, the specific heat exponent is then

$$\alpha_q|_{\tilde{\lambda}^2=0} = \frac{\epsilon}{2} - (N+2)\tilde{u}^*. \quad (5.35)$$

Therefore, positive α_q corresponds to a flow away from the $\tilde{\lambda}^2 = 0$ surface. Remembering the values for G and WF fixed points from section 2.4, we see that for $\epsilon > 0$ at G this condition is always fulfilled, thus, the elastic coupling is relevant, and at WF it is relevant for $N < 4$ and irrelevant for $N > 4$.

For finite elastic coupling $\tilde{\lambda} \neq 0$, we first consider the flow of the velocity ratio ϑ . Physically, its bare value ϑ_0 should always be positive. Then for $N \geq 1$ the RG flow of ϑ eq. (5.31) is always negative, only stopping for $\vartheta = 0$. It follows that c_l decreases faster than c under RG.

Interestingly, if we allow for a moment for N to be something else than a positive integer eq. (5.31) has a fixed point at a finite ϑ if $N \leq \frac{64}{81} \approx 0.79$. This is significant in that the absence of a fixed point where both ϑ and λ remain finite seems to be, in some sense, incidental. There is no obvious reason why in a theory that has analogs to the velocities c and c_l , but with slightly different combinatorics or differently formed integrals, there should not be non-trivial fixed points. However, in the case of the $O(N)$ model only the trivial fixed point exists.

We conclude that a true fixed point at finite elastic coupling can only exist in the

limit $\vartheta \rightarrow 0$. Formally, the RG flow equations have two additional solutions with a finite value for the dimensionless elastic coupling $\tilde{\lambda}^2$. However, only one of them is positioned at a real value of $\tilde{\lambda}$, corresponding to the modified Wilson-Fisher fixed point WF^* , see table 5.2.

Since this new fixed point exist only in the limit $\vartheta \rightarrow 0$, we can see from eq. (5.32) that all contributions from elastic coupling to the flow of Z_ϕ and \mathbf{r} vanish. Thus, WF^* will have identical critical exponents to its counterpart WF. However, as we see later, the new fixed point is characterized by a renormalized dynamical exponent of the phonon.

Table 5.2.: Fixed points of the $O(N)$ model coupled to an isotropic elastic medium, with values of the dimensionless couplings, the renormalized dynamical exponent of the phonons z_u , and the scaling dimension of the dimensionless elastic coupling $\tilde{\lambda}$.

Fixed point	ϑ	\tilde{u}	$\tilde{\lambda}^2$	z_u	$\frac{d \log \tilde{\lambda}^2}{d\ell} _{\tilde{\lambda}=\tilde{\lambda}^*}$
G	$\mathbb{R}_{>0}$	0	0	1	ϵ
WF ($\epsilon > 0$)	$\mathbb{R}_{>0}$	$\frac{\epsilon}{N+8}$	0	1	$\frac{4-N}{N+8}\epsilon$
$\text{WF}^*(\epsilon > 0, N > 4)$	0	$\frac{\epsilon}{N+8}$	$\frac{N-4}{N(N+8)}\epsilon$	$1 - \frac{4-N}{2(N+8)}\epsilon$	

The stability of a given fixed point and the direction of the RG flow within the $(\tilde{u}, \tilde{\lambda}^2)$ plane around it are determined by the matrix

$$\frac{d}{d\ell} \begin{pmatrix} \delta\tilde{u} \\ \delta\tilde{\lambda}^2 \end{pmatrix}_{\vartheta \rightarrow 0} = \begin{pmatrix} \epsilon - 2(N+8)\tilde{u}^* & 0 \\ -2(N+2)(\tilde{\lambda}^*)^2 & \epsilon + 2N(\tilde{\lambda}^*)^2 - 2(N+2)\tilde{u}^* \end{pmatrix} \begin{pmatrix} \delta\tilde{u} \\ \delta\tilde{\lambda}^2 \end{pmatrix}. \quad (5.36)$$

For $\epsilon > 0$, there are two scenarios for the RG flow corresponding to positive and negative α_q . For $N < 4$, we have a positive $\alpha_{q,\text{WF}}$, leading to relevant elastic coupling as expected. The RG flow for this case in the small ϑ limit is shown in fig. 5.1. There is no stable fixed point, and instead, we get runaway flow in $\tilde{\lambda}$. We will talk about the meaning of runaway flow later on.

For $N > 4$, where $\alpha_{q,\text{WF}}$ is negative, the WF fixed point is stable. The additional fixed point WF^* is present in the $\vartheta \rightarrow 0$ limit, which is repulsive along the $\tilde{\lambda}^2$ axis. The parameter space is split into a region of flow into WF and a region above a critical \tilde{u} -dependent threshold value of $\tilde{\lambda}^2$ where there is runaway flow again, as can be seen in fig. 5.2. The separatrix between the two regions goes through the WF^* fixed point.

Lifting the $\vartheta \rightarrow 0$ restriction, we find that in the three dimensional parameter space spanned by ϑ , \tilde{u} and $\tilde{\lambda}^2$, the separatrix is a sheet the form of which can be found numerically. It is shown in fig. 5.3.

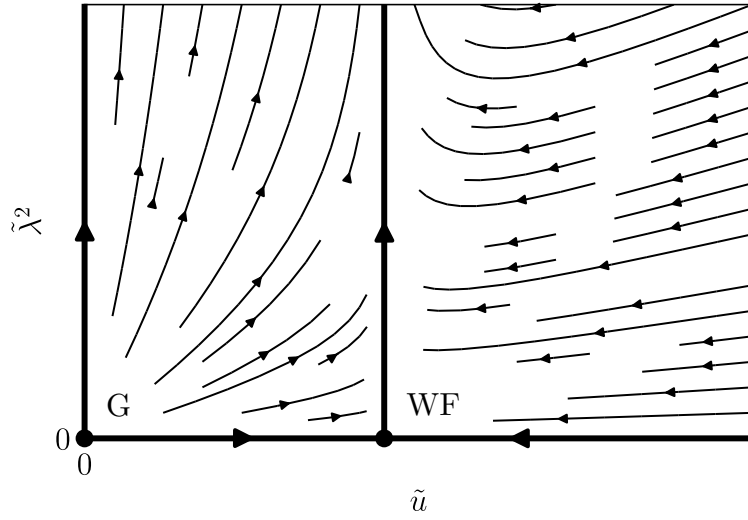


Figure 5.1.: RG flow for $\epsilon > 0$ and $1 \leq N < 4$ in the $\vartheta \ll 1$ limit. The G and WF fixed points are unstable with respect to the dimensionless elastic coupling $\tilde{\lambda}^2$ resulting in runaway flow.

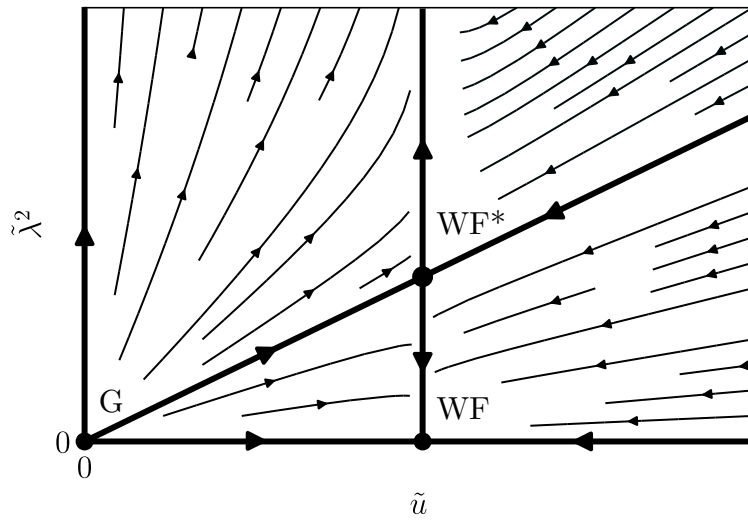


Figure 5.2.: RG flow for $\epsilon > 0$ and $N > 4$ in the $\vartheta \ll 1$ limit. G is unstable, while WF is stable. The additional fixed point WF* is repulsive with respect to the dimensionless elastic coupling $\tilde{\lambda}^2$ leading to runaway flow for sufficiently large elastic coupling, and flow towards WF otherwise.

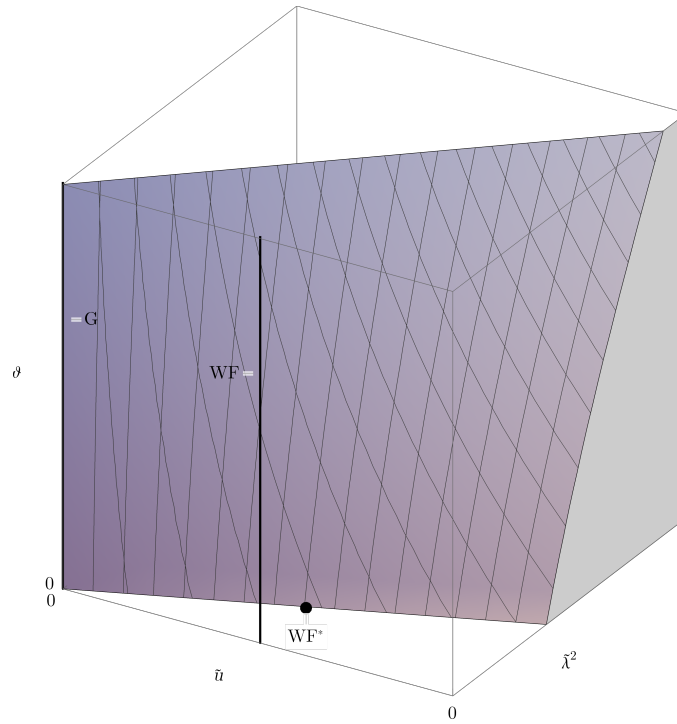


Figure 5.3.: Separatrix in $(\vartheta, \tilde{u}, \tilde{\lambda}^2)$ space for $\epsilon > 0$ and $N > 4$. Since G and WF are fixed points for every value of ϑ they are represented as lines in the $\tilde{\lambda} = 0$ plane. For initial values with $\tilde{\lambda}$ lower than the separatrix the flow is towards WF , above it is towards strong coupling. For initial values on the separatrix, the flow stays on the separatrix and approaches WF^* .

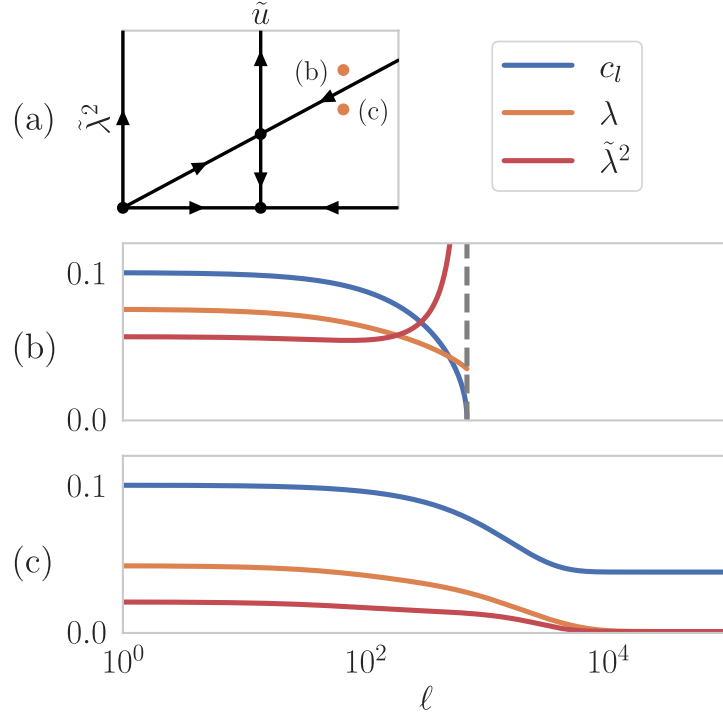


Figure 5.4.: RG flow of the dimensionful parameters c_l and λ as well as the dimensionless variable $\tilde{\lambda}$ for $\epsilon = 0.01$ and $N = 5$ using initial values $c_0 = 1$, $c_{0,l} = 0.1$, $u_0 = 0.5$, and (b) $\lambda_0 = 0.015$ above the separatrix leading to runaway flow and a vanishing phonon velocity, (c) $\lambda_0 = 0.009$ below the separatrix, and the flow is towards the WF fixed point with c_l saturating at a finite value.

To investigate the meaning of the instability that was encountered for $\epsilon > 0$ and $N < 4$ already at infinitesimal elastic coupling and in the other cases above some threshold value, an example of a numerically determined solution is shown in fig. 5.4. In the RG flow diagrams, the instability manifests as a diverging dimensionless coupling $\tilde{\lambda}$. A diverging $\tilde{\lambda}$ means that in terms of the dimensionful parameters λ , c , and c_l either λ diverges or at least one of the velocities vanishes. Since we have already established the $\vartheta \rightarrow 0$ limit, it would be c_l that vanishes. It turns out that, as shown in the scenario of runaway flow, both λ and c_l decrease. Since the flow in c_l is driven by the elastic coupling at large enough initial coupling λ_0 , c_l^2 decreases faster than λ^2 and vanishes at a finite RG scale. If the initial λ is small enough, then the elastic coupling vanishes asymptotically, but fast enough such that the flow of c_l tends to a finite value.

An interesting case happens at the boundary between the region of runaway flow and the basin of attraction of the WF fixed point. If initial values are on or sufficiently close to the separatrix shown in fig. 5.3, the flow is towards the WF* fixed point. The elastic coupling $\tilde{\lambda}^2$ then tends to a constant value $\tilde{\lambda}_{\text{WF}^*}^2$. Consequently, according to

eq. (5.29) while the RG flow is approaching WF^* the phonon velocity c_l vanishes asymptotically with a power law of b

$$c_l(\ell) \sim e^{-\frac{N\tilde{\lambda}_{\text{WF}^*}^2}{2}\ell} = b^{-\frac{4-N}{2(N+8)}\epsilon}. \quad (5.37)$$

This can be seen as a modification of the phonon dynamical exponent, which is usually fixed by the dispersion relation $\omega = c_l q$. The relation between correlation time and correlation length is then $\tau \propto c_l^{-1}(\xi)\xi = \xi^{z_u}$. The dynamical exponent of the phonon $z_u = 1 + \delta z$ is thus modified by the correction from the scaling of the sound velocity

$$\delta z = \frac{4-N}{2(N+8)}\epsilon = \alpha_{\text{WF}}. \quad (5.38)$$

An example of the power law behavior in c_l can be seen in fig. 5.5 in the region of influence of WF^* .

In any case, the renormalization of the dynamical exponent δz is given by the α_q exponent of the corresponding stable fixed point. The connection between the dynamical and specific heat exponent can be understood in terms of the perturbative argument brought forth in section 3.1 that the bulk modulus and thus the phonon velocity receive a correction that is proportional to the specific heat

$$\delta c_l^2 \propto \delta K \propto \frac{\partial \mathcal{F}}{\partial \epsilon^2} \propto \lambda^2 \langle \phi^2 \phi^2 \rangle \propto r^{-\alpha_q}. \quad (5.39)$$

Put in terms of the correction length, the connection is

$$\delta c_l \propto \xi^{-\frac{\alpha_q}{2\nu}} \quad (5.40)$$

So we should expect the correction to the dynamical exponent to be $\alpha_q/2\nu$, which agrees with our result eq. (5.38) up to first order in ϵ .

RG flow at the upper critical dimension

As we have seen in section 2.4 the corrections to scaling exponents at finite ϵ translate into logarithmic corrections at the upper critical dimension. Additionally, the $\epsilon = 0$ sometimes allows for analytic solutions of the RG flow equations, which can be interpreted more directly than the numerical examples we have seen so far.

The RG flow is still complicated by the flowing velocity ratio ϑ . However, in the limit of small ϑ , the equations simplify to

$$\begin{aligned} \frac{d\tilde{u}}{d\ell} &\approx -\frac{(N+8)}{2\pi^2}\tilde{u}^2, \\ \frac{d\tilde{\lambda}^2}{d\ell} &\approx -\frac{(N+2)}{\pi^2}\tilde{u}\tilde{\lambda}^2 + \frac{N}{2\pi^2}\tilde{\lambda}^4. \end{aligned} \quad (5.41)$$

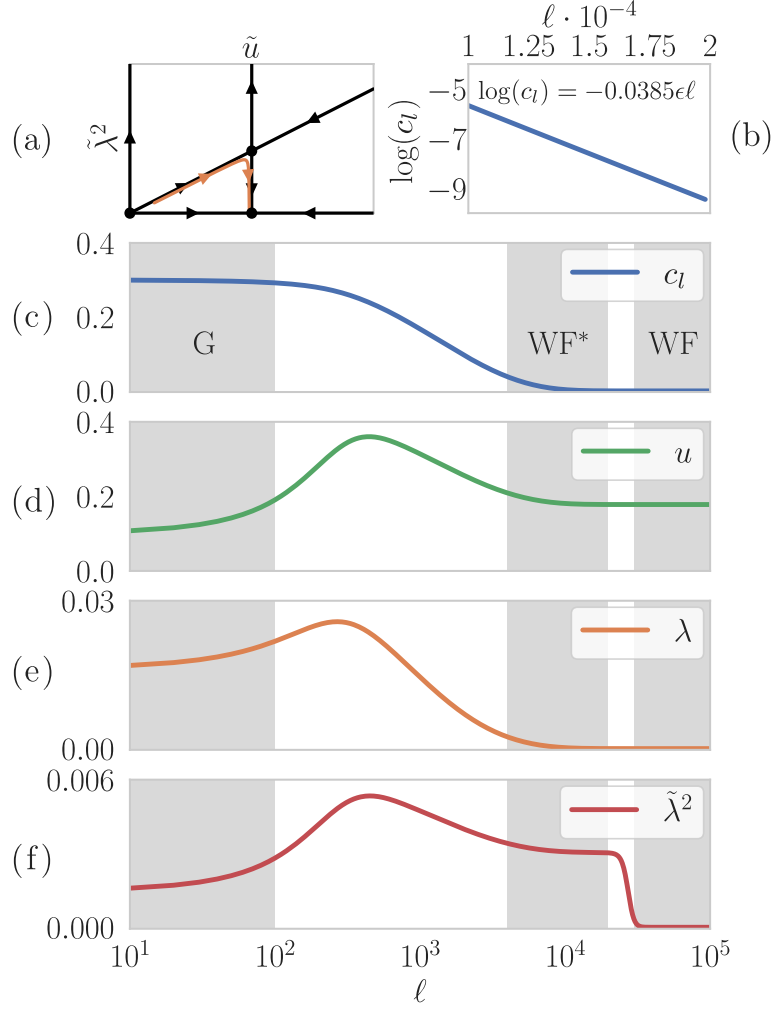


Figure 5.5.: RG flow in the domain of influence of the different fixed points, numerically calculated with $\epsilon = 0.01$ and $N = 5$. Initial values of the parameters are chosen just below the separatrix, with $c_0 = 1$, $c_{l,0} = 0.3$, $u_0 = 0.1$, and $\lambda_0 \approx 0.0163$. The flow is shown of (c) c_l , (d) u , (e) λ , and (f) $\tilde{\lambda}^2$ as a function of the RG scale ℓ . The shaded regions indicate the range of scale where the RG flow is governed by a specific fixed point with crossovers in between them. Initially, the flow is influenced by G. There is a range where the flow is dominated by WF* leading to a power-law dependence of the phonon velocity shown in (b) with the exponent $\delta z = \frac{1}{2} \frac{N-4}{N+8} \epsilon \approx 3.846 \times 10^{-4}$. Eventually, the flow is governed by the WF.

Notably, the RG flow of \tilde{u} is now decoupled from the elastic coupling $\tilde{\lambda}^2$. The solution is equivalent to the one we saw in section 2.4

$$\tilde{u}(\ell) = \frac{\tilde{u}_0}{(N+8)\tilde{u}_0\ell + 1}, \quad (5.42)$$

where \tilde{u}_0 is the bare value, $\tilde{u}(0) = \tilde{u}_0$. We may redefine the RG scale with a linear transformation

$$\tilde{\ell} = (N+8)\tilde{u}_0\ell + 1. \quad (5.43)$$

Thus, we conclude that $\tilde{u} \sim \tilde{\ell}^{-1} \sim (\log b)^{-1}$ is marginally irrelevant.

At $\tilde{u}_0 = 0$ one finds for the elastic coupling

$$\tilde{\lambda}^2(\ell) = \frac{\tilde{\lambda}_0^2}{1 - N\tilde{\lambda}_0^2\ell}. \quad (5.44)$$

The above solution diverges at a finite RG scale $\ell^* = (\tilde{\lambda}_0^2 N)^{-1}$, indicating a vanishing phonon velocity c_l .

For $\tilde{u}_0 \neq 0$ we may still find an analytic solution, by plugging in the solution eq. (5.42). The resulting first-order equation for $\tilde{\lambda}^2$ is solved by

$$\tilde{\lambda}^2(\ell) = \begin{cases} \frac{\frac{N-4}{N}\tilde{u}_0}{\left(\frac{N-4}{N}\frac{\tilde{u}_0}{\tilde{\lambda}_0^2} - 1\right)\tilde{\ell}^{\frac{2(N+2)}{N+8}} + \tilde{\ell}} & \text{for } N \neq 4 \\ \frac{3\tilde{u}_0\tilde{\lambda}_0^2}{\tilde{\ell}(3\tilde{u}_0 - \tilde{\lambda}_0^2 \log \tilde{\ell})} & \text{for } N = 4. \end{cases} \quad (5.45)$$

The behavior is quite similar to the finite ϵ case: For $N \leq 4$, $\tilde{\lambda}^2$ is marginally relevant and diverges at a finite ℓ . For $N > 4$, the divergent behavior is only observed for sufficiently strong initial elastic coupling, where the criterion can be read off the above solution

$$\tilde{\lambda}_0^2 > \frac{N-4}{N}\tilde{u}_0. \quad (5.46)$$

The separatrix seen earlier in the $\epsilon > 0$ and $N > 4$ case thus survives the $\epsilon \rightarrow 0$ limit as shown in fig. 5.6. Note that at finite ϑ the separatrix will be modified, analogous to the finite ϵ case.

The renormalization of the dynamical exponent also becomes a logarithmic correction at the upper critical dimension. If the initial couplings are on the separatrix, then c_l vanishes logarithmically

$$c_l \sim (\log b)^{-\frac{N-4}{2(N+8)}} \sim \left(\log \frac{\xi}{\xi_0}\right)^{-\frac{N-4}{2(N+8)}}, \quad (5.47)$$

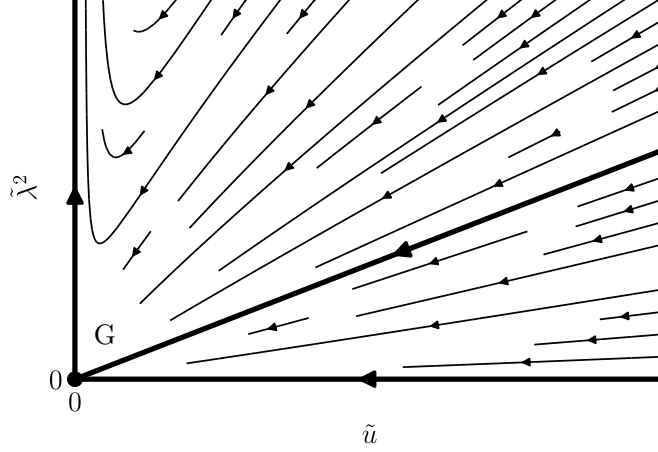


Figure 5.6.: RG flow at the upper critical dimension $\epsilon = 0$ for $\vartheta \ll 1$ and $N > 4$. There exists a separatrix below which the flow is towards the Gaussian fixed point. Above the separatrix the flow is towards strong coupling.

see fig. 5.7. Thus, there is a logarithmic correction to the dynamical exponent, with the correlation time depending on the correlation length like $\tau \sim \xi^z (\log \xi / \xi_0)^{-\hat{z}}$, where $\hat{z} = \frac{N-4}{2(N+8)}$.

5.3. Microscopic and macroscopic instability of the crystal lattice

So far, we have discussed the RG flow of the parameters that govern the microscopic fluctuations of both order parameter field ϕ and the displacement field \mathbf{u} . However, we still need to connect this to the macroscopic, observable, critical behavior of the system.

From the previous section, we know that, depending on the flavor number N and the initial values of the parameters, the flow can be either towards strong coupling $\tilde{\lambda}^2 \rightarrow \infty$, towards weak coupling $\tilde{\lambda}^2 \rightarrow 0$ or, as an edge case, if the coupling is exactly on the separatrix that exists for $N > 4$, towards a finite fixed point value of $\tilde{\lambda}^2$.

In any case, the renormalization of the elastic constants, and therefore the fate of the crystal lattice, is determined by the equation

$$\frac{dc_l^2}{dl} = -N\tilde{\lambda}^2 c_l^2. \quad (5.48)$$

As we have observed before, the right-hand side of this equation is always negative, and the flow is always to smaller values.

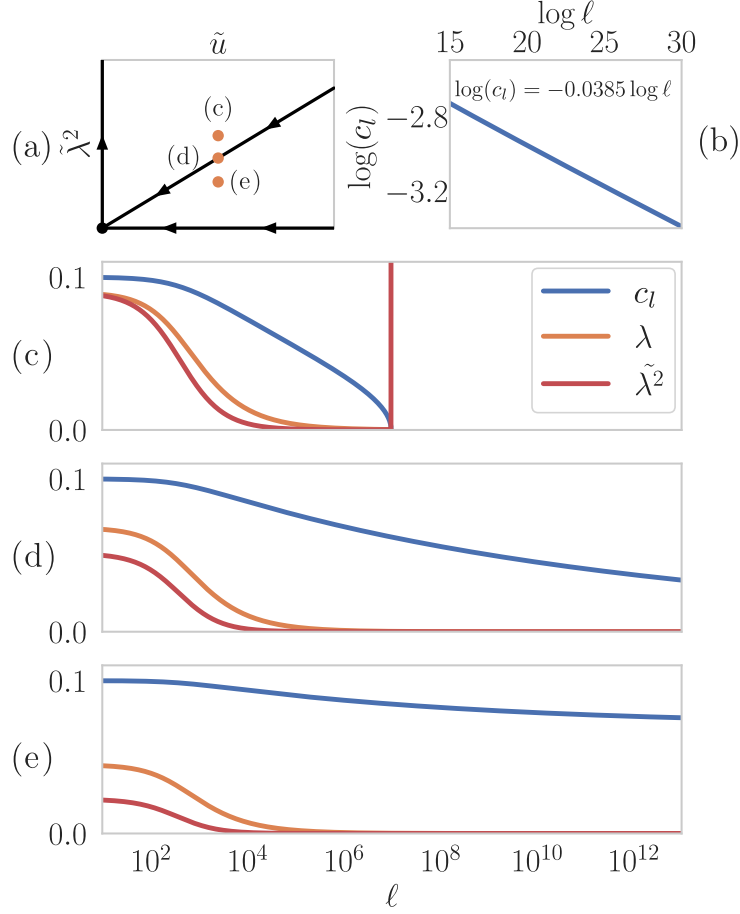


Figure 5.7.: RG flow at the upper critical dimension $\epsilon = 0$ for $N = 5$. with the starting values $c_0 = 1$, $c_{l,0} = 0.1$, $u_0 = 0.1$, and varying elastic couplings (c) $\lambda_0 = 0.006$, (d) $\lambda_0 \approx 0.0045$, and (e) $\lambda_0 = 0.003$ located above, on, and below the separatrix, respectively. Shown are the flow in c_l , λ , and $\tilde{\lambda}^2$ in each case. Above the separatrix (c) the phonon velocity vanishes at a finite RG scale. On the separatrix (d) the phonon velocity $c_l \sim \ell^{-\hat{z}}$ vanishes logarithmically with exponent $\hat{z} = \frac{N-4}{2(N+8)} = 0.03846\dots$, as illustrated in panel (b). Below the separatrix (e) c_l tends to a finite value.

If $\tilde{\lambda}^2$ diverges, the flow accelerates until c_l vanishes at a finite RG scale. Note that a diverging dimensionless coupling $\tilde{\lambda}$ this does not necessarily imply that the dimensionful elastic coupling λ becomes large, but rather that the longitudinal phonon velocity c_l becomes small. In other words, in an absolute sense, the interaction between lattice degrees of freedom does not become stronger, but the lattice becomes softer and therefore responds more strongly to the forces exerted on it.

With the phonon velocity c_l vanishing, the bulk crystal becomes unstable against longitudinal fluctuations, which results in a phase transition of the lattice. Since we are assuming an isotropic medium and therefore the phonon velocity vanishes in all directions simultaneously this transition would be isostructural, meaning that on both sides of the transition the crystal symmetry is the same. Isostructural transitions are generically first-order and are associated with a jump in the lattice constant, except for special points that require fine-tuning. The nature of such transitions was discussed in detail by Cowley (1976).

However, we may ask if this microscopic instability is ever reached. At finite phonon velocity, the system is microscopically stable. Microscopic stability is, however, not the same as macroscopic stability. Even though in a truly infinite system all modes are stable at finite phonon velocity, in reality, crystals are finite and have collective modes at a scale of the crystal size that are not captured by the usual phonon picture. The exact nature of these modes depends on the geometry and boundary conditions.

In the case of free boundary conditions, where the surface elements are allowed to adjust to applied forces, one generally finds that some of the macroscopic modes become unstable when one of the moduli vanishes. Therefore, the macroscopic stability of the crystal is not determined by the phonon velocities, but by the elastic moduli, in the isotropic case only K and μ . They are connected to the microscopic velocities via eq. (1.49). Since the transversal phonons do not couple to the order parameter field, the transversal phonon velocity is not renormalized, nor is the shear modulus. Solving for K yields

$$K(\ell) = \rho \left(c_l^2(\ell) - \frac{4}{3} c_t^2 \right). \quad (5.49)$$

Thus K vanishes once c_l reaches a threshold value given by $c_{l,\text{cr}}^2 = 4\mu/3\rho$. This would, analogous to the microscopic instability, trigger a first-order isostructural transition.

On the other extreme, we may apply pinned boundary conditions, holding every surface element at a fixed position, such as suggested by Bergman & Halperin (1976) for the classical equivalent. The pinned boundary stabilizes the crystal against the macroscopic instability. In this case, we expect the critical behavior to be determined by the microscopic degrees of freedom.

One may ask if pinning every single point on the surface is truly necessary to avoid the $K = 0$ instability, since this is experimentally unfeasible and thus is more a thought experiment than an actual one. The answer to this question is mostly unanswered and will depend on geometry. For simple geometries like a cube, one can show that fixing two faces is enough to avoid unstable modes, even at vanishing bulk modulus.

Since in any scenario, the sound velocity is lowered close to the transition, the discussion of the macroscopic instability also applies there. If the flow is towards weak coupling $\tilde{\lambda}^2 \rightarrow 0$. The phonon velocity is still renormalized but tends to a finite value. There is no microscopic instability since all phonon velocities remain finite. However, if the phonon velocity is lowered below the threshold value, the macroscopic instability may still be reached.

In the special case of flow on the separatrix towards the finite $\tilde{\lambda}^2$ fixed point WF*, which is possible for $N > 4$, the value that c_l tends asymptotically to 0. This case is similar to the classical theory (section 3.3) in the $N < 4$ case, At any finite RG scale, the value bulk system remains microscopically stable, but the system is guaranteed to encounter the macroscopic instability if boundary conditions allow it. However, contrary to the classical phase transition, where one finds Fisher-renormalized exponents, for the quantum transition, the exponents are Wilson-Fisher-type except for the dynamical exponent for the phonon z_u , which is renormalized as the phonon velocity vanishes as a power law

$$c_l \sim \xi^{-\delta z}, \quad (5.50)$$

where $z_u = 1 + \delta z$.

The case $\epsilon = 0$ is quite similar, except that here the corrections are logarithmic. For $N < 4$, the flow is towards strong coupling with logarithmically diverging $\tilde{\lambda}^2$. The microscopic instability is still present but at an exponentially large RG scale. For $N > 4$, it again depends on the initial values of the parameters. Flow is only towards strong coupling for sufficiently large values of $\tilde{\lambda}^2$. For initial couplings on the separatrix in fig. 5.6 the $\tilde{\lambda}^2$ logarithmically vanishes according to

$$\tilde{\lambda}^2(\ell) \approx \frac{2\pi^2(N-4)}{N(N+8)} \frac{1}{\ell}. \quad (5.51)$$

and so does the phonon velocity

$$c_l \sim \left(\log \frac{\xi}{\xi_0} \right)^{-\frac{N-4}{2(N+8)}} \quad (5.52)$$

as a function of $\xi = \xi_0 e^\ell$, resulting in a logarithmic correction to the phonon dynamical exponent. If the initial elastic coupling is small, then $\tilde{\lambda}^2$ vanishes fast enough such that c_l^2 tends towards a finite value. The argument of the macroscopic

instability still applies in all cases where c_l is renormalized below the threshold value.

In conclusion, we find the critical behavior near the quantum critical point to be quite different from the classical transition. In contrast to the finite temperature transition, the zero temperature transition does not show Fisher-renormalization but instead is microscopically unstable for $\alpha_q > 0$. In the inverse case $\alpha_q < 0$, we find that for small coupling, Wilson-Fisher physics is restored, analogous to the classical case, while for not too small coupling we predict a microscopic instability, or with coupling at the threshold between the two cases, a renormalized dynamical exponent.

6. Ferroelectric quantum criticality in an elastic medium

Ferroelectric transitions are of fundamental interest when it comes to questions of lattice effects on phase transitions because it is itself a kind of structural transition in the class of ferrodistoritive transitions. The ferroelectric order is essentially a frozen optical phonon, which induces a net polarization. Of course the condensing optical phonon branches couple to the acoustic phonons in ways dictated by the lattice symmetry. The form of this coupling can be derived by continuing the expansion in eq. (1.4) to the quartic level, keeping only terms that are relevant in the RG sense. The anharmonic coupling at the cubic level then represents the acoustic-optical phonon interaction and at the quartic level a self-interaction of the optical phonon.

In ferroelectrics that are also piezoelectric, the leading coupling is linear, and as a result, the transition is dominated by critical elasticity (Levanyuk & Sobyenin, 1970; Villain, 1970). If on the other hand, piezoelectricity is forbidden by symmetry the leading coupling is quadratic. An interesting set of materials where quadratic coupling dominates is the quantum paraelectrics, such as SrTiO_3 and KTaO_3 (Rowley et al., 2014), where ferroelectric order is suppressed by quantum fluctuations at low temperatures, but may be driven across a ferroelectric quantum critical point using pressure (Coak et al., 2020). They show an interesting temperature dependence that shows signatures of coupling to acoustic phonon in the low-temperature regime (Coak et al., 2020; Khmel'nitskii & Shneerson, 1971; Rowley et al., 2014).

An important ingredient for describing ferroelectric criticality is the inclusion of long-range dipolar interaction. It turns out that this significantly changes the critical behavior of the quantum $O(N)$ model. Khmel'nitskii & Shneerson (1973) first did this calculation for an $O(3)$ model with dipolar interaction in $3 + 1$ dimensions. They show that dipolar interaction changes the universality class of the transition from Wilson-Fisher (WF) to what we will refer to as Khmel'nitskii-Shneerson (KS) universality class. They also show that with the inclusion of dipolar interaction, cubic anisotropy becomes relevant, indicating an instability, where the effective quartic self-interaction vanishes, leading to a first-order transition.

Besides dipolar interaction, there is an important difference to the generic $O(N)$ model analyzed in section 5.2 in that the order parameter, representing an optical phonon is now a real space vector and is therefore bound to transform the same as

the displacement field \mathbf{u} under rotations. This allows for an isotropic coupling to shear strain, which leads to a renormalization of the transversal acoustic phonon velocity, not just the longitudinal one. This has important consequences for the critical behavior, since not only the bulk modulus is renormalized, but the shear modulus as well. In both the classical and quantum phase transition, we encounter a new type of instability, where the RG flow is towards a vanishing shear modulus.

In this chapter, section 6.1 covers the work by Khmel'nitskii & Shneerson (1973) on the criticality with dipolar interaction. After that, we move on to our own calculations. The RG flow of the isotropic ferroelectric with quadratic lattice coupling is derived in section 6.2, which combines KS physics with the insights we gained in chapter 5. We then take the classical limit and analyze the resulting RG equations in section 6.3. Finally, the instabilities found in the RG equations of the quantum transition are analyzed in section 6.4. The contents of section 6.2, section 6.3 and section 6.4 are original to this thesis, they have not been published yet.

6.1. Quantum criticality in the presence of dipolar interaction

If the order parameter field ϕ represents a degree of freedom that is associated with a dipole moment, such is the case in ferroelectrics or ferromagnets, there is a long-range dipole-dipole interaction between ϕ at different points. This gives a contribution to the action that is in the isotropic case of the form

$$\mathcal{S}_{\text{dipolar}} = s \int_{\mathbf{q}} \frac{(\mathbf{q} \cdot \phi)^2}{q^2}. \quad (6.1)$$

The above expression contains the scalar product between the reciprocal space vector \mathbf{q} and the order parameter ϕ , which is of course only meaningful if the flavor number is equal to the dimension $N = d$.

As a first step, we want to know what the effect of this term is in isolation, postponing the discussion of elastic coupling to section 6.2. We will also discuss how it changes the effect of cubic anisotropy. To not repeat ourselves too much we will include cubic anisotropy from the start, see section 2.5, obtaining the action

$$\begin{aligned} \mathcal{S} = & \int_{\mathbf{q}, \omega} \frac{1}{2} \phi_{\mathbf{q}}^T \left(\omega^2 + c^2 q^2 + r + s \hat{q} \hat{q}^T \right) \phi_{-\mathbf{q}} \\ & + \int_{\mathbf{q}, \omega} \int_{\mathbf{q}', \omega'} \int_{\mathbf{q}'', \omega''} V_{ijkl} \phi_{i, \mathbf{q}} \phi_{j, \mathbf{q}'} \phi_{k, \mathbf{q}''} \phi_{l, -\mathbf{q} - \mathbf{q}' - \mathbf{q}''}, \end{aligned} \quad (6.2)$$

where $\hat{q}_i = q_i/q$ is the unit vector in \mathbf{q} direction and the quadratic interaction is given by the tensor

$$V_{ijkl} = u\delta_{ij}\delta_{kl} + vg_{ijkl}. \quad (6.3)$$

At the Gaussian level, the dipolar term splits the d modes of ϕ into $d-1$ transversal modes ($\mathbf{q} \cdot \phi = 0$) and one longitudinal mode ($\mathbf{q} \cdot \phi \neq 0$). The longitudinal mode is the only one that sees the dipolar interaction in the form of a shifted gap $r_l = r + s$, while the transversal modes remain unchanged $r_t = r$. In general, the bare propagator is given by (Roussev & Millis, 2003)

$$G_{ij}^{(0)}(\mathbf{q}, \omega) = \frac{1}{\omega^2 + c^2q^2 + r} \left(\delta_{ij} - \hat{q}_i\hat{q}_j \frac{s}{\omega^2 + c^2q^2 + r + s} \right) \quad (6.4)$$

However, as the system approaches criticality the contribution of ω , q , and r will become negligible compared to the strength of dipolar interaction s . Assuming s is positive the longitudinal mode will be stabilized by dipolar interaction, so only the transversal modes become critical as r vanishes. Therefore we consider the Green's function only for the transversal modes

$$G_{ij}^{(0)}(\mathbf{q}, \omega) \approx \frac{\delta_{ij} - \hat{q}_i\hat{q}_j}{\omega^2 + c^2q^2 + r}. \quad (6.5)$$

We can now essentially repeat the RG analysis we made in section 2.5 with this modified propagator. We will need the following identities to solve the angle-dependent integrals

$$\begin{aligned} \int_{\hat{q}} \hat{q}_i\hat{q}_j &= \frac{S_d}{d} \delta_{ij} \\ \int_{\hat{q}} \hat{q}_i\hat{q}_j\hat{q}_k\hat{q}_l &= \frac{S_d}{d(d+2)} (\delta_{ij}\delta_{kl} + \delta_{ik}\delta_{jl} + \delta_{il}\delta_{jk}). \end{aligned} \quad (6.6)$$

Using these relations we calculate the one-loop self-energy correction. The rest of the calculation is simply about contracting the interaction tensors and projectors carefully. We obtain

$$\begin{aligned} \text{Diagram} &= \text{Diagram 1} + \text{Diagram 2} \\ \Sigma_{ij}^{(1L)} &= 2(2V_{ijkl} + 4V_{iklj}) \int_{\mathbf{q}} G_{kl} \\ &= 4I_1 \int_{\hat{q}} \left[(u\delta_{ij}\delta_{kl} + vg_{ijkl})(\delta_{kl} - \hat{q}_k\hat{q}_l) + 2(u\delta_{ik}\delta_{jl} + vg_{iklj})(\delta_{kl} - \hat{q}_k\hat{q}_l) \right] \\ &= 4I_1 \left[u\delta_{ij}(d-1) + v\delta_{ij} - \frac{1}{d}vg_{ijkl}\delta_{kl} \right. \\ &\quad \left. + 2 \left(u\delta_{ij} + v\delta_{ij} - \frac{1}{d}u\delta_{ij} - \frac{1}{d}vg_{iklj}\delta_{kl} \right) \right] \end{aligned} \quad (6.7)$$

$$= 4I_1 \left[\left(d + 1 - \frac{2}{d} \right) u + \left(3 - \frac{3}{d} \right) v \right] \delta_{ij} , \quad (6.8)$$

where the integral I_n is known from eq. (2.52). Similarly, we proceed with the vertex correction, which can be written as

$$\Gamma_{ijkl}^{(1L)} = \left[2^2 V_{ij'i'k'} V_{j'l'kl} + 2^4 V_{ij'i'k'} V_{j'kl'l} + 2^4 V_{ii'jk'} V_{j'kl'l} \right] \int_q G_{i'l'} G_{k'l'} \quad (6.9)$$

The calculation is somewhat involved, but conceptually completely analogous to the previous calculation of the self-energy correction. We skip the algebra and give the result for the overall vertex correction

$$\begin{aligned} \Gamma_{ijkl}^{(1L)} = & 4 \left[\left(d + 2 - \frac{8}{d} + \frac{12}{d(d+2)} + \frac{d}{d+2} + \frac{6}{d+2} \right) u^2 \right. \\ & \left. + 6 \left(1 - \frac{2}{d} + \frac{1}{d+2} + \frac{4}{d(d+2)} \right) uv + \frac{9}{d(d+2)} v^2 \right] \delta_{ij} \delta_{kl} \\ & + 16 \left(1 - \frac{2}{d} + \frac{1}{d(d+2)} \right) u^2 \delta_{ik} \delta_{jl} + \frac{16}{d(d+2)} u^2 \delta_{il} \delta_{jk} \\ & + \left[36 \left(1 - \frac{2}{d} + \frac{2}{d(d+2)} \right) v^2 + 48 \left(1 - \frac{2}{d} + \frac{2}{d(d+2)} \right) uv \right] g_{ijkl} . \end{aligned} \quad (6.10)$$

We have left the dimension d arbitrary as a way of bookkeeping, but since the expressions get unwieldy at a certain point we continue with $d = 3$.

Since the corrections only differ from the ones in section 2.5 by constant factors, the derivation of the RG equations is also analogous. In terms of the dimensionless couplings

$$\tilde{u} = \frac{u}{2\pi^2 c^3} , \quad \tilde{v} = \frac{v}{2\pi^2 c^3} , \quad (6.11)$$

we obtain the RG equations

$$\begin{aligned} \frac{dr}{dl} &= 2r - \frac{10}{3} \tilde{u} r - 2\tilde{v} r \\ \frac{d\tilde{u}}{dl} &= \epsilon \tilde{u} - \frac{34}{5} \tilde{u}^2 - \frac{24}{5} \tilde{u} \tilde{v} - \frac{3}{5} \tilde{v}^2 \\ \frac{d\tilde{v}}{dl} &= \epsilon \tilde{v} - \frac{21}{5} \tilde{v}^2 - \frac{28}{5} \tilde{u} \tilde{v} \end{aligned} \quad (6.12)$$

These equations are in agreement with the ones obtained by Khmel'nitskii &

Shneerson (1973) (equation (7)), up to a redefinition of the couplings.

Comparing these equations to eq. (2.80), we should note that, besides the change in numeric factors, there is an additional \tilde{v}^2 term in $d\tilde{u}/d\ell$. As we will see later this will have drastic consequences for the stability of the system.

Isotropic case $v = 0$

We first look at the case of vanishing anisotropy $v = 0$, to find out what the effect of the dipolar interaction is in isolation. The RG equations reduce to

$$\begin{aligned}\frac{dr}{d\ell} &= 2r - \frac{10}{3}r\tilde{u} \\ \frac{d\tilde{u}}{d\ell} &= \epsilon\tilde{u} - \frac{34}{5}\tilde{u}^2.\end{aligned}\tag{6.13}$$

These equations have two fixed points, the Gaussian (G) and a second one that we will call the Khmel'nitskii-Shneerson (KS) fixed point $\tilde{u}^* = \frac{5\epsilon}{34}$, analogous to the Wilson-Fisher (WF) fixed point we found for the $O(N)$ model. The KS fixed point is stable with respect to \tilde{u} and has the correlation length exponent

$$\nu_{\text{KS}} = \left(\frac{d \log r}{d \log b} \right)_{\tilde{u}=\tilde{u}_{\text{KS}}^*}^{-1} = 2 + \frac{25}{51}\epsilon\tag{6.14}$$

and consequently the specific heat exponent

$$\alpha_{\text{KS}} = 2 - (d+z)\nu_{\text{KS}} = \frac{1}{102}\epsilon + \mathcal{O}(\epsilon^2)\tag{6.15}$$

Note that these exponents are different from the Wilson-Fisher universality class, where we would expect for the corresponding case of $N = 3$ a correlation length exponent of $\nu_{\text{WF}} = 2 + \frac{5}{11}\epsilon$ and a specific heat exponent $\alpha_{\text{WF}} = \frac{1}{22}\epsilon$. In both classes α is positive for $\epsilon > 0$.

At the upper critical dimension $\epsilon = 0$, we have logarithmic corrections. The RG flow equation for r can then be solved exactly and we obtain

$$r \propto b^2 (\log b)^{-\frac{25}{51}}\tag{6.16}$$

We can extract the log correction to the correlation length in a similar fashion as in section 2.4, by taking the log on both sides ignoring log log terms and solving for b evaluated at the correlation length. The result is

$$\xi \propto r^{-\frac{1}{2}} (\log r)^{\frac{25}{51}},\tag{6.17}$$

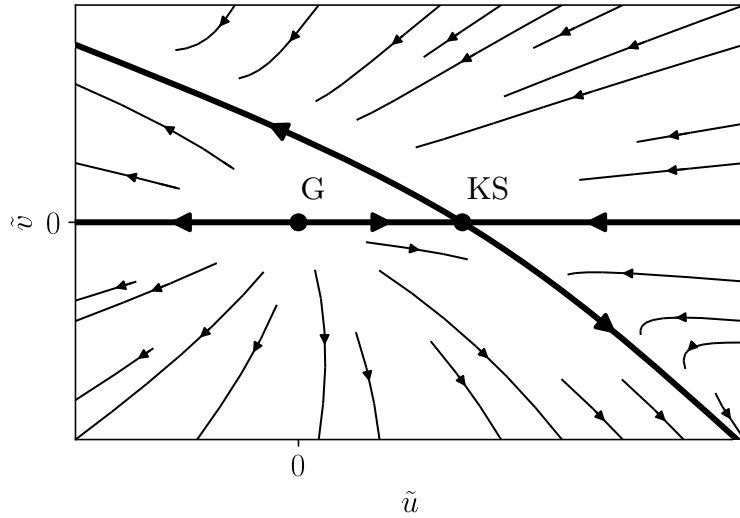


Figure 6.1.: RG flow in the presence of cubic anisotropy and dipolar interaction in $d = 3$ spatial dimensions.

such that $\hat{\nu} = 25/51$. This matches the result obtained by Khmel'nitskii & Shneerson (1973) for the logarithmic scaling in $3 + 1$ dimensions. We can contrast this with the prediction of the $O(3)$ model in the absence of dipolar interaction, which, as was shown in section 2.4, has $\hat{\nu} = 5/22$.

Relevance of cubic anisotropy in the presence of dipolar interaction

Including the cubic anisotropy, does not generate any additional fixed points. This is in strong contrast to the case described in section 2.5, where an Ising and a Cubic fixed point appeared in the absence of dipolar interaction. The situation is quite different here. We check the stability of the two existing fixed points G and KS. Expanding around the KS fixed point we obtain the linearized RG equations

$$\frac{d}{d\ell} \begin{pmatrix} \delta\tilde{u} \\ \delta\tilde{v} \end{pmatrix} = \begin{pmatrix} -\epsilon & -\frac{12}{17}\epsilon \\ 0 & \frac{3}{17}\epsilon \end{pmatrix} \begin{pmatrix} \delta\tilde{u} \\ \delta\tilde{v} \end{pmatrix}, \quad (6.18)$$

where the eigenvalues can be read off the diagonal. The positive eigenvalue indicates that the system is unstable with respect to the cubic anisotropy \tilde{v} . In other words, if the system starts with a non-vanishing cubic anisotropy, it will always eventually end up with runaway flow, with \tilde{v} diverging to $-\infty$. The G fixed point is unstable in both \tilde{u} and \tilde{v} direction, each with eigenvalue ϵ . The RG flow in the \tilde{u} - \tilde{v} -plane is shown in fig. 6.1.

Without dipolar interaction, we saw that above a certain flavor number ($N_c = 4$ at one-loop order), the cubic fixed point becomes stable. It turns out that, if we add dipolar interaction, there is also a critical flavor number above which the RG flow is qualitatively different. However, the flavor number is now tied to the spatial dimension. At one-loop order, in $d = 8$ dimensions and above an equivalent of the Cubic fixed point appears. Of course, this puts $d + z$ far above the upper critical dimension, and the Gaussian fixed point is stable.

It stands to reason that the critical flavor number will be modified, if one includes higher-order corrections into the RG procedure. However, in the limit of small ϵ the above results should be recovered. We therefore conclude that in $3 + 1$ dimensions ($\epsilon \rightarrow 0$) the cubic anisotropy diverges logarithmically in the presence of dipolar interactions.

6.2. RG flow equations of an isotropic elastic ferroelectric

We now seek to describe a ferroelectric transition coupled to an elastic medium. As usual, we use the minimal, most symmetric model that captures most of the physics. In this case, the minimal model is an isotropic elastic medium coupled to a Lorentz invariant ϕ^4 theory. It couples to the strain tensor ε , representing the acoustic branch, with a generic quadratic term.

$$\mathcal{S} = \int d^3r d\tau \left[\frac{1}{2} \boldsymbol{\phi}^T G^{(0)-1} \boldsymbol{\phi} + u(\phi^2)^2 + \lambda_1 \text{tr}\{\varepsilon\} \phi^2 + 2\lambda_2 \boldsymbol{\phi}^T \varepsilon \boldsymbol{\phi} + \frac{\rho}{2} \left((\partial_\tau \mathbf{u})^2 + c_l^2 \text{tr}\{\varepsilon\}^2 + 2c_t^2 \text{tr}\{\tilde{\varepsilon}\tilde{\varepsilon}\} \right) \right] \quad (6.19)$$

where c_l and c_t are the longitudinal and transversal sound velocity (see eq. (1.49)).

As described in the previous section we consider the limit of strong dipolar interaction, leading to a transversal projector in the bare propagator of the critical modes

$$G_{ij}^{(0)}(q, \omega) = \frac{\delta_{ij} - \hat{q}_i \hat{q}_j}{\omega^2 + c^2 q^2 + r}. \quad (6.20)$$

For the acoustic phonons on the other hand we have both longitudinal and transversal mode

$$\rho F_{ij}^{(0)}(\mathbf{q}, \omega) = \frac{\hat{q}_i \hat{q}_j}{\omega^2 + c_l^2 q^2} + \frac{\delta_{ij} - \hat{q}_i \hat{q}_j}{\omega^2 + c_t^2 q^2}. \quad (6.21)$$

In the previous chapter, we had ignored the second term, but now because of the additional coupling term λ_2 that couples shear strain to the order parameter we must include it and we expect a non-trivial RG flow for c_t . For convenience, we define a rank 4 tensor for the coupling

$$\lambda_{ijkl} = \lambda_1 \delta_{ij} \delta_{kl} + \lambda_2 (\delta_{ik} \delta_{jl} + \delta_{il} \delta_{jk}) \quad (6.22)$$

analogous to the isotropic stiffness tensor eq. (1.31). The interaction can then be written as

$$\lambda_1 \text{tr}\{\varepsilon\} \phi^2 + 2\lambda_2 \phi^T \varepsilon \phi = \lambda_{ijkl} \varepsilon_{ij} \phi_k \phi_l. \quad (6.23)$$

An important observation, that will become relevant later when we analyze the renormalization of the phonon velocities, is that the λ_2 term is not purely determined by shear strain, but instead a mixture of normal strain and shear strain. We can see this by rewriting the coupling in terms of the traceless strain tensor $\tilde{\varepsilon} = \varepsilon - \frac{1}{d} \text{tr}\{\varepsilon\} \mathbf{1}$

$$\begin{aligned} \lambda_1 \text{tr}\{\varepsilon\} \phi^2 + 2\lambda_2 \phi^T \varepsilon \phi &= \left(\lambda_1 + \frac{2}{d} \lambda_2 \right) \text{tr}\{\varepsilon\} \phi^2 + 2\lambda_2 \phi^T \tilde{\varepsilon} \phi \\ &\equiv \lambda_l \text{tr}\{\varepsilon\} \phi^2 + 2\lambda_t \phi^T \tilde{\varepsilon} \phi. \end{aligned} \quad (6.24)$$

So $\lambda_l = \lambda_1 + 2\lambda_2/d$ is the ‘‘longitudinal coupling’’ and $\lambda_t = \lambda_2$ is the transversal coupling.

Calculation of the corrections

The complete self-energy correction to one-loop order for the critical field amounts to

$$\begin{aligned} \text{---} \text{---} \text{---} &= \text{---} \text{---} \text{---} + \text{---} \text{---} \text{---} \\ \Sigma_{ll'}^{(1L)}(\mathbf{q}, \omega) &= 2u_0 \int_{q', \omega'} \left(2\delta_{ll'} G_{kk}^{(0)} + 4G_{ll'}^{(0)} \right) \\ &\quad - \frac{4}{\rho} \lambda_{0,ijkl} \lambda_{0,i'j'k'l'} \int_{q', \omega'} G_{kk'}^{(0)}(q' - q, \omega' - \omega) q'_i D_{jj'}^{(0)}(q', \omega) q'_{i'}. \end{aligned} \quad (6.25)$$

The first of the two corrections was already calculated in section 6.1

$$2u_0 \int_{q, \omega} \left(2\delta_{ij} G_{kk}^{(0)} + 4G_{ij}^{(0)} \right) = -\frac{1}{2\pi^2 c_0^3} \left(d + 1 - \frac{2}{d} \right) u_0 r_0 \log \Lambda \quad (6.26)$$

The second correction to the self-energy is more involved, since it depends on an external momentum and therefore contains projectors of the form

$$G_{ij}^{(0)}(q' - q, \omega' - \omega) \propto \left(\delta_{ij} - \frac{(q' - q)_i (q' - q)_j}{(q' - q)^2} \right). \quad (6.27)$$

Together with the momentum dependence of the phonon propagator it follows that the integrand has a complicated external momentum dependence. To keep the discussion here at least somewhat compact, the full calculation is done in chapter A, while here we simply give the result for the corrections to the wave function renormalization, the tuning parameter and the velocity of the critical mode

$$\begin{aligned}
Z_\phi^{-1} &= Z_{\phi,0}^{-1} \left(1 + \frac{2}{3\pi^2\rho} \left[\frac{3d-5}{2(d-1)} \frac{\lambda_1^2}{cc_l(c+c_l)^3} + \frac{\lambda_2^2}{cc_t(c+c_t)^3} \right] \log \Lambda \right) \\
r &= r_0 - \frac{1}{48\pi^2 c_0^3} \left(d+1 - \frac{2}{d} \right) u_0 r_0 \log \Lambda \\
&\quad + \frac{1}{3\pi^2\rho} \left[\frac{3d-5}{2(d-1)} \frac{2c+c_l}{c^3 c_l (c+c_l)^2} \lambda_1^2 + \frac{2c+c_t}{c^3 c_t (c+c_t)^2} \lambda_2^2 \right]_0 r_0 \log \Lambda \\
c^2 &= c_0^2 + \frac{1}{15\pi^2\rho(d-1)} \left[\frac{(5d-9)c-2c_l}{c_l(c+c_l)^3} \lambda_1^2 \right. \\
&\quad \left. + \frac{8}{cc_l(c+c_l)^2} ((c+2c_l)\lambda_1 + 4(c+c_l)\lambda_2) \lambda_2 \right. \\
&\quad \left. + 2 \frac{(4d-18)c^2 + (7d-33)cc_t + (4d-16)c_t^2}{cc_t(c+c_t)^3} \lambda_2^2 \right]_0 \log \Lambda,
\end{aligned} \tag{6.28}$$

where for conciseness of notation we just put the index 0 behind the brackets to mean that all parameters enclosed are bare parameters.

On the other hand, the acoustic phonon self-energy correction is given by

$$\begin{aligned}
\text{---} \text{---} \text{---} &= \text{---} \text{---} \text{---} \\
\Pi_{ii'}^{(1L)} &= 2q_j q_{j'} \lambda_{0,ijkl} \lambda_{0,i'j'k'v} \int_{q',\omega'} G_{kk'}^{(0)} G_{ll'}^{(0)},
\end{aligned} \tag{6.29}$$

where we express the propagator in terms of the elastic tensor C , which in an isotropic solid is of the form eq. (1.31). Using the relations eq. (6.6) we obtain the corrections to the phonon velocities, this amounts to

$$\begin{aligned}
\rho c_l^2 &= \rho c_{l,0}^2 - \frac{1}{4\pi^2 c_0^3} \left((d-1)\lambda_{0,1}^2 + 4 \frac{d-1}{d} \lambda_{0,1} \lambda_{0,2} + \frac{4}{d(d+2)} \lambda_{0,2}^2 \right) \log \Lambda \\
\rho c_t^2 &= \rho c_{t,0}^2 - \frac{1}{4\pi^2 c_0^3} \frac{d^2-2}{d(d+2)} \lambda_{0,2}^2 \log \Lambda
\end{aligned} \tag{6.30}$$

while $\rho = \rho_0$ is not renormalized (there is no non-trivial Z factor as there was for ϕ).

A similar procedure is used for the corrections on u , λ_1 and λ_2 . Here we have to be

careful with the different contractions again, for example

$$\begin{aligned}
\begin{array}{c} i \\ \diagdown \\ \bullet \\ \diagup \\ j \end{array} \begin{array}{c} k \\ \diagup \\ \bullet \\ \diagdown \\ l \end{array} &= \begin{array}{c} i \\ \diagdown \\ \bullet \\ \diagup \\ j \end{array} \begin{array}{c} i' \\ \diagdown \\ \bullet \\ \diagup \\ j' \end{array} \begin{array}{c} k \\ \diagup \\ \bullet \\ \diagdown \\ l \end{array} + \begin{array}{c} i \\ \diagdown \\ \bullet \\ \diagup \\ j \end{array} \begin{array}{c} i' \\ \diagdown \\ \bullet \\ \diagup \\ j' \end{array} \begin{array}{c} k \\ \diagup \\ \bullet \\ \diagdown \\ l \end{array} + \begin{array}{c} i \\ \diagdown \\ \bullet \\ \diagup \\ j \end{array} \begin{array}{c} i' \\ \diagdown \\ \bullet \\ \diagup \\ j' \end{array} \begin{array}{c} k \\ \diagup \\ \bullet \\ \diagdown \\ l \end{array} \\
&= \frac{1}{2} u_0^2 \left(2^3 \delta_{ij} \delta_{kl} \int_{q,\omega} G_{mn}^{(0)} G_{mn}^{(0)} + 2^5 \delta_{ij} \int_{q,\omega} G_{km}^{(0)} G_{ml}^{(0)} + 2^5 \int_{q,\omega} G_{ij}^{(0)} G_{kl}^{(0)} \right)
\end{aligned} \tag{6.31}$$

and

$$\begin{aligned}
\begin{array}{c} i \\ \diagdown \\ \bullet \\ \diagup \\ j \end{array} \begin{array}{c} k \\ \diagup \\ \bullet \\ \diagdown \\ l \end{array} &= \begin{array}{c} i \\ \diagdown \\ \bullet \\ \diagup \\ j \end{array} \begin{array}{c} i' \\ \diagdown \\ \bullet \\ \diagup \\ j' \end{array} \begin{array}{c} k' \\ \diagup \\ \bullet \\ \diagdown \\ l' \end{array} + \begin{array}{c} i \\ \diagdown \\ \bullet \\ \diagup \\ j \end{array} \begin{array}{c} i' \\ \diagdown \\ \bullet \\ \diagup \\ j' \end{array} \begin{array}{c} k' \\ \diagup \\ \bullet \\ \diagdown \\ l' \end{array} \\
&= \frac{u_0}{2\rho} \lambda_{kk'mm'} \lambda_{l'l'nn'} \int_{q,\omega} \left(2^4 \delta_{ij} G_{i'k'}^{(0)} G_{i'l'}^{(0)} + 2^5 G_{ik'}^{(0)} G_{jl'}^{(0)} \right) q_m D_{m'n}^0 q_{n'}
\end{aligned} \tag{6.32}$$

So in total for the dressed u -vertex we get

$$\begin{aligned}
\begin{array}{c} \diagdown \\ \bullet \\ \diagup \end{array} &= \begin{array}{c} \diagdown \\ \bullet \\ \diagup \end{array} + \begin{array}{c} \diagdown \\ \bullet \\ \diagup \end{array} + \begin{array}{c} \diagdown \\ \bullet \\ \diagup \end{array} \\
u - u_0 &= -4 \left(d + 7 - \frac{12}{d} + \frac{12}{d(d+2)} \right) u_0^2 I_{20} \\
&+ \frac{8}{\rho} \left[\frac{3d^2 + d - 4}{d(d+2)} \lambda_1^2 I_{21}(c_l) + \frac{d^2 + 3d - 4}{d(d+2)} \lambda_2^2 I_{21}(c_t) \right]_0 u_0 \\
&- \frac{4}{\rho^2} \frac{d-1}{d(d+2)} \left[(d+1) \lambda_1^4 I_{22}(c_l, c_l) + 2 \lambda_1^2 \lambda_2^2 I_{22}(c_l, c_t) + 3 \lambda_2^4 I_{22}(c_t, c_t) \right]_0
\end{aligned} \tag{6.33}$$

We also defined

$$I_{mn}(\{c_i\}) = \int_{q,\omega} \left(\frac{1}{\omega^2 + c^2 q^2 + r} \right)^m \prod_i^n \left(\frac{q^2}{\omega^2 + c_i^2 q^2} \right) \tag{6.34}$$

where c_i can be c_l or c_t . Now for the corrections to the λ -vertex we need

$$\begin{aligned}
\begin{array}{c} i \\ \diagdown \\ \bullet \\ \diagup \\ j \end{array} \begin{array}{c} k \\ \diagup \\ \bullet \\ \diagdown \\ l \end{array} &= \begin{array}{c} i \\ \diagdown \\ \bullet \\ \diagup \\ j \end{array} \begin{array}{c} k \\ \diagup \\ \bullet \\ \diagdown \\ l \end{array} + \begin{array}{c} i \\ \diagdown \\ \bullet \\ \diagup \\ j \end{array} \begin{array}{c} k \\ \diagup \\ \bullet \\ \diagdown \\ l \end{array} \\
&= \frac{2}{2!} u \lambda_{ij i' j'} \int_{q,\omega} \left(4 \delta_{kl} G_{i'k'}^{(0)} G_{j'l'}^{(0)} + 8 G_{i'k}^{(0)} G_{j'l}^{(0)} \right) .
\end{aligned} \tag{6.35}$$

The dressed vertex is then given by

$$\begin{aligned}
& (\lambda_1 - \lambda_{0,1})\delta_{ij}\delta_{kl} + (\lambda_2 - \lambda_{0,2})(\delta_{ik}\delta_{jl} + \delta_{il}\delta_{jk}) \\
&= -u_0\lambda_{ijj'j'} \int_{q,\omega} \left(4\delta_{kl}G_{i'k'}^{(0)}G_{j'k'}^{(0)} + 8G_{i'k'}^{(0)}G_{j'l}^{(0)}\right) \\
&+ \frac{4}{\rho}\lambda_{ijj'j'}\lambda_{kk'mm'}\lambda_{ll'nn'} \int_{q,\omega} G_{i'k'}^{(0)}G_{j'l}^{(0)}q_m D_{m'n}^0 q_{n'}
\end{aligned} \tag{6.36}$$

from which we obtain

$$\begin{aligned}
\lambda_1 - \lambda_{0,1} = & -4 \left[\frac{d^2 + d - 2}{d} \lambda_{0,1} + 2 \frac{d-1}{d+2} \lambda_{0,2} \right] u_0 I_{20} \\
& + \frac{4}{\rho} \left[\frac{d-1}{d} \lambda_1^3 I_{21}(c_l) + \frac{2}{d(d+2)} \lambda_1^2 \lambda_2 I_{21}(c_l) \right. \\
& \left. + \frac{d-1}{d} \lambda_1 \lambda_2^2 I_{21}(c_t) + 2 \frac{d+1}{d(d+2)} \lambda_2^3 I_{21}(c_t) \right]_0
\end{aligned} \tag{6.37}$$

$$\begin{aligned}
\lambda_2 - \lambda_{0,2} = & -8 \frac{d^2 - 2}{d(d+2)} \lambda_{0,2} u_0 I_{20} \\
& + \frac{4}{\rho} \left[\frac{d^2 - 2}{d(d+2)} \lambda_1^2 \lambda_2 I_{21}(c_l) - \frac{2}{d(d+2)} \lambda_2^3 I_{21}(c_t) \right]_0
\end{aligned} \tag{6.38}$$

To arrive at the RG equations we need to evaluate the integrals appearing in the above expressions. Most of them can be obtained from previous integrals as a derivative with respect to some parameter like

$$I_{21}(c_i) = -\frac{\partial}{\partial r} I_{11}(0, 0; c_i) = \frac{1}{8\pi^2} \frac{2c + c_i}{c^3 c_i (c + c_i)^2} \log \Lambda \tag{6.39}$$

and

$$I_{22}(c_i, c_i) = -\frac{1}{2c_i} \frac{\partial}{\partial c_i} I_{21}(c_i) = \frac{1}{8\pi^2} \frac{c^2 + 3cc_i + c_i^2}{c^3 c_i^3 (c + c_i)^3} \log \Lambda . \tag{6.40}$$

The integral $I_{22}(c_l, c_t)$ can not be derived in this way. However, extracting the logarithmic divergence is still possible by expanding in r (only 0th order contributes)

$$\begin{aligned}
I_{22}(c_l, c_t) &= \int_{q,\omega} \frac{q^4}{(\omega^2 + c^2 q^2)^2 (\omega^2 + c_l^2 q^2) (\omega^2 + c_t^2 q^2)} + \mathcal{O}(r) \\
&= \frac{1}{8\pi^2} \frac{2c^3 + (2c + c_l)(2c + c_t)(c_l + c_t)}{c^3 c_l c_t (c + c_l)^2 (c + c_t)^2 (c_l + c_t)} \log \Lambda
\end{aligned} \tag{6.41}$$

Note that in the case $c_l = c_t$ this is the same as $I_{22}(c_i, c_i)$.

RG flow equations

In analogy with previous chapters we perform the rescaling transformation $k = k'/b$, $\omega = \omega'/b$, which acts on the field with

$$\begin{aligned}\phi(\mathbf{q}, \omega) &= \sqrt{Z_\phi} b^{\frac{d+3z}{2}} \phi'(\mathbf{q}', \omega'), \\ \mathbf{u}(\mathbf{q}, \omega) &= \sqrt{Z_u} b^{\frac{d+3z}{2}} \mathbf{u}'(\mathbf{q}', \omega').\end{aligned}\tag{6.42}$$

The parameters are the rescaled

$$\begin{aligned}c^2 &= c'^2/(Z_\phi b^{2z-2}), & u &= u'/(Z_\phi^2 b^{3z-d}), \\ c_l^2 &= c_l'^2/(Z_u b^{2z-2}), & \lambda_1 &= \lambda_1'/(\sqrt{Z_u} Z_\phi b^{\frac{5z-d-2}{2}}), \\ c_t^2 &= c_t'^2/(Z_u b^{2z-2}), & \lambda_2 &= \lambda_2'/(\sqrt{Z_u} Z_\phi b^{\frac{5z-d-2}{2}}), \\ r &= r'/(Z_\phi b^{-2z}).\end{aligned}\tag{6.43}$$

With $z = 1$ and $d = 3 - \epsilon$ we arrive at

$$\begin{aligned}\frac{d \log Z_\phi}{d\ell} &= -\frac{2}{3\pi^2 \rho} \left[\frac{\lambda_1^2}{cc_l(c+c_l)^3} + \frac{\lambda_2^2}{cc_t(c+c_t)^3} \right] \\ \frac{d \log r}{d\ell} &= 2 - \frac{5}{3\pi^2 c^3} u + \frac{1}{3\pi^2 \rho c^3} \left[\frac{3c+c_l}{(c+c_l)^3} \lambda_1^2 + \frac{3c+c_t}{(c+c_t)^3} \lambda_2^2 \right] \\ \frac{dc^2}{d\ell} &= -\frac{1}{15\pi^2 \rho} \left[\frac{13c-c_l}{c_l(c+c_l)^3} \lambda_1^2 + \frac{4}{cc_l(c+c_l)^2} \left((c+2c_l)\lambda_1 + 4(c+c_l)\lambda_2 \right) \lambda_2 \right. \\ &\quad \left. + \frac{4(c^2-3cc_t-c_t^2)}{cc_t(c+c_t)^3} \lambda_2^2 \right]\end{aligned}\tag{6.44}$$

as well as the elastic constants

$$\begin{aligned}\frac{dc_l^2}{d\ell} &= -\frac{1}{2\pi^2 \rho c^3} \left(\lambda_1^2 + \frac{4}{3} \lambda_1 \lambda_2 + \frac{16}{15} \lambda_2^2 \right) \\ \frac{dc_t^2}{d\ell} &= -\frac{7}{30\pi^2 \rho c^3} \lambda_2^2\end{aligned}\tag{6.45}$$

where notably the flow of c_t only depends on the shear coupling λ_2 . The cross term the first of the two equations is a result of the compressive contribution to λ_2 and can be removed by switching to the longitudinal and transversal couplings, λ_l and λ_t . The couplings

$$\begin{aligned}\frac{d\lambda_1}{d\ell} &= \frac{\epsilon}{2} \lambda_1 - \frac{1}{\pi^2 c^3} \left(\frac{5}{3} \lambda_1 + \frac{2}{5} \lambda_2 \right) u + \frac{1}{3\pi^2 \rho c^3} \left(\frac{3c+c_l}{(c+c_l)^3} \lambda_1^2 + \frac{3c+c_t}{(c+c_t)^3} \lambda_2^2 \right) \lambda_1 \\ &\quad + \frac{1}{15\pi^2 \rho c^3} \left(\frac{2c+c_l}{c_l(c+c_l)^2} \lambda_1^2 + 2 \frac{2c+c_t}{c_t(c+c_t)^2} \lambda_2^2 \right) \lambda_2\end{aligned}\tag{6.46}$$

$$\begin{aligned} \frac{d\lambda_2}{d\ell} = & \frac{\epsilon}{2}\lambda_2 - \frac{7}{15\pi^2 c^3}\lambda_2 u \\ & + \frac{1}{30\pi^2 \rho c^3} \left(\frac{7c_l^2 + 21cc_l - 6c^2}{c_l(c+c_l)^3}\lambda_1^2 - 2\frac{c_t^2 + 3cc_t + 12c^2}{c_t(c+c_t)^3}\lambda_2^2 \right) \lambda_2 \end{aligned} \quad (6.47)$$

and

$$\begin{aligned} \frac{du}{d\ell} = & \epsilon u - \frac{17}{5\pi^2 c^3}u^2 \\ & + \frac{2}{15\pi^2 \rho c^3} \left(\frac{21c^2 + 39cc_l + 13c_l^2}{c_l(c+c_l)^3}\lambda_1^2 + \frac{27c^2 + 48cc_t + 16c_t^2}{c_t(c+c_t)^3}\lambda_2^2 \right) u \\ & - \frac{1}{15\pi^2 \rho c^3} \left(4\frac{c^2 + 3cc_l + c_l^2}{c_l^3(c+c_l)^3}\lambda_1^4 + 3\frac{c^2 + 3cc_t + c_t^2}{c_t^3(c+c_t)^3}\lambda_2^4 \right. \\ & \left. + 2\frac{2c^3 + (c_l+2c)(c_t+2c)(c_l+c_t)}{c_l c_t (c_l+c)^2 (c_t+c)^2 (c_l+c_t)}\lambda_1^2 \lambda_2^2 \right) \end{aligned} \quad (6.48)$$

It becomes immediately obvious that the RG equations have expanded considerably in complexity compared to the ones of the generic model eq. (5.29). The RG flow is fully described by a system of six coupled equations for the parameters c , c_l , c_t , λ_1 , λ_2 and u . We can reduce this to a system of five coupled equations, by switching to dimensionless variables. However, there is now no unique “natural” choice of dimensionless variables. For example, it is unclear which ratios between the three velocity parameters we should choose to describe the system.

We choose here a parametrization that is close to the one we had in the generic model, given by

$$\begin{aligned} \vartheta = \frac{c_l}{c}, \quad \tilde{\lambda}_l^2 = \frac{(\lambda_1 + \frac{2}{3}\lambda_2)^2}{4\pi^2 \rho c_l^2 c^3}, \quad \tilde{u} = \frac{1}{2\pi^2} \frac{u}{c^3}, \\ \zeta = \frac{c_t}{c_l}, \quad \tilde{\lambda}_t^2 = \frac{\lambda_2^2}{4\pi^2 \rho c_t^2 c^3}. \end{aligned} \quad (6.49)$$

Stability conditions

To identify and characteristic possible instabilities it helps to write down the stability requirements. The lattice is microscopically stable as long as

$$c_l^2 > 0 \quad \text{and} \quad c_t^2 > 0. \quad (6.50)$$

If one of the phonon velocities vanishes the system becomes microscopically unstable with respect to local distortions given by the corresponding phonon. For the dimensionless parameters, this implies that both ϑ and ζ have to be positive in a stable solid.

On the other hand, for macroscopic stability, it must hold that the elastic moduli

are positive

$$K = \rho \left(c_l^2 - \frac{4}{3} c_t^2 \right) > 0 \quad \text{and} \quad \mu = \rho c_t^2 > 0. \quad (6.51)$$

If open boundary conditions are applied, corresponding to constant pressure, and the bulk modulus K vanishes the system becomes unstable with respect to volume changes. For the dimensionless parameter ζ the global stability condition reads

$$K > 0 \iff c_l^2 > \frac{4}{3} c_t^2 \iff \zeta < \frac{\sqrt{3}}{2}. \quad (6.52)$$

If however the shear modulus μ vanishes the system is unstable with respect to changes in shape, causing a solid-liquid transition, i.e. melting. If μ vanishes, so does c_t and so does ζ . Thus stability requires that at constant pressure/open boundary ζ only lives on the interval $(0, \sqrt{3}/2)$, while at constant volume ζ lives on the positive real axis.

The RG flow equations for the bulk modulus $K = \rho(c_l^2 - \frac{4}{3}c_t^2)$ and shear modulus $\mu = \rho c_t^2$ are

$$\begin{aligned} \frac{dK}{d\ell} &= -\frac{1}{2\pi^2 c^3} \lambda_l^2, \\ \frac{d\mu}{d\ell} &= -\frac{7}{30\pi^2 c^3} \lambda_t^2, \end{aligned} \quad (6.53)$$

where $\lambda_l = \lambda_1 + \frac{2}{3}\lambda_2$ is the longitudinal coupling and $\lambda_t = \lambda_2$ is the transversal coupling.

RG flow equations in the absence of shear coupling $\lambda_2 = 0$

In the absence of shear coupling, the interaction is only with the longitudinal phonon mode. As a result, the transversal phonon velocity remains constant. We then have to deal only with three non-trivial RG equations in dimensionless variables, which are

$$\begin{aligned} \frac{d\vartheta}{d\ell} &= -\frac{15\vartheta + 19\vartheta^2 + 47\vartheta^3 + 15\vartheta^4}{15(1+\vartheta)^3} \tilde{\lambda}_l^2 \\ \frac{d\tilde{\lambda}_l^2}{d\ell} &= \epsilon \tilde{\lambda}_l^2 - \frac{20}{3} \tilde{u} \tilde{\lambda}_l^2 + \frac{30 + 168\vartheta + 204\vartheta^2 + 70\vartheta^3}{15(1+\vartheta)^3} \tilde{\lambda}_l^4 \\ \frac{d\tilde{u}}{d\ell} &= \epsilon \tilde{u} - \frac{34}{5} \tilde{u}^2 + \frac{246\vartheta + 306\vartheta^2 + 102\vartheta^3}{15(1+\vartheta)^3} \tilde{u} \tilde{\lambda}_l^2 - \frac{32\vartheta + 96\vartheta^2 + 32\vartheta^3}{15(1+\vartheta)^3} \tilde{\lambda}_l^4. \end{aligned} \quad (6.54)$$

Except for the numeric factors these equations are quite similar to the system we encountered in the generic model eq. (5.31), for $N < 4$. The same logic that applied then also applies here: ϑ is lowered by the elastic coupling and for small ϑ the remaining equations imply runaway flow in $\tilde{\lambda}_l^2$. The only stable trajectories start with $\tilde{\lambda}_l = 0$ where we recover Khmel'nitskii-Shneerson physics.

If we take the limit $\vartheta \rightarrow \infty$, neglecting effectively the quantum nature of the elastic degree of freedom, we obtain an RG flow analogous to the one found by Bergman & Halperin (1976) with a stable Fisher-renormalized Khmel'nitskii-Shneerson fixed point. This is exactly what we would expect for the classical transition since $\alpha_{\text{KS}} > 0$. We will elaborate further on this in the next section.

Overall we can say that in the absence of shear coupling λ_2 , the overall critical behavior is quite similar to the generic model, where a destabilization of the lattice and a subsequent first-order structural transition preempts the second-order phase transition of the rigid system.

6.3. Classical isotropic elastic ferroelectric criticality

We first concentrate on the classical ferroelectric transition. The corresponding RG equations can be derived from the quantum RG equations by taking the limit $\vartheta \rightarrow \infty$ in analogy to the situation that was discussed for the generic model in section 5.2. It turns out that the critical behavior of the classical transition already shows rich physics, when coupled to the elasticity. We find a situation similar to the one described by Bergman & Halperin (1976) in that there is a Fisher-renormalized fixed point at a finite value of the elastic coupling λ_l . However, to our knowledge, the theory of Fisher-renormalization has so far not been applied to models relevant to ferroelectric transition. Additionally, the inclusion of shear coupling leads to a much more complicated picture, which can not be explained by Fisher-renormalization.

We start by taking the classical limit of the RG flow equations in the previous section by $\vartheta \rightarrow \infty$. As a result, we obtain the classical equations

$$\begin{aligned}
\frac{d\zeta}{d\ell} &= \zeta \tilde{\lambda}_l^2 - \frac{7}{15} \zeta (1 - \frac{4}{3} \zeta^2) \tilde{\lambda}_t^2 \\
\frac{d\tilde{\lambda}_l}{d\ell} &= \frac{\epsilon}{2} \tilde{\lambda}_l - \frac{10}{3} \tilde{u} \tilde{\lambda}_l + \frac{4}{5} \zeta \tilde{u} \tilde{\lambda}_t + \frac{7}{3} \tilde{\lambda}_l^3 - \frac{8}{45} \zeta \tilde{\lambda}_l^2 \tilde{\lambda}_t + \frac{72 + 452\zeta^2}{135} \tilde{\lambda}_l \tilde{\lambda}_t^2 - \frac{4}{5} \zeta \tilde{\lambda}_t^3 \\
\frac{d\tilde{\lambda}_t}{d\ell} &= \frac{\epsilon}{2} \tilde{\lambda}_t^2 - \frac{14}{15} \tilde{u} \tilde{\lambda}_t + \frac{14}{15} \zeta \tilde{\lambda}_l^2 \tilde{\lambda}_t + \frac{16}{45} \zeta \tilde{\lambda}_l \tilde{\lambda}_t^2 - \frac{81 - 344\zeta^2}{135} \tilde{\lambda}_t^3 \\
\frac{d\tilde{u}}{d\ell} &= \epsilon \tilde{u} - \frac{34}{5} \tilde{u}^2 + \frac{104}{15} \tilde{u} \tilde{\lambda}_l^2 - \frac{272}{45} \zeta \tilde{u} \tilde{\lambda}_l \tilde{\lambda}_t + \frac{8(117 + 124\zeta^2)}{135} \tilde{u} \tilde{\lambda}_t^2 \\
&\quad - \frac{32}{15} \tilde{\lambda}_l^4 + \frac{256}{45} \zeta \tilde{\lambda}_l^3 \tilde{\lambda}_t - \frac{16(3 + 16\zeta^2)}{45} \tilde{\lambda}_l^2 \tilde{\lambda}_t^2 \\
&\quad + \frac{64\zeta(9 + 16\zeta^2)}{405} \tilde{\lambda}_l \tilde{\lambda}_t^3 - \frac{8(243 + 72\zeta^2 + 64\zeta^4)}{1215} \tilde{\lambda}_t^4.
\end{aligned} \tag{6.55}$$

In the case $\tilde{\lambda}_t = 0$ the equations for the couplings become independent of ζ , we can define

$$\bar{u} = \tilde{u} - \tilde{\lambda}_l^2 \tag{6.56}$$

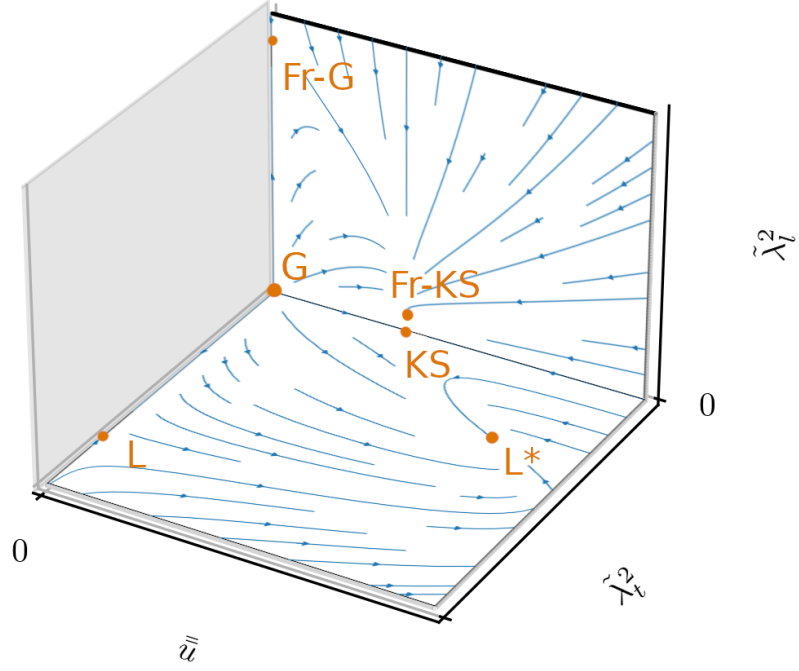


Figure 6.2.: RG flow of the classical elastic ferroelectric for small shear modulus, $\zeta \ll 1$. Shown are the $\tilde{\lambda}_l = 0$ plane and the $\tilde{\lambda}_t = 0$ plane, both of which have no out-of-plane flow. The G and WF fixed points are marked on the axis of vanishing coupling. The Fisher-renormalized fixed points exist in the plane of vanishing shear coupling but are both unstable with respect to infinitesimal $\tilde{\lambda}_t$. The L and L* fixed points are shown in the plane of vanishing λ_l , L* is stable in all directions. S is not shown since it is at finite ζ .

and obtain equations

$$\begin{aligned} \frac{d\bar{u}}{d\ell} \Big|_{\lambda_t=0} &= \epsilon\bar{u} - \frac{34}{5}\bar{u}^2 \\ \frac{d\tilde{\lambda}_l^2}{d\ell} \Big|_{\lambda_t=0} &= \epsilon\tilde{\lambda}_l^2 - \frac{20}{3}\bar{u}\tilde{\lambda}_l^2 - 2\tilde{\lambda}_l^4. \end{aligned} \quad (6.57)$$

which have the Fisher-renormalized Gaussian (Fr-G) and Fisher-renormalized Khmel'nitskii-Shneerson (Fr-KS) fixed points, each with the corresponding renormalized critical exponents.

Note that the converse case of finite $\tilde{\lambda}_t$ with vanishing longitudinal coupling $\tilde{\lambda}_l = 0$ is in general not stable, since $d\tilde{\lambda}_l/d\ell$ remains in general non-zero, with its sign depending on the sign of $\tilde{u} - \tilde{\lambda}_t^2$.

$$\frac{d\tilde{\lambda}_l}{d\ell} \Big|_{\lambda_t=0} = \frac{4}{5}\zeta\tilde{\lambda}_t(\tilde{u} - \tilde{\lambda}_t^2). \quad (6.58)$$

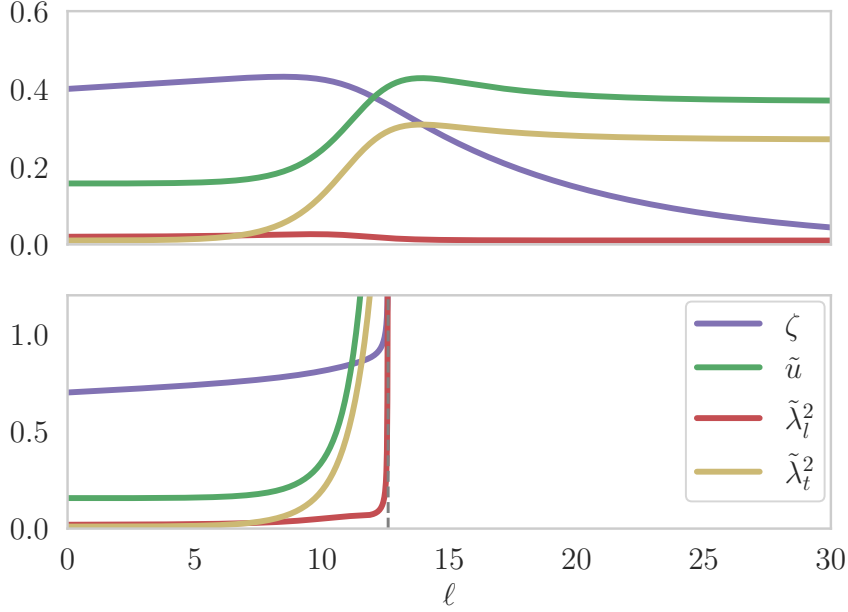


Figure 6.3.: Numerical solutions of the classical RG equations for small perturbations around the Fr-KS fixed point with a shear coupling $\tilde{\lambda}_{t,0} = 0.01$. The upper panel has $\zeta_0 = 0.4$ in which case the system quickly approaches L^* , and the lower panel has $\zeta_0 = 0.7$ for which the system becomes unstable at a finite RG scale because \tilde{u} diverges.

However, the flow in λ_l is small for small values of ζ . In the limit $\zeta \ll 1$ we can reframe the equations in the variable

$$\bar{u} = \tilde{u} - \tilde{\lambda}_t^2 - \frac{61 - \sqrt{1945}}{74} \tilde{\lambda}_t^2 \quad (6.59)$$

where the coefficient of the last term is chosen such that the $\tilde{\lambda}_t^4$ in $d\bar{u}/d\ell$ vanishes. The resulting RG flow equations are

$$\begin{aligned} \frac{d\tilde{\lambda}_t^2}{d\ell} \Big|_{\zeta \rightarrow 0} &= \epsilon \tilde{\lambda}_t^2 - \frac{20}{3} \bar{u} \tilde{\lambda}_t^2 - 2\tilde{\lambda}_t^4 - \frac{1229 - 25\sqrt{1945}}{555} \tilde{\lambda}_t^2 \tilde{\lambda}_t^2 \\ \frac{d\tilde{\lambda}_t^2}{d\ell} \Big|_{\zeta \rightarrow 0} &= \epsilon \tilde{\lambda}_t^2 - \frac{28}{15} \bar{u} \tilde{\lambda}_t^2 - \frac{760 - 7\sqrt{1945}}{555} \tilde{\lambda}_t^4 \\ \frac{d\bar{u}}{d\ell} \Big|_{\zeta \rightarrow 0} &= \epsilon \bar{u} - \frac{34}{5} \bar{u}^2 - \frac{8(190 - 11\sqrt{1945})}{555} \bar{u} \tilde{\lambda}_t^2 + \frac{24}{5} \tilde{\lambda}_t^2 \tilde{\lambda}_t^2. \end{aligned} \quad (6.60)$$

These equations have additional fixed points at vanishing $\tilde{\lambda}_l = 0$ but finite $\tilde{\lambda}_t$, which have been added to table 6.1. These fixed points exist only at $\zeta = 0$, a vanishing shear modulus, which corresponds to a liquid state, and we call them the L and L^* .

Table 6.1.: Fixed points of the classical ferroelectric transition coupled to an isotropic elastic medium, with values of the dimensionless couplings, as well as critical exponents ν and α .

Fixed point	ζ	\tilde{u}	$\tilde{\lambda}_l^2$	$\tilde{\lambda}_t^2$	ν	α
G	$\mathbb{R}_{>0}$	0	0	0	$\frac{1}{2}$	$\frac{\epsilon}{2}$
KS	$\mathbb{R}_{>0}$	$\frac{5\epsilon}{34}$	0	0	$\frac{1}{2} + \frac{25\epsilon}{204}$	$\frac{\epsilon}{102}$
Fr-G	$\mathbb{R}_{>0}$	$\frac{\epsilon}{2}$	$\frac{\epsilon}{2}$	0	$\frac{1}{2} + \frac{\epsilon}{4}$	$-\frac{\epsilon}{2}$
Fr-KS	$\mathbb{R}_{>0}$	$\frac{8\epsilon}{51}$	$\frac{\epsilon}{102}$	0	$\frac{1}{2} + \frac{13\epsilon}{102}$	$-\frac{\epsilon}{102}$
L	0	$\approx 0.37\epsilon$	0	$\approx 0.37\epsilon$	$\approx \frac{1}{2} + 0.29\epsilon$	$\approx -0.66\epsilon$
L*	0	$\approx 0.14\epsilon$	0	$\approx 0.61\epsilon$	$\approx \frac{1}{2} + 0.08\epsilon$	$\approx 0.20\epsilon$
S	≈ 0.84	$\approx 4.00\epsilon$	$\approx 0.08\epsilon$	$\approx 2.56\epsilon$	$\approx \frac{1}{2} + 1.56\epsilon$	$\approx -5.75\epsilon$

Additionally, we find a fixed point at finite ζ and finite shear coupling, which we call the S fixed point.

By expanding the RG equations around the individual fixed points we can learn about their stability. This way we can show that the Fr-KS fixed point, which would be stable in the case $\tilde{\lambda}_t = 0$, is unstable with respect to shear coupling. This can be seen in the form of a negative eigenvalue in the linearized equations, but we can also solve the non-linear problem numerically. In fig. 6.3 the RG trajectory for initial values at the KS fixed point plus a small shear coupling is shown.

The asymptotic flow depends on the initial value of ζ . If ζ_0 is small the flow is towards the L* fixed point. In this scenario, the longitudinal coupling $\tilde{\lambda}_l$ quickly goes to zero, while the transversal coupling $\tilde{\lambda}_t$ approaches a finite value $\tilde{\lambda}_t^*$. Thus ζ , and with it the transversal phonon velocity and the shear modulus, vanishes with a power law, where the exponent is determined by $\tilde{\lambda}_t^*$. If on the other hand, ζ_0 is above some critical value, $\tilde{\lambda}_t$ grows exponentially and the couplings diverge at a finite RG scale.

The L* fixed point is stable in all directions within the classical theory, indicating that within its basin of attraction, the asymptotic flow is similar to the example outlined above for small ζ_0 . This is supported by another numerical solution, shown in fig. 6.4, with initial values around the repulsive fixed point S, which is the only one that exists at both finite shear coupling and finite ζ . If ζ_0 is slightly smaller than the fixed point value at S, the flow is again towards L*, while for slightly larger ζ_0 we encounter an instability at a finite RG scale.

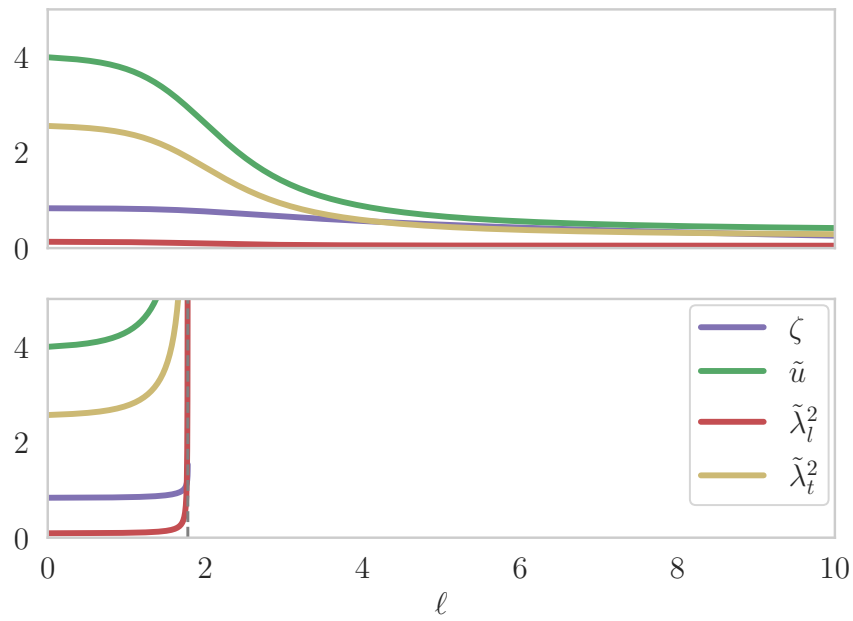


Figure 6.4.: Numerical solutions of the classical RG equations for small perturbations around the S fixed point in ζ direction. Initial values are $\zeta_0 = \zeta^* - 0.01$ in the upper panel and $\zeta_0 = \zeta^* - 0.01$ in the lower one.

6.4. Isotropic elastic ferroelectric quantum phase transition

The equations describing the quantum critical ferroelectric seem much more complicated. However, the phase diagram is much simpler as indicated by the smaller number of fixed points. The G and KS fixed points are still present at $\lambda_1 = \lambda_2 = 0$ independent of the values of η and ζ . Thus each represents a sheet in the 5-dimensional parameter space, on which the flow vanishes. One can find only one other fixed point

$$\vartheta^* \approx 0.73, \quad \zeta^* \approx 0.84, \quad \tilde{\lambda}_i^* \approx \pm 0.26\sqrt{\epsilon}, \quad \tilde{\lambda}_t^* \approx \pm 1.47\sqrt{\epsilon}, \quad \tilde{u}^* \approx 2.03\epsilon \quad (6.61)$$

or rather two fixed points, since the sign of the elastic coupling is ambiguous. Notably, $\zeta^* < \sqrt{3}/2$ is below the threshold of macroscopic stability, meaning that the fixed point is accessible for both open and pinned boundary conditions.

From an expansion of the RG equation around the fixed points, we can determine the matrix

$$\frac{d}{d\ell} \begin{pmatrix} \delta\vartheta \\ \delta\zeta \\ \delta\tilde{\lambda}_1 \\ \delta\tilde{\lambda}_2 \\ \delta\tilde{u} \end{pmatrix} \approx \begin{pmatrix} 0.19\epsilon & -0.19\epsilon & \pm 0.28\epsilon^{\frac{1}{2}} & \pm 0.11\epsilon^{\frac{1}{2}} & 0 \\ 0 & 2.30\epsilon & \mp 0.43\epsilon^{\frac{1}{2}} & \mp 0.17\epsilon^{\frac{1}{2}} & 0 \\ \pm 0.74\epsilon^{\frac{3}{2}} & \pm 5.97\epsilon^{\frac{3}{2}} & -3.01\epsilon & -3.19\epsilon & -1.75\epsilon^{\frac{1}{2}} \\ \mp 0.70\epsilon^{\frac{3}{2}} & \mp 5.38\epsilon^{\frac{3}{2}} & -0.10\epsilon & 2.75\epsilon & 2.74\epsilon^{\frac{1}{2}} \\ 7.60\epsilon^2 & 12.79\epsilon^2 & 3.36\epsilon^{\frac{3}{2}} & -13.80\epsilon^{\frac{3}{2}} & -11.89\epsilon \end{pmatrix} \begin{pmatrix} \delta\vartheta \\ \delta\zeta \\ \delta\tilde{\lambda}_1 \\ \delta\tilde{\lambda}_2 \\ \delta\tilde{u} \end{pmatrix}, \quad (6.62)$$

and since of the eigenvalues, two are positive and three are negative, we conclude that the fixed points are repulsive. From eq. (6.44) we can extract the critical exponent, which are

$$\nu \approx 2 - 3.69\epsilon \quad \eta \approx -0.96\epsilon \quad (6.63)$$

which corresponds to an $\alpha \approx -3.19\epsilon$.

Much like the classical theory the KS fixed point becomes unstable with respect to elastic coupling, as we have already seen in the $\lambda_2 = 0$ case. We therefore conclude that there are no stable fixed points.

We use repulsive fixed point at finite elastic coupling as a starting point to determine the fate of the system with numerical solutions, see fig. 6.5. If ζ_0 is slightly smaller than ζ^* then the flow is towards $\zeta = 0$. This point is reached at a finite RG scale and the shear coupling $\tilde{\lambda}_t$ diverges at this point, indicating a microscopic instability at which the transversal phonon velocity c_t vanishes. As discussed before this is associated with a solid-liquid transition.

If ζ_0 is slightly larger than ζ^* the result is quite different. In this scenario, ζ grows and finally diverges at a finite RG scale, along with all couplings $\tilde{\lambda}_i$, $\tilde{\lambda}_t$, and \tilde{u} . Looking at

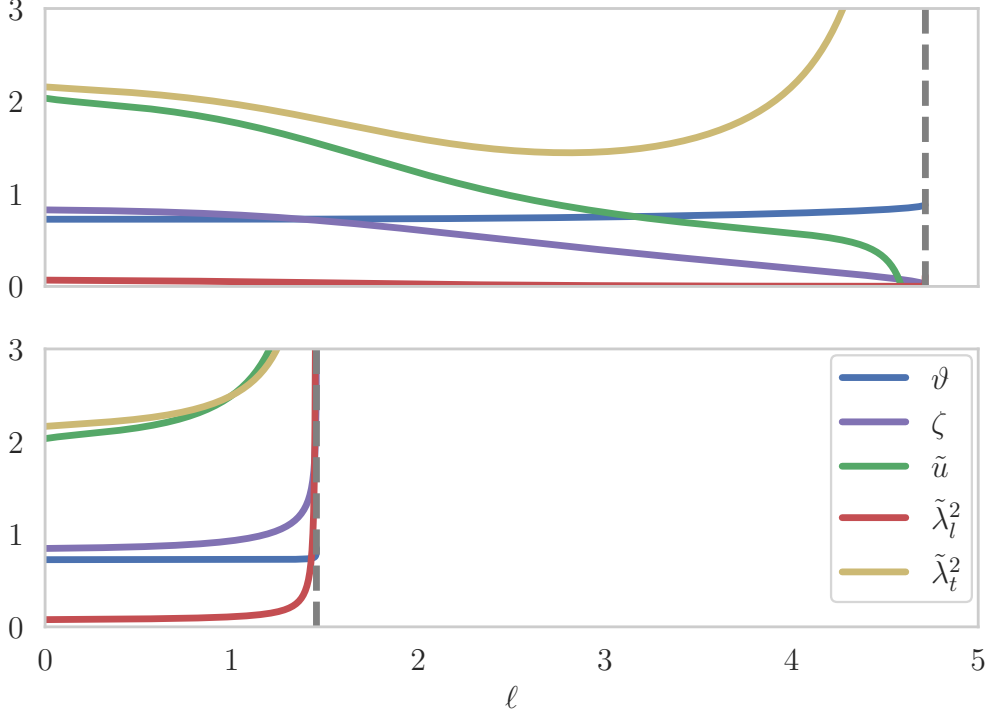


Figure 6.5.: Examples of the RG flow of a quantum critical elastic ferroelectric around the finite coupling fixed point. The upper panel is for $\zeta_0 = \zeta^* - 0.01$, where the flow is eventually to $\zeta = 0$. The lower panel is for $\zeta_0 = \zeta^* + 0.01$, where ζ diverges along with the couplings.

the results of the equivalent numerical experiment for dimensionful parameters, we can find that this divergence corresponds to both the longitudinal phonon velocity c_l and the critical velocity c vanishing. In the case of open boundary conditions, the vanishing bulk modulus will trigger an isostructural transition already before that point. If pinned boundary conditions are applied the microscopic instability is reached. The vanishing of the critical velocity is generally associated with a Lifshitz point. To describe such a point appropriately higher gradients up to $\mathcal{O}(q^4)$ must be considered in the action.

Part II.

Chiral Magnetoelasticity

7. Chiral magnets in the micromagnetic framework

The following chapter introduces the theory of chiral magnets in the framework of micromagnetism, the semi-classical, continuum description of magnetism that is valid on a length scale much longer than the atomic scale. In section 7.1 we derive some important features of this theory, which are important ingredients for the standard model of bulk chiral magnets. This model is then discussed in detail in section 7.2, where we treat it as a Landau theory and explore selected regions of the phase diagram.

7.1. The continuum limit of magnetism

When describing ferromagnetism, one often discusses a Heisenberg-type model, with a symmetric exchange interaction. In the case of chiral magnets, broken inversion symmetry also allows for an antisymmetric exchange, which is called *Dzyaloshinsky-Moriya interaction* (DMI), resulting from spin-orbit coupling in second-order perturbation theory (Dzyaloshinsky, 1958; Moriya, 1960). The Hamiltonian is then of the form

$$H = -J \sum_{\langle mn \rangle} \mathbf{S}_m \cdot \mathbf{S}_n + \sum_{\langle mn \rangle} \mathbf{D}_{mn} \cdot (\mathbf{S}_m \times \mathbf{S}_n). \quad (7.1)$$

A positive J describes a ferromagnet, while a negative J describes an antiferromagnet. We will only consider ferromagnetic systems in this context. The vector \mathbf{D}_{mn} describes the DMI for the specific bond between the sites m and n .

The Heisenberg exchange term favors aligned spins, while the DMI term favors orthogonal spins, where the exact orientation depends on the vector \mathbf{D}_{mn} . The competition between these two couplings, often together with other energy terms such as anisotropy and a Zeeman field, can stabilize a variety of modulated spin textures, such as magnetic helices, cycloids, or skyrmions.

If DMI is weak, which is to be expected for weak spin-orbit coupling, the length scale of the modulation becomes large. Common examples of bulk chiral magnets include MnSi, FeGe and Cu₂OSeO₃, which are of the so-called B20 structure, have helices with a period on the order of 20 nm, 70 nm and 60 nm (Adams et al., 2012)

respectively. On these scales, it makes little sense to consider every individual spin, but instead, we will move to a semi-classical, continuum description.

First, we move from individual magnetic moments to a continuous function $\mathbf{S}_n \rightarrow \mathbf{M}(\mathbf{R}_n)$, describing the coarse-grained magnetization of the volume element around the lattice site at position \mathbf{R}_n . We then suppose the distance between neighboring sites is small and use a series expansion in the lattice constants. Rewriting the sum over pairs first as a sum over site and bond vectors \mathbf{a} , then as an integral, the exchange interaction becomes

$$\begin{aligned} \sum_{\langle mn \rangle} \mathbf{S}_m \cdot \mathbf{S}_n &\propto \frac{1}{2} \sum_n \sum_{\mathbf{a}} \mathbf{M}(\mathbf{R}_n) \cdot \mathbf{M}(\mathbf{R}_n + \mathbf{a}) \\ &= \frac{1}{2V} \int d^3r \sum_{\mathbf{a}} \left(\mathbf{M}(\mathbf{r})^2 + \frac{1}{2} \mathbf{M}(\mathbf{r}) \cdot (\mathbf{a} \cdot \nabla)^2 \mathbf{M}(\mathbf{r}) \right) + \mathcal{O}(\delta^3) \end{aligned} \quad (7.2)$$

where V is the volume of integration. The factor of $1/2$ compensates for the double counting of bonds from summing over all bonds at every site. Here, we already used the fact that the first-order term vanishes, which can be seen using integration by parts.

If we assume that the total magnetic moment at a specific site is fixed, the quantity $\mathbf{M}(\mathbf{r})^2$ is a spatial constant that can be ignored. We describe the $\mathbf{M} = M_s \mathbf{m}$ where \mathbf{m} is the unit vector in magnetization direction and M_s is the saturation magnetization. What is left is evaluating the sum over bonds for the specific crystal structure. For a cubic system, we find the exchange energy

$$E_{\text{ex}} = \int d^3r A (\partial_i \mathbf{m}(\mathbf{r}) \cdot \partial_i \mathbf{m}(\mathbf{r})) \quad (7.3)$$

with $A = JM_s^2/(2a)$ for a simple cubic lattice with only nearest-neighbor interaction and lattice constant a . The sum over repeated indices is implied.

For DMI we apply the analogous reasoning, with the important distinction that the DMI vector is a function of the bond vector $\mathbf{D}_{mn} \rightarrow \mathbf{D}(\mathbf{a})$. We use this to define the DMI tensor $\tilde{D}_{ij} = D_i(\hat{e}_j)$ and write

$$\begin{aligned} \sum_{\langle mn \rangle} \mathbf{D}_{mn} \cdot (\mathbf{S}_m \times \mathbf{S}_n) &\propto \frac{1}{2} \sum_n \sum_{\mathbf{a}} \epsilon_{ijk} D_i(\mathbf{a}) M_j(\mathbf{R}_n) M_k(\mathbf{R}_n + \mathbf{a}) \\ &= \frac{1}{2V} \int d^3r \sum_{\mathbf{a}} \epsilon_{ijk} \tilde{D}_{il}(\mathbf{a}) M_j(\mathbf{r}) \partial_l M_k(\mathbf{r}) + \mathcal{O}(\delta^2) \end{aligned} \quad (7.4)$$

where now the first order is leading. The 0th order term vanishes with $\mathbf{S} \times \mathbf{S}$. We define the Lifshitz invariants

$$w_{ij} = \epsilon_{ikl} m_i \partial_j m_l. \quad (7.5)$$

The DMI energy can then be compactly written as

$$E_{\text{DMI}} = \int d^3r D_{ij} w_{ij} \quad (7.6)$$

where $D_{ij} = M_s^2 \tilde{D}_{ij}$. Depending on the form of the tensor, we obtain different types of DMI. If the DMI vector is parallel to the bond vector, the $D_{ij} = D\delta_{ij}$ gives a *Bloch-type DMI*

$$E_{\text{Bloch}} = \int d^3r D \text{tr}\{w\} = \int d^3r D \mathbf{m} \cdot (\nabla \times \mathbf{m}), \quad (7.7)$$

where D is now just a constant number. This is the most symmetric type of DMI since it only breaks inversion symmetry, but not rotational symmetry. The sign of D determines the chirality.

If we allow the DMI vector to point in a different direction than the bond vector, we need another vector to disambiguate the direction. Assuming this additional symmetry-breaking direction is independent of the bond vector, we may write $D_{ij} = D\epsilon_{ijk}d_k$, with some anisotropy axis \hat{d} . The result is called *Néel-type DMI*

$$E_{\text{Néel}} = \int d^3r D\epsilon_{ijk}w_{ij}d_k = \int d^3r D \left((\mathbf{m} \cdot \nabla)(\hat{d} \cdot \mathbf{m}) - (\mathbf{m} \cdot \hat{d})(\nabla \cdot \mathbf{m}) \right) \quad (7.8)$$

Bulk chiral magnets generally have Bloch-type DMI, because it has a higher symmetry. In the presence of additional symmetry breaking, such as at surfaces, an additional Néel-type coupling is present, often also called interfacial DMI. We will, for the most part, only consider the effects of Bloch-type DMI.

7.2. The minimal micromagnetic model for bulk chiral magnets

Much of the physics of bulk chiral magnets, such as the B20 compounds, turns out to be surprisingly well captured in a rather simple model. Uniaxial anisotropy acts as a mechanism to stabilize a skyrmion phase as a magnetic ground state. In bulk chiral magnets at finite temperature the skyrmion phase is often stabilized by thermal fluctuations instead. However, in practice, it turns out that many statements are independent of the stabilization mechanism.

We have established so far the micromagnetic form of exchange interaction and DMI. Here we add another term for the Zeeman energy in an external magnetic field H , and a uniaxial anisotropy K with an anisotropy axis \hat{e}_a .

$$\mathcal{E} = A(\partial_i \mathbf{m})^2 + D \mathbf{m} \cdot (\nabla \times \mathbf{m}) - \mathcal{K}(\hat{e}_a \cdot \mathbf{m})^2 - \mu_0 M_s \mathbf{H} \cdot \mathbf{m} \quad (7.9)$$

In the presence of a surface, minimizing the above energy functional, implies the non-trivial boundary condition

$$[A(\hat{\mathbf{s}} \cdot \nabla)\mathbf{m} - D(\mathbf{s} \times \mathbf{m})]_{\partial V} = 0, \quad (7.10)$$

where $\hat{\mathbf{s}}$ is the unit vector normal to the surface. It contains contributions from both the magnetization itself and its derivative (Robin boundary condition). This leads to interesting surface effects which we explore in detail in chapter 9.

As we have hinted at before the competition between exchange interaction A and DMI D defines a characteristic length scale. When inserting a periodic ansatz, such as the helical state $\mathbf{m} \propto \cos(Qz)\hat{\mathbf{x}} + \sin(Qz)\hat{\mathbf{y}}$ with a wavelength $\lambda = 2\pi/Q$, one finds that the energy is minimized by $Q = 2A/D$. The energy density is on the order of $D^2/(2A)$. We can use these natural scales to define a convenient unit system, that effectively reduces the number of free parameters of the model. We make the substitution $\mathbf{r} = \frac{2A}{D}\tilde{\mathbf{r}}$, $\nabla = \frac{D}{2A}\tilde{\nabla}$ and find

$$\tilde{\mathcal{E}} = \frac{\mathcal{E}}{\frac{D^2}{2A}} = \frac{1}{2}(\tilde{\partial}_i\mathbf{m})^2 + \mathbf{m} \cdot (\tilde{\nabla} \times \mathbf{m}) - \kappa(\hat{\mathbf{e}}_a \cdot \mathbf{m})^2 - \mathbf{h} \cdot \mathbf{m} \quad (7.11)$$

where $\kappa = \mathcal{K}/\frac{D^2}{2A}$ and $\mathbf{h} = \mu_0 M_s \mathbf{H}/\frac{D^2}{2A}$, are now the only free parameters left. Additionally, there is the “hidden” parameter $2A/D$. In the following, we drop the $\tilde{}$ on the gradients for convenience and have it understood that whenever we work in the dimensionless model, length scales are measured in $2A/D$.

The phase diagram as a function of κ and \mathbf{h} has been explored in depth (Butenko et al., 2010; Güngördü et al., 2016; Rowland, Banerjee, & Randeria, 2016; M. N. Wilson et al., 2014). Easy-plane anisotropy ($\kappa < 0$) favors a conical state, while easy-axis anisotropy ($\kappa > 0$) can stabilize a helical, conical, or skyrmion lattice phase, depending on the parameters. For every value of κ there is a critical field h_c above which the ground state is uniformly polarized along the direction of the applied magnetic field. We will take a closer look at some of these phases in the following.

Conical phase

In the case $\kappa = 0$, the model has only the applied magnetic field as a free parameter. Since the remaining terms are invariant under combined rotations or real space and spin space, the magnetic field direction is arbitrary. Lets say $\mathbf{h} = h\hat{\mathbf{e}}_z$. It turns out that the ground state of this model can be captured with the ansatz

$$\mathbf{m} = \begin{pmatrix} \sin \theta \cos(Qz) \\ \sin \theta \sin(Qz) \\ \cos \theta \end{pmatrix} \quad (7.12)$$

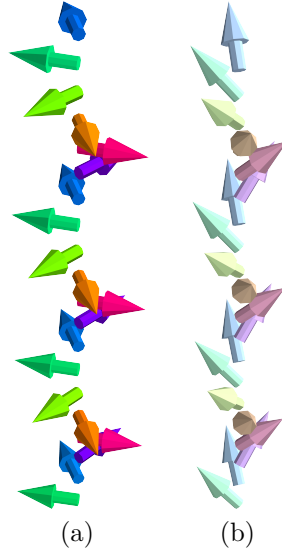


Figure 7.1.: 3D representation of the magnetization in the conical state conical state with (a) $\theta = \frac{\pi}{2}$ (Helix) and (b) $\theta = \frac{\pi}{4}$.

Inserting this ansatz into the model, we obtain the energy density

$$\mathcal{E} = \left(\frac{1}{2}Q^2 - Q \right) \sin^2 \theta - h \cos \theta . \quad (7.13)$$

Clearly, the energy is minimal for $Q = 1$ since this is how we defined the unit system. Minimizing the energy with respect to θ , it turns out that there is a phase transition at $h_c = 1$ where the second order of \mathcal{E} in θ vanishes. The $h > 1$ phase we call the *field polarized* phase and $h < 1$ the conical phase since there we have a finite cone angle

$$\theta = \begin{cases} \arccos h & \text{if } h < 1 \\ 0 & \text{if } h \geq 1 . \end{cases} \quad (7.14)$$

In dimensionful quantities the critical field for the conical-polarized transition is

$$H_c = \frac{D^2}{2A\mu_0 M_s} . \quad (7.15)$$

Skyrmion phase

Skyrmions are topologically non-trivial excitation of the non-linear sigma model (Skyrme, 1962). Magnetic skyrmions have been predicted a long time ago (Bogdanov & Yablonskii, 1989), but have more recently been discovered in chiral magnets (Muhlbauer et al., 2009). To be more precise, magnetic skyrmions are two-

dimensional skyrmions in a plane, in bulk chiral magnets the one perpendicular to the applied magnetic field.

The topological nature of an isolated magnetic texture manifests in the fact that assuming the magnetization is continuous everywhere and becomes continuous far away from the texture the integral

$$\frac{1}{4\pi} \int \mathbf{m} \cdot (\partial_x \mathbf{m} \times \partial_y \mathbf{m}) dx dy = N \quad (7.16)$$

must necessarily be an integer. N is called the winding number and if $N = -1$ the texture is classified as a skyrmion.

For topological classification to be well-defined the magnetic texture needs to be localized, therefore the magnetization approaches a homogeneous background magnetization within a typical length scale R_s , which we may identify as the skyrmion radius. To understand what determines this radius in a stable state look at the energy functional in two-dimensions

$$\tilde{E}_m = \int \left(\frac{1}{2} (\partial_i \mathbf{m})^2 + \mathbf{m} \cdot (\nabla \times \mathbf{m}) - \kappa (\hat{\mathbf{e}}_a \cdot \mathbf{m}) - \mathbf{h} \cdot \mathbf{m} \right) dx dy \quad (7.17)$$

and rescale the coordinate $\mathbf{r} \rightarrow \mathbf{r}/R_s$ after which the energy takes the form

$$\tilde{E}_m = \tilde{E}_{\text{ex}} + \tilde{E}_{\text{DMI}} R_s + (\tilde{E}_a + \tilde{E}_Z) R_s^2, \quad (7.18)$$

with some coefficients \tilde{E}_i which depend on the exact skyrmion profile. The effect of DMI is to introduce a linear term, shifting the energy minimum from 0 to a finite value. Thus DMI stabilizes finite-size skyrmions, in the sense that in the absence of any other mechanism for skyrmion annihilation such as surfaces or defects, there is no continuous path in configuration space that connects the skyrmion to the homogeneously polarized state.

Of course, this is different from the question of the ground state, i.e. which field configuration has the lowest energy. If the creation of a single skyrmion is energetically favorable, then many skyrmions are even more favorable and they form a typically hexagonal lattice. Like every periodic function, the magnetization describing the skyrmion lattice can be written as a Fourier series

$$\mathbf{m}(\mathbf{r}) = \sum_{\mathbf{G}} a_{\mathbf{G}} \left(\hat{\mathbf{e}}_{\mathbf{G}} \sin(\mathbf{G} \cdot \mathbf{r}) + \hat{\mathbf{z}} \cos(\mathbf{G} \cdot \mathbf{r}) \right), \quad (7.19)$$

where \mathbf{G} is a reciprocal lattice vector of the two-dimensional skyrmion lattice and we have used the symmetries $m_{1/2}(-\mathbf{r}) = -m_{1/2}(\mathbf{r})$ and $m_3(-\mathbf{r}) = m_3(\mathbf{r})$ to combine the \mathbf{G} and $-\mathbf{G}$ contributions. $a_{\mathbf{q}}$ is the amplitude of the respective Fourier component and $\hat{\mathbf{e}}_{\mathbf{q}}$ a polarization vector.

As long as we do not introduce in-plane anisotropy, symmetry demands that $a_{\mathbf{q}}$

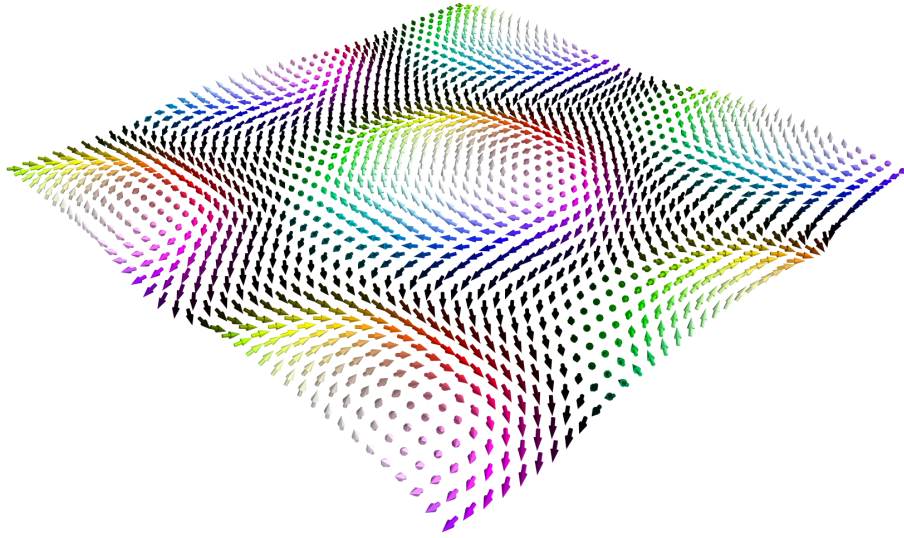


Figure 7.2.: Bloch-type skyrmion lattice

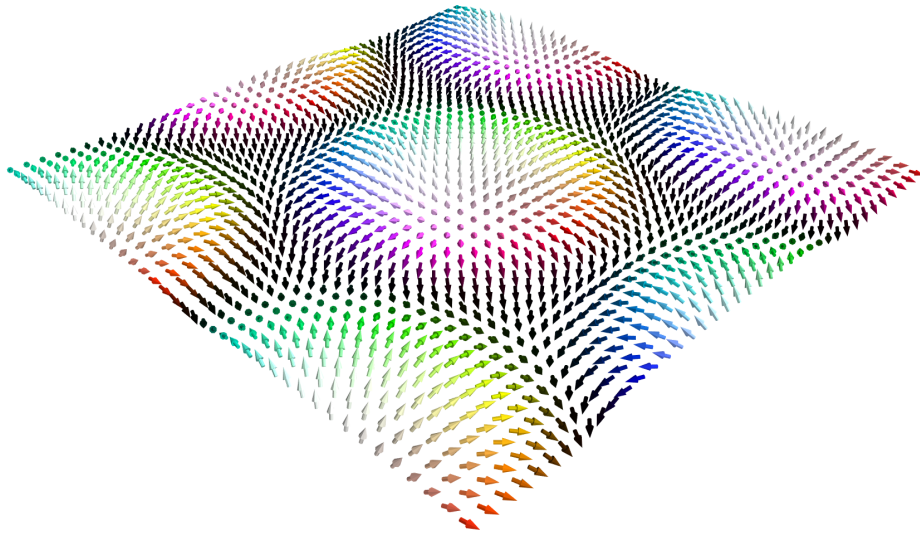


Figure 7.3.: Néel-type skyrmion lattice

must be the same for all \mathbf{q} with the same magnitude $|\mathbf{q}|$. The polarization vector we assume to be in-plane and is characterized by the angle χ to the \mathbf{q} vector

$$\hat{\mathbf{e}}_{\mathbf{G}} = \hat{\mathbf{G}} \cos \chi + \hat{\mathbf{z}} \times \hat{\mathbf{G}} \sin \chi, \quad (7.20)$$

where $\hat{\mathbf{G}} = \mathbf{G}/|\mathbf{G}|$ is the unit vector in \mathbf{G} direction. The parameter χ is called the *skyrmion helicity*. In general, the helicity could be different for each reciprocal lattice vector $\chi_{\mathbf{G}}$, but in this work, we will only be interested in the helicity of smallest non-trivial \mathbf{G} -vectors, the first “ring” of the hexagonal reciprocal lattice around the Γ -point. This ring is characterized by $|\mathbf{G}| = Q_{\text{SKL}} = 2\pi/a_{\text{SKL}}$, where Q_{SKL} and a_{SKL} are the lattice constants of the reciprocal and real space lattices respectively. If we restrict the summation in eq. (7.19) only to this first ring, a configuration known as *triple- \mathbf{q} -state*, and insert this ansatz into the DMI energy we obtain the helicity dependence

$$\tilde{E}_{\text{DMI}}^{\text{Bloch}} \propto \sin \chi, \quad \tilde{E}_{\text{DMI}}^{\text{Néel}} \propto \cos \chi. \quad (7.21)$$

For Bloch-type DMI the energy minimum is localized at a helicity of $\pm\pi/2$, depending on the sign of D , and the corresponding configuration is known as *Bloch skyrmions*. For Néel-type DMI on the other hand, the minimum is at 0 or π , which are called *Néel skyrmions*. Lattices of Bloch and Néel skyrmions are shown in figs. 7.2 and 7.3

Concerning the skyrmion lattice constant, although for the triple- \mathbf{q} state, the energy is minimal for $Q_{\text{SKL}} = 1$ in natural units, meaning it is equal to the pitch in the helical state, with the inclusion of higher harmonics this changes. Q_{SKL} is in general a function of h and κ .

8. Theory of magnetoelastic coupling in chiral magnets

After developing an understanding of the theory of the magnetic sector, we now explore the consequences of coupling to elasticity. Since both sectors are effectively described by a continuum theory, we treat the coupling on the same footing. To justify this approach and develop a better understanding of the physical meaning behind this coupling we first show how magnetoelastic coupling naturally appears in the derivation of the magnetic energy terms if one allows for lattice fluctuations section 8.1. It turns out that just to find and parametrize the correct form of magnetoelastic coupling, already comes with some insight into how special chiral magnets are in this regard, as we will see in section 8.2. When describing physical phenomena with magnetoelasticity, it turns out to be already a non-trivial exercise to decide which couplings to include and which to neglect. To gain some intuition about the effect of these couplings, we show some simple examples for the case of magnetostrictive coupling (section 8.3) and coupling to Lifshitz invariants (section 8.3).

8.1. Microscopic origins of magnetoelastic coupling

We revisit the spin Hamiltonian form eq. (7.1), with the idea that spins are allowed to deviate from their equilibrium position. Compared to the rigid model, this requires for example for the Heisenberg exchange interaction a generalization to site-dependent coupling $J \rightarrow J_{mn}$ since displacements vary from site to site. We assume that the coupling is only a function of relative position. Thus, the contribution of the symmetric exchange interaction to the Hamiltonian is

$$H_{\text{ex}} = \sum_{\langle mn \rangle} J_{mn} \mathbf{S}_m \cdot \mathbf{S}_n = \sum_{\langle mn \rangle} J(\mathbf{r}_m - \mathbf{r}_n) \mathbf{S}(\mathbf{r}_m) \cdot \mathbf{S}(\mathbf{r}_n). \quad (8.1)$$

Of course, the same reasoning holds for the DMI contribution

$$H_{\text{DMI}} = \sum_{\langle mn \rangle} \mathbf{D}_{mn} \cdot (\mathbf{S}_m \times \mathbf{S}_n) = \sum_{\langle mn \rangle} \mathbf{D}(\mathbf{r}_m - \mathbf{r}_n) \cdot (\mathbf{S}(\mathbf{r}_m) \times \mathbf{S}(\mathbf{r}_n)). \quad (8.2)$$

To keep the coming calculations brief, we combine both contributions into using tensor notation

$$H = H_{\text{ex}} + H_{\text{DMI}} = \sum_{\langle mn \rangle} \mathcal{J}^{\alpha\beta}(\mathbf{r}_m - \mathbf{r}_n) S_\alpha(\mathbf{r}_m) S_\beta(\mathbf{r}_n), \quad (8.3)$$

where we defined the exchange tensor with a symmetric and an antisymmetric contribution

$$\mathcal{J}^{\alpha\beta}(\mathbf{r}) = \delta_{\alpha\beta} J(\mathbf{r}) + \epsilon_{\alpha\beta\gamma} D_\gamma(\mathbf{r}) \quad (8.4)$$

Using $\mathbf{r}_n = \mathbf{R}_n + \mathbf{u}_n$, where \mathbf{R}_n is the equilibrium position and \mathbf{u}_n is the displacement, and rewriting in terms of the relative position of neighboring sites $\mathbf{R}_m = \mathbf{R}_n + \mathbf{a}$, where \mathbf{a} goes over the nearest neighbours of the n^{th} site, we obtain

$$\begin{aligned} & \sum_{\langle mn \rangle} \mathcal{J}^{\alpha\beta}(\mathbf{r}_m - \mathbf{r}_n) S_\alpha(\mathbf{r}_m) S_\beta(\mathbf{r}_n) \\ &= \frac{1}{2} \sum_{\mathbf{R}, \mathbf{a}} \mathcal{J}^{\alpha\beta}(\mathbf{a} + \mathbf{u}(\mathbf{R}) - \mathbf{u}(\mathbf{R} + \mathbf{a})) S_\alpha(\mathbf{R} + \mathbf{u}(\mathbf{R})) S_\beta(\mathbf{R} + \mathbf{a} + \mathbf{u}(\mathbf{R} + \mathbf{a})) \end{aligned} \quad (8.5)$$

We now have two small parameters: The displacement \mathbf{u} and the lattice spacing \mathbf{a} . First, we expand in \mathbf{u} . The 0th order describes the rigid interaction, which has been discussed in section 7.1. To extract the contribution to linear elasticity, we consider the 1st order. Decomposing the Hamiltonian into different u orders $H = H|_{\mathbf{u}=0} + H_{\text{me}} + \mathcal{O}(u^2)$ and neglecting higher orders we obtain

$$\begin{aligned} H_{\text{me}} &= \frac{1}{2} \int d\mathbf{r} \sum_{\mathbf{a}} \left[(\mathbf{u}(\mathbf{r}) - \mathbf{u}(\mathbf{r} + \mathbf{a})) \cdot \nabla \mathcal{J}^{\alpha\beta}(\mathbf{a}) S_\alpha(\mathbf{r}) S_\beta(\mathbf{r} + \mathbf{a}) \right. \\ & \quad \left. + \mathcal{J}^{\alpha\beta}(\mathbf{a}) \left(S_\beta(\mathbf{r} + \mathbf{a}) (\mathbf{u}(\mathbf{r}) \cdot \nabla) S_\alpha(\mathbf{r}) + S_\alpha(\mathbf{r}) (\mathbf{u}(\mathbf{r} + \mathbf{a}) \cdot \nabla) S_\beta(\mathbf{r} + \mathbf{a}) \right) \right] \end{aligned} \quad (8.6)$$

Eventually, we want to write the interaction in terms of strain, to make explicit the fact that the energy can not depend on \mathbf{u} directly, only its derivatives, by translational invariance. For this, we find it convenient to rewrite the last term using integration by parts and ignoring the boundary terms, resulting in

$$\begin{aligned} H_{\text{me}} &= \frac{1}{2} \int d\mathbf{r} \sum_{\mathbf{a}} \left[- \mathcal{J}^{\alpha\beta}(\mathbf{a}) (\nabla \cdot \mathbf{u}(\mathbf{r} + \mathbf{a})) S_\alpha(\mathbf{r}) S_\beta(\mathbf{r} + \mathbf{a}) \right. \\ & \quad \left. + (u_j(\mathbf{r}) - u_j(\mathbf{r} + \mathbf{a})) \left(\partial_j \mathcal{J}^{\alpha\beta}(\mathbf{a}) S_\alpha(\mathbf{r}) S_\beta(\mathbf{r} + \mathbf{a}) + \mathcal{J}^{\alpha\beta}(\mathbf{a}) S_\beta(\mathbf{r} + \mathbf{a}) \partial_j S_\alpha(\mathbf{r}) \right) \right]. \end{aligned} \quad (8.7)$$

Finally, we may expand in \mathbf{a} . We replace $\mathbf{u}(\mathbf{r}) - \mathbf{u}(\mathbf{r} + \mathbf{a})$ with the derivative of \mathbf{u} along \mathbf{a} . Shifting around the derivatives using integration by parts, we may bring the remaining terms into the form

$$\begin{aligned} & (\nabla \cdot \mathbf{u}(\mathbf{r} + \mathbf{a})) S_\alpha(\mathbf{r}) S_\beta(\mathbf{r} + \mathbf{a}) \\ & \rightarrow (\nabla \cdot \mathbf{u}) \left(S_\alpha S_\beta - S_\beta(\mathbf{a} \cdot \nabla) S_\alpha + \frac{1}{2} S_\beta(\mathbf{a} \cdot \nabla)^2 S_\alpha \right) + \mathcal{O}(a^3) \end{aligned} \quad (8.8)$$

and

$$\begin{aligned}
& (u_j(\mathbf{r}) - u_j(\mathbf{r} + \mathbf{a})) \left(\partial_j \mathcal{J}^{\alpha\beta}(\mathbf{a}) S_\alpha(\mathbf{r}) S_\beta(\mathbf{r} + \mathbf{a}) + \mathcal{J}^{\alpha\beta}(\mathbf{a}) S_\beta(\mathbf{r} + \mathbf{a}) \partial_j S_\alpha(\mathbf{r}) \right) \\
& \rightarrow -(\mathbf{a} \cdot \nabla) u_j(\mathbf{r}) \left(\partial_j \mathcal{J}^{\alpha\beta} S_\alpha S_\beta + \mathcal{J}^{\alpha\beta} S_\beta \partial_j S_\alpha \right. \\
& \quad \left. + \frac{1}{2} \partial_j \mathcal{J}^{\alpha\beta} (\mathbf{a} \cdot \nabla) (S_\alpha S_\beta) + \frac{1}{2} \mathcal{J}^{\alpha\beta} (\mathbf{a} \cdot \nabla) (S_\beta \partial_j S_\alpha) + \mathcal{O}(a^3) \right).
\end{aligned} \tag{8.9}$$

We sort all these terms according to the number of derivatives.

As a result, we obtain the overall magnetoelastic energy up to second order in lattice coupling

$$\mathcal{E}_{me} = \varepsilon_{ij} \lambda_{ij}^{\alpha\beta} M_\alpha M_\beta + \varepsilon_{ij} \lambda_{ijk}^{\alpha\beta} M_\alpha \partial_k M_\beta + \varepsilon_{ij} \lambda_{ijkl}^{\alpha\beta} M_\alpha \partial_k \partial_l M_\beta \tag{8.10}$$

where the coupling tensors are given by

$$\begin{aligned}
\lambda_{ij}^{\alpha\beta} &= - \sum_{\mathbf{a}} (\delta_{ij} \mathcal{J}^{\alpha\beta}(\mathbf{a}) + \frac{1}{2} (a_i \partial_j \mathcal{J}^{\alpha\beta}(\mathbf{a}) + a_j \partial_i \mathcal{J}^{\alpha\beta}(\mathbf{a}))) \\
\lambda_{ijk}^{\alpha\beta} &= \sum_{\mathbf{a}} (\delta_{ij} J(\mathbf{a}) + (a_i \partial_j + a_j \partial_i) J(\mathbf{a}) a_k + (a_i \delta_{jk} + a_j \delta_{ik}) J(\mathbf{a})) \\
\lambda_{ijkl}^{\alpha\beta} &= \sum_{\mathbf{a}} (a_i \delta_{jk} + a_j \delta_{ik}) a_l J(\mathbf{a})
\end{aligned} \tag{8.11}$$

These couplings depend of course on the properties of the exchange tensor \mathcal{J} . Since we have assumed the original Hamiltonian to be symmetric under combined rotations of spin space and real space, this will be reflected in these tensors. However, we could plug a more general exchange tensor into these equations and obtain the elastic coupling tensors for the respective symmetry class.

In conclusion, the origin of magnetoelastic coupling can be traced back to the distance and direction dependence of the microscopic interactions. We have derived the expression for the magnetoelastic couplings up to second order in lattice spacing, to be consistent with the derivation done in the rigid system. However, determining the actual coupling tensors requires knowledge about \mathcal{J} and its derivative, which is in general hard to obtain from first principles. For more general considerations, see (Brown, 1966).

8.2. Classification of magnetoelastic couplings

Since it is often difficult to find out about the microscopic details of magnetic interactions, it is simpler to take the intuition gained from the previous section and write down a phenomenological model. In this context, we view the model as a gradient expansion in the fields \mathbf{m} , \mathbf{u} , and their derivatives, keeping all symmetry-allowed terms up to a certain order. As in any expansion, we hope that higher

orders contribute less and less to the overall behavior of the system and cut off the expansion at some point. Determining where this point is, may not always be easy. A basic assumption of our original model was that spin-orbit coupling (SOC) is weak, leading to magnetic textures on length scales where the continuum limit is justified. We may therefore take the strength of SOC as a small parameter λ_{SOC} . Since we include DMI as an essential ingredient for non-trivial magnetic textures, and DMI is $\mathcal{O}(\lambda_{\text{SOC}}^2)$ it is natural to include all terms up until this order.

The type of magnetoelastic coupling in lowest order in the gradient expansion, which is commonly mentioned in textbooks (Landau & Lifshitz, 1963) is often referred to as *magnetostriction* and has the energy contribution

$$\mathcal{E}_{\text{ms}} = \varepsilon_{ij} \lambda_{ijkl} m_k m_l . \quad (8.12)$$

This term contains contributions up to $\mathcal{O}(\lambda_{\text{SOC}}^2)$. For a cubic chiral magnet with point group 23, the tensor λ has four independent components with a tensor as discussed in section 1.2. For a derivation of the general coupling tensor see (E. Callen & Callen, 1965). However, if we assume $m^2 = 1$, we can reduce the effective number of parameters by sorting the λ_{12} and λ_{21} contributions into a chiral ($\lambda_{12} - \lambda_{21}$) and a non-chiral ($\lambda_{12} + \lambda_{21}$) contribution

$$\begin{aligned} & \frac{1}{2}(\lambda_{12} + \lambda_{21})(\varepsilon_{11}(m_2^2 + m_3^2) + \varepsilon_{22}(m_3^2 + m_1^2) + \varepsilon_{33}(m_1^2 + m_2^2)) \\ & + \frac{1}{2}(\lambda_{12} - \lambda_{21})(\varepsilon_{11}(m_2^2 - m_3^2) + \varepsilon_{22}(m_3^2 - m_1^2) + \varepsilon_{33}(m_1^2 - m_2^2)) \end{aligned} \quad (8.13)$$

and rewriting

$$\begin{aligned} & \varepsilon_{11}(m_2^2 + m_3^2) + \varepsilon_{22}(m_3^2 + m_1^2) + \varepsilon_{33}(m_1^2 + m_2^2) \\ & = \text{tr}\{\varepsilon\} + \varepsilon_{11}m_1^2 + \varepsilon_{22}m_2^2 + \varepsilon_{33}m_3^2 . \end{aligned} \quad (8.14)$$

Thus, we can get rid of the non-chiral term by shifting $\lambda_{11} \rightarrow \lambda_{11} + (\lambda_{12} + \lambda_{21})/2$ which introduces a term that is linear in the trace of the strain tensor but independent of magnetization

$$\mathcal{E} \rightarrow \mathcal{E} + \frac{1}{2}(\lambda_{12} + \lambda_{21}) \text{tr}\{\varepsilon\} . \quad (8.15)$$

The extra term is effectively an isotropic stress that causes a volume change proportional to the coupling $\lambda_{12} + \lambda_{21}$. The effect of this volume change can be absorbed into the existing model parameters. Thus, we can reduce the number of independent components to three and write $\lambda_{12} \rightarrow \lambda_{12} - (\lambda_{12} + \lambda_{21})/2$

$$\lambda^V = \begin{pmatrix} \lambda_{11} & \lambda_{12} & -\lambda_{12} & 0 & 0 & 0 \\ -\lambda_{12} & \lambda_{11} & \lambda_{12} & 0 & 0 & 0 \\ \lambda_{12} & -\lambda_{12} & \lambda_{11} & 0 & 0 & 0 \\ 0 & 0 & 0 & \lambda_{44} & 0 & 0 \\ 0 & 0 & 0 & 0 & \lambda_{44} & 0 \\ 0 & 0 & 0 & 0 & 0 & \lambda_{44} \end{pmatrix} . \quad (8.16)$$

One order higher in the gradient expansion the coupling is most naturally expressed in the Lifshitz invariants $w_{ij} = \epsilon_{ikl} m_k \partial_j m_l$, which allows us to write all five independent couplings (Kitchaev, Beyerlein, & Van der Ven, 2018). This *DMI-type coupling* may be written in tensor notation as

$$\mathcal{E}_{\text{meDMI}} = \varepsilon_{ij} \mu_{ijkl} w_{kl}^s + \mu_a (\varepsilon_{12} w_{12}^a + \varepsilon_{23} w_{23}^a + \varepsilon_{31} w_{31}^a) . \quad (8.17)$$

where we introduced the symmetrized and antisymmetrized Lifshitz invariants, $w_{ij}^s = (w_{ij} + w_{ji})/2$ and $w_{ij}^a = (w_{ij} - w_{ji})/2$.

For completeness, we also write down the energy term representing the effect of elasticity on the gradient on a distorted background $\nabla \rightarrow (1 + \varepsilon)\nabla$, which modifies the exchange interaction. This exchange-type coupling may be written as

$$\mathcal{E}_{\text{meEx}} = \varepsilon_{ij} \nu_{ijkl} \partial_k \mathbf{m} \cdot \partial_l \mathbf{m} \quad (8.18)$$

with four independent parameters in space group 23.

There is another type of ME coupling that is only relevant at surfaces, called *magnetorotation* (Maekawa & Tachiki, 1976). Magnetorotation couples the magnetization to the antisymmetrized displacement gradient (eq. (1.25)), describing local rotations.

$$\mathcal{E}_{\text{m-rot}} = \lambda_r (\omega_{12} m_1 m_2 + \omega_{23} m_2 m_3 + \omega_{31} m_3 m_1) . \quad (8.19)$$

In general, there will be also a rotational version of the coupling to Lifshitz invariants as well as the exchange-type terms.

$$\begin{aligned} \mathcal{E}_{\text{ch-rot}} &= \mu_r (\omega_{12} w_{12} + \omega_{23} w_{23} + \omega_{31} w_{31}) \\ \mathcal{E}_{\text{ex-rot}} &= -\nu_r \mathbf{m} \cdot (\omega_{12} \partial_1 \partial_2 + \omega_{23} \partial_2 \partial_3 + \omega_{31} \partial_3 \partial_1) \mathbf{m} \end{aligned} \quad (8.20)$$

However, we will not make use of these in this work and only list them here for completeness.

The inclusion of elastic couplings introduces a considerable amount of new parameters to the micromagnetic model. Even if we assume $m^2 = 1$ magnetostriction adds three independent parameters. The DMI-type coupling adds five, and the exchange-type coupling another four. In total, that makes 12 independent parameters, plus magnetorotation if applicable. Additionally, the stiffness tensor must be known, however, this can usually be achieved by independent measurements, such as resonant ultrasound experiments (Migliori et al., 1993). Of course, this is not a feasible model for making definite predictive statements about physical phenomena, since with such a large number of parameters we can probably fit anything. Instead, we will make reasonable assumptions about which kind of coupling contributes the most in the specific case under consideration.

8.3. Selected examples

To elucidate the effect of the unusual form of the magnetoelastic coupling tensors we discuss some examples including the magnetostriction term, where the chiral nature of the coupling tensor becomes important. It turns out that even in the absence of microscopic variations of the magnetization there can be non-trivial effect of magnetoelastic coupling on the static configuration of the system.

Homogeneous chiral magnetostriction

For strong enough external magnetic fields (above a critical field H_c) the magnetic state will be homogeneously polarized. In this scenario, only the homogeneous strain E_{ij} is non-zero. The elasticity theory for this state is thus given by the energy density

$$\mathcal{E} = \frac{1}{2} E_{ij} C_{ijkl} E_{kl} + E_{ij} \lambda_{ijkl} m_k m_l. \quad (8.21)$$

The ground state is then trivially found by minimizing this quadratic function. We express the solution to the equation of state conveniently using Mandel notation (see eq. (1.40))

$$E^M = -(C^M)^{-1} \lambda^M \langle (mm^T)^M \rangle_{\mathcal{V}}. \quad (8.22)$$

Assuming for example a constant magnetization $\mathbf{m} = (0, 0, 1)$ as a result of a magnetic field applied in [001] direction, we obtain the following strain

$$\begin{aligned} E_{11} &= \frac{C_{12}\lambda_{11} + (C_{11} + 2C_{12})\lambda_{12}}{C_{11}^2 + C_{11}C_{12} - 2C_{12}^2} \\ E_{22} &= \frac{C_{12}\lambda_{11} - (C_{11} + 2C_{12})\lambda_{12}}{C_{11}^2 + C_{11}C_{12} - 2C_{12}^2} \\ E_{33} &= -\frac{(C_{11} + C_{12})\lambda_{11}}{C_{11}^2 + C_{11}C_{12} - 2C_{12}^2} \end{aligned} \quad (8.23)$$

while the three shear strain components vanish. Notice that the strains in x and y direction differ by the sign of the λ_{12} term. The effect of magnetostriction is thus not only a tetragonal distortion, as would be expected for a centrosymmetric cubic magnet, but an orthorhombic distortion (see fig. 8.1). Note that this effect requires not only inversion symmetry breaking but also rotational symmetry breaking since a 4-fold rotation symmetry around the magnetic field axis would not allow this effect. Interestingly, because the interaction is quadratic in magnetization, inverting the direction of the magnetic field does not change the strain at all.

If the magnetic field is instead applied along the [111] direction, this chiral effect on magnetostriction vanishes, resulting in a rhombohedral distortion. This is reasonable since in this scenario no crystal axis has a special role.

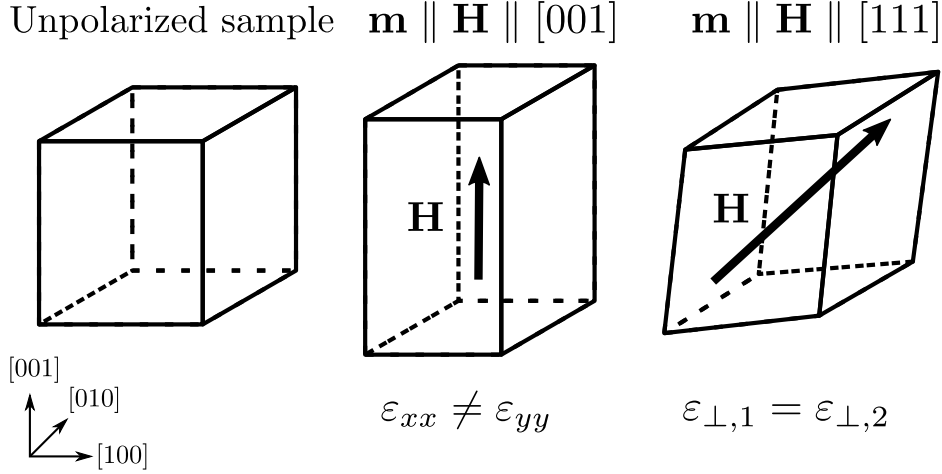


Figure 8.1.: Schematic picture of the effect of chiral magnetostriction for homogeneous magnetization. Left is the unpolarized and unstrained crystal. In the middle, the polarization is along one of the crystal axes, thus the strain breaks chiral symmetry. On the right, the polarization is along the $[111]$ axis, the strain is not chiral since not crystal axis is favored.

Helix orientation in chiral magnetoelastic potential

In the helical phase with a helix orientation along a particular axis $\hat{\mathbf{q}}$ the magnetization is described by the ansatz

$$\mathbf{m}(\mathbf{r}) = \sin(\mathbf{q} \cdot \mathbf{r})\hat{\mathbf{e}}_2 + \cos(\mathbf{q} \cdot \mathbf{r})\hat{\mathbf{e}}_3 \quad (8.24)$$

in an orthonormal basis where $\hat{\mathbf{e}}_1 \parallel \mathbf{q}$ and $\hat{\mathbf{e}}_2, \hat{\mathbf{e}}_3 \perp \mathbf{q}$. In the isotropic magnetic model, the direction of the helix is ambiguous. However, the magnetostriction coupling will introduce some anisotropy depending on the coupling parameters λ_{11} , λ_{12} and λ_{44} , since the presence of the helix in the magnetization leads to a corresponding periodic lattice distortion. These directions-dependent lattice distortions create an effective potential in which the helix will orient to the minimum at equilibrium. Therefore we use the ansatz in eq. (8.24) for an arbitrary wavevector $\mathbf{q} = Q(\sin \psi \cos \chi, \sin \psi \sin \chi, \cos \psi)$ to get the magnetoelastic energy as a function of helix orientation

$$\mathcal{V}(\psi, \chi) = \int d^3r \mathcal{E}(\mathbf{m}(\psi, \chi)) \quad (8.25)$$

The result is shown graphically in fig. 8.2. We see two anisotropic contributions one from the introduced cubic anisotropy, which goes with $\lambda_a = \lambda_{11} - 2\lambda_{44}$ and one chiral term from λ_{12} . Since the overall strength of the coupling is not relevant to

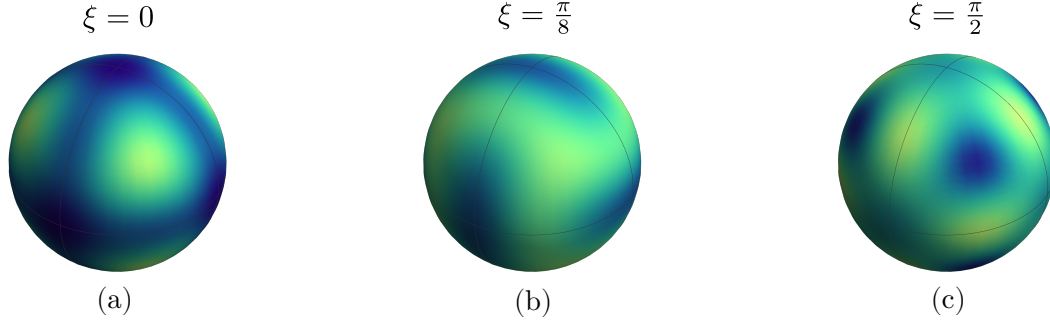


Figure 8.2.: Effective helix potential from lattice distortions for different values of the coupling parameters. (a) For purely centrosymmetric coupling ($\lambda_{12} = 0$) the minimum is in the $[111]$ direction like in MnSi. (b) For mixed coupling the potential has a chiral twist. (c) For purely chiral coupling ($\lambda_a = 0$) the minimum is in $[110]$ direction.

the helix orientation we can parametrize the two effects such that

$$\begin{aligned}\lambda_{12} &\equiv \lambda_0 \sin \xi \\ \lambda_a &\equiv \lambda_0 \cos \xi .\end{aligned}\tag{8.26}$$

The most interesting feature of this potential is that the chiral magnetoelastic coupling λ_{12} has a clear preference for a helix in the $[110]$ direction. This is unusual since the leading cubic anisotropy of the form m_i^4 can have a minimum only in the $[001]$ or $[111]$ direction. A helix oriented in the $[110]$ direction has been observed in iron-doped MnSi (Kindervater et al., 2020).

Magnon-phonon hybrid through DMI-type elastic coupling

To show an example of where the DMI-type coupling becomes relevant we discuss a non-reciprocity in the sound velocity that was seen in ultrasound experiments field polarized phase of Cu_2OSeO_3 (Nomura et al., 2019). The non-reciprocity is a result of magnon-phonon hybridization, which lifts the degeneracy between the two transversal acoustic phonons. This magneto-chiral phonon inherits its chirality from DMI.

To describe this effect theoretically we use linear spin wave theory based on the Landau-Lifshitz (LL) equation

$$\partial_t \mathbf{m} = \mathbf{m} \times \frac{\delta \mathcal{E}}{\delta \mathbf{m}}\tag{8.27}$$

where we have absorbed the gyromagnetic ratio into the time coordinate. The

elastic dynamics are given by

$$\partial_t^2 \mathbf{u} = \frac{\delta \mathcal{E}}{\delta \mathbf{u}} . \quad (8.28)$$

To calculate the spectrum we linearize the LL equation in fluctuations around the ground state in both magnetization and displacement using the decomposition

$$\mathbf{m}(r, t) = \mathbf{m}_0(r) + \boldsymbol{\mu}(r, t), \quad \mathbf{u}(r, t) = \mathbf{u}_0(r) + \boldsymbol{\eta}(r, t) . \quad (8.29)$$

The ground state $(\mathbf{m}_0, \mathbf{u}_0)$ is then defined by

$$\left. \frac{\delta \mathcal{E}}{\delta \mathbf{m}} \right|_{\mathbf{m}=\mathbf{m}_0} = 0 \quad \left. \frac{\delta \mathcal{E}}{\delta \mathbf{u}} \right|_{\mathbf{u}=\mathbf{u}_0} = 0 . \quad (8.30)$$

The ingredients for the model are as follows: We include exchange interaction and DMI to obtain a chiral magnon mode, a strong magnetic field $h > h_c$, such that the ground state magnetization is uniformly polarized, and a magnetoelastic coupling to facilitate the hybridization. The energy functional \mathcal{E} is thus given by

$$\mathcal{E} = A(\partial_i m_j)^2 + D\mathbf{m} \cdot (\nabla \times \mathbf{m}) - \mathbf{h} \cdot \mathbf{m} + \varepsilon_{ij} \mu_{ijkl} w_{kl} + \frac{1}{2} \varepsilon_{ij} C_{ijkl} \varepsilon_{kl} . \quad (8.31)$$

We omit here the coupling antisymmetrized Lifshitz invariants, since it is not needed to explain the effect and only makes the expressions unnecessarily long.

Since all the spatial derivatives of \mathbf{m}_0 vanish $\partial_i m_{0,j} = 0$ all the Lifshitz invariants $w_{ij} = 0$ also vanish and the elastic ground state is trivial $\varepsilon_0 = 0$.

Coupling with $\mathbf{m}_0 = \text{const.}$ and $\mathbf{u}_0 = 0$

$$\frac{\delta \mathcal{E}_{\text{meDMI}}}{\delta m_n} = -\mu_{ijkl} \varepsilon_{knm} m_{0,m} \partial_l \partial_i \eta_j \quad (8.32)$$

Inserting this into the LL equation and Fourier transforming with respect to time and space coordinates we obtain

$$i\omega \mu_i(\mathbf{q}, \omega) = \varepsilon_{ijk} m_{0,j} \left[(q^2 + h) \mu_k(\mathbf{q}, \omega) + 2i \varepsilon_{kln} q_l \mu_n(\mathbf{q}, \omega) - \varepsilon_{kln} m_{0,n} \mu_{mop} q_o q_p \eta_m(\mathbf{q}, \omega) \right] + \mathcal{O}(\mu^2) . \quad (8.33)$$

The same procedure may be applied to the phonon equation of motion. We use

$$\frac{\delta \mathcal{E}_{\text{meDMI}}}{\delta u_i} = \mu_{ijkl} \partial_j w_{kl} = \mu_{ijkl} \varepsilon_{kmn} m_{0,m} \partial_j \partial_l \mu_n + \mathcal{O}(\mu^2) \quad (8.34)$$

to obtain the Fourier-transformed equation

$$\rho \omega^2 \eta_i = C_{ijkl} q_j q_k \eta_l + \mu_{ijkl} \varepsilon_{kmn} m_{0,m} q_j q_l \mu_n . \quad (8.35)$$

There is at this point a slight technical issue, since the LL equation is first order in time, the elastic equation of motion on the other hand is second order. To combine them into a single linear equation, which would allow us to determine the spectrum by diagonalization of the corresponding matrix, we define the auxiliary field

$$\boldsymbol{\zeta} = \rho \partial_t \boldsymbol{\eta} , \quad (8.36)$$

which allows us to split the elastic equation of motion into two first-order equations. The full system of equations is then

$$\begin{aligned} i\omega \boldsymbol{\mu} &= H \boldsymbol{\mu} + J \boldsymbol{\eta} \\ i\omega \boldsymbol{\eta} &= \frac{1}{\rho} \boldsymbol{\zeta} \\ i\omega \boldsymbol{\zeta} &= D \boldsymbol{\eta} + L \boldsymbol{\mu} \end{aligned} \quad (8.37)$$

where the matrices are given by

$$\begin{aligned} H_{in} &= \epsilon_{ijk} m_{0,j} \left[(q^2 + h) \delta_{kn} + 2i \epsilon_{kln} q_l \right] \\ J_{im} &= -\epsilon_{ijk} m_{0,j} \epsilon_{kln} m_{0,l} \mu_{mopn} q_o q_p \\ D_{il} &= C_{ijkl} q_j q_k \\ L_{in} &= \mu_{ijkl} \epsilon_{kmn} m_{0,m} q_j q_l \end{aligned} \quad (8.38)$$

We now simply have to diagonalize the linear system of equations, obtaining the eigenfrequencies, see fig. 8.3.

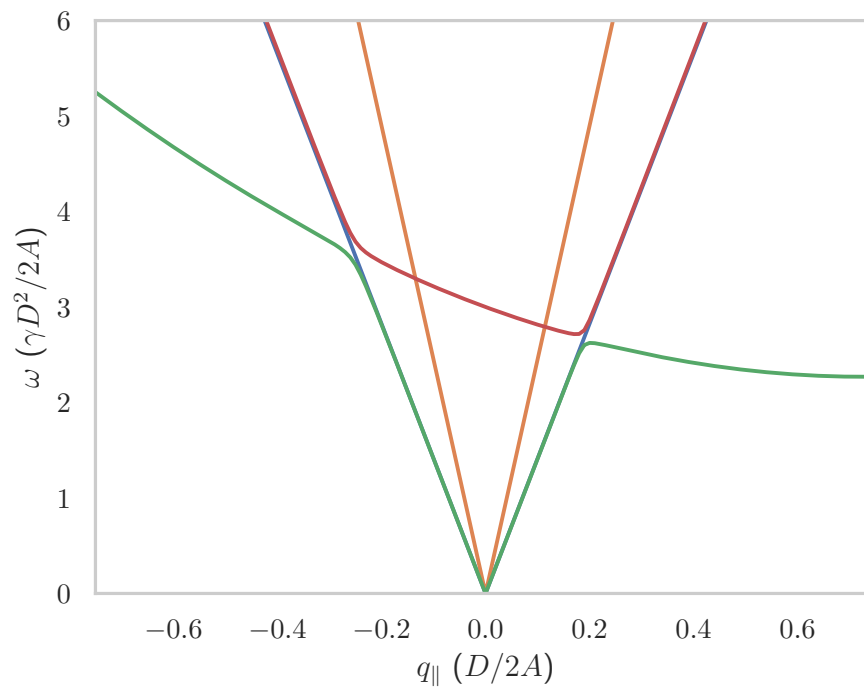


Figure 8.3.: Spectrum of magnon-phonon hybrid for momentum along the magnetic field. One of the transversal acoustic phonon branches hybridizes with the magnon, and the other phonon branches are unaffected.

9. Magnetoelastic effects on chiral surface twists

One of the many interesting features of the chiral magnets is the fact that as a result of uncompensated DMI at the surface, the magnetization follows nontrivial boundary conditions (eq. (7.10)). To accommodate these boundary conditions, various magnetic textures show an effect called surface twist. Even in the field-polarized phase, this surface twist appears as the magnetization is tilted away from the magnetic field axis close to the surface (Aqeel et al., 2021; Rybakov et al., 2013). The chiral surface twist can also affect the stability of other magnetic textures (Leonov et al., 2016; Meynell et al., 2014) and can be used as a mechanism for the creation of skyrmions (Müller, Rosch, & Garst, 2016). In section 9.1 we show how the magnetization profile at the surface is affected by magnetoelastic coupling.

Skyrmions also show a surface twist in the helicity (Zhang et al., 2018), if the magnetic field, and consequently the skyrmion axis, is parallel to the surface normal. We present a simple analytical model of this effect in section 9.2 which is in close agreement with micromagnetic simulations. Interestingly, this clear prediction of the well-established and usually accurate minimal micromagnetic model, is in harsh disagreement with experimental results (Schneider et al., 2018; Zhang et al., 2018). We look at the effect of magnetoelastic coupling on the surface twist in section 9.2 as a possible explanation. However, it turns out that the effect is far too small to explain experimental observations. Even worse, more recent experiments on a field-cooled meta-stable skyrmion lattice, show that at low temperatures the length scale of the surface twist tends towards value predicted by the minimal model (Tan et al., 2024), while magnetoelastic coupling is expected to have larger effects at low temperatures. We explore several other explanations, but overall this remains an open question.

9.1. Surface twist in the field polarized and helical state

As discussed in section 7.2 the phase diagram of bulk chiral magnets contains a helical phase at low magnetic fields and a field-polarized phase at strong magnetic

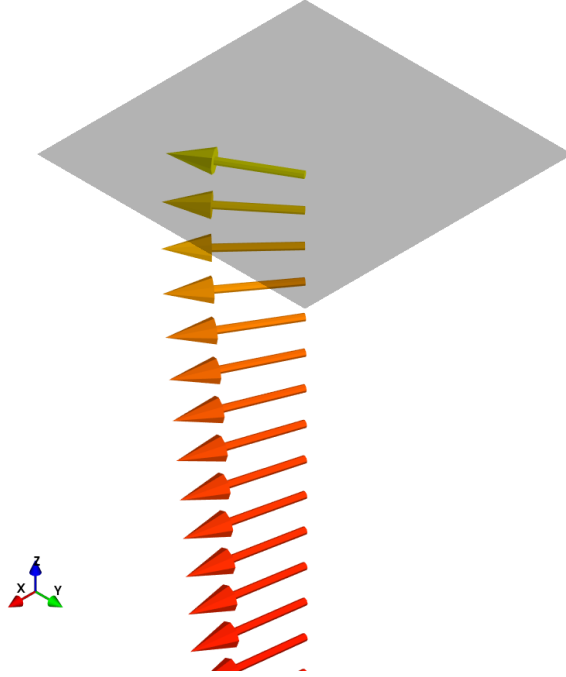


Figure 9.1.: Magnetization profile of the surface twist in the field polarized phase. The surface is at $z = 0$, the magnetic field is applied in x direction, at the surface the magnetization twists out of the magnetic field axis and has a finite y -component.

fields. Since uniaxial anisotropy is not necessary to discuss these phases we neglect it ($\kappa = 0$) and consider the energy

$$\tilde{\mathcal{E}}_m = \frac{1}{2}(\partial_i \mathbf{m})^2 + \mathbf{m} \cdot (\nabla \times \mathbf{m}) - \mathbf{h} \cdot \mathbf{m} . \quad (9.1)$$

The bulk ground state depends on $h = |\mathbf{h}|$. For $h = 0$, we have a helical state. At finite h this induces a conical state with a cone angle depending on h . For $h > 1$, we have a fully polarized state.

Let the surface normal be in z -direction with the normal vector $\hat{\mathbf{s}} \parallel \hat{\mathbf{z}}$. An external magnetic field is applied parallel to the surface in the x -direction $h\hat{\mathbf{x}}$. We make an ansatz that is a modification of the bulk conical state, with an additional twist by an angle ψ around the surface normal, that will depend on the distance to the

surface

$$\mathbf{m} = R_z(\psi(z))R_x(Qx)R_z(\theta(z))\hat{\mathbf{x}} = \begin{pmatrix} \cos \theta \cos \psi - \cos Qx \sin \theta \sin \psi \\ \cos \theta \sin \psi + \cos Qx \sin \theta \cos \psi \\ \sin Qx \sin \theta \end{pmatrix} \quad (9.2)$$

In general, the cone angle may also change close to the surface, as indicated by the argument z . Inserting this ansatz into the energy and integrating over the x direction we can derive the effective one-dimensional theory, given by the energy functional

$$E_m = \int_0^\infty dz \left(\frac{1}{2}(\theta')^2 + \frac{1}{8}(3 + \cos 2\theta)\psi'(\psi' - 2) + \mathcal{V}(\theta, \psi) \right), \quad (9.3)$$

where we defined the effective potential \mathcal{V} for the cone and twist angles

$$\mathcal{V}(\theta, \psi) = \frac{1}{2} \left(\sin^2 \theta - \cos \psi (1 + 2h \cos \theta - \cos 2\theta) \right) \quad (9.4)$$

If h is small, then $\theta \approx \pi/2$ and the ψ dependent term vanishes. The same holds for large $h > h_c$ with $\theta = 0$. However, if $h \lesssim h_c$ the twist angle will influence the cone angle and vice versa. Thus analytical solutions are only possible for the polarized state ($h \geq 1$) and the helix ($h = 0$).

The resulting equations of motion are in general not analytically solvable. We can obtain solvable equations, if we assume that the cone angle θ is not influenced by the surface twist and just set θ to its bulk value

$$\theta = \begin{cases} \arccos h & \text{if } h < 1 \\ 0 & \text{if } h \geq 1. \end{cases} \quad (9.5)$$

Using this assumption, we obtain as the equation of state for the twist angle ψ the well-known *sine-Gordon equation* and Neumann boundary condition

$$\psi'' = \frac{1}{L^2(h)} \sin \psi \quad \psi'(0) = \begin{cases} -\frac{1}{2}(1 + h^2) & \text{if } h < 1 \\ -1 & \text{if } h \geq 1 \end{cases} \quad (9.6)$$

where we defined

$$L(h) = \begin{cases} \sqrt{\frac{1 + h^2}{2}} & \text{if } h \ll 1 \\ \frac{1}{\sqrt{h}} & \text{if } h \geq 1. \end{cases} \quad (9.7)$$

In both cases we apply the additional condition $\psi(z \rightarrow \infty) = 0$, requiring that the magnetization approaches its bulk state far away from the surface. The solution of

the sine-Gordon equation under these conditions is unique and given by

$$\psi(z) = 4 \arctan \left(e^{-\frac{z-z_0(h)}{L(h)}} \right) \quad (9.8)$$

which is parametrized by only two numbers, both of which depend on the external magnetic field: The shift in z direction

$$z_0(h) = -L(h) \operatorname{Arcosh} \left\{ \begin{array}{ll} \frac{2}{L^3(h)} & \text{if } h \ll 1 \\ \frac{2}{L(h)} & \text{if } h \geq 1 \end{array} \right\} \quad (9.9)$$

and $L(h)$ which turns out to be the length scale of the surface twist. Thus the length scale of the surface twist depends strongly on the applied magnetic field.

Magnetoelastic effect on the surface twist in the field polarized phase

In the conical phase, the non-trivial boundary conditions for the displacement field do not allow us to easily integrate out strain. However, in the polarized phase, the problem becomes effectively one-dimensional, since there is no modulation to the surface, and all x and y derivatives have to vanish by symmetry. In this one-dimensional problem, the boundary conditions are trivially fulfilled, and this makes reasoning about this problem much easier. We therefore concentrate on the field polarized phase from now on

$$\mathbf{m} = \begin{pmatrix} \cos \psi \\ \sin \psi \\ 0 \end{pmatrix} \quad (9.10)$$

where the only degree of freedom left is the twisting angle $\psi(z)$. We investigate the effect of magnetostriction on the chiral surface twist. The energy density including the elastic degrees of freedom is then

$$\tilde{\mathcal{E}} = \tilde{\mathcal{E}}_m + \varepsilon_{ij} \lambda_{ijkl} m_k m_l + \frac{1}{2} \varepsilon_{ij} C_{ijkl} \varepsilon_{kl} \quad (9.11)$$

where the elastic constants and couplings are measured in the magnetic energy scale $\lambda \rightarrow \lambda \frac{D^2}{2A}$ and $C \rightarrow C \frac{D^2}{2A}$, to maintain the dimensionless units. We will assume here that both C and λ tensor have the form corresponding to point group 23, and that $m^2 = 1$ such that λ can be written as in eq. (8.16), in the principal coordinates of the crystal lattice. However, here we have to consider the relative orientation of the crystal structure to the surface and magnetic field. To stay in the

previously used convention of the surface normal vector $\hat{\mathbf{s}}$ pointing in z -direction and the external magnetic field \mathbf{h} pointing in the x -direction, we rotate the elastic tensors.

Let C and λ be the elastic tensors in the principle coordinates of the lattice, which in the cubic crystal system is orthogonal. The rotation matrix $R(\alpha, \beta, \gamma) \equiv R_z(\alpha)R_x(\beta)R_z(\gamma)$ connects the vectors $\hat{\mathbf{s}}$ and \mathbf{h} with the lattice directions [001] and [100] such that $\hat{\mathbf{s}} = R\hat{\mathbf{e}}_{[001]}$ and $\mathbf{h}/h = R\hat{\mathbf{e}}_{[100]}$ using the Euler angles α , β and γ . To transform the elastic tensors into the coordinate system, where $\hat{\mathbf{s}}$ and \mathbf{h} point into the desired direction we apply the inverse rotation,

$$C'_{i_1 j_1 k_1 l_1} = R_{i_1 i_2}^T R_{j_1 j_2}^T R_{k_1 k_2}^T R_{l_1 l_2}^T C_{i_2 j_2 k_2 l_2} . \quad (9.12)$$

Since the general expressions get unwieldy quickly, we concentrate on the high symmetry directions.

To derive the effective theory governing the surface twist we integrate out strain. We do this separately for the homogeneous strain components E_{ij} , which only depend on the bulk state where $\psi = 0$. The homogeneous strain is then calculated in analogy to section 8.3, with rotated tensors. Because of the symmetry of the problem, the remaining inhomogeneous strain, and thus the displacement field, can only depend on the z -coordinate. Using this assumption and the boundary condition that in the bulk \mathbf{u} has to vanish, we derive the strain profile at the surface.

As an example for a [001] surface with an external magnetic field in [100] direction, R is a unit matrix and evaluating the proper tensor contractions we find that the only non-vanishing, inhomogeneous strain component is given by

$$\partial_z u_3 = -\frac{2\lambda_{12}}{C_{11}} \sin^2 \psi . \quad (9.13)$$

Note that for this orientation the surface strain is purely determined by the chiral coupling λ_{12} . If we reinsert this into the energy functional and derive the equation of state for the twisting angle ψ using the ansatz $\mathbf{m} = (\cos \psi, \sin \psi, 0)$.

$$\psi'' = h \sin \psi + \frac{\lambda_{11}^2 + 3\lambda_{12}^2}{C_{11} - C_{12}} \sin 2\psi + \frac{\lambda_{12}^2}{C_{11}} \sin 4\psi \quad (9.14)$$

where the $\sin 2\psi$ term represents an effective uniaxial anisotropy from the homogeneous distortion, caused by the polarized ground state, and the $\sin 4\psi$ term represents a cubic anisotropy inherited from the lattice.

It is also important to check how the critical field changes under the inclusion of magnetostriction since we need to make sure that the uniform magnetization which we assumed is the true bulk ground state. This can be done by inserting the ansatz for the magnetization in the conical state and expanding in the cone angle θ , effectively deriving a Landau functional for the conical-polarized transition.

Still in the $\hat{\mathbf{s}} \parallel [001]$ and $\mathbf{h} \parallel [100]$ orientation, the critical field h_c which makes the quadratic term vanish is

$$h_c = 1 - \frac{2\lambda_{11}^2}{C_{11} - C_{12}} - \frac{6\lambda_{12}^2}{C_{11} - C_{12}} + \frac{4\lambda_{44}}{C_{44}}. \quad (9.15)$$

For an isotropic lattice $C_{11} - C_{12} = 2C_{44}$ and coupling $\lambda_{11} = 2\lambda_{44}$, $\lambda_{12} = 0$ the magnetostriction contribution vanishes, showing that the effect is one of lattice anisotropy.

After multiplying the equation of state with ψ' , integrating over z and eliminating the integration constant by enforcing the constraint $\psi'(z \rightarrow \infty) = \psi(z \rightarrow \infty) = 0$ we obtain the first-order equation

$$\psi' = \sqrt{2\mathcal{V}(\psi)} = \sqrt{2h(1 - \cos \psi) + 2\mathcal{V}_{\text{me}}(\psi)} \quad (9.16)$$

where the magnetoelastic contribution to the effective potential is given by

$$\mathcal{V}_{\text{me}}(\psi) = \mathfrak{L}_u(1 - \cos 2\psi) + \mathfrak{L}_c(1 - \cos 4\psi). \quad (9.17)$$

The boundary conditions are unmodified $\psi'(0) = -1$. The coefficients \mathfrak{L}_u and \mathfrak{L}_c depend on the crystallographic orientation. For selected lattice orientations the uniaxial anisotropy is given by

$$\mathfrak{L}_u = \begin{cases} \frac{\lambda_{11}^2 + 3\lambda_{12}^2}{2(C_{11} - C_{12})} & \hat{\mathbf{s}} \parallel [001], \mathbf{h} \parallel [100] \\ \frac{1}{3} \left(\frac{\lambda_{11}^2 + 3\lambda_{12}^2}{2(C_{11} - C_{12})} + \frac{2\lambda_{44}^2}{C_{44}} \right) & \hat{\mathbf{s}} \parallel [111], \mathbf{h} \parallel [1\bar{1}0], \end{cases} \quad (9.18)$$

and the cubic anisotropy by

$$\mathfrak{L}_c = \begin{cases} \frac{\lambda_{12}^2}{4C_{11}} & \hat{\mathbf{s}} \parallel [001], \mathbf{h} \parallel [100] \\ 0 & \hat{\mathbf{s}} \parallel [111], \mathbf{h} \parallel [1\bar{1}0] \end{cases} \quad (9.19)$$

Integrating eq. (9.16) exactly is in general not possible. However, we can find numerical solutions, such as the ones shown in fig. 9.2. As long as the elastic coupling is not too large the profile is still approximately exponential, with a characteristic length scale L_{tw} that gets smaller with increased coupling. The length scale can be determined by a fit of $\psi \sim e^{-z/L_{\text{tw}}}$, and the result is also shown in fig. 9.2 as a function of the couplings and for different values of the applied field h .

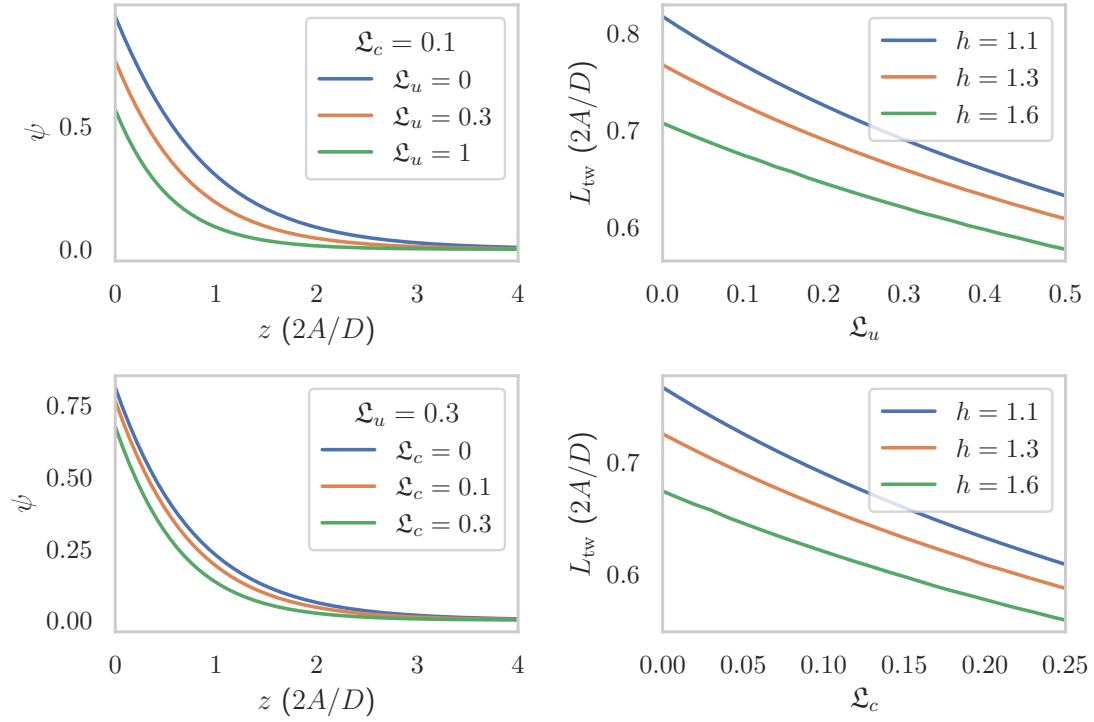


Figure 9.2.: Numerically determined profile of the chiral surface twist in the field polarized phase for different values of the magnetoelastic couplings (left), and length scale of the twist L_{tw} , determined by exponential fit as a function of the couplings.

9.2. Skyrmion surface twist

The skyrmion surface twist is a phenomenon that appears when the skyrmion axis is along the surface normal vector. Here, the boundary conditions force a twist in the skyrmion helicity, which is typically Bloch type in the bulk, towards a mixed Bloch-Néel state. Since helicity characterizes an in-plane magnetization angle, the twist angle of the skyrmion surface twist does not directly depend on the out-of-plane applied magnetic field, but instead is determined only by intrinsic material parameters.

Minimal analytical model

At first, we need to understand the prediction of the purely magnetic model. For this, we consider the skyrmions lattice phase of the model

$$\tilde{\mathcal{E}}_m = \frac{1}{2}(\partial_i \mathbf{m})^2 + \mathbf{m} \cdot (\nabla \times \mathbf{m}) - \kappa m_z^2 - h m_z, \quad (9.20)$$

with a surface in the x - y -plane. The magnetic field, anisotropy axis, and surface normal are thus all aligned along the z -direction, $\hat{\mathbf{s}} \parallel \mathbf{h} \parallel \hat{\mathbf{e}}_a \parallel \hat{\mathbf{z}}$. The lattice of skyrmion tubes, which orients along the same axis, is periodic in the x - y -plane and may be represented as a Fourier series

$$\mathbf{m}(\mathbf{r}) = \sum_{\mathbf{G}} a_{\mathbf{G}} \left((\hat{\mathbf{G}} \cos \chi(z) + \hat{\mathbf{z}} \times \hat{\mathbf{G}} \sin \chi(z)) \sin(\mathbf{G} \cdot \mathbf{r}) + \hat{\mathbf{z}} \cos(\mathbf{G} \cdot \mathbf{r}) \right), \quad (9.21)$$

where \mathbf{G} is a vector of the reciprocal lattice of the two-dimensional, hexagonal skyrmion crystal and $\hat{\mathbf{G}} = \mathbf{G}/|\mathbf{G}|$ is the corresponding unit vector. The z -dependent angle χ is the skyrmion helicity. Since χ describes an angle in the x - y -plane, it does not appear in anisotropy and magnetic field terms, which only couple to out-of-plane degrees of freedom. Hence, the helicity is unaffected by the parameters κ and h .

In the above ansatz, we have made already a strong assumption: χ is the same for all \mathbf{q} . In general, this would not be valid, however, we are mainly interested in a model that reproduces the length scale of the surface twist. The longest length scale will be determined by the smallest \mathbf{G} vectors, therefore we argue that the long-range physics will be captured by modeling the skyrmion lattice as the so-called triple- \mathbf{q} -state, where we only consider reciprocal lattice vectors with $|\mathbf{G}| = Q_{\text{SKL}}$ which Q_{SKL} is the reciprocal lattice constant. Thus the sum only goes over

$$\hat{\mathbf{G}} \in \left\{ \begin{pmatrix} 1 \\ 0 \\ 0 \end{pmatrix}, \begin{pmatrix} -\frac{1}{2} \\ \frac{\sqrt{3}}{2} \\ 0 \end{pmatrix}, \begin{pmatrix} -\frac{1}{2} \\ -\frac{\sqrt{3}}{2} \\ 0 \end{pmatrix} \right\} \quad (9.22)$$

and the Γ -point, representing a uniform magnetization contribution. By symmetry the amplitude $a_{\mathbf{G}} = a$ is then independent of \mathbf{G} . Inserting the triple- \mathbf{q} -ansatz into the minimal model and executing the integral over x and y , we arrive at an effective one-dimensional theory for χ ,

$$\tilde{E}_m = \frac{3a^2}{2} \int dz \left(\frac{1}{2} (\partial_z \chi)^2 + Q_{\text{SKL}}^2 + \partial_z \chi - 2Q_{\text{SKL}} \sin \chi \right) + \text{const.}, \quad (9.23)$$

In the bulk of the chiral magnet, we have translational invariance in z -direction. Thus the bulk helicity χ_0 is simply given by the minimum of the sin-potential, $\chi_0 = \pi/2$. We assume that the skyrmion lattice periodicity is determined by bulk properties and minimizing the above energy for $\chi = \chi_0$ yields $Q_{\text{SKL}} = 1$, in other words, the periodicity of the triple- q -state is the same at the helix period. We have learned in section 7.2 that this is in general not true since Q_{SKL} depends on the parameters κ and h . The simplification is an artifact of the triple- q -state approximation.

The equation of state for χ is the familiar sine-Gordon equation

$$\chi'' = 2 \sin(\chi - \chi_0) \quad (9.24)$$

where $\chi_0 = \pi/2$ is the bulk helicity, which for our model is Bloch-type. The boundary condition eq. (7.10) evaluates to $\chi'(0) = -1$ and of course we impose the condition that far away from the surface the helicity approaches the bulk value. The solution is thus in analogy with eq. (9.8)

$$\chi(z) - \chi_0 = 4 \arctan \left(e^{-\sqrt{2}(z-z_0)} \right). \quad (9.25)$$

We can read off the length scale of the skyrmion surface twist. Converting back from our natural units, we obtain

$$L_{\text{twist}} = \frac{1}{\sqrt{2}} \frac{2A}{D}. \quad (9.26)$$

In this simplified model the twist length depends only on the ratio of exchange interaction and DMI, similar to the magnetic modulation length $\lambda = \frac{4\pi}{A}/D$. The prediction of the minimal model is thus that the skyrmion surface twist has a length scale of $L_{\text{twist}} = \frac{\lambda}{\sqrt{22}\pi}$. This is lower than the estimate that one would get from dimensional analysis, $2A/D$, which is commonly found in the literature (Laan, Zhang, & Hesjedal, 2021; Zhang et al., 2018), by a factor of $1/\sqrt{2}$. This makes the discrepancy between theory and experiment even more striking, since the experimental value is several times larger than the theoretical estimate.

In the bulk chiral magnet Cu_2OSeO_3 the magnetic modulation length is approximately $\lambda = 62$ nm (Adams et al., 2012; Zhang et al., 2018). The prediction of the minimal model is thus $L_{\text{twist}} \approx 7$ nm, which agrees well with micromagnetic

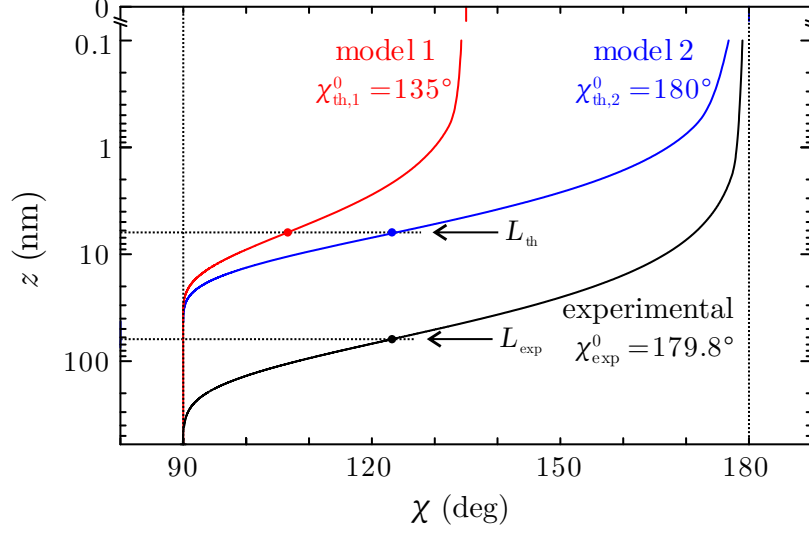


Figure 9.3.: Helicity profile from X-ray scattering experiments in Cu_2OSeO_3 and theoretical predictions from micromagnetic simulations (Zhang et al., 2018). In the theoretical model, the skyrmions twist has a length scale of $L_{\text{th}} = 5.4$ nm. Experimentally, a length scale of $L_{\text{exp}} = 62.5$ nm was observed.

modeling (Zhang et al., 2018). However, experimental observation of the twist length in the stable skyrmion lattice phase using depth-dependent circular dichroic resonant elastic X-ray scattering are in the range of 50 – 60 nm (Tan et al., 2024; Zhang et al., 2018), see fig. 9.3. The reason for this strong discrepancy is unknown, which motivates us to explore the effect of extending the model with magnetoelastic coupling on the surface twist.

Estimation of the bulk helicity length scale

If we are only interested in the length scale of changes in the helicity, in the above example $\sqrt{2}$, it is interesting to note that this scale was already encoded in the equation of state eq. (9.24), which is valid everywhere in the bulk, not just close to the surface. The surface merely acts as a perturbation, that forces the helicity to deviate from the bulk values to fulfill the boundary conditions. The range of this perturbation was dictated by bulk physics.

Practically, it is therefore not necessary to solve eq. (9.24) exactly, to extract the relevant length scale as will be shown below. Instead, we can imagine an infinitesimal perturbation $\delta\chi$ of the helicity $\chi(z) = \chi_0 + \delta\chi(z)$ somewhere along the skyrmion string in the bulk of the system and ask how this perturbation decays along the string.

We can expand the energy eq. (9.23) in $\delta\chi$ to obtain

$$\tilde{E}_m \approx \frac{1}{2} \int dz \left((\partial_z \delta\chi)^2 - 2\delta\chi^2 \right). \quad (9.27)$$

Since we are describing the helicity in the bulk, where translational invariance in z -direction holds, we can simply Fourier transform and obtain

$$\tilde{E}_m = \frac{1}{2} \int dq \left(q^2 + 2 \right) \delta\chi_q \delta\chi_{-q} \quad (9.28)$$

So the correlation function

$$\langle \delta\chi_q \delta\chi_{-q} \rangle = \frac{1}{q^2 + 2} \quad (9.29)$$

has a pole at $q = \pm i\sqrt{2}$, which is exactly the prediction of the minimal model for the twist length in dimensionless units.

Effect of magnetostriction

Already in one of the original publications describing the long-range surface reconstruction of the skyrmion lattice (Zhang et al., 2018) the magnetoelastic coupling is mentioned as a possible explanation. The intuition behind it is that the skyrmion lattice state leads to a crystal lattice distortion, which will be especially strong at the surface because of the skyrmion surface twist. If the crystal lattice distortion favors a Néel-type skyrmion, a self-consistent solution may show an enhancement of the surface twist.

To test this hypothesis we consider the effect of adding magnetostriction to the setup described above. The full energy density is given by

$$\tilde{\mathcal{E}} = \frac{1}{2} (\partial_i \mathbf{m})^2 + \mathbf{m} \cdot (\nabla \times \mathbf{m}) - \kappa m_z^2 - h m_z + \varepsilon_{ij} \lambda_{ijkl} m_k m_l + \frac{1}{2} \varepsilon_{ij} C_{ijkl} \varepsilon_{kl}. \quad (9.30)$$

To solve this model in the skyrmion lattice state analytically is challenging and promises only limited insight. We therefore resolve to numerical methods for this particular problem. The model was implemented as a finite element simulation of combined magnetic and elastic dynamics with high damping. The magnetic dynamics is given by the Landau-Lifshitz-Gilbert equation

$$\partial_t \mathbf{m} = \mathbf{m} \times \frac{\delta \mathcal{E}}{\delta \mathbf{m}} + \alpha \mathbf{m} \times \partial_t \mathbf{m} \quad (9.31)$$

where we have absorbed the gyromagnetic factor into the time coordinate. The parameter α represents the strength of the Gilbert damping. The elastic dynamics are given by the equation

$$\partial_t^2 \mathbf{u} = \frac{\delta \mathcal{E}}{\delta \mathbf{u}} + \eta \partial_t \mathbf{u} \quad (9.32)$$

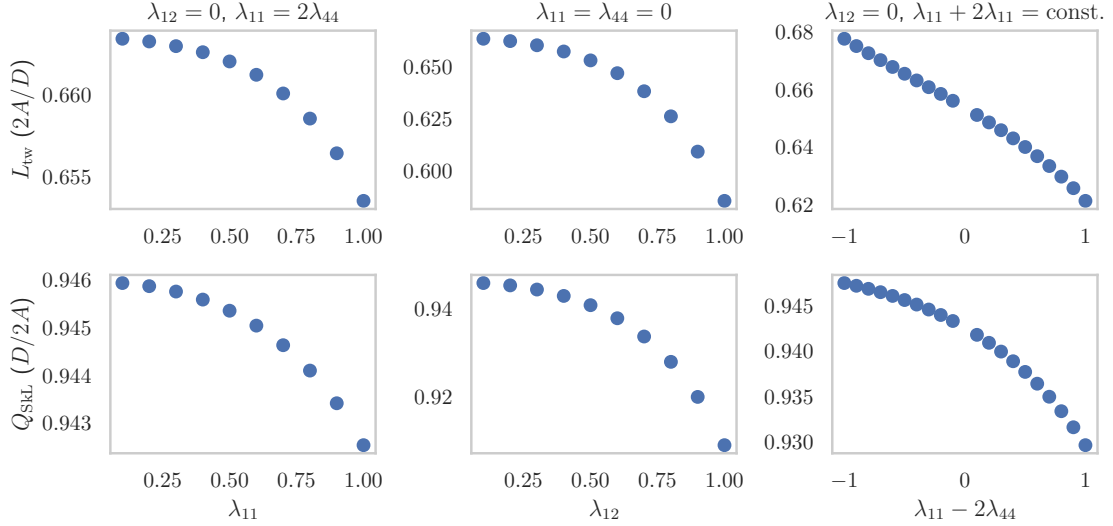


Figure 9.4.: Length scale of the skyrmion surface twist and skyrmion lattice constant as a function of magnetoelastic coupling parameters, determined using finite element simulations. The effect of isotropic coupling is to suppress the range of the surface twist, the same is the case for chiral coupling. The cubic anisotropic coupling can have a positive or negative effect, depending on the sign of $\lambda_{11} - 2\lambda_{44}$.

where η is the elastic damping, and the mass density was absorbed into the time coordinate. The simulation was done with the FEniCS framework (Alnaes et al., 2015; *Automated solution of differential equations by the finite element method*, 2012).

The skyrmion lattice was modeled with a rectangular unit cell containing two skyrmions, with periodic boundary conditions in x and y directions. In z -direction the simulation domain extended over a length on the order of the experimentally observed surface twist scale $L_z \sim 2\pi/Q_{\text{SKL}}$.

The simulations were performed in two steps. First, the bulk ground state was found by applying Neumann boundary conditions on both sides of the domain, simultaneously minimizing the energy as a function of Q_{SKL} and E_{ij} . The resulting values of these parameters were subsequently fixed for the second step of the simulation, in which Robin boundary conditions eq. (7.10) were applied to the $z = 0$ surface. The system was then allowed to relax and the helicity was extracted using the projection on the triple- q -fourier components. The length scale of the twist was determined by an exponential fit.

The effect of magnetostriction on the surface twist depends on the values chosen for the coupling tensor. For an isotropic coupling it holds $\lambda_{11} - 2\lambda_{44} = 0$ and $\lambda_{12} = 0$. These conditions leave only a single free coupling parameter. It can be seen in fig. 9.4, that the effect of the isotropic magnetostriction is to suppress the range

of the surface twist. At the same time Q_{SKL} is getting smaller, meaning that the skyrmion lattice is expanding slightly. This effect can be attributed to uniaxial anisotropy, caused by the tetragonal distortion of the lattice, which is known to have a small effect on Q_{SKL} .

The effect of the chirality magnetoelastic coupling is stronger than the isotropic coupling, but also lowers the length scale of the surface twist.

The only enhancement of the surface twist from magnetostriction is caused by the anisotropic coupling $\lambda_{11} - 2\lambda_{44}$ being negative, meaning that shear coupling λ_{44} is stronger than normal coupling λ_{11} . A similar effect can be found when lowering the shear stiffness C_{44} . However, if λ_{44} is increased above a certain threshold value such that λ_{44}/C_{44} is of order unity, the strong cubic anisotropy destabilizes the skyrmion lattice and the system transitions to a tilted polarized phase. In the tilted polarized phase the magnetization is homogeneous and tilted away from the magnetic field axis in [001] direction, because the cubic anisotropy favors the [111] direction.

These results should be taken with a grain of salt, since in the simulation, a hexagonal symmetry is imposed on the skyrmion lattice by setting the simulation domain to a rectangular unit cell with a fixed aspect ratio, while the cubic anisotropy breaks the hexagonal symmetry of the skyrmion lattice.

Discussion

We have seen from the simulation that the effect of magnetoelastic coupling on the skyrmion surface twist is generally small for realistic values of the coupling constants. An enhancement of the length scale of the surface twist could be seen for large λ_{44} , however, at large coupling, the skyrmion lattice was destabilized by the induced cubic anisotropy, such that a length scale comparable with exponential observations can not be reached this way.

Generally, a modification of the length scale of the surface twist L_{twist} is associated with a modification of the skyrmion lattice period $2\pi/Q_{\text{SKL}}$ of similar relative size. Thus a much larger ratio $L_{\text{twist}}Q_{\text{SKL}}$, such as was seen experimentally, seems even further out of reach. We therefore conclude that magnetoelastic is not the explanation for this effect.

More recent experiments performed by Tan et al. (2024) on the metastable skyrmion lattice at various temperatures, show a strong dependence of the surface twist on temperature. The large length scale that was observed earlier (Zhang et al., 2018) is only reproduced in the stable skyrmion phase at around 56 K, while for low temperatures the length scale approaches the prediction of the minimal model. This is another contradiction with the magnetoelastic hypothesis since the effect of magnetoelastic coupling is expected to be strongest for low temperatures. If we assume that the temperature dependence of the model parameters is dominated by

the temperature dependence of the saturation magnetization $M_s(T)$, this follows immediately from the M_s dependence of the various coupling parameters. From dimensional analysis, we can argue that $A \sim M_s^2$ and $D \sim M_s^2$, which should scale like $M_s^2 \sim T_c - T$. The magnetostriction however represents an anisotropy and thus one has to be more careful about the temperature dependence (H. B. Callen & Callen, 1966). We assume $\lambda \sim (T_c - T)^{\frac{3}{2}}$, C does not depend on M_s . Overall, the effect of magnetoelastic coupling is given by the energy scale

$$\frac{\lambda^2}{C} / \frac{D^2}{2A} \sim (T_c - T)^2, \quad (9.33)$$

thus the effect vanishes quickly when approaching the phase boundary to the paramagnetic phase.

A similar reasoning applies to DMI-type elastic coupling μ but with the more straightforward temperature dependence $\mu \sim M_s^2 \sim (T_c - T)$. A linear temperature scaling of an effect caused by DMI-type magnetoelastic coupling was indeed seen in experiments (Nomura et al., 2019) (also see section 8.3).

Conclusion and outlook

Throughout this thesis, we have seen several examples of elastic coupling to microscopic degrees of freedom influencing the physics at large scales. Both in the case of continuous phase transitions and chiral magnetism, we have learned a lot.

In part 1 we asked how the nature of continuous phase transitions is changed by elastic coupling. For classical phase transitions, this question has been sufficiently answered in the literature (Bergman & Halperin, 1976; Fisher, 1968; Larkin & Pikin, 1969). It was found that at constant pressure the transition becomes first order, while at constant volume one expects Fisher-renormalized exponents. Bergman & Halperin (1976) pointed out that the condition of “constant volume” is more accurately described by pinned boundary conditions, where all surface atoms are fixed to their position to stabilize the magnetoelastic crystal. It is however unclear if this purely theoretical construct is truly necessary, and we find that may warrant further research. We applied the classical theory to the tricritical point in chapter 4 and saw that if the critical exponent of specific heat α is positive, at constant pressure, the tricritical point is completely suppressed by elastic fluctuations through the Larkin-Pikin mechanism, while at constant volume Fisher-renormalized tricritical exponents emerge. In contrast, the effect of elastic coupling on quantum criticality turned out to be very different, as we discussed in detail in chapter 5 in the context of a generic $O(N)$ model. In the quantum critical theory elastic coupling is also non-perturbative if the corresponding critical exponent α_q is positive, but unlike the classical theory the RG flow is not towards a stable fixed point with Fisher-renormalized exponents. Instead, the lattice shows a microscopic instability at a finite RG scale through a vanish sound velocity. At $\alpha_q < 0$ we found a new repulsive fixed point that is characterized by a modified dynamical exponent for the longitudinal phonon. Overall, these results emphasize how the quantum nature of the fluctuations that drive the transition leads to fundamentally different and generally more singular critical behavior.

The elastic coupling at a ferroelectric transition, which was the topic of chapter 6, allows for coupling to shear strain, additionally to the generic compressive coupling. In the absence of this shear coupling, the ferroelectric critical behavior turned out to be modified by elastic coupling in a completely analogous way to the generic $O(N)$ model: The classical transition has a stable Fisher-renormalized fixed point, while the quantum transition has runaway flow leading to a microscopic instability. However, the theory turned out to be unstable with respect to above mentioned

shear coupling in both cases, leading to much richer physics. The classical theory has an additional fixed point at finite shear coupling, but vanishing shear modulus, indicating an instability towards a solid-liquid transition in the case of an isotropic medium. The nature of these new fixed points is at this point poorly understood and will be the topic of future research. The quantum theory has again no stable fixed points, but there are two different kinds of microscopic instabilities, one characterized by a vanishing longitudinal and the other by a vanishing transversal phonon velocity. The consequences of these instabilities are at this point unclear and need to be studied in more detail. Additionally, the role of flexoelectricity in relation to the theory outlined in chapter 6 has not been addressed.

In part 2 we explored the effect of magnetoelastic coupling on the non-collinear phases in chiral magnets. This is a partially unexplored field with many open questions. We saw in chapter 9 that the chiral surface twist in the field polarized phase has led to a non-trivial strain near the surface, which lowers the length scale of the surface twist. In the case of the skyrmion surface twist, we have shown that magnetoelastic coupling is *not* the reason for the large-scale surface reconstruction of the skyrmion lattice. We saw that there are certain regions in the vast parameter space of the magnetoelastic couplings, where the surface twist is enhanced, but this is by no means enough to explain the order or magnitude difference between the prediction of the purely micromagnetic theory and experimental results (Zhang et al., 2018). The question of the actual reason for the stark discrepancy between theory and experiment is still open, but in light of recent experimental results (Tan et al., 2024) it is much more likely to be answered with temperature-dependent effects, such as thermal fluctuations.

The understanding of combined magnetic and elastic dynamics that we have gained in the process is a good starting point to investigate a wide range of other phenomena. For example, magnetoelastic coupling will cause a magnon phonon hybridization, and in the skyrmion lattice phase, this may have interesting effects on the magnon band structure. The surface twist in the polarized phase is known to lead to magnon bound states (Müller et al., 2016), which may show interesting interactions with surface acoustic waves. Hybridization between spin waves and surface acoustic waves is an active field at the moment (Xu et al., 2020), and it would be interesting to see how this plays out in chiral magnets.

Acknowledgements

I would like to thank all the people who have made this thesis possible. First of all Markus Garst for giving me the opportunity to do this research in such a stimulating research environment. I would also like to thank Indranil Paul who hosted me during my research stay in Paris, where we worked together on the ferroelectric quantum criticality project. Thanks go also to my co-authors Saheli Sarkar and Nikolas Grivas on the quantum criticality on a compressible lattice (Sarkar et al., 2023), especially Saheli, who also helped me understand some of the older works on ferroelectric criticality. Also thanks to Jan Masell for the discussions on the skyrmion surface twist.

Lastly, I would like to acknowledge all the people who proofread some of this work and gave me valuable feedback, namely Daniel Hauck, Riccardo Ciola, Konrad Scharff, Sopheak Sorn, and Mark Currle. Also thanks to Kevin Klinge and Luzie Franke for finding my most embarrassing typos.

A. Calculation of self-energy diagram with transversal and longitudinal projectors

In the calculation of the self-energy correction for the isotropic ferroelectric with elastic coupling in section 6.2 the following diagram appears.

$$(A.1)$$

It resolves to the expression

$$\Sigma_{kk'}(\nu, p) = \frac{4}{\rho} \lambda_{ijkl} \lambda_{i'j'k'l'} \int_{q, \omega} G_{ll'}^0(p-q, \nu-\omega) q_i D_{jj'}^0(q, \omega) q_{i'} . \quad (A.2)$$

up to a combinatorial factor. The dependence of the integral on the external momentum is complicated by the transversal projector in the Green's function

$$G_{ij}^0(q, \omega) = \frac{\delta_{ij} - \hat{q}_i \hat{q}_j}{\omega^2 + c_0^2 q^2 + r_0} . \quad (A.3)$$

We will therefore need to calculate products of projectors on different momentum vectors such as

$$\left(\delta_{ij} - \frac{(p-q)_i (p-q)_j}{(p-q)^2} \right) \left[\frac{q_k q_l}{q^2} D_l(q, \omega) + \left(\delta_{kl} - \frac{q_k q_l}{q^2} \right) D_t(q, \omega) \right] \quad (A.4)$$

However, this also simplifies the calculation somewhat, since the self energy correction also split into longitudinal and transversal part

$$\Sigma_{ij}(\nu, p) = \sigma_l(\nu, p) \hat{p}_i \hat{p}_j + \sigma_t(\nu, p) (\delta_{ij} - \hat{p}_i \hat{p}_j) , \quad (A.5)$$

and we are only interested in the correction to the transversal modes. Therefore we extract the scalar function σ_t using the relation

$$\text{tr} \Sigma(\nu, p) - \hat{p}_i \Sigma_{ij}(\nu, p) \hat{p}_j = (d-1) \sigma_t(\nu, p). \quad (\text{A.6})$$

We will then assume that we can ignore the longitudinal mode and only renormalize the transversal one

$$Z_\phi^{-1}(\omega^2 + c^2 q^2 + r) = \omega + c_0^2 q^2 + r_0 - \sigma_t(\omega, q). \quad (\text{A.7})$$

Working out the algebra we find

$$\sigma_t(\nu, p) = \frac{4}{\rho} \int_{q, \omega} \frac{q^2}{(\nu - \omega)^2 + c^2(p - q)^2 + r} \left[\frac{f_l(p, q)}{\omega^2 + c_l^2 q^2} + \frac{f_t(p, q)}{\omega^2 + c_t^2 q^2} \right] \quad (\text{A.8})$$

with

$$\begin{aligned} f_l(p, q) &= \frac{\lambda_1^2}{d-1} \left(d-1 + \frac{q^2}{(p-q)^2} \left((\hat{p} \cdot \hat{q})^2 - 1 \right) \right) \\ &+ \frac{4\lambda_1 \lambda_2}{d-1} \left(\frac{q^2 - (p \cdot q)}{(p-q)^2} - 1 \right) \left((\hat{p} \cdot \hat{q})^2 - 1 \right) \\ &+ \frac{4\lambda_2^2}{d-1} \left(\frac{p^2 \left((\hat{p} \cdot \hat{q})^2 - 1 \right) + (p-q)^2}{(p-q)^2} - 1 \right) \left((\hat{p} \cdot \hat{q})^2 - 1 \right) \\ f_t(p, q) &= \frac{\lambda_2^2}{d-1} \left(\frac{(\hat{p} \cdot \hat{q})^2 [p^2(8-d-4(\hat{p} \cdot \hat{q})^2) + q^2] + (d-4)p^2 - q^2}{(p-q)^2} \right. \\ &\quad \left. + d(1 - (\hat{p} \cdot \hat{q})^2) \right) \end{aligned} \quad (\text{A.9})$$

However, since the problem is spherically symmetric, σ_t can not depend on the direction of external momentum \hat{p} . We can therefore choose p to be in z -direction such that $\hat{p} \cdot \hat{q} = \cos \theta$.

$$\begin{aligned} f_l(p, q, \theta) &= \frac{\lambda_1^2}{d-1} \left(d-1 - \frac{q^2}{p^2 + q^2 - 2pq \cos \theta} \sin^2 \theta \right) \\ &- \frac{4\lambda_1 \lambda_2}{d-1} \left(\frac{q^2 - pq \cos \theta}{p^2 + q^2 - 2pq \cos \theta} - 1 \right) \sin^2 \theta \\ &- \frac{4\lambda_2^2}{d-1} \left(\frac{p^2 \cos^2 \theta + q^2 - 2pq \cos \theta}{p^2 + q^2 - 2pq \cos \theta} - 1 \right) \sin^2 \theta \\ f_t(p, q, \theta) &= \frac{\lambda_2^2}{d-1} \left(\frac{\cos^2 \theta [p^2(8-d-4 \cos^2 \theta) + q^2] + (d-4)p^2 - q^2}{p^2 + q^2 - 2pq \cos \theta} \right. \\ &\quad \left. + d \sin^2 \theta \right) \end{aligned} \quad (\text{A.10})$$

Assuming that σ_t already has the form required by eq. (A.7) we can simplify the calculation by expanding in ν , p and r separately

$$\sigma_t(p, \nu) \sim \frac{1}{2} \frac{\partial^2 \sigma_t}{\partial \nu^2} \Big|_{\substack{\nu=0 \\ p=0 \\ r=0}} \nu^2 + \frac{1}{2} \frac{\partial^2 \sigma_t}{\partial p^2} \Big|_{\substack{\nu=0 \\ p=0 \\ r=0}} p^2 + \frac{\partial \sigma_t}{\partial r} \Big|_{\substack{\nu=0 \\ p=0 \\ r=0}} r \quad (\text{A.11})$$

at least at the level of logarithmic divergences. Keeping in mind that the self energy is *subtracted* from the bare propagator, we can then identify

$$\begin{aligned} 1 - Z_\phi^{-1} &= \frac{1}{2} \frac{\partial^2 \sigma_t}{\partial \nu^2} \Big|_{\substack{\nu=0 \\ p=0 \\ r=0}} = \frac{4}{\rho} \int_{q,\omega} \frac{q^2 (3\omega^2 - c^2 q^2)}{(\omega^2 + c^2 q^2)^3} \left[\frac{f_l(0, q, \theta)}{\omega^2 + c_l^2 q^2} + \frac{f_t(0, q, \theta)}{\omega^2 + c_t^2 q^2} \right] \\ r_0 - r &= \frac{\partial \sigma_t}{\partial r} \Big|_{\substack{\nu=0 \\ p=0 \\ r=0}} = -\frac{4}{\rho} \int_{q,\omega} \frac{q^2}{(\omega^2 + c^2 q^2)^2} \left[\frac{f_l(0, q, \theta)}{\omega^2 + c_l^2 q^2} + \frac{f_t(0, q, \theta)}{\omega^2 + c_t^2 q^2} \right] \end{aligned} \quad (\text{A.12})$$

For the ν and r derivatives we notice $f_{l/t}(0, q, \theta) = f_{l/t}(\theta)$ and write

$$\begin{aligned} f_l(\theta) &= \lambda_1^2 \left(1 - \frac{\sin^2 \theta}{d-1} \right) \\ f_t(\theta) &= \lambda_2^2 \sin^2 \theta \end{aligned} \quad (\text{A.13})$$

With this we can straightforwardly calculate the integrals and combine everything to get

$$\begin{aligned} Z_\phi^{-1} &= 1 + \frac{16K_4}{3\rho} \left[\frac{3d-5}{2(d-1)} \frac{\lambda_1^2}{c c_l (c+c_l)^3} + \frac{\lambda_2^2}{c c_t (c+c_t)^3} \right] \log b \\ r &= Z_\phi b^{-2z} \left(r - \frac{K_4}{6c^3} \left(d+1 - \frac{2}{d} \right) ur \log b \right. \\ &\quad \left. + \frac{8K_4}{3\rho} \left[\frac{3d-5}{2(d-1)} \frac{2c+c_l}{c^3 c_l (c+c_l)^2} \lambda_1^2 + \frac{2c+c_t}{c^3 c_t (c+c_t)^2} \lambda_2^2 \right] r \log b \right) \end{aligned} \quad (\text{A.14})$$

Only for the c correction we have to actually calculate derivatives of $f_{l/t}$ as well

$$c_0^2 - c^2 = \frac{1}{2} \frac{\partial^2 \sigma_t}{\partial p^2} \Big|_{\substack{\nu=0 \\ p=0 \\ r=0}} = \frac{2}{\rho} \int_{q,\omega} \left(\frac{\partial^2}{\partial p^2} \frac{q^2}{\omega^2 + c^2(p-q)^2} \left[\frac{f_l(p, q, \theta)}{\omega^2 + c_l^2 q^2} + \frac{f_t(p, q, \theta)}{\omega^2 + c_t^2 q^2} \right] \right)_{p=0} \quad (\text{A.15})$$

As a result we get

$$\begin{aligned}
c^2 = Z_\phi b^{2-2z} & \left(c^2 - \frac{8K_4}{15\rho(d-1)} \left[\frac{(5d-9)c - 2c_l}{c_l(c+c_l)^3} \lambda_1^2 \right. \right. \\
& + \frac{8}{cc_l(c+c_l)^2} ((c+2c_l)\lambda_1 + 4(c+c_l)\lambda_2) \lambda_2 \\
& \left. \left. + 2 \frac{(4d-18)c^2 + (7d-33)cc_t + (4d-16)c_t^2}{cc_t(c+c_t)^3} \lambda_2^2 \right] \log b \right)
\end{aligned} \tag{A.16}$$

Finally, we arrive at the RG flow equations for the parameters of the propagator of the longitudinal optical mode:

$$\begin{aligned}
\frac{dZ_\phi}{d\ell} &= -\frac{16K_4}{3\rho} \left[\frac{\lambda_1^2}{cc_l(c+c_l)^3} + \frac{\lambda_2^2}{cc_t(c+c_t)^3} \right] \\
\frac{dc^2}{d\ell} &= -\frac{8K_4}{15\rho} \left[\frac{13c - c_l}{c_l(c+c_l)^3} \lambda_1^2 + \frac{4}{cc_l(c+c_l)^2} ((c+2c_l)\lambda_1 + 4(c+c_l)\lambda_2) \lambda_2 \right. \\
& \quad \left. + \frac{4(c^2 - 3cc_t - c_t^2)}{cc_t(c+c_t)^3} \lambda_2^2 \right] \\
\frac{dr}{d\ell} &= \left(2 - \frac{5K_4}{9c^3} u + \frac{8K_4}{3\rho} \left[\frac{3c + c_l}{c^3(c+c_l)^3} \lambda_1^2 + \frac{3c + c_t}{c^3(c+c_t)^3} \lambda_2^2 \right] \right) r
\end{aligned} \tag{A.17}$$

Bibliography

- Adams, T., Chacon, A., Wagner, M., Bauer, A., Brandl, G., Pedersen, B., ... Pfeleiderer, C. (2012). Long-wavelength helimagnetic order and skyrmion lattice phase in Cu_2OSeO_3 . *Physical Review Letters*, 108(23). <https://doi.org/10.1103/physrevlett.108.237204>
- Alnaes, M. S., Blechta, J., Hake, J., Johansson, A., Kehlet, B., Logg, A., ... Wells, G. N. (2015). The FEniCS project version 1.5. *Archive of Numerical Software*, 3. <https://doi.org/10.11588/ans.2015.100.20553>
- Altland, A., & Simons, B. (2023). *Condensed matter field theory*. Cambridge University Press. <https://doi.org/10.1017/9781108781244>
- Anfuso, F., Garst, M., Rosch, A., Heyer, O., Lorenz, T., Rüegg, C., & Krämer, K. (2008). Spin-spin correlations of the spin-ladder compound $(\text{C}_5\text{H}_{12}\text{N})_2\text{CuBr}_4$ measured by magnetostriction and comparison to quantum monte carlo results. *Phys. Rev. B*, 77, 235113. <https://doi.org/10.1103/PhysRevB.77.235113>
- Aqeel, A., Azhar, M., Vlietstra, N., Pozzi, A., Sahliger, J., Huebl, H., ... Mostovoy, M. (2021). All-electrical detection of skyrmion lattice state and chiral surface twists. *Physical Review B*, 103(10). <https://doi.org/10.1103/physrevb.103.1100410>
- Automated solution of differential equations by the finite element method: The FEniCS book*. (2012). *Lecture Notes in Computational Science and Engineering*. Springer Berlin Heidelberg. <https://doi.org/10.1007/978-3-642-23099-8>
- Baker, G. A., & Essam, J. W. (1970). Effects of lattice compressibility on critical behavior. *Physical Review Letters*, 24(9), 447–449. <https://doi.org/10.1103/physrevlett.24.447>
- Baker, G. A., & Essam, J. W. (1971). Statistical mechanics of a compressible ising model with application to β brass. *The Journal of Chemical Physics*, 55(2), 861–879. <https://doi.org/10.1063/1.1676156>
- Bergman, D. J., & Halperin, B. I. (1976). Critical behavior of an ising model on a cubic compressible lattice. *Phys. Rev. B*, 13, 2145–2175. <https://doi.org/10.1103/PhysRevB.13.2145>
- Bogdanov, A. N., & Yablonskii, D. A. (1989). Thermodynamically stable “vortices” in magnetically ordered crystals. The mixed state of magnets. *Zh. Eksp. Teor. Fiz*, 95(1), 178.
- Brown, W. F. (1966). *Magnetoelastic interactions* (Vol. 9). Springer.
- Bruno, J., & Sak, J. (1980). Renormalization group for first-order phase transitions: Equation of state of the compressible ising magnet. *Phys. Rev. B*, 22, 3302–3318. <https://doi.org/10.1103/PhysRevB.22.3302>

- Butenko, A. B., Leonov, A. A., Röbner, U. K., & Bogdanov, A. N. (2010). Stabilization of skyrmion textures by uniaxial distortions in noncentrosymmetric cubic helimagnets. *Physical Review B*, *82*(5). <https://doi.org/10.1103/physrevb.82.052403>
- Callen, E., & Callen, H. B. (1965). Magnetostriction, forced magnetostriction, and anomalous thermal expansion in ferromagnets. *Physical Review*, *139*(2A), A455–A471. <https://doi.org/10.1103/physrev.139.a455>
- Callen, H. B., & Callen, E. (1966). The present status of the temperature dependence of magnetocrystalline anisotropy, and the power law. *Journal of Physics and Chemistry of Solids*, *27*(8), 1271–1285. [https://doi.org/10.1016/0022-3697\(66\)90012-6](https://doi.org/10.1016/0022-3697(66)90012-6)
- Cardy, J. (1996). *Scaling and renormalization in statistical physics*. Cambridge University Press. <https://doi.org/10.1017/cbo9781316036440>
- Chandra, P., Coleman, P., Continentino, M. A., & Lonzarich, G. G. (2020). Quantum annealed criticality: A scaling description. *Phys. Rev. Res.*, *2*, 043440. <https://doi.org/10.1103/PhysRevResearch.2.043440>
- Coak, M. J., Haines, C. R. S., Liu, C., Rowley, S. E., Lonzarich, G. G., & Saxena, S. S. (2020). Quantum critical phenomena in a compressible displacive ferroelectric. *Proceedings of the National Academy of Sciences*, *117*(23), 12707–12712. <https://doi.org/10.1073/pnas.1922151117>
- Cowley, R. A. (1976). Acoustic phonon instabilities and structural phase transitions. *Physical Review B*, *13*(11), 4877–4885. <https://doi.org/10.1103/physrevb.13.4877>
- Di Francesco, P., Mathieu, P., & Sénéchal, D. (1997). *Conformal field theory*. *Graduate Texts in Contemporary Physics*. Springer New York. <https://doi.org/10.1007/978-1-4612-2256-9>
- Domb, C. (1956). *J. Chem. Phys.*, *25*, 783. <https://doi.org/10.1063/1.1743060>
- Dünweg, B. (2000). Computersimulationen zu phasenübergängen und kritischen phänomenen. *Habilitationsschrift*. Retrieved from <https://www2.mpip-mainz.mpg.de/~duenweg/Public/PDFsOfPreprints/habil.pdf>
- Dzyaloshinsky, I. (1958). A thermodynamic theory of “weak” ferromagnetism of antiferromagnetics. *Journal of Physics and Chemistry of Solids*, *4*(4), 241–255. [https://doi.org/10.1016/0022-3697\(58\)90076-3](https://doi.org/10.1016/0022-3697(58)90076-3)
- Fisher, M. E. (1968). Renormalization of critical exponents by hidden variables. *Phys. Rev.*, *176*, 257–272. <https://doi.org/10.1103/PhysRev.176.257>
- Gati, E., Garst, M., Manna, R. S., Tutsch, U., Wolf, B., Bartosch, L., . . . Lang, M. (2016). Breakdown of hooke’s law of elasticity at the mott critical endpoint in an organic conductor. *Science Advances*, *2*(12). <https://doi.org/10.1126/sciadv.1601646>
- Güngördü, U., Nepal, R., Tretiakov, O. A., Belashchenko, K., & Kovalev, A. A. (2016). Stability of skyrmion lattices and symmetries of quasi-two-dimensional chiral magnets. *Physical Review B*, *93*(6). <https://doi.org/10.1103/physrevb.93.064428>
- Han, S., Lee, J., & Moon, E.-G. (2021). Lattice vibration as a knob on exotic quantum criticality. *Physical Review B*, *103*(1). <https://doi.org/10.1103/physre>

vb.103.014435

- Harris, A. B. (1974). Effect of random defects on the critical behaviour of ising models. *Journal of Physics C: Solid State Physics*, 7(9), 1671–1692. <https://doi.org/10.1088/0022-3719/7/9/009>
- Kenna, R., Johnston, D. A., & Janke, W. (2006). Scaling relations for logarithmic corrections. *Physical Review Letters*, 96(11). <https://doi.org/10.1103/physrevlett.96.115701>
- Khmel'nitskii, D. E., & Shneerson, V. L. (1971). Low-temperature displacement-type phase transition in crystals. *Soviet Physics Solid State, USSR*, 13(3), 687–+.
- Khmel'nitskii, D. E., & Shneerson, V. L. (1973). Phase transitions of the displacement type in crystals at very low temperatures. *Journal of Experimental and Theoretical Physics*, 37, 164. Retrieved from <https://api.semanticscholar.org/CorpusID:232617065>
- Kindervater, J., Adams, T., Bauer, A., Haslbeck, F. X., Chacon, A., Mühlbauer, S., ... Pfeleiderer, C. (2020). Evolution of magnetocrystalline anisotropies in $\text{Mn}_{1-x}\text{Fe}_x\text{Si}$ and $\text{Mn}_{1-x}\text{Co}_x\text{Si}$ as inferred from small-angle neutron scattering and bulk properties. *Physical Review B*, 101(10). <https://doi.org/10.1103/physrevb.101.104406>
- Kitchaev, D. A., Beyerlein, I. J., & Van der Ven, A. (2018). Phenomenology of chiral dzyaloshinskii-moriya interactions in strained materials. *Physical Review B*, 98(21). <https://doi.org/10.1103/physrevb.98.214414>
- Laan, G. van der, Zhang, S. L., & Hesjedal, T. (2021). Depth profiling of 3D skyrmion lattices in a chiral magnet—a story with a twist. *AIP Advances*, 11(1). <https://doi.org/10.1063/9.0000072>
- Landau, L., & Lifshitz, E. (1959). *Theory of elasticity*. Pergamon.
- Landau, L., & Lifshitz, E. (1963). *Electrodynamics of continuous media*. Pergamon.
- Larkin, A., & Pikin, S. (1969). Phase transitions of the first order but nearly of the second. *Sov. Phys. JETP*, 29, 891. Retrieved from <http://www.tcm.phy.cam.ac.uk/~dek12/courses/phase/Ap2.pdf>
- Leonov, A. O., Togawa, Y., Monchesky, T. L., Bogdanov, A. N., Kishine, J., Kousaka, Y., ... Inoue, K. (2016). Chiral surface twists and skyrmion stability in nanolayers of cubic helimagnets. *Physical Review Letters*, 117(8). <https://doi.org/10.1103/physrevlett.117.087202>
- Levanyuk, A. P., & Sobyenin, A. A. (1970). Second-order phase transitions without divergences in the second derivatives of the thermodynamic potential. *ZhETF Pisma Redaktsiiu*, 11, 540.
- Luijten, E., & Blöte, H. W. J. (1997). Classical critical behavior of spin models with long-range interactions. *Physical Review B*, 56(14), 8945–8958. <https://doi.org/10.1103/physrevb.56.8945>
- Maekawa, S., & Tachiki, M. (1976). Surface acoustic attenuation due to surface spin wave in ferro- and antiferromagnets. In *AIP conference proceedings* (Vol. 29, pp. 542–543). AIP. <https://doi.org/10.1063/1.30437>
- Mandel, J. (1965). Generalisation de la theorie de plasticite de w. T. koiter.

- International Journal of Solids and Structures*, 1(3), 273–295. [https://doi.org/10.1016/0020-7683\(65\)90034-x](https://doi.org/10.1016/0020-7683(65)90034-x)
- Meynell, S. A., Wilson, M. N., Fritzsche, H., Bogdanov, A. N., & Monchesky, T. L. (2014). Surface twist instabilities and skyrmion states in chiral ferromagnets. *Physical Review B*, 90(1). <https://doi.org/10.1103/physrevb.90.014406>
- Migliori, A., Sarrao, J. L., Visscher, W. M., Bell, T. M., Lei, M., Fisk, Z., & Leisure, R. G. (1993). Resonant ultrasound spectroscopic techniques for measurement of the elastic moduli of solids. *Physica B: Condensed Matter*, 183(1–2), 1–24. [https://doi.org/10.1016/0921-4526\(93\)90048-b](https://doi.org/10.1016/0921-4526(93)90048-b)
- Moriya, T. (1960). Anisotropic superexchange interaction and weak ferromagnetism. *Physical Review*, 120(1), 91–98. <https://doi.org/10.1103/physrev.120.91>
- Moura, M. A. de, Lubensky, T. C., Imry, Y., & Aharony, A. (1976). Coupling to anisotropic elastic media: Magnetic and liquid-crystal phase transitions. *Physical Review B*, 13(5), 2176–2185. <https://doi.org/10.1103/physrevb.13.2176>
- Mühlbauer, S., Binz, B., Jonietz, F., Pfleiderer, C., Rosch, A., Neubauer, A., ... Boni, P. (2009). Skyrmion lattice in a chiral magnet. *Science*, 323(5916), 915–919. <https://doi.org/10.1126/science.1166767>
- Müller, J., Rosch, A., & Garst, M. (2016). Edge instabilities and skyrmion creation in magnetic layers. *New Journal of Physics*, 18(6), 065006. <https://doi.org/10.1088/1367-2630/18/6/065006>
- Nattermann, T. (1977). Critical behaviour of a compressible n-component model with cubic anisotropy. *Journal of Physics A: Mathematical and General*, 10(10), 1757–1772. <https://doi.org/10.1088/0305-4470/10/10/010>
- Nomura, T., Zhang, X.-X., Zherlitsyn, S., Wosnitza, J., Tokura, Y., Nagaosa, N., & Seki, S. (2019). Phonon magneto-chiral effect. *Physical Review Letters*, 122(14). <https://doi.org/10.1103/physrevlett.122.145901>
- Paul, I., & Garst, M. (2017). Lattice effects on nematic quantum criticality in metals. *Physical Review Letters*, 118(22). <https://doi.org/10.1103/physrevlett.118.227601>
- Pelissetto, A., & Vicari, E. (2002). Critical phenomena and renormalization-group theory. *Physics Reports*, 368(6), 549–727. [https://doi.org/10.1016/s0370-1573\(02\)00219-3](https://doi.org/10.1016/s0370-1573(02)00219-3)
- Reiss, P., Graf, D., Haghighirad, A. A., Knafo, W., Drigo, L., Bristow, M., ... Coldea, A. I. (2019). Quenched nematic criticality and two superconducting domes in an iron-based superconductor. *Nature Physics*, 16(1), 89–94. <https://doi.org/10.1038/s41567-019-0694-2>
- Rice, O. K. (1954). Thermodynamics of phase transitions in compressible solid lattices. *J. Chem. Phys.*, 22, 1535. <https://doi.org/10.1063/1.1740453>
- Riedel, E. K., & Wegner, F. J. (1972). Tricritical exponents and scaling fields. *Physical Review Letters*, 29(6), 349–352. <https://doi.org/10.1103/physrevlett.29.349>
- Roussev, R., & Millis, A. J. (2003). Theory of the quantum paraelectric-ferroelectric transition. *Physical Review B*, 67(1). <https://doi.org/10.1103/physrevb.67.014105>

- Rowland, J., Banerjee, S., & Randeria, M. (2016). Skyrmions in chiral magnets with Rashba and Dresselhaus spin-orbit coupling. *Physical Review B*, *93*(2). <https://doi.org/10.1103/physrevb.93.020404>
- Rowley, S. E., Spalek, L. J., Smith, R. P., Dean, M. P. M., Itoh, M., Scott, J. F., ... Saxena, S. S. (2014). Ferroelectric quantum criticality. *Nature Physics*, *10*(5), 367–372. <https://doi.org/10.1038/nphys2924>
- Rüegg, Ch., Normand, B., Matsumoto, M., Furrer, A., McMorrow, D. F., Krämer, K. W., ... Boehm, M. (2008). Quantum magnets under pressure: Controlling elementary excitations in TiCuCl. *Physical Review Letters*, *100*(20). <https://doi.org/10.1103/physrevlett.100.205701>
- Rybakov, F. N., Borisov, A. B., & Bogdanov, A. N. (2013). Three-dimensional skyrmion states in thin films of cubic helimagnets. *Physical Review B*, *87*(9). <https://doi.org/10.1103/physrevb.87.094424>
- Sachdev, S. (2011). *Quantum phase transitions*. Cambridge University Press. <https://doi.org/10.1017/cbo9780511973765>
- Sak, J. (1974). Critical behavior of compressible magnets. *Phys. Rev. B*, *10*, 3957–3960. <https://doi.org/10.1103/PhysRevB.10.3957>
- Samanta, A., Shimshoni, E., & Podolsky, D. (2022). Phonon-induced modification of quantum criticality. *Phys. Rev. B*, *106*, 035154. <https://doi.org/10.1103/PhysRevB.106.035154>
- Sarkar, S., Franke, L., Grivas, N., & Garst, M. (2023). Quantum criticality on a compressible lattice. *Physical Review B*, *108*(23). <https://doi.org/10.1103/physrevb.108.235126>
- Schneider, S., Wolf, D., Stolt, M. J., Jin, S., Pohl, D., Rellinghaus, B., ... Lubk, A. (2018). Induction mapping of the 3D-modulated spin texture of skyrmions in thin helimagnets. *Physical Review Letters*, *120*(21). <https://doi.org/10.1103/physrevlett.120.217201>
- Skyrme, T. H. R. (1962). A unified field theory of mesons and baryons. *Nuclear Physics*, *31*, 556–569. [https://doi.org/10.1016/0029-5582\(62\)90775-7](https://doi.org/10.1016/0029-5582(62)90775-7)
- Tan, W., Jin, H., Fan, R., Ran, K., & Zhang, S. (2024). Evidence for giant surface dzyaloshinskii-moriya interaction in the chiral magnetic insulator Cu₂OSeO₃. *Physical Review B*, *109*(22). <https://doi.org/10.1103/physrevb.109.1220402>
- Villain, J. (1970). Self consistency of Landau's model in the transition from piezoelectricity to ferroelectricity. *Solid State Communications*, *8*(5), 295–297. [https://doi.org/10.1016/0038-1098\(70\)90453-9](https://doi.org/10.1016/0038-1098(70)90453-9)
- Wilson, K. G., & Fisher, M. E. (1972). Critical exponents in 3.99 dimensions. *Physical Review Letters*, *28*(4), 240–243. <https://doi.org/10.1103/physrevlett.28.240>
- Wilson, M. N., Butenko, A. B., Bogdanov, A. N., & Monchesky, T. L. (2014). Chiral skyrmions in cubic helimagnet films: The role of uniaxial anisotropy. *Physical Review B*, *89*(9). <https://doi.org/10.1103/physrevb.89.094411>
- Xu, M., Yamamoto, K., Puebla, J., Baumgaertl, K., Rana, B., Miura, K., ... Otani, Y. (2020). Nonreciprocal surface acoustic wave propagation via magneto-rotation coupling. *Science Advances*, *6*(32). <https://doi.org/10.1126/sciadv.abb1724>

- Zacharias, M., Bartosch, L., & Garst, M. (2012). Mott metal-insulator transition on compressible lattices. *Physical Review Letters*, *109*(17). <https://doi.org/10.1103/physrevlett.109.176401>
- Zacharias, M., Paul, I., & Garst, M. (2015). Quantum critical elasticity. *Physical Review Letters*, *115*(2). <https://doi.org/10.1103/physrevlett.115.025703>
- Zhang, S., Laan, G. van der, Müller, J., Heinen, L., Garst, M., Bauer, A., ... Hesjedal, T. (2018). Reciprocal space tomography of 3D skyrmion lattice order in a chiral magnet. *Proceedings of the National Academy of Sciences*, *115*(25), 6386–6391. <https://doi.org/10.1073/pnas.1803367115>
- Zinn-Justin, J. (2021). *Quantum field theory and critical phenomena: Fifth edition*. Oxford University PressOxford. <https://doi.org/10.1093/oso/9780198834625.001.0001>